SPALLATION-FISSION SYMBIOSIS

by

© WOLFGANG JOACHIM HARTMANN

A Thesis

Submitted to the School of Graduate Studies

in Partial Fulfilment of the Requirements

for the Degree

Doctor of Philosophy

McMaster University

March 1983

SPALLATION-FISSION SYMBIOSIS

DOCTOR OF PHILOSOPHY (1983)
(Nuclear Engineering)

McMASTER UNIVERSITY
Hamilton, Ontario

TITLE: SPALLATION-FISSION SYMBIOSIS

AUTHOR: Wolfgang Joachim Hartmann,

B.Sc. (University of Calgary)
M.Eng. (McMaster University)

SUPERVISOR: Dr. A.A. Harms

NUMBER OF PAGES: xiii, 250

ABSTRACT

The search for an enhancement of nuclear energy suggests that breeding of fissile fuel from fertile materials as well as the rejuvenation of spent nuclear fuel is of major importance. With the development of linear accelerator breeders it is possible, in principle, to enrich depleted nuclear fuel and to reenrich spent thermal reactor fuel for continued burnup without reprocessing. The management of separated fissile isotopes is thus largely avoided.

The symbiotic nuclear reactor system analyzed here consists of a linear accelerator breeder and a conventional nuclear converter reactor capable of burning natural uranium fuel. With repeated breed-burn cycles the system nuclear fuel can be brought to fuel burnups of up to and exceeding 27 times the conventional system once-through fuel burnup.

The analysis undertaken here shows considerable potential for uranium based fuel cycles relative to that for thorium fuel cycles for the case of low fuel burnup rejuvenation without reprocessing. Consequently uranium-plutonium fuel cycles are analyzed for schemes with periodic chemical fuel reprocessing as well as without reprocessing.

This analysis involves the development of a detailed

symbiotic system dynamic mass-energy conservation formulation, yielding results ranging from detailed system isotopic concentration histories to general system fuel mass flow and energy flow. A comparison is made between the major parameters of the symbiotic reactor system and its equivalent conventional system.

Optimum symbiotic system characteristics are generally obtained for net accumulated fuel burnups below 9 times the conventional once-through fuel burnup. For the presently estimated fuel to capital-operational cost fraction a marginally favorable symbiotic system is only obtained with an energy self-sufficient breeder subsystem. For increased fuel cost fractions, however, the symbiotic system shows highly improved system characteristics even for net power consuming breeder subsystems.

ACKNOWLEDGEMENTS

The author wishes to thank Dr. A.A. Harms, Department of Engineering Physics, for his guidance in the preparation of this thesis. Special thanks also to Dr. D.A. Thompson, Department of Engineering Physics, and Dr. Y. Nogami, Department of Physics, for their support in completing this work. The author also wishes to thank his parents, as well as Dr. A.C. Whittier and Mr. A.R. Dastur, both of Atomic Energy of Canada Limited, for their continued support and encouragement. Further, the careful final typing by the Engineering Word Processing is appreciated with thanks.

TABLE OF CONTENTS

TABLE OF CONTENTS (continued)

TABLE OF CONTENTS (continued)

LIST OF FIGURES

LIST OF FIGURES (continued)

LIST OF FIGURES (continued)

LIST OF FIGURES (continued)

LIST OF TABLES

CHAPTER 1

INTRODUCTION

1.1 Motivation

Conventional nuclear power reactors are dependent upon the availability of fissile fuels such as uranium-235, plutonium-239, plutonium-241, or uranium-233. However, the only naturally occuring fissile isotope is uranium-235, which constitutes 0.71% of natural uranium with the remainder being uranium-238.

Fissile isotopes such as uranium-233 and plutonium-239 however can be produced by nuclear transmutation from the more abundant fertile isotopes thorium-232 and uranium-238 respectively:

$$^{232}\mathrm{Th} + n \rightarrow {}^{233}\mathrm{Th} \xrightarrow{\beta^-} {}^{233}\mathrm{Pa} \xrightarrow{\beta^-} {}^{233}\mathrm{U} \qquad (1.1.1)$$

and

$$^{238}\mathrm{U} + n \rightarrow {}^{239}\mathrm{U} \xrightarrow{\beta^-} {}^{239}\mathrm{Np} \xrightarrow{\beta^-} {}^{239}\mathrm{Pu} \qquad (1.1.2)$$

The neutron source necessary for fissile fuel breeding can be the fission reaction itself. This, in fact, extends the fissile fuel resources of conventional reactors by breeding fissile isotopes of the plutonium chain directly into the fuel element during regular burnup. However, due to high

non-breeding neutron absorption in thermal nuclear reactors, the fissile fuel destruction rate generally exceeds the fissile fuel breeding rate resulting in fissioning of only about 1% of the heavy element fuel.

It is known that a fast flux environment, with neutrons in the keV range, enhances fissile fuel breeding. Based on this feature, fast breeder reactors may be able to extend fissile fuel resources. However, high fissile fuel inventory requirements and associated fissile fuel reprocessing limit the efficiency of such breeders.

It is recognized that a fission-independent neutron source would not have such limitations. Presently interesting fission-independent neutron sources are fusion reactions and spallation reactions. The importance of neutron producing spallation reactions in fissile fuel breeding strategies has been recognized as early as 1952 by W.B. Lewis[1], who realized the possibility of producing more energy by fissioning of a fissile atom than was needed by breeding the isotope in an accelerator target environment.

With the emergence of non-fission neutron sources, nuclear systems based on fissile fuel rejuvenation without reprocessing become attractive alternatives. The nuclear system considered here uses an accelerator target neutron source to breed fissile fuel directly in a thermal nuclear

reactor fuel element. The fuel element can subsequently be burnt directly in a conventional reactor. The specific system investigated consists of a 1 GeV proton linear accelerator breeder associated with a conventional reactor capable of burning natural uranium, such as a Canadian-Deuterium-Uranium Reactor (CANDU).

1.2 Spallation Reactions

Since the realization of the value of spallation produced neutrons for research and commercial applications in the late 1940's and early 1950's, considerable effort has been expended on the theory of associated reaction mechanisms. Reactions typically involve a target exposed to a charged particle beam with particle energies in the intermediate MeV to low GeV range. Interaction mechanisms in this range are based on compound nucleus theory[2] for reaction particle energies less than 50 MeV, and on the Serber model[3] for high energy nuclear reactions above 50 MeV. Detailed reviews of the reaction mechanisms, calculation methods, as well as experimental results have been reported by Yaffe[4], Hyde[5], and Shen and Merker[6].

Spallation reactions can generally be characterized as inelastic nuclear reactions in which at least one collision partner is a complex nucleus and the energy of the initial incident particle exceeds 50 MeV. The spallation

reaction can then be described by a two step model[3]. The initial step, also called the intranuclear cascade, knock-on or fast stage, occurs within a time interval of 10^{-22} seconds and is comparable to the transit time of a high energy particle through a complex nucleus. The final step, also called the evaporation, de-exitation or slow stage, occurs within 10^{-18} to 10^{-17} seconds. In the initial stage a high energy particle, such as 1 GeV proton, enters a high-Z target such as lead or uranium and interacts with individual nucleons of the complex nucleus. The result is the ejection of a few nucleons, the formation of pions, as well as the emergence of clusters of nucleons or fragments. This leaves the remaining nucleus in an excited stage. In the final step the excited nucleus de-excites by the emission of single nucleons, small clusters of nucleons, or, for actinide nuclei, also by fission. The particles emitted in the first step typically have energies above 50 MeV while the second step produces particles with a kinetic energy of a few MeV. In thick targets the emitted particles from both steps can undergo further spallation and associated compound nucleus reactions in what is generally called the nuclear cascade. Depending on the incident particle type and energy as well as the complex nucleus type, over 100 neutrons may be released per initial incident particle thus setting the stage for fissile fuel breeding.

1.3 Spallation Calculations and Experiments

The production of secondary neutrons by spallation reactions was first observed by E.O. Lawrence[7] and independently suggested by N.N. Semenov[8] in the late 1940's. Its' research and commercial importance was realized as early as the 1950's[1] resulting in continued research to the present[9-14].

Because of the complexity of spallation reactions theoretical research has mainly focused on Monte-Carlo computer simulations of the physical processes. Thus, since the early 1950's, several Monte-Carlo programs[6,15-18] have been written based on versions of the basic Serber model. Recent calculations in the United States and Canada are primarily being based on the code NMTC[17], which takes into account reactions with particle energies above 15 MeV. A comparative study of major transport codes[19] showed remarkably similar results for the intranuclear cascade calculations although results were somewhat sensitive to the details of the evaporation calculations. To obtain the total spallation based neutron yield, transport calculations for neutrons below 15 MeV are performed employing several Monte-Carlo codes such as O5R[20] and MORSE[21], while discrete ordinate codes such as ANISN[22] are also used. At present, the total calculated neutron yield per incident high energy particle is expected to be within 10% of the

actual yield.

Experimental studies and associated calculations can be divided into two major groups: those dealing with small spallation targets and those dealing with large or infinite spallation targets. For small targets neutron absorption by the target is minimized and the neutron yield is essentially the number of neutrons leaking from the target and is measured as neutrons absorbed in the moderator surrounding the target. In large targets neutron leakage is kept to a minimum and the neutron yield is basically the number of neutrons absorbed in the target.

Research oriented spallation neutron sources favor small targets producing high neutron leakage fluxes to be used in various experiments. Figure 1.3.1 summarizes the neutron leakage yields for high energy protons incident on small uranium and lead targets obtained from major experiments and associated calculations[7,9,23-27], with calculations being generally within 15% of the experimental findings. For small targets an increase in target size also increases the neutron leakage yield since high energy particles including spallation products have a greater interaction volume. However, neutron moderation and the associated increase in capture cross sections eventually will reduce the leakage neutron yield with increasing target size.

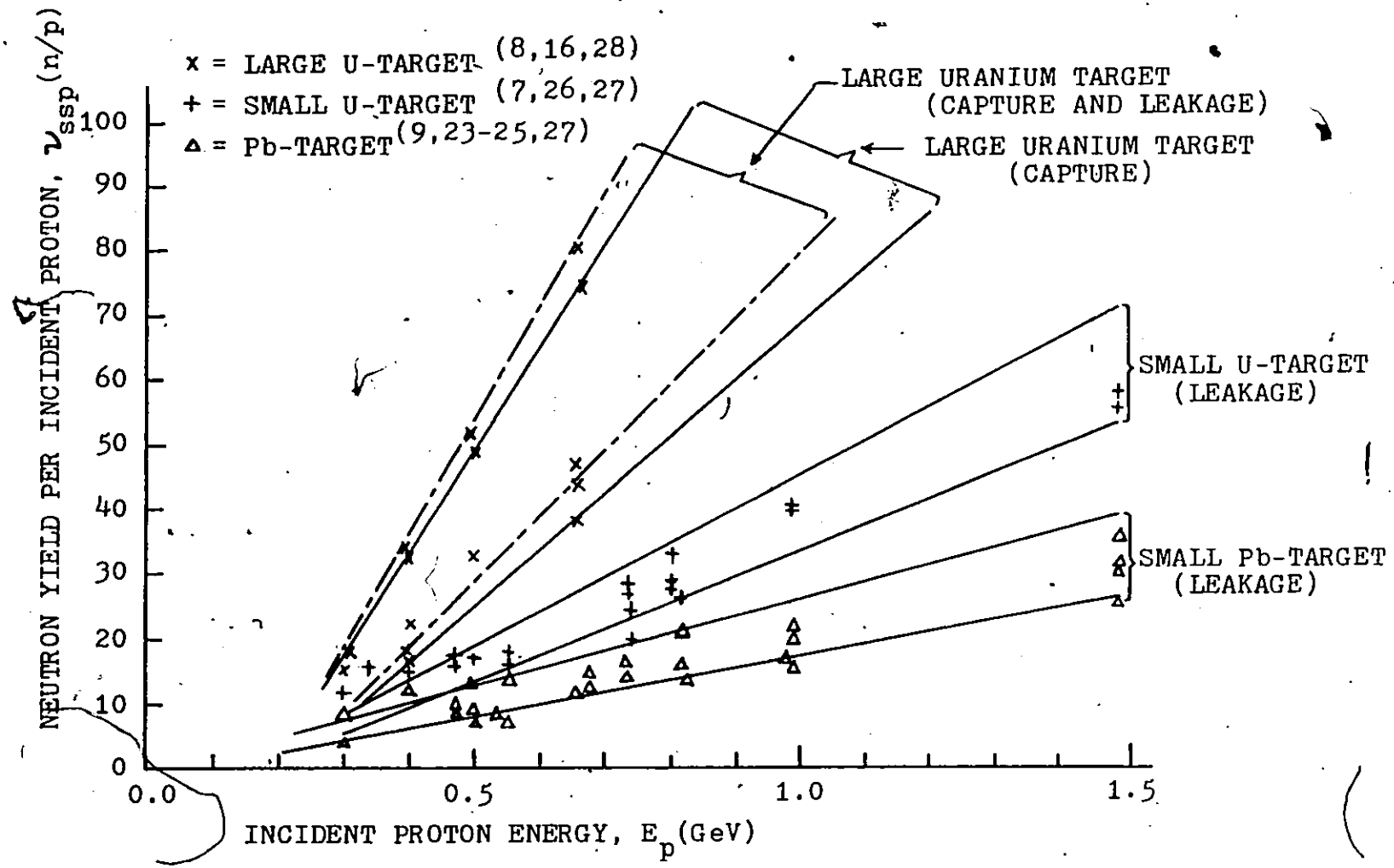

Fig. 1.3.1 Proton-initiated spallation neutron yield. The ranges shown indicate the domain of calculated and experimental results.

The neutron yield as absorbed by large uranium targets as well as the corresponding total neutron yield is also shown in Fig. 1.3.1. The neutron leakage of these targets is typically between 20% and 30% of the total neutron yield. The upper limits for large uranium targets are based on early calculations by Barashenkov and Toneev[16]; in this work, however, π-meson generation processes were not taken into consideration and fission barrier simulations were oversimplified[27] resulting in an overestimation of the neutron yields as suggested by experimental measurements[8]. Independent calculations for large uranium targets have been performed by Nakahara and Takahashi[28] using the NMTC-code and yielded results about 20% lower than experimental values[8], attributable to the fact that high energy fission reactions were not taken into account by NMTC[29]. Calculations have shown[30] that neutron absorption in small uranium targets can be as high as 50% of the total neutron yield. This makes the total neutron yield of large uranium targets consistent with the leakage yield of small uranium targets, where some allowance is made for further neutron multiplication of the small target leakage neutrons.

High energy reactions with incident particles other than protons have also been considered[7,25,31] and yield, in the case of deuteron interactions, 20% to 30% higher

neutron yields. Nevertheless protons are generally preferred choices due to the associated reduced technical problems of high-energy high-current beam production.

As shown in Fig. 1.3.1, uranium spallation target-blanket assemblies show the greatest fissile fuel breeding potential. For commercial applications, however, high beam powers are required which are expected to produce high power densities in the uranium target. Realistic target-blanket designs would therefore typically consist of non-fissioning target materials, such as lead or bismuth, surrounded by uranium oxide, UO_2, or thorium oxide, ThO_2, blankets and moderator-coolants such as light water, H_2O, or heavy water, D_2O.

Calculations using the NMTC-code produced total spallation neutron yields of 35 neutrons per 1 GeV proton for infinite lead or uranium oxide targets[32]. The introduction of a moderator-coolant consisting of different densities of light water or of heavy water, reduced the spallation neutron yield to between 28 and 31 neutrons per 1 GeV proton. The total non-fission spallation neutron yield of a small lead target surrounded by a fuel-coolant composition consisting of a mixture of uranium-oxide and light water or uranium oxide and heavy water may, therefore, conservatively be taken as 30 neutrons per 1 GeV proton. A target-blanket configuration of this type would be typical

for a system of fissile fuel rejuvenation without reprocessing.

1.4 Synergetic Nuclear Energy Systems

With the potential availability of non-fission neutron sources produced by fusion[33] or spallation reactions[6], the analysis of their impact on breeder-depleter synergetic systems becomes of major importance. The need for the analysis of fission independent breeder-depleter synergetic systems has been realized as early as the late 1960's when Jung[34] and Lidsky[35] discussed fusion-fission symbiotic systems. Since then numerous papers on synergetic nuclear energy systems have been published, as described in a recent overview of synergetic systems[36], which includes systems based on accelerator-spallation neutron sources. The accelerator based synergetic system employing spallation neutron sources is considered to be technically feasible and seems nearest to industrial practicability[37].

Spallation-based fissile fuel breeding systems have been studied widely under such names as spallation breeders[38-40], accelerator breeders[41-48], electrical breeders[49,50], electronuclear breeders[51-53], or fuel producers[54-56], and clean breeders[41]. The main advantages of a suitably designed accelerator based

synergetic system are:

1) avoidance of criticality accidents,
2) higher burnup levels due to lack of criticality constraints,
3) low fissile fuel inventories as compared to fast breeder reactors,
4) unlimited xenon override,
5) relaxed doubling time limitations as compared to fast breeder reactors,
6) high breeding ratios,
7) avoidance of non-fissile fuel breeding as compared to fusion systems, and
8) efficient integration with present technology.

The major disadvantages appear to be:

1) high fuel burnup material integrity limitations for systems with limited reprocessing,
2) high neutron flux levels,
3) high power gradients, and
4) high power densities.

In the development of accelerator based breeder reactors it is apparent that a wide range of operational options are possible. Three distinct overlapping systems have emerged:

1) the accelerator driven power reactor (ADPR)[57-60]
2) the accelerator fuel producer (AFP)[32,38-56]

3) the accelerator fuel regenerator or rejuvenator (AFR)[32,59-66].

The ADPR system, shown schematically in Fig. 1.4.1, would typically breed little or no net fissile fuel with the fissile fuel produced mainly consumed by the reactor itself. The AFP system, shown schematically in Fig. 1.4.2, would typically produce substantial amounts of fissile fuel, but the power production of the breeder would be lower. Fissile fuel separation and reprocessing is a necessity in this system since fissile fuel inventory is kept to a minimum. The AFR system, shown schematically in Fig. 1.4.3, has the potential of reenriching spent nuclear fuel from fission reactors with sufficient fissile fuel such that it can be reinserted into the fission reactor for continued burnup. No fuel reprocessing is to take place in this system. The fissile fuel production of the AFR is expected to be lower than the production of the AFP, since only limited spectral shaping is possible. This is due to the restraint of no reprocessing of fuel elements, requiring the same fuel element structure and materials for both the breeding reactor and its associated fission companion. Additional fissile fuel absorption losses in the AFR, as compared to the AFP, can be expected due to the higher fissile fuel inventory in the breeder. Here the fissile fuel inventory of the AFR fuel is dictated by the criticality requirements

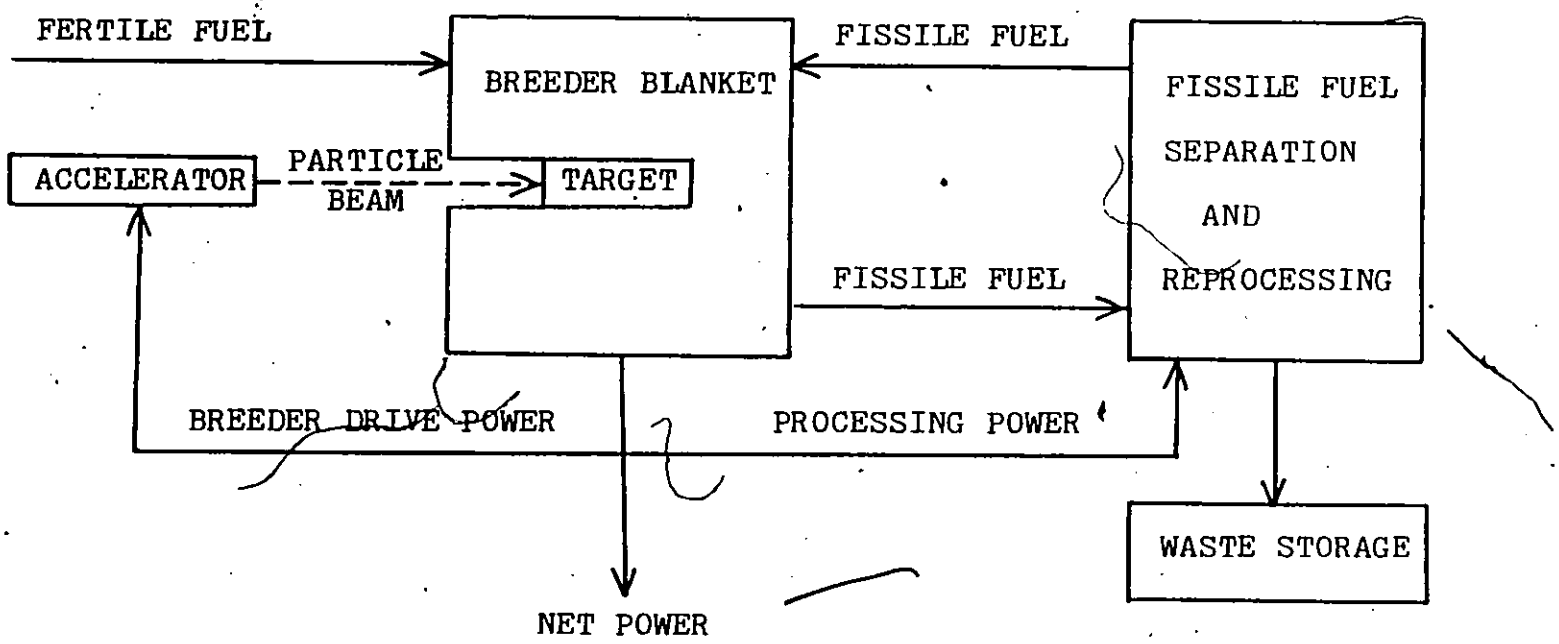

Fig. 1.4.1 The schematic representation of the accelerator driven power reactor (ADPR).

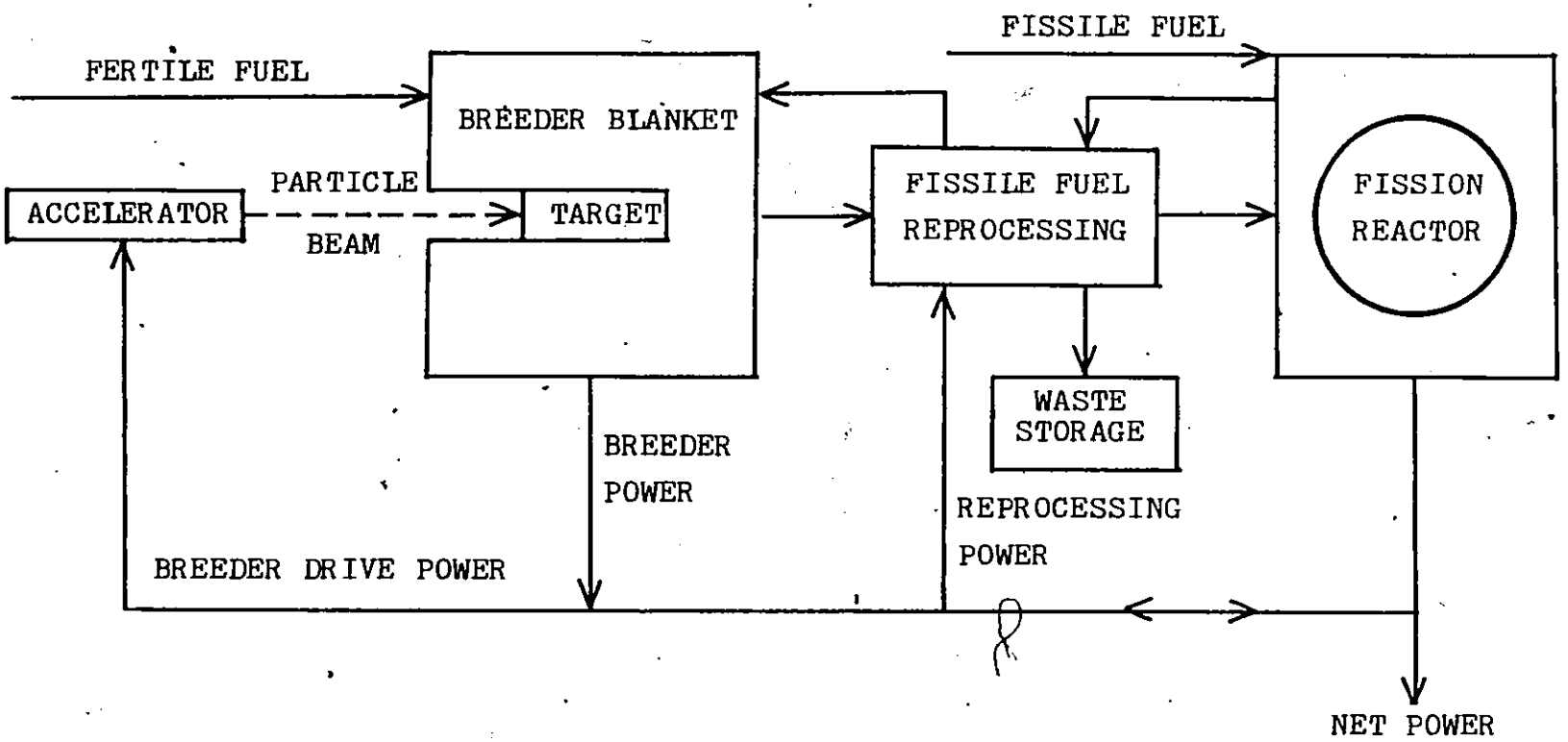

Fig. 1.4.2 The schematic representation of the accelerator fuel producer (AFP).

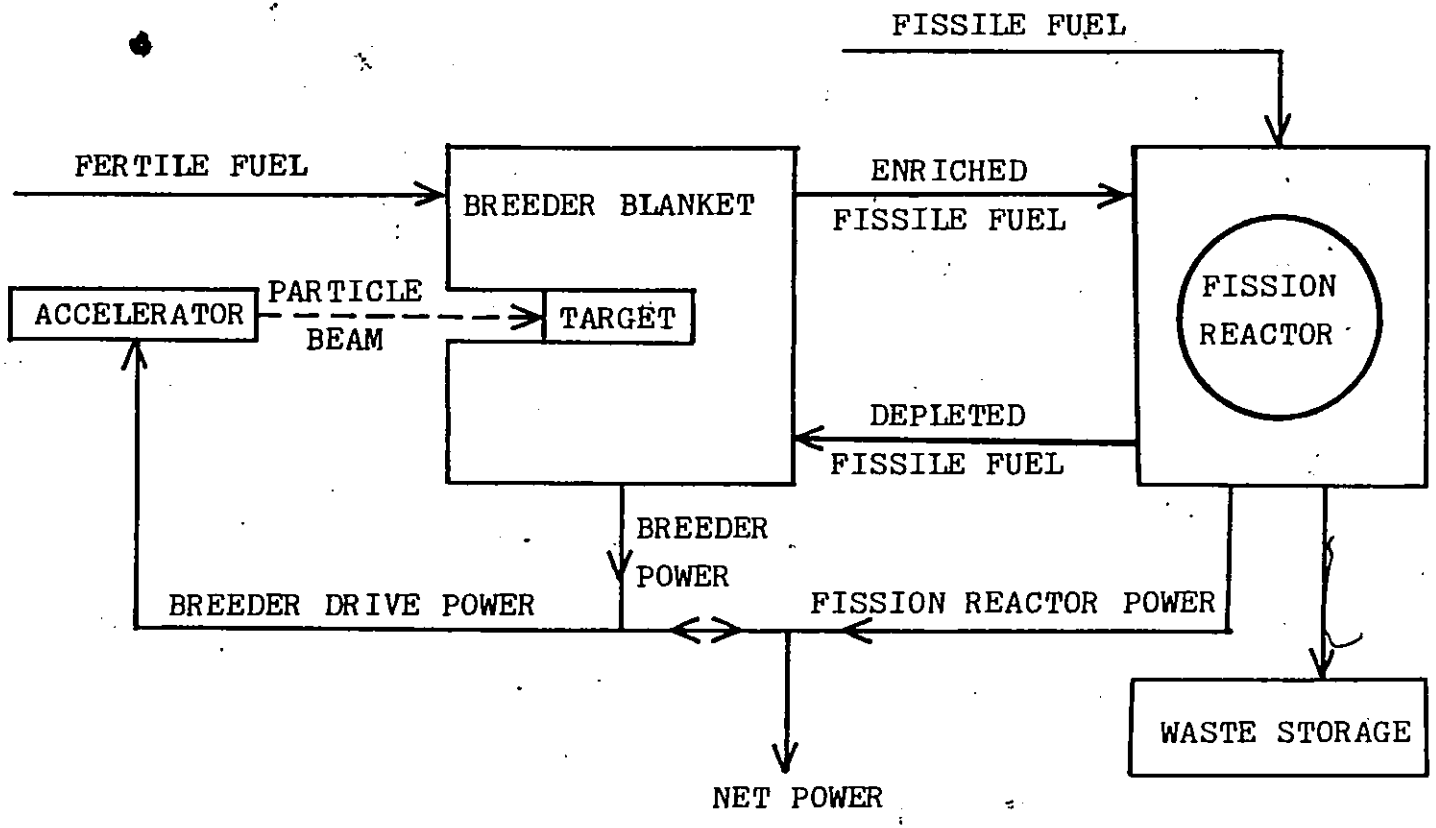

Fig. 1.4.3 The schematic representation of the accelerator fuel regenerator (AFR).

of the companion conventional reactor.

In this dissertation we explore a special case of the synergetic interaction of an AFR with a conventional reactor system; specifically we analyze the uranium-plutonium fuel cycle without reprocessing of linear accelerator based, low fissile fuel inventory symbiotic nuclear reactor systems.

1.5 Research Outline

This dissertation is structured to yield a sequential concept development, each chapter being based on previous ones. Figure 1.5.1 shows the schematic representation of the flow of the conceptual ideas. The system data and results are presented concurrently with appropriate development of the associated formalism.

In Chapter 2 the target-blanket spatial flux distribution characteristics as determined by the fission independent target neutron source are formulated. The functional forms of the breeder-blanket neutron flux and the associated accelerator target flux are obtained using the basic coordinate systems in one and two dimensions for neutrons of one energy group.

In Chapter 3 the characteristic spallation energy spectrum is explored resulting in a formulation of basic cross section data to be used in isotope depletion calculations. Here a two-component flux analysis,

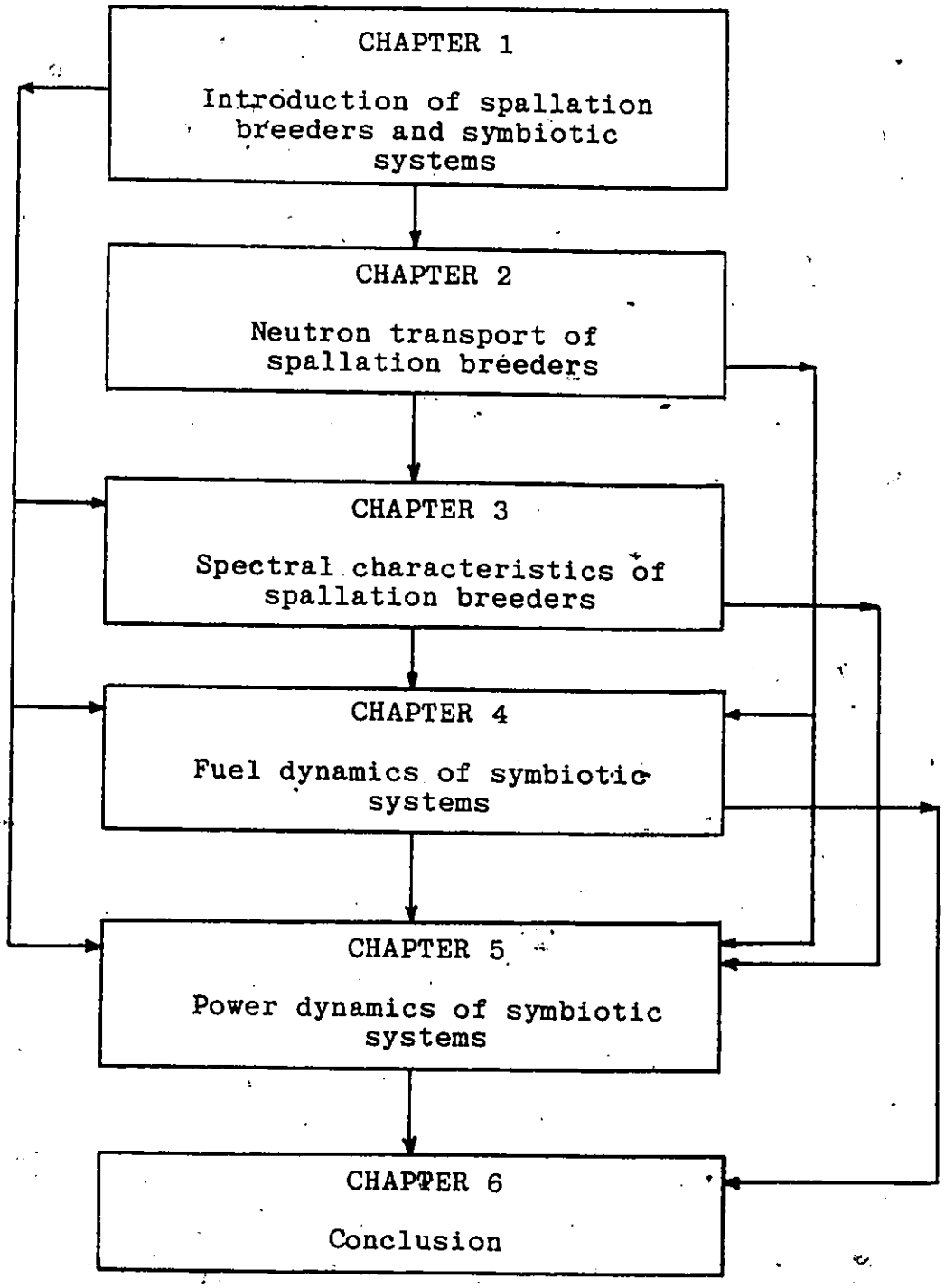

Fig. 1.5.1: Schematic overview of research

consisting of overlapping neutron energy groups, is employed.

Chapter 2 and Chapter 3 deal specifically with the breeder subsystem of the symbiotic system. In Chapter 4 the depleter subsystem is incorporated into the analysis. Here the symbiotic system fuel dynamics are specifically dealt with using a lumped parameter analysis and subsequently a detailed system mass-energy flow analysis is undertaken starting from basic conservation principles. The spatial and spectral breeder characteristics formulated in Chapter 2 and Chapter 3 respectively are incorporated in these calculations.

Chapter 5 further expands the symbiotic system analysis to include system power dynamics. Here the major system parameters are set into perspective by comparing the symbiotic system with the equivalent conventional system.

Chapter 6 highlights the major characteristics and conclusions of the explored systems.

CHAPTER 2

MATHEMATICAL FORMALISM OF THE ONE-COMPONENT ANALYSIS

2.1 Basic One-Component Formalism

The basic one-component formalism is the conventional approach in solving nuclear reactor problems. The starting point is the general neutron transport equation[67,68] given by

$$\frac{1}{v}\frac{\partial}{\partial t}\psi(\vec{r},\vec{\Omega},E,t) + \vec{\Omega}\cdot\nabla\psi(\vec{r},\vec{\Omega},E,t) + \Sigma_t(\vec{r},E,t)\,\psi(\vec{r},\vec{\Omega},E,t) =$$

$$\left(\int dE' \int d\vec{\Omega}'\, f_t'(\vec{r},\vec{\Omega}'\to\vec{\Omega},E'\to E)\, c(\vec{r},E')\, \Sigma_t(\vec{r},E',t)\right.$$

$$\left.\psi(\vec{r},\vec{\Omega}',E',t)\right) + T(\vec{r},\vec{\Omega},E,t), \qquad (2.1.1)$$

where the symbols are defined as follows: $\psi(\vec{r},\vec{\Omega},E,t)$ is the angular neutron flux at position $\vec{r}$, direction $\vec{\Omega}$, and energy E at time t. v is the neutron speed and $T(\vec{r},\vec{\Omega},E,t)$ defines flux independent neutron sources. $c(\vec{r},E')$ is the average neutron yield per reaction of cross-section $\Sigma_t(\vec{r},E',t)$, while $f_t'(\vec{r},\vec{\Omega}'\to\vec{\Omega},E'\to E)$ defines the fraction of neutrons of incident energy E' and direction $\vec{\Omega}'$ emerging from the interaction with energy E and direction $\vec{\Omega}$. Applying Eq. 2.1.1 to a bare target for the case of steady state gives

$$\vec{\Omega}\cdot\nabla\psi_{tb} + \Sigma_t(\vec{r},E)\,\psi_{tb} = \left(\int dE' \int d\vec{\Omega}'\, f_t'(\vec{r},\vec{\Omega}'\to\vec{\Omega},E'\to E)\right.$$

$$\left. c(\vec{r},E')\,\Sigma_t(\vec{r},E')\,\psi_{tb}'\right) + T_{tb}(\vec{r},\vec{\Omega},E). \qquad (2.1.2)$$

Here, $T_{tb}(\vec{r},\vec{\Omega},E)$ is the target neutron source produced by

spallation reactions. At the target boundary, $\vec{a}$, for a bare target one requires

$$\psi_{tb}(\vec{a},\vec{\Omega},E) = 0 \text{ for } \hat{n}\cdot\vec{\Omega} < 0, \qquad (2.1.3)$$

where the unit vector, $\hat{n}$, is the target surface vector.

Equation 2.1.2 can be solved in principle to obtain a bare target neutron leakage flux $\psi_{tb}(\vec{a},\vec{\Omega},E)$. This leakage flux becomes the neutron boundary source condition for repetitive subcritical breeding-blanket optimization calculations. It is clear that, as long as the target is not changed, sophisticated target calculations need not be repeated for each blanket optimization step. Figure 2.1.1 shows a typical target system.

The appropriate transport equation for the blanket is given by

$$\vec{\Omega}\cdot\nabla\psi_b + \Sigma_t(\vec{r},E)\,\psi_b = \left(\int dE' \int d\vec{\Omega}'\, f_t'(\vec{r},\vec{\Omega}'\to\vec{\Omega},E'\to E)\right.$$
$$\left. c(\vec{r},E')\,\Sigma_t(\vec{r},E')\,\psi_b'\right) + T_b(\vec{r},\vec{\Omega},E), \qquad (2.1.4)$$

with its associated blanket-to-target leakage flux component defined by

$$\vec{\Omega}\cdot\nabla\psi_{tl} + \Sigma_t(\vec{r},E)\,\psi_{tl} = \left(\int dE' \int d\vec{\Omega}'\, f_t'(\vec{r},\vec{\Omega}'\to\vec{\Omega},E'\to E)\right.$$
$$\left. c(\vec{r},E')\,\Sigma_t(\vec{r},E')\,\psi_{tl}'\right) + T_{tl}(\vec{r},\vec{\Omega},E). \qquad (2.1.5)$$

This target-blanket system is shown in Fig. 2.1.2. The total target neutron flux is therefore

$$\psi_{tt}(\vec{r},\vec{\Omega},E) = \psi_{tb}(\vec{r},\vec{\Omega},E) + \psi_{tl}(\vec{r},\vec{\Omega},E) \qquad (2.1.6)$$

and can be obtained by superimposing the system represented by Fig. 2.1.1 onto the system of Fig. 2.1.2. The interface

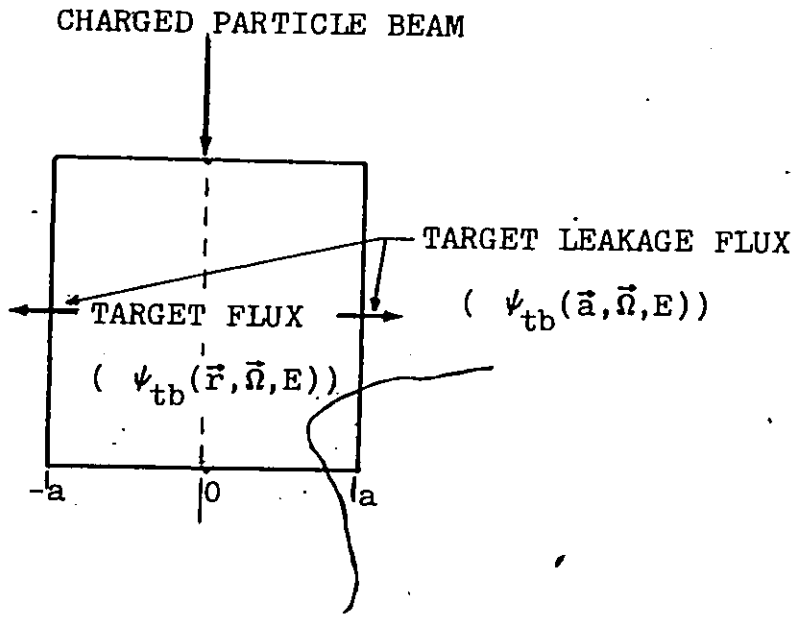

Fig. 2.1.1 Bare target model of an accelerator breeder.

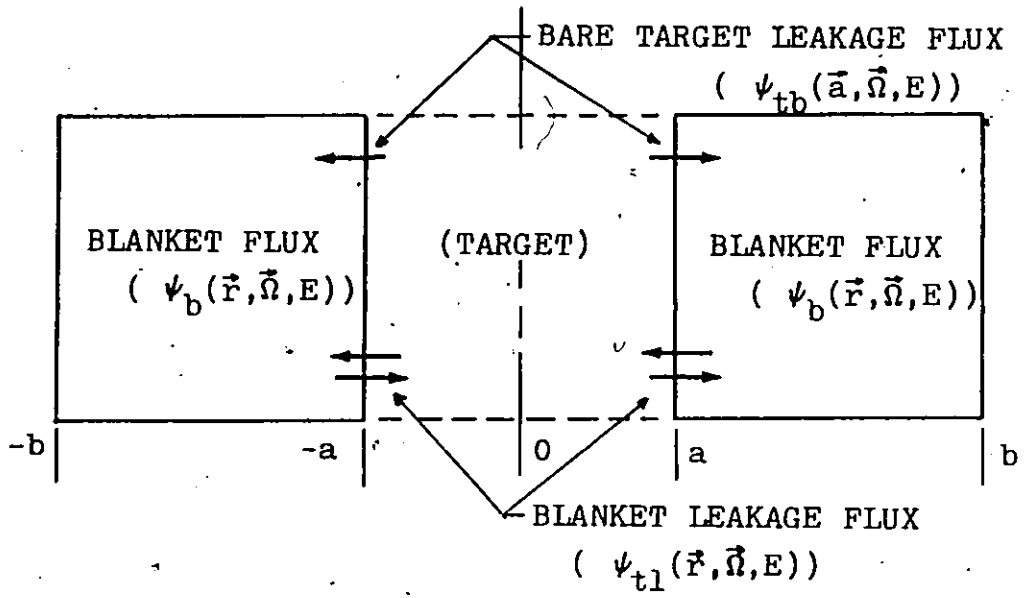

Fig. 2.1.2 Subcritical target-blanket model of an accelerator breeder.

boundary condition between the target and the blanket at $\vec{a}$ requires a continous neutron flux expressed by

$$\psi_{tt}(\vec{a},\vec{\Omega},E) = \psi_b(\vec{a},\vec{\Omega},E) \qquad (2.1.7)$$

or

$$\psi_{tl}(\vec{a},\vec{\Omega},E) = \psi_b(\vec{a},\vec{\Omega},E) - \psi_{tb}(\vec{a},\vec{\Omega},E), \qquad (2.1.8)$$

which becomes

$$\psi_{tl}(\vec{a},\vec{\Omega},E) = \psi_b(\vec{a},\vec{\Omega},E) \text{ for } \hat{n}\cdot\vec{\Omega} < 0. \qquad (2.1.9)$$

In most practical target-blanket designs, the neutron flux can only be calculated by numerical methods. Valuable insight into the basic characteristics of a target-blanket system can, however, be obtained from the analytic solutions of the neutron diffusion approximation to the transport equation.

2.2 One-Component One-Energy Group Diffusion Analysis

It has been found that a one group diffusion analysis of a fast breeder reactor yielded adequate results for scoping and parametric studies. Similar results should also be obtained for a ADPR with a high neutron multiplication value, since the relatively small number of target-produced spallation neutrons has little effect on the overall flux spectrum. This is especially true for the blanket flux at locations reasonably distant from blanket boundaries.

The use of Fick's law in Eq. 2.1.2 yields the standard neutron diffusion balance equation

$$D_j \nabla^2 \phi_j(\vec{r}) - (1 - c_j)\, \Sigma_{tj}\, \phi_j(\vec{r}) = -T_j(\vec{r}). \qquad (2.2.1)$$

Here, D_j is the diffusion coefficient and $\phi_j(\vec{r})$ is the space dependent neutron flux, where the subscript j defines the assembly location and the flux-component type. Using the equality

$$(1 - c_j)\, \Sigma_{tj} = (1 - k_{\infty j})\, \Sigma_{aj}, \qquad (2.2.2)$$

where Σ_{aj} is the medium absorption cross section, Eq. 2.2.1 becomes

$$D_j \nabla^2 \phi_j(\vec{r}) - (1 - k_{\infty j})\, \Sigma_{aj}\, \phi_j(\vec{r}) = -T_j(\vec{r}). \qquad (2.2.3)$$

Further simplification yields

$$\nabla^2 \phi_j(\vec{r}) - \omega_j^2\, \phi_j(\vec{r}) = -\frac{T_j(\vec{r})}{D_j}, \qquad (2.2.4)$$

where

$$\omega_j^2 = \frac{(1 - k_{\infty j})\, \Sigma_{aj}}{D_j} > 0, \qquad (2.2.5)$$

since the driven assembly necessarily has to be subcritical.

A blanket flux is now defined to be a flux with negligible non-neutron induced neutron production reactions, or

$$T_b(\vec{r}) = 0 \qquad (2.2.6)$$

and

$$T_{tl}(\vec{r}) = 0 \qquad (2.2.7)$$

for the blanket flux and the blanket-to-target leakage flux respectively. Equation 2.2.4 thus becomes

$$\nabla^2 \phi_j(\vec{r}) - \omega_j^2 \phi_j(\vec{r}) = 0. \qquad (2.2.8)$$

The appropriate interface boundary condition for the bare target is

$$\left|\vec{J}_{tb}(\vec{a})\right| = \phi_{tb}(\vec{a})/2, \qquad (2.2.9)$$

where the neutron current, $\vec{J}_{tb}(\vec{a})$, is related to the flux, $\phi_{tb}(\vec{a})$, by Fick's law. The subcritical target-blanket system requires

$$\phi_{tl}(\vec{a}) = \phi_b(\vec{a}) - \left|2\,\vec{J}_{tb}(\vec{a})\right| \qquad (2.2.10)$$

and

$$\vec{J}_{tl}(\vec{a}) = \vec{J}_b(\vec{a}) - \vec{J}_{tb}(\vec{a}), \qquad (2.2.11)$$

which, by using Fick's law, is rewritten as

$$D_{tl}\,\nabla\phi_{tl}(\vec{r})\Big|_{\vec{a}} = D_b\,\nabla\phi_b(\vec{r})\Big|_{\vec{a}} + \vec{S}(\vec{a}). \qquad (2.2.12)$$

Here, the source term, $\vec{S}(\vec{a})$, is the boundary source needed to drive the subcritical target-blanket system defined by

$$\vec{S}(\vec{a}) = \vec{J}_{tb}(\vec{a}). \qquad (2.2.13)$$

Equation 2.2.8 with its appropriate interface conditions can be expressed in Cartesian, cylindrical, and spherical coordinate systems as appropriate:

a) In the Cartesian coordinate system, the diffusion equation becomes

$$\frac{\partial^2}{\partial x^2}\phi_j(\vec{r}) + \frac{\partial^2}{\partial y^2}\phi_j(\vec{r}) + \frac{\partial^2}{\partial z^2}\phi_j(\vec{r}) - \omega_j^2\,\phi_j(\vec{r}) = 0, \qquad (2.2.14)$$

with the interface boundary conditions

$$\phi_{tl}(\vec{a}) = \phi_b(\vec{a}) - \left|2\vec{S}(\vec{a})\right| \qquad (2.2.15)$$

and

$$D_{t1} \frac{\partial}{\partial x} \phi_{t1}(\vec{r})\Big|_{\vec{a}} \hat{x} + D_{t1} \frac{\partial}{\partial y} \phi_{t1}(\vec{r})\Big|_{\vec{a}} \hat{y}$$

$$+ D_{t1} \frac{\partial}{\partial z} \phi_{t1}(\vec{r})\Big|_{\vec{a}} \hat{z}$$

$$= D_b \frac{\partial}{\partial x} \phi_b(\vec{r})\Big|_{\vec{a}} \hat{x} + D_b \frac{\partial}{\partial y} \phi_b(\vec{r})\Big|_{\vec{a}} \hat{y}$$

$$+ D_b \frac{\partial}{\partial z} \phi_b(\vec{r})\Big|_{\vec{a}} \hat{z} + \vec{S}(\vec{a}). \qquad (2.2.16)$$

b) In the cylindrical coordinate system, the diffusion equation becomes

$$\frac{\partial^2}{\partial r^2} \phi_j(\vec{r}) + \frac{1}{r} \frac{\partial}{\partial r} \phi_j(\vec{r}) + \frac{1}{r^2} \frac{\partial^2}{\partial \theta^2} \phi_j(\vec{r}) + \frac{\partial^2}{\partial z^2} \phi_j(\vec{r})$$

$$- \omega_j^2 \phi_j(\vec{r}) = 0, \qquad (2.2.17)$$

with the interface condition of Eq. 2.2.15 and

$$D_{t1} \frac{\partial}{\partial r} \phi_{t1}(\vec{r})\Big|_{\vec{a}} \hat{r} + D_{t1} \frac{1}{r} \frac{\partial}{\partial \theta} \phi_{t1}(\vec{r})\Big|_{\vec{a}} \hat{\theta}$$

$$+ D_{t1} \frac{\partial}{\partial z} \phi_{t1}(\vec{r})\Big|_{\vec{a}} \hat{z}$$

$$= D_b \frac{\partial}{\partial r} \phi_b(\vec{r})\Big|_{\vec{a}} \hat{r} + D_b \frac{1}{r} \frac{\partial}{\partial \theta} \phi_b(\vec{r})\Big|_{\vec{a}} \hat{\theta}$$

$$+ D_b \frac{\partial}{\partial z} \phi_b(\vec{r})\Big|_{\vec{a}} \hat{z} + \vec{S}(\vec{a}). \qquad (2.2.18)$$

c) In the spherical coordinate system, the diffusion equation becomes

$$\frac{1}{r^2}\left(\frac{\partial}{\partial r}\left(r^2\,\frac{\partial}{\partial r}\,\phi_j(\vec{r})\right)+\frac{1}{\sin\theta}\,\frac{\partial}{\partial\theta}\left(\sin\theta\,\frac{\partial}{\partial\theta}\,\phi_j(\vec{r})\right)\right.$$

$$\left.+\frac{1}{\sin^2\theta}\,\frac{\partial^2}{\partial\phi^2}\,\phi_j(\vec{r})\right)-\omega^2\,\phi_j(\vec{r})=0, \qquad (2.2.19)$$

with the interface boundary condition of Eq. 2.2.15 and

$$D_{t1}\,\frac{\partial}{\partial r}\,\phi_{t1}(\vec{r})\Big|_{\vec{a}}\,\hat{r}+D_{t1}\,\frac{1}{r}\,\frac{\partial}{\partial\theta}\,\phi_{t1}(\vec{r})\Big|_{\vec{a}}\,\hat{\theta}$$

$$+\frac{1}{r\sin\theta}\,\frac{\partial}{\partial\phi}\,\phi_{t1}(\vec{r})\Big|_{\vec{a}}\,\hat{\phi}=D_b\,\frac{\partial}{\partial r}\,\widetilde{\phi_b}(\vec{r})\Big|_{\vec{a}}\,\hat{r}$$

$$+D_b\,\frac{1}{r}\,\frac{\partial}{\partial\theta}\,\phi_b(\vec{r})\Big|_{\vec{a}}\,\hat{\theta}+\frac{1}{r\sin\theta}\,\frac{\partial}{\partial\phi}\,\phi_b(\vec{r})\Big|_{\vec{a}}\,\hat{\phi}+\vec{S}(\vec{a}). \qquad (2.2.20)$$

Equations 2.2.14, 2.2.17 and 2.2.19 are solved for special cases in the following sections. These equations are clearly only valid as long as direct spallation neutron sources initiated by particles other than neutrons can be neglected.

2.3 One-Component One-Energy Group Diffusion Approximation in Cartesian Coordinates and One Dimension

For a one-dimensional case in the Cartesian coordinate system, we impose

$$\frac{\partial}{\partial y}\,\phi_j(\vec{r})=0 \qquad (2.3.1)$$

and

$$\frac{\partial}{\partial z}\,\phi_j(\vec{r})=0 \qquad (2.3.2)$$

on Equation 2.2.4 to yield

$$\frac{\partial^2}{\partial x^2} \phi_j(x) - \omega^2 \phi_j(x) = 0. \qquad (2.3.3)$$

The appropriate interface boundary conditions follow from Eq. 2.2.15 and Eq. 2.2.16 to give

$$\phi_{t1}(a) = \phi_b(a) - 2S(a) \qquad (2.3.4)$$

and

$$D_{t1} \frac{\partial}{\partial x} \phi_{t1}(x)\Big|_a = D_b \frac{\partial}{\partial x} \phi_b(x)\Big|_a + S(a). \qquad (2.3.5)$$

The general solution of Eq. 2.3.3 for the target volume becomes

$$\phi_{t1}(x) = A_1 \cosh(\omega_{t1} x), \qquad (2.3.6)$$

while for the blanket volume, this yields

$$\phi_b(x) = A_2 \exp(-\omega_b x) + A_3 \exp(\omega_b x), \qquad (2.3.7)$$

and for a possible reflector, we obtain

$$\phi_r(x) = A_4 \exp(-\omega_r x). \qquad (2.3.8)$$

Here each volume is taken to be filled with a homogeneous material mixture. A schematic representation of the model is given in Fig. 2.3.1.

For an infinite blanket, one requires a finite flux at all coordinates and Eq. 2.3.6 and Eq. 2.3.7 become

$$\phi_{t1i}(x) = A_{1i} \cosh(\omega_{t1} x) \qquad (2.3.9)$$

and

$$\phi_{bi}(x) = A_{2i} \exp(-\omega_b x). \qquad (2.3.10)$$

For a bare blanket of thickness, d, we obtain the boundary

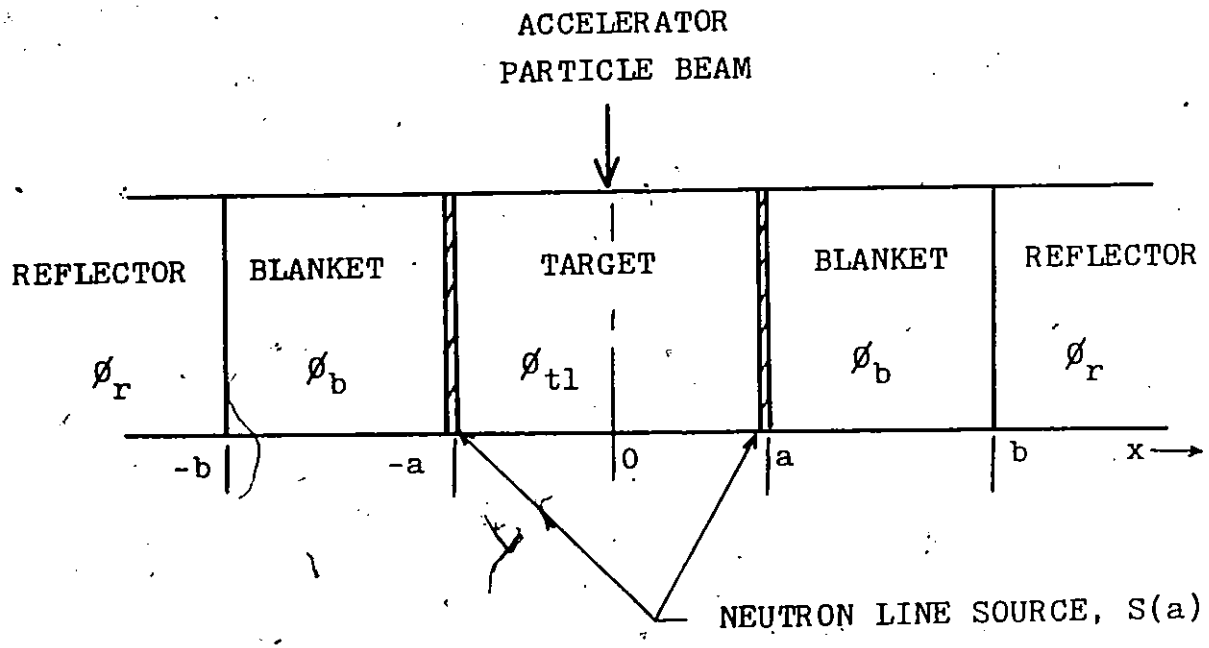

Fig. 2.3.1 One-dimensional target-blanket-reflector model of an accelerator breeder.

condition

$$\phi_b(b) = -2D_b \frac{\partial}{\partial x}\phi_b(x)\Big|_b \qquad (2.3.11)$$

from Eq. 2.2.9. The system location, b, is defined by

$$b = a + d. \qquad (2.3.12)$$

The solutions therefore become

$$\phi_{tlb}(x) = A_{1b} \cosh(\omega_{tl}\, x) \qquad (2.3.13)$$

and

$$\phi_{bb}(x) = A_{2b} \exp(-\omega_b\, x) + A_{3b} \exp(\omega_b\, x). \qquad (2.3.14)$$

In the presence of a perfect reflector at location, b, we require that.

$$\frac{\partial}{\partial x}\phi_b(x)\Big|_b = 0, \qquad (2.3.15)$$

which yields the solutions

$$\phi_{tlp}(x) = A_{1p} \cosh(\omega_{tl}\, x) \qquad (2.3.16)$$

and

$$\phi_{bp}(x) = A_{2p}(\exp(-\omega_b\, x) + \exp(-(2b-x)\omega_b)). \qquad (2.3.17)$$

Expressions for the constants, A_{mn}, are found with the aid of appropriate boundary conditions.

2.4 One-Component One-Energy Group Diffusion Approximation in Cylindrical Coordinates and One Dimension

For a one-dimensional case in the cylindrical coordinate system, we take

$$\frac{\partial}{\partial \theta}\phi_j(\vec{r}) = 0 \qquad (2.4.1)$$

and

$$\frac{\partial}{\partial z} \phi_j(\vec{r}) = 0 \qquad (2.4.2)$$

to obtain for Eq. 2.2.17

$$r^2 \frac{\partial^2}{\partial r^2} \phi_j(r) + r \frac{\partial}{\partial r} \phi_j(r) - \omega_j^2 r^2 \phi(r) = 0. \qquad (2.4.3)$$

The appropriate interface boundary conditions follow from Eq. 2.2.15 and Eq. 2.2.18 to give

$$\phi_{tl}(a) = \phi_b(a) - 2\, S(a) \qquad (2.4.4)$$

and

$$D_{tl} \frac{\partial}{\partial r} \phi_{tl}(r)\Big|_a = D_b \frac{\partial}{\partial r} \phi_b(r)\Big|_a + S(a). \qquad (2.4.5)$$

The general solutions of Eq. 2.4.3 are in the form of modified Bessel functions and can be written as

$$\phi_{tl}(r) = A_1 I_o(\omega_{tl} r), \qquad (2.4.6)$$

$$\phi_b(r) = A_2 I_o(\omega_b r) + A_3 K_o(\omega_b r), \qquad (2.4.7)$$

and

$$\phi_r(r) = A_4 K_o(\omega_r r) \qquad (2.4.8)$$

for homogenous target, blanket, and reflector volumes respectively.

For an infinite blanket, we require a finite flux at all reactor locations and therefore Eq. 2.4.6 and Eq. 2.4.7 become

$$\phi_{tli}(r) = A_{1i} I_o(\omega_{tl} r) \qquad (2.4.9)$$

and

$$\phi_b(r) = A_{3i}\, K_o(\omega_b\, r), \tag{2.4.10}$$

where the constants, A_{mn}, are obtained from the appropriate boundary conditions.

In the presence of a perfect reflector at location, b, we have

$$\frac{\partial}{\partial r}\, \phi_b(r)\Big|_b = 0 \tag{2.4.11}$$

which yields the solutions

$$\phi_{tlp}(r) = A_{lp}\, I_o(\omega_{tl}\, r) \tag{2.4.12}$$

and

$$\phi_{bp}(r) = A_{3p}\left(I_o(\omega_b\, r)\, \frac{K_1(\omega_b\, b)}{I_1(\omega_b\, b)} + K_o(\omega_b\, r)\right), \tag{2.4.13}$$

where the constants, A_{lp} and A_{3p}, are obtained from the interface boundary conditions between the target and the blanket at the location, a.

2.5 One-Component One-Energy Group Diffusion Approximations in Spherical Coordinates and One Dimension

For a one-dimensional case in the spherical coordinate system, we write

$$\frac{\partial}{\partial \theta}\, \phi_j(\vec{r}) = 0 \tag{2.5.1}$$

and

$$\frac{\partial}{\partial \phi}\, \phi_j(\vec{r}) = 0 \tag{2.5.2}$$

so that Eq. 2.2.19 becomes

$$\frac{1}{r^2} \frac{\partial}{\partial r} r^2 \frac{\partial}{\partial r} \phi_j(r) - \omega_j^2 \phi_j(r) = 0. \qquad (2.5.3)$$

The appropriate interface boundary conditions follow from Eq. 2.2.15 and Eq. 2.2.20 to give

$$\phi_{t1}(a) = \phi_b(a) - 2\, S(a) \qquad (2.5.4)$$

and

$$D_{t1} \frac{\partial}{\partial r} \phi_{t1}(r)\Big|_a = D_b \frac{\partial}{\partial r} \phi_b(r)\Big|_a + S(a). \qquad (2.5.5)$$

Equation 2.5.3 can be rewritten as

$$\frac{\partial^2}{\partial r^2} \phi_j(r) + \frac{2}{r} \frac{\partial}{\partial r} \phi_j(r) - \omega_j^2 \phi_j(r) = 0, \qquad (2.5.6)$$

which by substitution of

$$\phi_j(r) = \frac{\phi'_j(r)}{r} \qquad (2.5.7)$$

becomes

$$\frac{\partial^2}{\partial r^2} \phi'_j(r) - \omega_j^2 \phi'_j(r) = 0. \qquad (2.5.8)$$

This form of the diffusion equation can be solved to yield the general solutions

$$\phi_{t1}(r) = A_1 \sinh(\omega_{t1} r)/r, \qquad (2.5.9)$$

$$\phi_b(r) = A_2 \exp(-\omega_b r)/r + A_3 \exp(\omega_b r)/r, \qquad (2.5.10)$$

and

$$\phi_r(r) = A_4 \exp(-\omega_b r)/r \qquad (2.5.11)$$

for homogeneous target, blanket, and reflector volumes

respectively.

For an infinite blanket, we require a finite flux at all reactor locations and Eq. 2.5.9 and Eq. 2.5.10 become

$$\phi_{tli}(r) = A_{1i} \sinh(\omega_{tl} r)/r \qquad (2.5.12)$$

and

$$\phi_{bi}(r) = A_{2i} \exp(-\omega_b r)/r, \qquad (2.5.13)$$

where the constants, A_{mn}, are obtained from the appropriate boundary conditions.

In the presence of a perfect reflector at location, b, we impose

$$\frac{\partial}{\partial r} \phi_b(r)\Big|_b = 0, \qquad (2.5.14)$$

which yields the solutions

$$\phi_{tlp}(r) = A_{1p} \sinh(\omega_{tl} r)/r \qquad (2.5.15)$$

and

$$\phi_{bp}(r) = A_{2p}\left(\exp(-\omega_b r)/r + \frac{(b\omega_b + 1)}{(b\omega_b - 1)} \exp(\omega_b r)/r\right), \qquad (2.5.16)$$

where the constants, A_{1p} and A_{2p}, are obtained from the interface boundary conditions between the target and the blanket at a.

2.6 One-Component One-Energy Group Diffusion Approximation in Cartesian Coordinates and Two Dimensions

The major shortcoming of a one-dimensional treatment of the diffusion equation is that a neutron line-source of a

finite target cannot be simulated. A two-dimensional treatment with Cartesian coordinates greatly improves the model although complete elimination of the problem can only be achieved by a two-dimensional treatment in the cylindrical coordinate system.

A realistic model is defined in Fig. 2.6.1, where the interface boundary condition at the location, x=a, is given by

$$\vec{J}_{tl}(\vec{r})\Big|_{x=a} = \vec{J}_b(\vec{r})\Big|_{x=a} - \vec{S}(\vec{r})\Big|_{x=a}. \qquad (2.6.1)$$

Here, $\vec{S}(\vec{r})\Big|_{x=a}$ is the neutron leakage current created by a bare target at the interface location, x=a. Applying Eq. 2.3.1 as the appropriate leakage condition in the y-direction, yields the two-dimensional diffusion equation from Eq. 2.2.14 to give

$$\frac{\partial^2}{\partial x^2}\phi_j(\vec{r}) + \frac{\partial^2}{\partial z^2}\phi_j(\vec{r}) - \omega_j^2\,\phi_j(\vec{r}) = 0. \qquad (2.6.2)$$

The interface boundary conditions are obtained from Eq. 2.6.1 and are

$$D_{tl}\frac{\partial}{\partial x}\phi_{tl}(x,z)\Big|_{x=a} = D_b\frac{\partial}{\partial x}\phi_b(x,z)\Big|_{x=a} + S_x(a,z) \qquad (2.6.3)$$

and

$$D_{tl}\frac{\partial}{\partial z}\phi_{tl}(x,z)\Big|_{x=a} = D_b\frac{\partial}{\partial z}\phi_b(x,z)\Big|_{x=a} + S_z(a,z), \qquad (2.6.4)$$

where

$$\vec{S}(\vec{r}) = S_x(\vec{r})\hat{x} + S_y(\vec{r})\hat{y} + S_z(\vec{r})\hat{z}. \qquad (2.6.5)$$

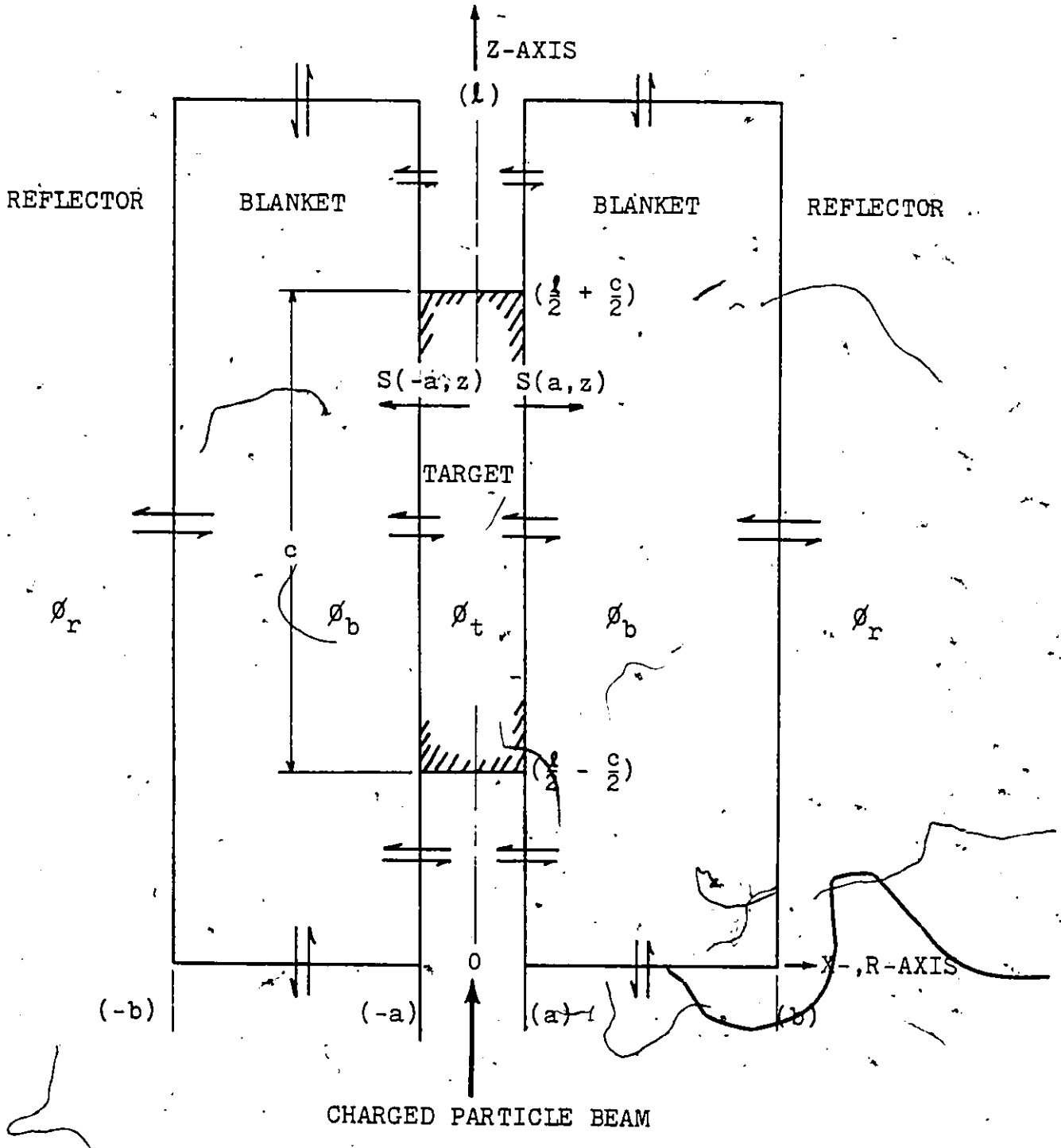

Fig. 2.6.1 Two-dimensional model of an accelerator breeder.

Equation 2.6.2 can be solved by the method of separation of variables. Hence,

$$\phi_j(\vec{r}) = X_j(x)\, Z_j(z), \tag{2.6.6}$$

and we rewrite Eq. 2.6.2 as

$$\beta_j^2 - \gamma_j^2 - \omega_j^2 = 0. \tag{2.6.7}$$

Here

$$\beta_j^2 = \frac{1}{X_j(x)} \frac{\partial^2}{\partial x^2} X_j(x) \tag{2.6.8}$$

and

$$\gamma_j^2 = \frac{-1}{Z_j(z)} \frac{\partial^2}{\partial z^2} Z_j(z). \tag{2.6.9}$$

The general solution for Eq. 2.6.8 is

$$X_j(x) = A_{1j} \exp(-\beta_j x) + A_{2j} \exp(\beta_j x), \tag{2.6.10}$$

while for Eq. 2.6.9, we write

$$Z_j(a) = A_{3j} \cos(\gamma_j z) + A_{4j} \sin(\gamma_j z). \tag{2.6.11}$$

To obtain solutions for the constants, A_{mj}, boundary conditions at z=0, z=ℓ, and x=b are now introduced. Only the extreme cases defined by black boundary conditions and white boundary conditions are considered.

For a bare blanket, black boundary conditions are introduced to yield

$$X_{bb}(b,-b) = 0 \tag{2.6.12}$$

and

$$Z_{bb}(0,\ell) = 0. \tag{2.6.13}$$

Here, the boundary locations are the standard extrapolated boundaries used in the diffusion approximations. The

boundary condition

$$\phi(r') = 2\left|\vec{J}(r')\right|, \tag{2.6.14}$$

where r' is a real boundary location, can be used but yields more complex solutions. The boundary condition at location z=0 requires that

$$A_{3bb} = 0, \tag{2.6.15}$$

while the condition at location z=ℓ gives

$$\gamma_{bn} = \frac{n\pi}{\ell} \text{ for } n = 1, 2, 3, \ldots . \tag{2.6.16}$$

The solution for Eq. 2.6.11 thus becomes

$$Z_{bbn}(z) = A_{4bn} \sin(\frac{n\pi}{\ell} z). \tag{2.6.17}$$

Using Eq. 2.6.7, we obtain

$$\beta_{bn}^2 = (\frac{n\pi}{\ell})^2 + \omega_b^2. \tag{2.6.18}$$

Applying Eq. 2.6.12 to Eq. 2.6.10 gives

$$X_{bbn}(x) = A_{1bn}\left(\exp(-\beta_{bn} x) - \exp(-\beta_{bn} 2b + \beta_{bn} x)\right). \tag{2.6.19}$$

By substituting Eq. 2.6.17 and Eq. 2.6.19 into Eq. 2.6.6, we finally obtain the solution

$$\phi_{bb}(x,z) = \sum_{n=1}^{\infty} C_{bbn}\left(\exp(-\beta_{bn} x) - \exp(-\beta_{bn} 2b + \beta_{bn} x)\right) \sin(\frac{n\pi}{\ell} z) \tag{2.6.20}$$

for the total blanket flux. The constants, C_{bbn}, can be calculated directly from $\phi(\pm a,z)$ by using the conventional

Fourier-series theory or from Eq. 2.6.3 and Eq. 2.6,4. A knowledge of the target flux, $\phi_{tlb}(x,z)$, is however required. Due to the complexity of the target, this solution, $\phi_{tlb}(x,z)$, is difficult to obtain. This difficulty, however, can be avoided by requiring that neutrons originating in the blanket are reflected at the boundary locations x=a, and x=-a. Under certain favourable conditions[30], this is a reasonable requirement. The condition can be expressed as

$$J_{tlx}(\pm a) = 0 \tag{2.6.21}$$

and Eq. 2.6.3 and Eq. 2.6.4 become

$$S_x(a,z) = -D_b \frac{\partial}{\partial x} \phi_{bb}(x,z)\Big|_{x=a} \tag{2.6.22}$$

and

$$S_z(a,z) = -D_b \frac{\partial}{\partial z} \phi_{bb}(x,z)\Big|_{x=a} + D_{tl} \frac{\partial}{\partial z} \phi_{tlb}(x,z)\Big|_{x=a} \tag{2.6.23}$$

Here, Eq. 2.6.23 defines the target flux, $\phi_{tlb}(x,z)$, required to produce the white boundary condition. Substituting Eq. 2.6.20 into Eq. 2.6.22, we get

$$S_x(a,z) = \sum_{n=1}^{\infty} C_{bbn} D_b \beta_{bn} \left(\exp(-\beta_{bn} a) + \exp(-\beta_{bn} 2b + \beta_{bn} a)\right) \sin\left(\frac{n\pi}{\ell} z\right). \tag{2.6.24}$$

The predetermined x-component of the bare target leakage current, $S_x(a,z)$, can be expanded in a Fourier series such that

$$S_x(a,z) = \sum_{n=1}^{\infty} A_n \sin\left(\frac{n\pi}{\ell} z\right), \tag{2.6.25}$$

where

$$A_n = \frac{2}{\ell} \int_0^{\ell} dz\, S_x(a,z) \sin\left(\frac{n\pi}{\ell} z\right). \tag{2.6.26}$$

Substituting Eq. 2.6.25 into Eq. 2.6.24 yields

$$C_{bbn} = A_n/\left[D_b\, \beta_{bn}\left(\exp(-\beta_{bn}\, a) + \exp(-\beta_{bn} 2b + \beta_{bn}\, a)\right)\right]. \tag{2.6.27}$$

For a blanket surrounded by a perfect reflector, we apply the white boundary conditions

$$\left.\frac{\partial X_{bp}(x)}{\partial x}\right|_{x=b} = 0 \tag{2.6.28}$$

and

$$\left.\frac{\partial Z_{bp}(z)}{\partial z}\right|_{z=0,\ell} = 0. \tag{2.6.29}$$

Applying the conditions defined by Eq. 2.6.29 to Eq. 2.6.11 gives

$$Z_{bpn}(z) = A_{3pn} \cos\left(\frac{n\pi}{\ell} z\right) \text{ for } n = 0,1,2,\ldots, \tag{2.6.30}$$

while applying Eq. 2.6.28 to Eq. 2.6.10 yields

$$X_{bpn}(x) = A_{1pn}\left(\exp(-\beta_{bn}\, x) + \exp(-2\beta_{bn}\, b + \beta_{bn}\, x)\right). \tag{2.6.31}$$

The boundary source term, $S_x(a,z)$, can be expanded to give

$$S_x(a,z) = \frac{A_o}{2} + \sum_{n=1}^{\infty} A_n \cos\left(\frac{n\pi}{\ell} z\right), \tag{2.6.32}$$

where

$$A_n = \frac{2}{\ell} \int_0^{\ell} dz\, S_x(a,z) \cos\left(\frac{n\pi}{\ell} z\right) \text{ for } n = 1,2,3,\ldots . \quad (2.6.33)$$

Combining Eq. 2.6.30 and Eq. 2.6.31 one obtains the final solution

$$\phi_{bp}(x,z) = \sum_{n=0}^{\infty} C_{bpn}\left(\exp(-\beta_{bn} x) + \exp(-2\beta_{bn} b + \beta_{bn} x)\right) \cos\left(\frac{n\pi}{\ell} z\right). \quad (2.6.34)$$

Here, the constants, C_{bpn}, are obtained from the boundary source, $S_x(a,z)$, to yield

$$C_{bpo} = A_o/(2D_b \beta_{bn}(\exp(-\beta_{bn} a) - \exp(-2\beta_{bn} b + \beta_{bn} a))) \quad (2.6.35)$$

and

$$C_{bpn} = A_n/(D_b \beta_{bn}(\exp(-\beta_{bn} a) + \exp(-2\beta_{bn} b + \beta_{bn} a))). \quad (2.6.36)$$

2.7 One-Component One-Energy Group Diffusion Approximation in Cylindrical Coordinates and Two Dimensions

A two-dimensional treatment of the spallation-breeder reactor blanket in cylindrical coordinates with axial symmetry gives a three-dimensional, realistic model. The model is defined by Fig. 2.6.1. For this case, we have

$$\frac{\partial}{\partial\theta} \phi_j(\vec{r}) = 0 \quad (2.7.1)$$

in Eq. 2.2.17 to obtain

$$\frac{\partial^2}{\partial r^2} \phi_j(\vec{r}) + \frac{1}{r} \frac{\partial}{\partial r}\phi_j(\vec{r}) + \frac{\partial^2}{\partial z^2} \phi_j(\vec{r}) - \omega_j^2 \phi_j(\vec{r}) = 0. \quad (2.7.2)$$

Similar to Eq. 2.6.21, we require

$$J_{tlr}(a,z) = 0 \quad (2.7.3)$$

and Eq. 2.2.18 thus yields

$$S_r(a,z) = -D_b \frac{\partial}{\partial r} \phi_b(r,z)\Big|_{r=a} \quad (2.7.4)$$

and

$$S_z(a,z) = -D_b \frac{\partial}{\partial z} \phi_b(r,z)\Big|_{r=a} + D_{tl} \frac{\partial}{\partial z} \phi_{tl}(r,z)\Big|_{r=a}. \quad (2.7.5)$$

Equation 2.7.2 can be solved by the method of separation of variables such that

$$\phi_j(r,z) = Z_j(r)\, R_j(r). \quad (2.7.6)$$

By applying the bare blanket boundary conditions

$$R_{bb}(+b,-b) = 0 \quad (2.7.7)$$

and

$$Z_{bb}(0,\ell) = 0 \quad (2.7.8)$$

we obtain the solution

$$\phi_{bb}(r,z) = \sum_{n=1}^{\infty} C'_{bbn} \left(I_o(\beta_{bn}\, r) - \frac{I_o(\beta_{bn}\, b)}{K_o(\beta_{bn}\, b)} K_o(\beta_{bn}\, r)\right)$$

$$\sin\left(\frac{n\pi}{\ell} z\right). \quad (2.7.9)$$

Expanding the r-component of the neutron source, $S_r(a,z)$, in terms of the Fourier series yields

$$S_r(a,z) = \sum_{n=1}^{\infty} A'_n \sin\left(\frac{n\pi}{\ell} z\right), \quad (2.7.10)$$

where

$$A'_n = \frac{2}{\ell} \int_0^{\ell} dz\, S_r(a,z) \sin\left(\frac{n\pi}{\ell} z\right), \qquad (2.7.11)$$

and applying the boundary condition given by Eq. 2.7.4 results in

$$C'_{bbn} = -A_n / \left[D_b\, \beta_{bn} \left(I_1(\beta_{bn}\, a) + \frac{I_o(\beta_{bn}\, b)}{K_o(\beta_{bn}\, b)} K_1(\beta_{bn}\, a)\right)\right]. \qquad (2.7.12)$$

Similarly, for a blanket with a perfect reflector, we require

$$\left.\frac{\partial R_{bp}(r)}{\partial r}\right|_{r=b} = 0 \qquad (2.7.13)$$

and

$$\left.\frac{\partial Z_{bp}(z)}{\partial z}\right|_{z=0,\ell} = 0 \qquad (2.7.14)$$

to obtain the solution as

$$\phi_{bp}(r,z) = \sum_{n=0}^{\infty} C'_{bpn} \left[I_o(\beta_{bn}\, r) + \frac{I_1(\beta_{bn}\, b)}{K_1(\beta_{bn}\, b)} K_o(\beta_{bn}\, r)\right] \cos\left(\frac{n\pi}{\ell} z\right). \qquad (2.7.15)$$

From the boundary conditions given by Eq. 2.7.4 and the expansion

$$S_r(a,z) = \frac{A'_o}{2} + \sum_{n=1}^{\infty} A'_n \cos\left(\frac{n\pi}{\ell} z\right), \qquad (2.7.16)$$

where

$$A'_n = \frac{2}{\ell} \int_0^{\ell} dz\, S_r(a,z) \cos\left(\frac{n\pi}{\ell} z\right), \qquad (2.7.17)$$

we get by substitution,

$$C'_{bpo} = A'_o/(2D_b\ \omega_b(\frac{I_1(\omega_b\ b)}{K_1(\omega_b\ b)}\ K_1(\omega_b\ a) - I_1(\omega_b\ a))) \qquad (2.7.18)$$

and

$$C'_{bpn} = A'_n/(D_b\ \beta_{bn}(\frac{I_1(\beta_{bn}\ b)}{K_1(\beta_{bn}\ b)}\ K_1(\beta_{bn}\ a) - I_1(\beta_{bn}\ a))), \qquad (2.7.19)$$

the required constants of Eq. 2.7.15.

CHAPTER 3

MATHEMATICAL FORMALISM OF THE TWO-COMPONENT ANALYSIS

3.1 Basic Two-Component Analysis

Typical driven breeder-reactor calculations are costly and time consuming[13,28]. There are, however, reactor problems requiring calculations of repetitive nature suggesting that redundant calculations may be avoided by choosing a systematic solution procedure. Three such situations seem to be of interest:

1) an unchanged driven spallation target associated with different blanket designs;
2) an unchanged driven blanket associated with different target spectra;
3) an unchanged driven spallation target associated with slightly differing blanket properties; this latter situation is usually found in depletion calculations, where fissile fuel concentrations vary slightly.

The first situation can be dealt with by spatial isolation of the target from the blanket. The bare target leakage neutron current is calculated once and becomes a target-blanket boundary source for independent target-blanket calculations where only blanket properties are altered. This situation is treated in Chapter 2.

In the second and third situations a two-component flux analysis can be advantageous. The two-component approach can best be described by considering individual neutron histories. A neutron is produced by spallation reactions, undergoes scattering and multiplicative reactions, and is finally captured or decays. The neutron flux so created can be divided into two components such that

$$\psi(\vec{r},\vec{\Omega},E) = \psi_s(\vec{r},\vec{\Omega},E) + \psi_b(\vec{r},\vec{\Omega},E), \qquad (3.1.1)$$

where $\psi_s(\vec{r},\vec{\Omega},E)$ and $\psi_b(\vec{r},\vec{\Omega},E)$ are the S-component and B-component flux respectively.

The S-component consists of neutrons that are produced by high energy spallation reactions and interact with target-blanket material to produce second generation neutrons. Some of the emerging neutrons may now be defined as B-component neutrons. The choice of B-component creation reactions is made according to spectral requirements and may involve all reactions or just certain reactions under appropriate conditions. Generally the S-component flux will consist of mainly high energy neutrons while the B-component flux has a softer spectrum which is prefered for fissile fuel breeding. It should be noted here that by an appropriate choice of component transfer reactions, a standard two-energy group neutron transport formulation can be obtained. Here, however, it is required that the B-component

is spectrally independent of the S-component, which generally results in spectrally overlapping flux components.

The difference in component spectral characteristics suggests that solution methods of different degrees of sophistication can be applied to obtain a solution for each component. The S-component, for example, can typically be solved by Monte-Carlo and high energy neutron transport methods, while transport corrected diffusion approximations may be sufficient for B-component calculations. For the second situation it therefore follows from the component spectral independence requirement that only additional S-component calculations have to be done while the B-component flux only changes in amplitude depending on the magnitude of the component transfer term. Both spectral separation and spectral independence aid in reducing computational effort.

By substituting Eq. 3.1.1 into Eq. 2.1.2 and collecting terms refering to similar components, two equations defining the S-component and the B-component are obtained as follows:

$$\vec{\Omega} \cdot \nabla\psi_s(\vec{r},\vec{\Omega},E) + \Sigma_t(\vec{r},E)\,\psi_s(\vec{r},\vec{\Omega},E) = \left(\int dE' \int d\vec{\Omega}'\right.$$
$$\left. f'_t(\vec{r},\vec{\Omega}'\to\vec{\Omega},E'\to E)\; c(\vec{r},E')\; \Sigma_t(\vec{r},E')\; \psi_s(\vec{r},\vec{\Omega}',E')\right)$$
$$+ T(\vec{r},\vec{\Omega},E) - T_{sb}(\vec{r},\vec{\Omega},E) \qquad (3.\text{[illegible]}2)$$

and

$$\hat{\Omega} \cdot \nabla \psi_b(\vec{r},\hat{\Omega},E) + \Sigma_t(\vec{r},E)\,\psi_b(\vec{r},\hat{\Omega},E) = \left(\int dE' \int d\hat{\Omega}'\right.$$
$$f'_t(\vec{r},\hat{\Omega}'\to\hat{\Omega},E'\to E)\; c(\vec{r},E')\;\Sigma_t(\vec{r},E')\;\psi_b(\vec{r},\hat{\Omega}'E'))$$
$$+ T_{sb}(\vec{r},\hat{\Omega},E), \qquad (3.1.3)$$

where the component coupling term is defined by

$$T_{sb}(\vec{r},\hat{\Omega},E) = \int dE' \int d\hat{\Omega}'\; f'_{tsb}(\vec{r},\hat{\Omega}'\to\hat{\Omega},E'\to E)$$
$$c(\vec{r},E')\;\Sigma_t(\vec{r},E')\;\psi_s(\vec{r},\hat{\Omega}',E'). \qquad (3.1.4)$$

The independent source term, $T(\vec{r},\hat{\Omega},E)$, contributes only to the S-component. The basic requirement of the two-component analysis developed here is the indistinguishability of the coupling production spectrum, Eq. 3.1.4, from the production spectrum of the B-component flux. This condition ensures spectral independence of S- and B-components and can be expressed by

$$T_{sb}(\vec{r},\hat{\Omega},E) = \gamma_{sb} \int dE' \int d\hat{\Omega}'\; f'_t(\vec{r},\hat{\Omega}'\to\hat{\Omega},E'\to E)$$
$$c(\vec{r},E')\;\Sigma_t(\vec{r},E')\;\psi_b(\vec{r},\hat{\Omega}',E'), \qquad (3.1.5)$$

γ_{sb} taken to be a constant. Comparing Eq. 3.1.4 with Eq. 3.1.5 yields

$$f'_{tsb}(\vec{r},\hat{\Omega}'\to\hat{\Omega},E'\to E) = f'_t(\vec{r},\hat{\Omega}'\to\hat{\Omega},E'\to E)\;\gamma_{sb}\;\frac{\psi_b(\vec{r},\hat{\Omega}',E')}{\psi_s(\vec{r},\hat{\Omega}',E')}, \qquad (3.1.6)$$

where it is required that the component coupling term not exceed the S-component production term or

$$\gamma_{sb} \le \frac{\psi_s(\vec{r},\hat{\Omega},E)}{\psi_b(\vec{r},\hat{\Omega},E)}. \qquad (3.1.7)$$

Using Eq. 3.1.4 and Eq. 3.1.6, Eq. 3.1.2 and Eq. 3.1.3 can

be rewritten to yield

$$\vec{\Omega} \cdot \nabla\psi_s(\vec{r},\vec{\Omega},E) + \Sigma_t(\vec{r},E)\,\psi_s(\vec{r},\vec{\Omega},E)$$
$$= \left(\int dE' \int d\vec{\Omega}'\, f_t'(\vec{r},\vec{\Omega}' \to \vec{\Omega},\, E' \to E)\right.$$
$$c(\vec{r},E')\,\Sigma_t(\vec{r},E')\,(\psi_s(\vec{r},\vec{\Omega}',E') - \gamma_{sb}$$
$$\left.\psi_b(\vec{r},\vec{\Omega}',E'))\right) + T(\vec{r},\vec{\Omega},E) \qquad (3.1.8)$$

and

$$\vec{\Omega} \cdot \nabla\psi_b(\vec{r},\vec{\Omega},E) + \Sigma_t(\vec{r},E)\,\psi_b(\vec{r},\vec{\Omega},E)$$
$$= (1 + \gamma_{sb}) \int dE' \int d\vec{\Omega}'\, f_t'(\vec{r},\vec{\Omega}' \to \vec{\Omega}, E' \to E)$$
$$c(\vec{r},E')\,\Sigma_t(\vec{r},E')\,\psi_b(\vec{r},\vec{\Omega}',E'). \qquad (3.1.9)$$

The appropriate system boundary conditions at $\vec{a}$ are

$$\psi_s(\vec{a},\vec{\Omega},E) = 0 \qquad (3.1.10)$$

and

$$\psi_b(\vec{a},\vec{\Omega},E) = 0 \qquad (3.1.11)$$

for all angular flux components satisfying

$$\hat{n} \cdot \vec{\Omega} < 0, \qquad (3.1.12)$$

where $\hat{n}$ is the normal surface vector of the system.

We note here that Eq. 3.1.9 is similar to those describing conventional reactor systems, with γ_{sb} being chosen to yield a critical system. Equation 3.1.9, therefore, uniquely defines γ_{sb} and the spectral shape of $\psi_b(\vec{r},\vec{\Omega},E)$, while the amplitude of $\psi_b(\vec{r},\vec{\Omega},E)$ remains arbitrary. Consequently, Eq. 3.1.8 can be solved to yield $\psi_s(\vec{r},\vec{\Omega},E)$ while the magnitude of $\psi_b(\vec{r},\vec{\Omega},E)$ is obtained according to the constraint given by Eq. 3.1.7. For target-blanket systems with slightly differing properties,

corresponding to the third situation, only γ_{sb} is changed when solving Eq. 3.1.9. This change is to have no spectral effect on the S- or B-component flux and therefore the spectral calculations of Eq. 3.1.8 and Eq. 3.1.9 need not be repeated. The relative magnitudes of $\psi_s(\vec{r},\vec{\Omega},E)$ and $\psi_b(\vec{r},\vec{\Omega},E)$, however, change according to Eq. 3.1.7. Spectral shifts of the total flux as given by Eq. 3.1.1 are nevertheless included due to the relative change in magnitude of ψ_s and ψ_b. The similarity of the two-component flux analysis and a two-energy group analysis is apparent. In a two-component analysis each component is however truly independent, while in a two-group approach this is only approximated. This suggests that for large spectral differences between components the two-component analysis is preferred while for small differences a two-energy group treatment is more advantageous.

3.2 Reaction-Decoupled Two-Component Analysis

In Sec. 1 of this chapter the determination of the component coupling term T_{sb}, Eq. 3.1.5, required the knowledge of the B-component angular flux. This requirement introduces considerable complexity to the solution method. The condition of spectral independence can also be obtained through neutron multiplication reactions producing neutrons independent of the original flux spectrum. For such a

reaction, y, it is required that

$$f'_y(\vec{r},\hat{\Omega},E) = f'_y(\vec{r},\hat{\Omega}'\to\hat{\Omega},E'\to E). \qquad (3.2.1)$$

Letting

$$f'_t(\vec{r},\hat{\Omega}'\to\hat{\Omega},E'\to E) = f'_n(\vec{r},\hat{\Omega}'\to\hat{\Omega},E'\to E) + f'_y(\vec{r},\hat{\Omega},E), \qquad (3.2.2)$$

the appropriate two-component transport equations can be obtained from Eq. 3.1.2 and Eq. 3.1.3 to yield

$$\hat{\Omega}\cdot\nabla\psi_s(\vec{r},\hat{\Omega},E) + \Sigma_t(\vec{r},E)\,\psi_s(\vec{r},\hat{\Omega},E) = \left(\int dE' \int d\hat{\Omega}'\right.$$
$$f'_n(\vec{r},\hat{\Omega}'\to\hat{\Omega},E'\to E)\; c(\vec{r},E')\;\Sigma_t(\vec{r},E')$$
$$\left.\psi_s(\vec{r},\hat{\Omega}',E')\right) + T(\vec{r},\hat{\Omega},E) \qquad (3.2.3)$$

and

$$\hat{\Omega}\cdot\nabla\psi_b(\vec{r},\hat{\Omega},E) + \Sigma_t(\vec{r},E)\,\psi_b(\vec{r},\hat{\Omega},E) = \left(\int dE' \int d\hat{\Omega}'\right.$$
$$f'_n(\vec{r},\hat{\Omega}'\to\hat{\Omega},E'\to E)\; c(\vec{r},E')\;\Sigma_t(\vec{r},E')\;\psi_b(\vec{r},\hat{\Omega}',E') + f'_y(\vec{r},\hat{\Omega},E)$$
$$\left.c(\vec{r},E')\;\Sigma_t(\vec{r},E')\;(\psi_b(\vec{r},\hat{\Omega}',E') + \psi_s(\vec{r},\hat{\Omega}',E'))\right). \qquad (3.2.4)$$

The S-component flux, $\psi_s(\vec{r},\hat{\Omega},E)$, can now be obtained by directly solving Eq. 3.2.3, while the B-component flux, $\psi_b(\vec{r},\hat{\Omega},E)$, is obtained by solving Eq. 3.2.4.

The fission reaction is generally known to produce neutrons with an energy source spectrum practically independent of the reaction initiating neutron energy, angle of incidence, or fissioning isotope and element. This is especially true for initiating neutrons having low energies, E'. The fission neutron therefore satisfies the condition of Eq. 3.2.1, where appropriate energies, E', and fissionable isotopes have to be chosen according to the required accuracy in satisfying Eq. 3.2.1. For conditions

such that Eq. 3.2.1 has to be satisfied only approximately, n-xn reactions as well as all fission reactions can be included in the set of component transfer reactions.

3.3 Integrated Two-Component Analysis

In determining overall system breeding characteristics it is required to integrate the component transport equations, Eq. 3.2.3 and Eq. 3.2.4, over angular flux directions, neutron energies, and system volume to yield

$$L_s + \Sigma_{ts} \phi_s = c_{ns} \Sigma_{ns} \phi_s + T \qquad (3.3.1)$$

and

$$L_b + \Sigma_{tb}\phi_b = c_{nb}\Sigma_{nb}\phi_b + c_{ys}\Sigma_{ys}\phi_s + c_{yb}\Sigma_{yb}\phi_b. \qquad (3.3.2)$$

The net neutron leakage current, L, for each component is given by

$$L_x = \int_V d\vec{r} \int_E dE \int_\Omega d\vec{\Omega}\, \vec{\Omega} \cdot \nabla\psi_x(\vec{r},\vec{\Omega},E), \quad x = s,b, \qquad (3.3.3)$$

while a scalar neutron flux, ϕ_x, is defined by

$$\phi_x = \int_V d\vec{r} \int_E dE \int_\Omega d\vec{\Omega}\, \psi_x(\vec{r},\vec{\Omega},E), \quad x = s,b. \qquad (3.3.4)$$

The macroscopic component cross section, Σ_k, can be expressed by

$$\Sigma_{kx} = \int_V d\vec{r} \int_E dE \int_\Omega d\vec{\Omega}\, \Sigma_k(\vec{r},E)\, \psi_x(\vec{r},\vec{\Omega},E)/\phi_x, \qquad (3.3.5)$$

such that

$$\Sigma_{tx}(\vec{r},E) = \sum_k \Sigma_{kx}(\vec{r},E), \qquad (3.3.6)$$

where the subscripts k and x define appropriate reaction types and flux components respectively. The independent internal neutron source, T, is given by

$$T = \int_V d\vec{r} \int_E dE \int_\Omega d\vec{\Omega}\, T(\vec{r},\vec{\Omega},E), \tag{3.3.7}$$

while the average neutron yield of reaction type 'k' is given by

$$c_{kx} = \int_V d\vec{r} \int_E dE \int_\Omega d\vec{\Omega} \int_{E'} dE' \int_{\Omega'} d\vec{\Omega}'\, f'_k(\vec{r},\vec{\Omega}'\to\vec{\Omega},E'\to E)$$

$$c_k(\vec{r},E')\, \Sigma_k(\vec{r},E')\, \psi_x(\vec{r},\vec{\Omega}',E')/\Sigma_{kx}\phi_x, \tag{3.3.8}$$

where

$$f'_t(\vec{r},\vec{\Omega}'\to\vec{\Omega},E'\to E)\, c(\vec{r},E')\, \Sigma_t(\vec{r},E') =$$

$$= \sum_k f'_k(\vec{r},\vec{\Omega}'\to\vec{\Omega},E'\to E)\, c_k(\vec{r},E')\, \Sigma_k(\vec{r},E'). \tag{3.3.9}$$

For subcritical breeding systems, the integrated leakage terms L_s and L_b can be made arbitrarily small by choosing an appropriate distance between drive source and reactor boundary to yield the condition

$$L_s = 0 \tag{3.3.10}$$

and

$$L_b = 0 \tag{3.3.11}$$

for any degree of accuracy. For these conditions Eq. 3.3.1 and Eq. 3.3.2 can be solved to yield the integrated component flux

$$\phi_s = T/(\Sigma_{ts} - c_{ns}\Sigma_{ns}) \tag{3.3.12}$$

and

$$\phi_b = T\, c_{ys}\Sigma_{ys}/((\Sigma_{ts} - c_{ns}\Sigma_{ns})\,(1-c_{tb})\,\Sigma_{tb}). \tag{3.3.13}$$

Appropriate reaction rates R_{ki}, for isotope i needed in depletion calculations, are defined by

$$R_{ki} = \Sigma_{ki} \phi \ , \qquad (3.3.14)$$

where the component averaged macroscopic cross section is given by

$$\Sigma_{ki} = (\Sigma_{ksi} \phi_s + \Sigma_{kbi} \phi_b) \ / \ \phi \qquad (3.3.15)$$

and the total integrated system scalar flux is defined as

$$\phi = \phi_s + \phi_b . \qquad (3.3.16)$$

For a reactor system with constant isotopic density distributions, n_i, Eq. 3.3.15 can be rewritten to yield

$$\Sigma_{ki} = \sigma_{ki} n_i \ , \qquad (3.3.17)$$

where

$$\sigma_{ki} = (\sigma_{ksi} \phi_s + \sigma_{kbi} \phi_b) \ / \ \phi \qquad (3.3.18)$$

and use was made of the general definition of the macroscopic cross section

$$\Sigma_{ki}(\vec{r},E) = \sigma_{ki}(E) \ n_i(\vec{r}) . \qquad (3.3.19)$$

In a fast neutron flux environment, a system with little neutron moderation, one-energy group reactor calculations where shown to be generally acceptable[69]. Since breeding of fissile fuel is highly favourable under such conditions, a spallation breeder reactor would necessarily operate under similar conditions. A one-energy group treatment of this neutron environment, however, would not be appropriate for depletion calculations, since neutron multiplication in such calculations is exaggerated. This is

due to the condition of a fissile isotope increased neutron fission source not having the high multiplication neutron yield properties of a spallation neutron source. In a spallation based breeding system a two-component analysis, using fission as a component transfer reaction, accurately simulates the shift from a spallation originating spectrum to a fission originating neutron spectrum. A one-energy group two-component analysis would therefore yield results similar in accuracy to one-energy group fast reactor calculations.

From considerations of heat production in a spallation breeder it is generally not feasible to have fissile fuel directly exposed to the spallation drive source[48]. A spallation target and a breeding blanket have to be identified for direct enrichment of fuel elements since conventional reactor fuel contains considerable amounts of fissile fuel and can therefore not be used as a target. For a system with fuel rejuvenation without reprocessing any fissile fuel bred in the target is therefore of no direct relevance. In the analysis of such systems Eq. 3.3.1 and Eq. 3.3.2 are still valid with the spatial integral being performed over the active breeding blanket. The leakage integrals L_s and L_b however cannot be neglected. For this case L_s becomes the major driving current, while T is generally negligible. The B-component

flux at the target-blanket interface is high and L_b may not be omitted, especially if a strong absorber such as uranium is used as a target material.

The simplicity of the solutions of the component equations, Eq. 3.3.12 and Eq. 3.3.13 can be retained by introducing a component leakage transfer term, L_{st}, in the integrated two-component equations to yield

$$\Sigma_{tbs}\phi_{sb} = c_{nsb}\Sigma_{nsb}\phi_{sb} + S_n \qquad (3.3.20)$$

and

$$\Sigma_{tbb}\phi_{bb} = c_{nbb}\Sigma_{nbb}\phi_{bb} + c_{ysb}\Sigma_{ysb}\phi_{sb} + c_{ybb}\Sigma_{ybb}\phi_{bb} + (L_{st}-L_{bb}), \qquad (3.3.21)$$

where

$$L_{st} = L_{bb} \qquad (3.3.22)$$

and an effective blanket drive source is defined by

$$S_n = T_b - L_{sb} - L_{st}\ , \qquad (3.3.23)$$

here the additional subscript b denotes the blanket volume integration. Clearly with the condition given by Eq. 3.3.22, Eq. 3.3.20 and Eq. 3.3.21 are equivalent to Eq. 3.3.1 and Eq. 3.3.2 and their corresponding solutions given by Eq. 3.3.12 and Eq. 3.3.13, where the internal neutron source T, Eq. 3.3.7, is replaced by the effective neutron drive source S_n, Eq. 3.3.23.

Each term in Eq. 3.3.23 can be expressed as a fraction of the blanket independent neutron source T_{ltb} to yield

$$S_n = \gamma_{be}\, T_{1tb}, \tag{3.3.24}$$

where the fraction γ_{be} is defined by

$$\gamma_{be} = T_b/T_{1tb} - L_{sb}/T_{1tb} - L_{st}/T_{1tb} \tag{3.3.25}$$

and

$$T_{1tb} = \int_V d\vec{r} \int_E dE \int_\Omega d\hat{\Omega}\, \hat{\Omega} \cdot \nabla \psi_{tb}(\vec{r},\hat{\Omega},E) + T_b. \tag{3.3.26}$$

Here the bare target angular flux $\psi_{tb}(\vec{r},\hat{\Omega},E)$, is defined by Eq. 2.1.2. We note here that for a blanket as defined in Chapter 2, T_b is taken to be zero. The ratio L_{sb}/T_{1tb} is the highly directional, predominantly target produced neutron drive source and therefore basically independent of breeding blanket properties. The B-component leakage fraction L_{st}/T_{1tb}, although much smaller in absolute value than L_{sb}/T_{1tb}, is strongly dependent on the B-component flux in the vicinity of the target-blanket interface and therefore is generally not constant as fissile isotope concentrations change during depletion calculations. The target-blanket geometry, however, can be changed to counteract the depletion dependence, producing a constant ratio, L_{st}/T_{1tb}.

To obtain a constant ratio, L_{st}/T_{1tb}, the blanket-to-target, neutron leakage loss can be reduced by introducing a cavity between the breeding blanket and the target to result in a smaller effective cross-sectional target area. At the same time, the blanket power density is reduced due to the

increase in distance between drive source and blanket. Similar geometric adjustments can be made to keep the peak blanket power density constant during depletion calculations. Since the B-component neutron source is proportional to the blanket fission power, the associated increase in target-blanket distance will keep the blanket-to-target net leakage constant due to the corresponding decrease in target cross-sectional area. This view is based on the blanket property producing the maximum blanket power density close to the blanket-target surface. Conditions yielding displacement independent target cross-sectional areas are also assumed. For a realistic breeder system analysis, especially in consideration of the present degree of accuracy in determining spallation neutron yields, the effective neutron source fraction γ_{be} can be taken as constant with respect to material composition changes during depletion calculations.

For realistic breeder systems it can therefore be concluded that, by defining an appropriate neutron drive source, a two-region target breeding-blanket system can be treated like a one-region homogeneous fissile fuel breeding system.

CHAPTER 4

FUEL DYNAMICS WITH LIMITED REPROCESSING

4.1 Introduction

As discussed in Chapter 1, spallation-fission symbiotic systems can play a major role in the enhancement of fissile fuel utilization. It is further realized that fissile fuel enrichment with reprocessing can practically be eliminated if the depleted fuel element of a conventional thermal reactor is placed in a fast neutron flux environment to breed fissile fuel directly in the fuel element. Continued burnup of the fuel element in a thermal reactor is then possible. This breed-burn cycle can be repeated as desired. In each breed-burn cycle a certain amount of fuel mass is converted into energy. The mass-energy inventory, consisting of the system mass and the mass fraction converted to energy, has to be conserved during each breed-burn cycle. This fundamental law of conservation of mass-energy forms the basis for the following system analysis.

A typical nuclear symbiotic reactor system, as shown in Fig. 4.1.1, accepts fresh nuclear fuel and converts it into energy and fuel ash. The symbiotic system generally consists of three basic subsystems,

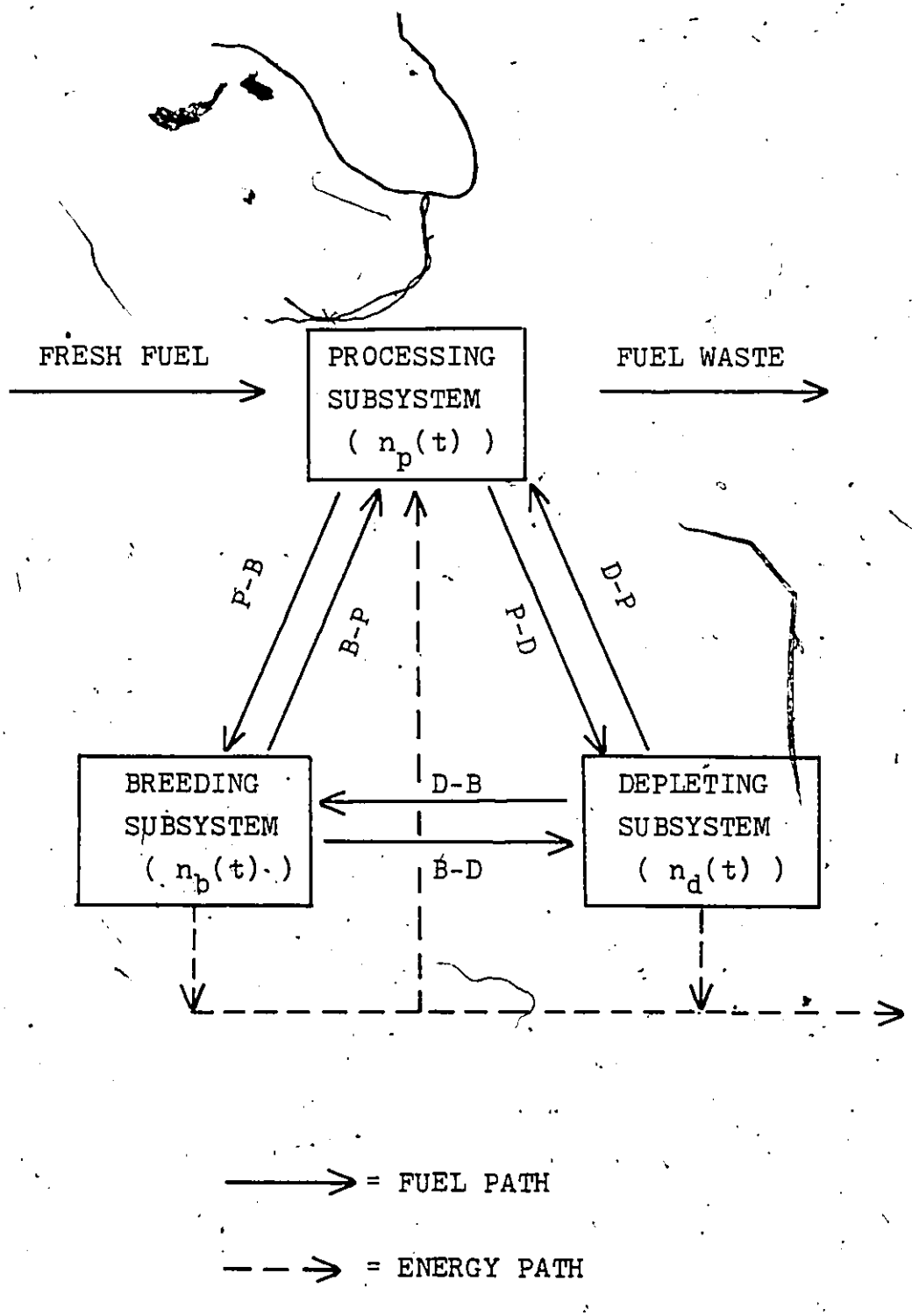

Fig. 4.1.1 Symbiotic nuclear reactor system.

1) the reprocessing subsystem, where fuel enrichment, reprocessing, fabrication, and disposal processing takes place;

2) the breeding subsystem, where predominantly breeding of fissile fuel from fertile fuel takes place;

3) the depleting subsystem, where predominantly depletion of fissile fuel occurs.

For a conventional reactor the breeding subsystem is absent and the fuel movement links, as shown in Fig. 4.1.1, are required once for a once-through fuel cycle and several times if waste fissile fuel is reused. A fast breeder-reactor consists of all three subsystems with links B-D and D-B missing. For the symbiotic system without reprocessing, which is of interest here, links B-P and P-B are absent. High energy neutrons required for breeding in such a system are typically obtained from spallation or fusion reactions. It may be noted here that the breeder-depletion system of a fast-breeder reactor is neutronically coupled, while the breeder-depletion system of a spallation breeder or of a fusion breeder is decoupled. The analysis presented here only deals with neutronically decoupled systems, which are better suited for fuel rejuvenation without reprocessing.

For each subsystem and for the entire system a mass-energy density, $n_{mx}(\vec{r},t)$, can be formulated such that a general system mass-energy inventory is defined by

$$n_x(t) = \sum_m \int_{V_x} d\vec{r}\ n_{mx}(\vec{r},t), \qquad (4.1.1)$$

here m are the system mass-energy components of system x occupying volume V_x. A general rate of system inventory change therefore becomes

$$I_x(t) = \frac{dn_x(t)}{dt} . \qquad (4.1.2)$$

Similarly, for each system x a mass-energy feed rate and a mass-energy extraction rate can be expressed as

$$R_i(t) = \frac{-dn_i(t)}{dt} \qquad (4.1.3)$$

and

$$R_f(t) = \frac{dn_f(t)}{dt} , \qquad (4.1.4)$$

where i denotes the initial feed mass-energy stockpile system, while f stands for the final extraction mass-energy stockpile system. Conservation consideration demands

$$I_x(t) = R_i(t) - R_f(t) . \qquad (4.1.5)$$

This equation becomes of primary importance in a complex system mass-energy flow analysis.

4.2 Physics Aspects of Nuclear Reactor Systems

The subsystems of major importance in a symbiotic reactor system, as shown in Fig. 4.1.1, are of the breeding type and the depleting type depending on the dominant mode of neutron absorption. For each of these subsystems,

mass-energy balance equations of the general form given by Eq. 4.1.5, can be formulated. A general neutron balance equation can be written as

$$\frac{dN_n(t)}{dt} = S_n(t) + \sum_k^L \sum_i \int_E dE \int_V d\vec{r}\, (\nu_{kni}(E) - 1)$$

$$\sigma_{kni}(E)\, n_i(\vec{r},t)\, \psi_n(\vec{r},E,t), \qquad (4.2.1)$$

here $N_n(t)$ is the system time dependent neutron population. The integrations are carried out over the system volume V and neutron energies E. The subscript n identifies variables and parameters involving neutrons. The number of neutrons produced per interaction type k of the neutron flux $\psi_n(\vec{r},E,t)$ with isotope i of number density n is given by $\nu_{kni}(E)$, while the associated microscopic reaction cross section is denoted by $\sigma_{kni}(E)$.

The system neutron source or sink, used in Eq. 4.2.1, is defined by

$$S_n(t) = -\int_E dE \int_S d\vec{s}\, \vec{J}_{ns}(\vec{r},E,t) \cdot \hat{n} + S_{nsp}(t)$$

$$+ \sum_k \sum_{j\neq n} \sum_i \int_E dE \int_V d\vec{r}\, \nu_{kji}(E)\, \sigma_{kji}(E)\, n_i(\vec{r},t)$$

$$\psi_j(\vec{r},E,t)$$

$$+ \sum_k^H \sum_i \int_E dE \int_V d\vec{r}\, (\nu_{kni}(E)-1)\, \sigma_{kni}(E)\, n_i(\vec{r},t)$$

$$\psi_n(\vec{r},E,t)\ . \qquad (4.2.2)$$

Here the first term defines the net neutron current crossing the system boundary S, where the integrations of the neutron current, $\vec{J}_{ns}(\vec{r},E,t)$, are performed over all neutron energies E, and the system surface S. The unit vector, $\hat{n}$, is perpendicular to the volume surface. In the case of a conventional critical reactor this term is the neutron leakage of the reactor, while for a breeding blanket it would also include the externally supplied driving neutron current. The second term of Eq. 4.2.2 defines spontaneous neutron sources and is generally negligible. The third term accounts for neutron sources produced by reactions induced by non-neutrons of type j. The last term defines neutron yields of neutron induced reactions of reaction set H. Here reaction set H consists of all neutron initiated reactions not contained in reaction set L used in Eq. 4.2.1. The grouping into reaction sets H and L is completely arbitrary and set H may not exist at all. In the formulation of Eq. 3.3.23, as well as in fission based conventional reactor systems, such reaction groupings are generally not made. The preferred grouping consists of spallation and nonspallation reactions, set H and set L respectively. For calculations based on the high-energy particle transport code NMTC[17], reaction set H consists of neutron reactions above 15 MeV.

The neutron flux $\psi_n(\vec{r},E,t)$, in Eq. 4.2.1 can be

expressed as the product

$$\psi_n(\vec{r},E,t) = \Phi_n(\vec{r},E,t)\ \phi_n(t), \tag{4.2.3}$$

which by making use of the normalization

$$\int_E dE \int_V d\vec{r}\ \Phi_n(\vec{r},E,t) = 1, \tag{4.2.4}$$

yields

$$\phi_n(t) = \int_E dE \int_V d\vec{r}\ \psi_n(\vec{r},E,t). \tag{4.2.5}$$

A system macroscopic absorption cross section can therefore be defined as

$$\Sigma_{an}(t) = \sum_i \overset{a}{\sum_k} \int_E dE \int_V d\vec{r}\ \sigma_{kni}(E)\ n_i(\vec{r},t)\ \Phi_n(\vec{r},E,t), \tag{4.2.6}$$

while a general neutron absorption rate is given by

$$R_{an}(t) = \Sigma_{an}(t)\ \phi_n(t). \tag{4.2.7}$$

Similarly a macroscopic production cross section can be defined by

$$\Sigma_{pn}(t) = \sum_i \overset{P}{\sum_k} \int_E dE \int_V d\vec{r}\ \sigma_{kni}(E)\ n_i(\vec{r},t)\ \Phi_n(\vec{r},E,t), \tag{4.2.8}$$

while an average neutron yield per production reaction is given by

$$\nu_{pn}(t) = \sum_{i}^{P} \sum_{k} \int_{E} dE \int_{V} d\vec{r}\, \nu_{kni}(E)\, \sigma_{kni}(E)\, n_i(\vec{r},t)$$

$$\phi_n(\vec{r},E,t) \,/\, \Sigma_{pn}(t). \qquad (4.2.9)$$

A general neutron production rate can therefore be expressed as

$$R_{pn}(t) = \nu_{pn}(t)\, \Sigma_{pn}(t)\, \phi_n(t). \qquad (4.2.10)$$

For a system operating under steady state conditions Eq. 4.2.1 must yield

$$\frac{dN_n(t)}{dt} = 0. \qquad (4.2.11)$$

Substituting appropriate parameters into Eq. 4.2.1 under this condition and rearranging yields

$$\phi_n(t) = S_n(t) \,/\, (1 - k(t))\, \Sigma_{an}(t), \qquad (4.2.12)$$

where

$$k(t) = \nu_{pn}(t)\, \Sigma_{pn}(t) \,/\, \Sigma_{an}(t), \qquad (4.2.13)$$

the system neutron multiplication ratio. Equation 4.2.12 is of considerable importance in a subcritical breeder analysis, since it relates the drive source $S_n(t)$ to the breeder flux $\phi_n(t)$.

A general specific power of a nuclear system is defined as

$$p_n(t) = \sum_{i}^{P} \sum_{k} \int_{E} dE \int_{V} d\vec{r}\, U_{kni}(E)\, \sigma_{kni}(E)\, n_i(\vec{r},t)$$

$$\phi_n(\vec{r},E,t), \qquad (4.2.14)$$

where $U_{kni}(E)$ is the thermal energy released per specified reaction. An average fuel burnup of a nuclear system is

expressed by

$$\beta_n = \int_\tau dt\ p_n(t)\ \phi_n(t)\ /\ M_{oh}, \qquad (4.2.15)$$

the ratio of the total energy produced by the fuel during its' system average residence time τ to the initial heavy element fuel inventory mass given by

$$M_{oh} = \frac{1}{N_a} \sum_i^h \int_V d\vec{r}\ n_i(r,0)\ M_i, \qquad (4.2.16)$$

where N_a is Avogadro's number and M_i is the gram-atomic weight of element i. In Eq. 4.2.16 the summation is carried out over all fissile and fertile isotopes h. Substituting Eq. 4.2.12 into Eq. 4.2.15 yields

$$\beta_n = \int_\tau dt\ p_n(t)\ S_n(t)/((1 - k(t))\ \Sigma_{an}(t)\ M_{oh}). \qquad (4.2.17)$$

The general mass-energy flow rate of a reactor system can be expressed as

$$R_{oh} = M_{oh}/\tau. \qquad (4.2.18)$$

The thermal power associated with the neutron flux of a reactor system is defined by

$$P_{tn}(t) = p_n(t)\ \phi_n(t), \qquad (4.2.19)$$

where the specific power, $p_n(t)$, is given by Eq. 4.2.14, while a fuel residence time averaged power is given by

$$P_{tn} = \int_\tau dt\ P_n(t)/\tau. \qquad (4.2.20)$$

Comparing Eq. 4.2.20 with Eq. 4.2.15 and Eq. 4.2.18 yields

$$P_{tn} = \beta_n\ R_{oh}. \qquad (4.2.21)$$

The fuel system average time τ required to solve Eq. 4.2.18 and Eq. 4.2.20 is extracted from Eq. 4.2.17 subject to general system burnup constraints discussed later in this section.

Although Eq. 4.2.1 to Eq. 4.2.21 refer primarily to neutrons, identical system equations can be obtained for other system particle interactions. A total system generated power can thus be written as

$$P_t(t) = \sum_k \sum_j \sum_i \int_E dE \int_V d\vec{r}\, U_{kji}(E)\, \sigma_{kji}(E)\, n_i(\vec{r},t)\, \psi_j(\vec{r},E,t) , \qquad (4.2.22)$$

where, as before, the subscripts k, j, and i denote reaction type, particle flux type, and material type respectively.

The depletion subsystem of a symbiotic system, as shown in Fig. 4.1.1, generally consists of a critical reactor. Using Eq. 4.2.21 the average thermal power produced by this subsystem is given by

$$P_{td} = R_{odh}\, \beta_d(k_d), \qquad (4.2.23)$$

where the subscript n has been omitted, since only the neutron flux is of relevance. The final fuel burnup β_d is dependent on the subsystem's criticality constraint, denoted by (k_d). This means that the fuel burnup has to be chosen, such that Eq. 4.2.1 is satisfied over the entire subsystem. The fuel feed rate R_{odh} can be given arbitrary constraints defining the size or thermal power of the subsystem.

The breeder subsystem of a symbiotic system, as shown

in Fig. 4.1.1, generally consists of a subcritical driven reactor. Its' fuel produced thermal power is given by

$$P_{tbb} = R_{obh}(\tau_b)\ \beta_b(k_d). \qquad (4.2.24)$$

Here the final fuel burnup $\beta_b(k_d)$ has no breeder subsystem criticality constraints, since the subsystem is driven by an external neutron source. In the case of fuel rejuvenation without reprocessing, however, the breeder enriched fuel has to meet reactivity constraints of the critical depleter subsystem as indicated by its' multiplication constant k_d in Eq. 4.2.24. The breeder fuel feed rate $R_{obh}(\tau_b)$ is constrained by the average breeder fuel resistance time τ_b, which in turn is dependent on both the breeder fuel burnup $\beta_b(k_d)$ and the neutron drive source $S_b(t)$.

A total system fuel burnup can be defined as

$$\beta_t = \beta_b + \beta_d, \qquad (4.2.25)$$

the sum of the breeder fuel burnup and the depleter fuel burnup.

The symbiotic systems investigated are based on the uranium-plutonium chain, as shown in Fig. 4.2.1, where the depleter subsystem is capable of burning natural uranium in oxide form, UO_2, as in heavy-water moderated converter reactors.

The depletion equations for isotopes of density n_i are of the general form

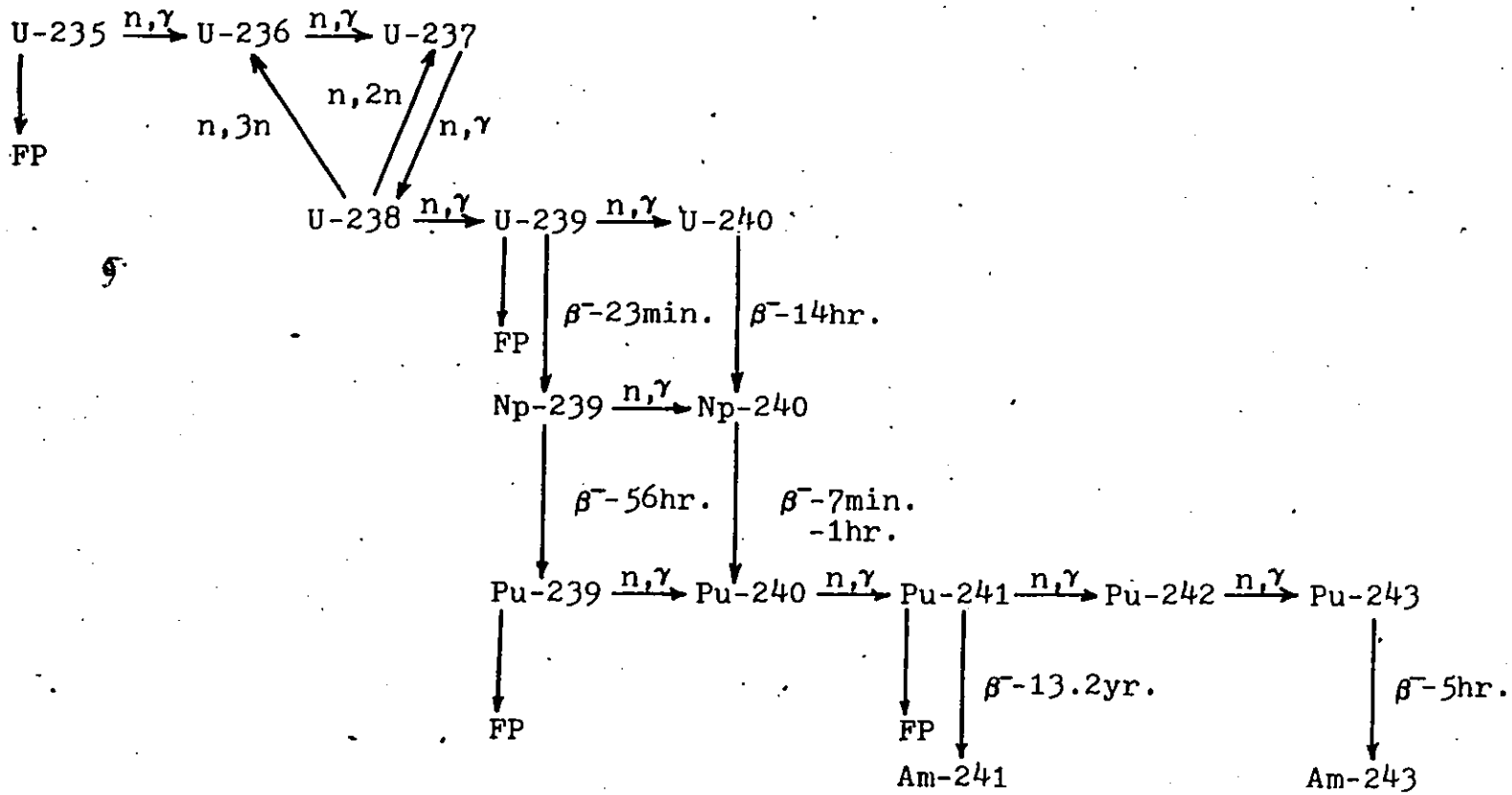

Fig. 4.2.1 Chain of isotopes created by neutron irradiation of U-238 and U-235.

$$\frac{dn_i(t)}{dt} = \sum_k \sum_j \sum_o \int_E dE \int_V d\vec{r}\ \sigma_{kjo}(o\to i,E)\ n_o(\vec{r},t)\ \psi_j(\vec{r},E,t) + \sum_o \int_V d\vec{r}\ \lambda_o(o\to i)\ n_o(\vec{r},t) - \sum_k \sum_j \int_E dE \int_V d\vec{r}\ \sigma_{kji}(i\to o,E)\ n_i(\vec{r},t)\ \psi_j(\vec{r},E,t) - \int_V d\vec{r}\ \lambda_i\ n_i(\vec{r},t)\ , \qquad (4.2.26)$$

where $\sigma_{kjo}(\vec{r},o\to i,E)$ and $\lambda_o(o\to i)$ are the microscopic cross section of reaction type k and decay constant respectively transforming isotope o into isotope i. λ_i is the decay constant of isotope i. To obtain the densities of the fuel isotopes, Eq. 4.2.26 was solved analytically, with frequent cross section updates, as required by changes in the neutron energy spectrum. The energy spectrum averaged microscopic cross sections for the depleter reactor were based on published values by C.H. Westcott[70,71], while average cross sections of the breeder blanket were obtained from ENDF/B-IV cross sections and the two-component analysis described in Sec. 3.3. Here the S-component of the two-component analysis consisted of typical spallation target leakage spectra, while the B-component spectrum was a typical fast neutron flux spectrum, peaked in the 10 keV to 1 MeV range[27,62]. This choice yielded high breeding and low power production breeder blanket characteristics, typical of uranium-oxide fuels with low fissile fuel inventories[32,48,56,61,62]. The neutron irradiation

dependent fission product load was similated using three pseudo fission products[71,72]. The pseudo fission product densities were obtained by solving

$$\frac{dn_p(t)}{dt} = \sum_o \int_E dE \int_V d\vec{r}\ {}^{p}w_o(E)\ \sigma_{fno}(E)\ n_o(\vec{r},t)\ \psi_n(\vec{r},E,t) - \int_E dE \int_V d\vec{r}\ \sigma_{anp}\ n_p(\vec{r},t)\ \psi_n(\vec{r},E,t), \quad (4.2.27)$$

where ${}^{p}w_o(E)$ is the yield of pseudo fission product p produced through fission of isotope o, while σ_{anp} are the three microscopic neutron absorption cross sections of 50 barns, 300 barns, and 800 barns for the corresponding pseudo fission products[72], of a thermal reactor. The pseudo fission product cross section for the fast neutron spectrum breeder subsystem is taken to be 0.5 barns[73].

An effective neutron multiplication ratio of a fuel element can be defined by

$$k_{ef}(t) = \frac{R_{pnf}(t)}{R_{anf}(t) - S_{nf}(t)}, \quad (4.2.28)$$

where the neutron production rate $R_{pnf}(t)$ is given by Eq. 4.2.10, while a total neutron destruction rate becomes the difference of $R_{anf}(t)$, Eq. 4.2.7, and $S_{nf}(t)$, Eq. 4.2.2. The space dependent integrals being carried out over the appropriate fuel element, denoted by the subscript f.

The effective neutron multiplication ratio over the entire critical reactor therefore yields

$$k_{ed}(t) = \frac{\sum_{f}^{F} R_{pnf}(t)}{\sum_{f}^{F} (R_{anf}(t) - S_{nf}(t))} = 1, \qquad (4.2.29)$$

where the summations are carried out over the set of all fuel elements F. Appropriate integration of Eq. 4.2.29 over the fuel residence time τ_d yields

$$k_{ed} = \frac{\sum_{f}^{F} \int_{\tau_d} dt\, R_{pnf}(t)}{\sum_{f}^{F} (\int_{\tau_d} dt\, R_{anf}(t) - \int_{\tau_d} dt\, S_{nf}(t))} = 1. \qquad (4.2.30)$$

A reactor simulation can be idealized such that one fuel element becomes representative of the entire reactor to yield

$$k_{efd} = \frac{\int_{\tau_d} dt\, R_{pnf}(t)}{\int_{\tau_d} dt\, R_{anf}(t) - \int_{\tau_d} dt\, S_{nf}(t)} = 1, \qquad (4.2.31)$$

by simplifying Eq. 4.2.30. Equation 4.2.31 can be interpreted as the depleter subsystem criticality constraint condition. During each rejuvenation cycle fuel is burned until Eq. 4.2.31 is satisfied, thus uniquely defining the final depleter fuel burnup $\beta_d(k_{efd}(\tau_d))$ required by Eq. 4.2.23. The fuel elements in the breeder subsystem have no criticality constraints and the initial depleter multiplication ratio $k_{efd}(0)$, Eq. 4.2.28, can be arbitrarily chosen. In the systems studied the multiplication ratio

$k_{efd}(0)$ was not allowed to exceed the maximum value of $k_{efd}(t)$ obtained during fuel burnup in the conventional once-through depleter system, thus uniquely defining the burnup $\beta_b(k_{efd}(0))$ in Eq. 4.2.24 as well as defining the breeder fuel residence time τ_b[61]. An increase in this upper limit would decrease the breeding effectiveness, since fissile fuel inventory is increased. At the same time the fuel residence times would also be increased, making refuelling operations less frequent. Figure 4.2.2 shows the temporal history of the important fissile isotopes as a function of the total fuel burnup, for 40 rejuvenation-burn cycles. The important feature to note here is the relative rapid depletion of uranium-235 and the "saw-tooth" asymptotic build-up of the fissile plutonium isotopes. The associated fission product load, that is the sum of the pseudo fission product densities, is also shown. The cycle averaged fissile isotope concentration increase with burnup can be attributed to the increased fission product load.

A second symbiotic system involves rejuvenation of fissile fuel with periodic fission product removal[66]. Although reprocessing introduces a cost penalty, it may be necessary to overcome high burnup material integrity limitations. At the same time possible reactor design limitations due to the large range of fissile isotope

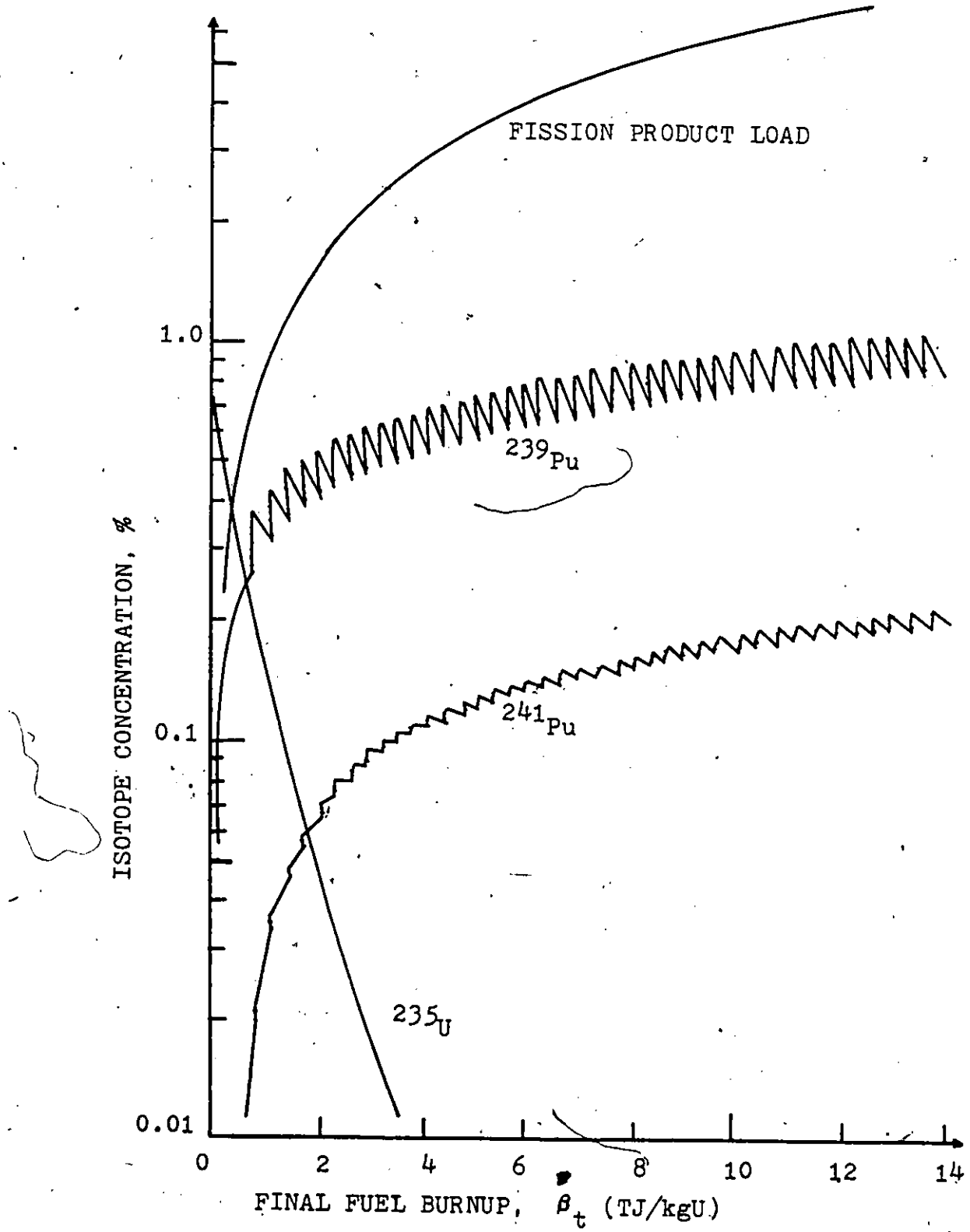

Fig. 4.2.2 Fissile fuel variations for fuel cycles without reprocessing.

concentrations are eliminated since fission product removal reduces fissile inventory requirements. Consequently the breeding ratio and the conversion ratio of each rejuvenation cycle is increased resulting in better breeding characteristics of the entire system. To optimize the effect of fission product removal, rejuvenation cycles without reprocessing take place when the negative reactivity of accumulated fission products equals the reactivity gain of a reenrichment exposure. For a fission product removal cycle no breeder subsystem is therefore required and an increase in net breeder supported depleter power is achieved. Figure 4.2.3 shows the temporal history of the important fissile isotopes as well as the fission product load for three reprocessing periods. The remaining reprocessing cycles are not shown since an equilibrium period is already obtained after the first two reprocessing steps.

4.3 Breeder-Converter Symbiotic System Analysis

The main factors contributing to the performance of a complex system are more easily recognized in an approximate lumped-parameter type analysis[39,40,57,60] rather than from detailed, high accuracy, computer based analyses. In addition to increasing the conceptual understanding, it can also be used for quick perturbation calculations and for

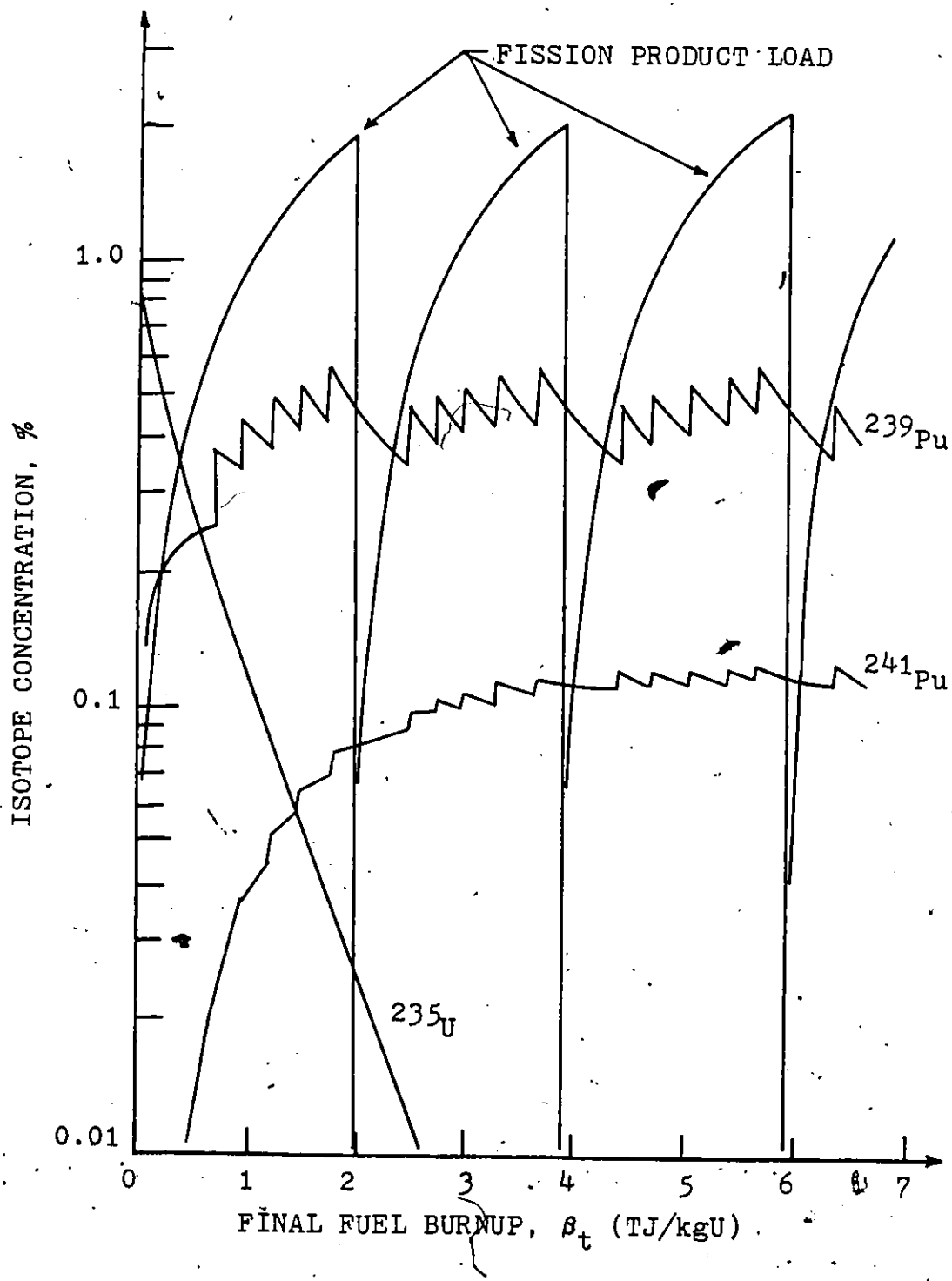

Fig. 4.2.3 Fissile fuel variations for fuel cycles with periodic reprocessing and fission product removal.

comparisons of detailed computer based analyses. Such a lumped-parameter analysis is now presented for spallation-breeder symbiotic systems.

A subcritical breeder blanket can be thought of as being driven by an externally supplied neutron current of S_n neutrons per second, formally defined by Eq. 4.2.2. Expressed in the formalism of Eq. 3.3.24, Eq. 4.2.2 becomes

$$S_n = \gamma_{be}\, T_{ltb}. \tag{4.3.1}$$

A spallation neutron yield ν_{ssp} per accelerator drive particle can therefore be defined as

$$\nu_{ssp} = \frac{S_n\, q}{I_q\, \gamma_{be}}, \tag{4.3.2}$$

where I_q is the accelerator beam current and q is the associated beam particle charge. In the breeding blanket the target produced neutrons are multiplied by fission and n-xn reactions. The upper limit of neutrons available for breeding is therefore

$$S_{max} = \frac{I_q}{q}\, \gamma_{be}\, \nu_{ssp}\, M_b, \tag{4.3.3}$$

where the neutron blanket multiplication factor, M_b, is given by

$$M_b = \left(\frac{1}{1-k_b}\right)\left(\frac{\Sigma_{anb} - \Sigma_{pnb}}{\Sigma_{anb}}\right). \tag{4.3.4}$$

Here the blanket multiplication ratio, k_b, defined by Eq. 4.2.13, is

$$k_b = \frac{\nu_{pnb}\,\Sigma_{pnb}}{\Sigma_{anb}}, \qquad (4.3.5)$$

where ν_{pnb} is defined by Eq. 4.2.9. The blanket macroscopic production cross section, Σ_{pnb}, and absorption cross section, Σ_{anb}, are defined by Eq. 4.2.8 and Eq. 4.2.6 respectively. The first fraction in Eq. 4.3.4 is the total infinite blanket neutron multiplication factor while the second factor is the ratio of neutrons not absorbed by neutron multiplication reactions to total blanket absorbed neutrons. A blanket consisting of only fertile isotopes will therefore breed S_n fissile atoms per second which can subsequently be burned in a converter reactor.

In the converter reactor, additional fissile atoms are bred according to its' conversion ratio C_d, defined by

$$C_d = \frac{fe_{\Sigma_{cnd}}}{fi_{\Sigma_{and}}}, \qquad (4.3.6)$$

where $fe_{\Sigma_{cnd}}$ and $fi_{\Sigma_{and}}$ are the depleter reactor macroscopic fertile isotope capture cross section and fissile isotope absorption cross section respectively. For a conversion ratio less than 1, typical for depleter or converter reactors, the system maximum rate of fissile isotope production becomes

$$m_{R_{pfi}} = \frac{I_q}{q}\,\gamma_{be}\,\nu_{ssp}\,\hat{M}_b\,\frac{1}{1-C_d}. \qquad (4.3.7)$$

Assuming that all fissile atoms are burned in the converter reactor, the total breeder supported thermal converter reactor power, generally defined by Eq. 4.2.23, can be written as

$$m_{P_{td}} = S_n M_b \frac{1}{1-C_d} E_{ad} , \qquad (4.3.8)$$

where E_{ad} is the thermal energy produced per fissile atom absorption reaction and defined by

$$E_{ad} = \frac{fi_{\Sigma_{fnd}}}{fi_{\Sigma_{and}}} \left(\frac{fe_{\Sigma_{fnd}}}{fi_{\Sigma_{fnd}}} + 1\right) U_{fnd} . \qquad (4.3.9)$$

Here $fi_{\Sigma_{fnd}}$ and $fe_{\Sigma_{fnd}}$ are the macroscopic depleter fission cross sections of fissile and fertile isotopes respectively. The effective energy produced per depleter fission reaction is given by U_{fnd}. Equation 4.3.8 and Eq. 4.3.9 can only be considered as upper limits of fissile isotope production rate and thermal converter power. To obtain realistic parameters, several loss fractions are now identified.

The breeding blanket generally does not consist of only fertile isotopes and therefore a breeding loss fraction due to non fertile fuel parasitic blanket capture can be defined as

$$F_c = \frac{fe_{\Sigma_{cnb}}}{\Sigma_{cnb}} , \qquad (4.3.10)$$

where the macroscopic blanket capture cross section Σ_{cnb}, includes neutron capture by fissile isotopes. Since the

breeder blanket may also contain fissile fuel, a fissile fuel absorption loss fraction can be defined as

$$F_a = \frac{{}^{fe}\Sigma_{cnb} - {}^{fi}\Sigma_{anb}}{{}^{fe}\Sigma_{cnb}} . \qquad (4.3.11)$$

A breeder net fissile isotope production rate can therefore be expressed by

$${}^{b}R_{pfi} = S_{max} F_c F_a , \qquad (4.3.12)$$

where S_{max}, F_c, and F_a are given by Eq. 4.3.3, Eq. 4.3.10, and Eq. 4.3.11 respectively.

Not all of the fissile isotopes produced by the breeder may be consumed by the depleter system. Fissile fuel may be lost as high burnup fuel waste or as reprocessing waste. An actual depleter reactor absorbed to breeder reactor produced fissile isotope consumption fraction can hence be expressed as

$${}^{b}F_i = {}^{b}R_{ifi} / {}^{b}R_{pfi} , \qquad (4.3.13)$$

where ${}^{b}R_{pfi}$ is defined by Eq. 4.3.12. The breeder-produced fissile fuel converter depletion rate, ${}^{b}R_{ifi}$, is defined by

$${}^{b}R_{ifi} = \frac{d}{dt} \left(\Sigma_{fi} \int_{V_d} d\vec{r}\ {}^{b}n_{fi}(\vec{r},t) \right), \qquad (4.3.14)$$

where the breeder-based fissile isotope densities, ${}^{b}n_{fi}(\vec{r},t)$ are integrated over the depleter reactor volume V_d. The summation in Eq. 4.3.14 is carried out over all fissile isotope types.

An effective symbiotic system conversion ratio is now

defined as

$$C_{eff} = 1 - (F_c\ F_a\ {}^{b}F_i\ \frac{1}{1-C_d})^{-1}\ , \qquad (4.3.15)$$

where F_c, F_a, ${}^{b}F_i$, and C_d are defined by Eq. 4.3.10, Eq. 4.3.11, Eq. 4.3.13, and Eq. 4.3.6 respectively.

A breeder based converter fissile fuel absorption per breeder drive neutron can therefore be expressed as

$$N_{fi} = M_b\ \frac{1}{1 - C_{eff}}\ , \qquad (4.3.16)$$

where the breeder multiplication is given by Eq. 4.3.4. With the definition of Eq. 4.3.16 the breeder based converter fissile fuel absorption rate becomes

$$R_{afi} = S_n\ N_{fi}\ , \qquad (4.3.17)$$

where S_n is defined by Eq. 4.3.1, while the breeder supported thermal depleter reactor power is given by

$$P_{td} = S_n\ N_{fi}\ E_{ad}\ , \qquad (4.3.18)$$

the energy per fissile isotope absorption, E_{ad}, being given by Eq. 4.3.9. It should be noted here that Eq. 4.3.17 and Eq. 4.3.18 are equivalent to Eq. 4.3.7 and Eq. 4.3.8 respectively, with C_d being replaced by C_{eff}.

Similar to Eq. 4.3.18 a breeder blanket fuel power can be defined by

$$P_{tbb} = S_n\ \frac{1}{1 - k_b}\ E_{ab}\ ; \qquad (4.3.19)$$

where E_{ab} is the energy produced per blanket neutron absorption expressed by

$$E_{ab} = \frac{\Sigma_{pnb} U_{pnb}}{\Sigma_{anb}}, \qquad (4.3.20)$$

with the cross sections Σ_{pnb} and Σ_{anb} defined by Eq. 4.2.8 and Eq. 4.2.6 respectively, and

$$U_{pnb} = p_{nbb}/\Sigma_{pnb}. \qquad (4.3.21)$$

Here the specific power of the breeder blanket, p_{nbb}, is given by Eq. 4.2.14.

The general breeder core power is

$$P_{tcb} = P_{tb} - P_{tbb} + P_{te}, \qquad (4.3.22)$$

where the total breeder power, P_{tb}, is generally defined by Eq. 4.2.22, while the breeder-blanket fuel produced power, P_{tbb}, is given by Eq. 4.3.19. The externally supplied breeder drive power, P_{te}, for an accelerator driven breeder can be obtained from

$$P_{te} = \frac{I_q}{q} E_q, \qquad (4.3.23)$$

where E_q is the energy of the accelerator beam charged particle of charge q and current I_q.

A breeder core Q value can be expressed as

$$Q_{tcb} = P_{tcb}/P_{te}, \qquad (4.3.24)$$

while a breeder blanket Q value is given by

$$Q_{tbb} = P_{tbb}/P_{te}. \qquad (4.3.25)$$

Here P_{tcb}, P_{tbb}, and P_{te} are defined by Eq. 4.2.22,

Eq. 4.3.19, and Eq. 4.3.23 respectively. Using Eq. 4.3.24 and Eq. 4.3.25 a total breeder Q value takes the form of the summation

$$Q_{tb} = Q_{tcb} + Q_{tbb}, \qquad (4.3.26)$$

a parameter of considerable importance in the power balance of the symbiotic system.

4.4 Breeder-Converter Symbiotic Comparisons

Several uranium-oxide and thorium-oxide accelerator breeder systems have recently been studied[32,48,56,62]. A summary description of selected case studies of the referenced work as well as this work is given in Table 4.4.1, while the corresponding parameter comparison is shown in Table 4.4.2.

One of the most critical factors in evaluating a breeder-converter system is the strength of the externally supplied blanket neutron source, S_n, defined by Eq. 4.3.1. Due to the high particle energies involved, this neutron source is also the most difficult parameter to be obtained theoretically or experimentally. As explored in Sec. 1.3, the spallation target neutron yield varies considerably with particle type, particle energy, and target material of the accelerator-breeder subsystem. In recent studies[46,49]

Table 4.4.1 Accelerator breeder systems

Case	Fuel	Moderator	Moderator Density (g/cm^3)	References
a	UO_2 (0.71% U-235)	D_2O (44%)	0.77	32,56,62
b	UO_2	H_2O	0.7	
c	UO_2	H_2O	0.35	
d	UO_2	H_2O	0.175	
e	ThO_2 (100% Th-232)	D_2O (44%)	0.77	32,56,62
f	ThO_2	H_2O	0.7	
g	ThO_2	H_2O	0.35	
h	ThO_2	H_2O	0.175	
i	UO_2 (0% Pu-239)	Na-Fe (50%)	-	48
j	UO_2 (2% Pu-239)	Na-Fe		
k	ThO_2 (0% U-233)	Na-Fe (50%)	-	48
l	ThO_2 (2% U-233)	Na-Fe		
m	ThO_2 (0%-2% U-233)	H_2O-D_2O	-	this work
n	ThO_2	H_2O-D_2O		based on
o	ThO_2	H_2O-D_2O		references 48,62,74
p	UO_2 (0.5%-1% Pu-239&U-235)	H_2O-D_2O	-	this work
q	UO_2	H_2O-D_2O		
r	UO_2	H_2O-D_2O		
s	UO_2	H_2O-D_2O		

Table 4.4.2a Breeder-converter system parameters

Description (case)		k_b Eq. 4.3.5	M_b Eq. 4.3.4	F_c Eq. 4.3.10	F_a Eq. 4.3.11	b_{F_i} Eq. 4.3.13
UO_2-D_2O	(a)	0.30	1.27	0.98	0.95	1.00
UO_2-H_2O	(b)	0.54	1.75	0.98	0.94	1.00
	(c)	0.48	1.58	0.98	0.94	1.00
	(d)	0.43	1.47	0.98	0.94	1.00
ThO_2-D_2O	(e)	0.068	1.04	0.98	0.97	1.00
ThO_2-H_2O	(f)	0.065	1.04	0.98	0.97	1.00
	(g)	0.078	1.05	0.98	0.97	1.00
	(h)	0.093	1.06	0.98	0.97	1.00
UO_2-Na	(i)	0.27	1.23	0.98	0.95	1.00
	(j)	0.47	1.53	0.98	0.84	1.00
ThO_2-Na	(k)	0.063	1.05	0.98	0.97	1.00
	(l)	0.32	1.27	0.98	0.80	1.00
ThO_2-Mod	(m)	0.28	1.22	0.98	0.83	0.21
	(n)	0.31	1.27	0.97	0.83	0.80
	(o)	0.29	1.25	0.98	0.83	0.33
UO_2-Mod	(p)	0.418	1.46	0.98	0.94	0.99
	(q)	0.436	1.49	0.97	0.92	0.89
	(r)	0.515	1.68	0.92	0.83	0.98
	(s)	0.430	1.48	0.97	0.93	0.94

Table 4.4.2b Breeder-converter system parameters

Description (case) →	C_d Eq. 4.3.6	C_{eff} Eq. 4.3.15	N_{fi} Eq. 4.3.16 (a/n_{sp})	E_{ad} Eq. 4.3.9 (MeV)	E_{ab} Eq. 4.2.20 (MeV)
UO_2-D_2O (a)	0.75	0.73	4.73	146	21.8
UO_2-H_2O (b)	0.75	0.73	6.45	146	39.2
(c)	0.75	0.73	5.82	146	34.8
(d)	0.75	0.73	5.41	146	31.2
ThO_2-D_2O (e)	0.88	0.87	8.27	178	5.1
ThO_2-H_2O (f)	0.88	0.87	8.25	178	4.9
(g)	0.88	0.87	8.33	178	5.8
(h)	0.88	0.87	8.41	178	7.0
UO_2-Na (i)	0.75	0.73	4.59	146	20.5
(j)	0.75	0.68	4.82	146	38.1
ThO_2-Na (k)	0.88	0.87	8.33	178	3.3
(l)	0.88	0.85	8.25	178	27.7
ThO_2-Mod (m)	0.88	0.30	1.74	178	20.9
(n)	0.88	0.81	6.80	178	23.2
(o)	0.88	0.56	2.80	178	21.7
UO_2-Mod (p)	0.74	0.72	5.22	146	26.3
(q)	0.67	0.58	3.56	146	27.5
(r)	0.45	0.27	2.30	146	32.4
(s)	0.70	0.64	4.12	146	27.1

Table 4.4.2c Breeder-converter system parameters

Description (case)	ν_{ssp} Eq. 4.3.2 (n/p)	β_t Eq. 4.2.25 (TJ/kgHE)	P_{td}* Eq. 4.3.18 (GW_t)	P_{tbb}* Eq. 4.3.19 (MW_t)	Q_{tbb} Eq. 4.3.25
UO_2-D_2O (a)	28.2±2.2	0.0	5.86	262	0.9
UO_2-H_2O (b)	28.2±2.2	0.0	7.98	721	2.4
(c)	27.8±2.6	0.0	7.10	559	1.9
(d)	29.5±2.7	0.0	7.04	484	1.6
ThO_2-D_2O (e)	29.8±4.3	0.0	13.2	49	0.2
ThO_2-H_2O (f)	29.8±4.3	0.0	13.2	47	0.2
(g)	30.9±3.9	0.0	13.8	59	0.2
(h)	30.8±3.2	0.0	13.9	71	0.2
UO_2-Na (i)	30.	0.0	6.05	252	0.8
(j)	30.	0.0	6.35	651	2.3
ThO_2-Na (k)	30.	0.0	13.4	32	0.1
(l)	30.	0.0	13.2	366	1.2
ThO_2-Mod (m)	30.0	2.55	2.79	262	0.9
(n)	30.0	2.55	10.9	302	1.0
(o)	30.0	5.10	4.49	576	0.9
UO_2-Mod (p)	30.0	0.289	6.87+.5%	407+3.0%	1.4
(q)	30.0	0.297	4.69+.4%	438+2.8%	1.5
(r)	30.0	0.370	3.03-.3%	602+1.2%	2.0
(s)	30.0	2.64	5.43+1.%	427+3.4%	1.4

* γ_{be} = 1.0 (see Eq. 4.3.1 and Eq. 4.3.2).

a 0.3 A, 1 GeV proton beam was found to be a realistic and practical breeder drive source, while lead, uranium, or thorium are generally considered the main target materials. The spallation neutron yield for these heavy elements, ν_{ssp}, defined by Eq. 4.3.2 falls typically between 20 n/p and 40 n/p, and is further multiplied by fission reactions and to a lesser extent by n-xn reactions, to produce a total neutron yield up to and exceeding 100 n/p as shown in Fig. 1.3.1. For UO_2 and H_2O moderated assemblies, the spallation neutron yield for 1 GeV protons ranges from 27 n/p to 31 n/p, depending on the moderator to fuel volume ratio and moderator density[32]. The standard deviation for each set of Monte-Carlo calculations with the NMTC-code ranges typically between 2 n/p and 3 n/p. Table 4.4.2c gives ν_{ssp} and the associated standard deviation for the selected cases. Here for cases i to s 30 n/p has been found to be an appropriate value. The assemblies of all cases consisted of lead targets surrounded by breeding blankets containing the heavy element fertile fuel. Moderator-coolants such as sodium, light water, and heavy water were used as indicated in Table 4.4.1.

The total fuel burnup, β_t, defined by Eq. 4.2.25, is also summarized in Table 4.4.2c for each case. No burnup calculations were performed for cases a to l, describing initial burnup-free system conditions. The burnup for these

cases is shown as zero. For cases m to o breeder-converter system parameter estimates were based on depletion calculations of thorium fuels with uranium-235 topping[74]. Case m refers to the first breed-burn cycle, case n refers to the second breed-burn cycle, while case o represents a two cycle breed-burn system, consisting of a combination of case m and n. System parameters for cases p to s were obtained from detailed depletion calculation of this work. They apply to a breed-burn scheme described in Sec. 4.2, with the specific system fuel depletion history being shown in Fig. 4.4.2 for the major fissile isotopes. Case p refers to cycle two in Fig. 4.4.2, which is the first cycle requiring a breeder subsystem, case q refers to the 8th breed-burn cycle, while case r refers to the 49th breed-burn cycle. Case s refers to a system average of cycles 2 to 8.

The neutron multiplication factor, M_b, defined by Eq. 4.3.4, and its' associated generation multiplication constant, k_b, defined by Eq. 4.3.5, are summarized in Table 4.4.2a. Neutron multiplication is generally low, typical for nuclear fuels with low fissile fuel inventory requirements. It should be noted here that cases a to l are based on NMTC calculations for particle transport solutions above 15 MeV. This code, however, does not take neutron multiplication by fission reactions into account. Considering experimental results, as discussed in Sec. 1.3,

this is thought to underestimate neutron yields by up to 20% for large uranium targets. By including this effect in oxide fuel breeding blankets it is estimated that the neutron multiplication factor, M_b, will be increased by up to 15%.

The major system parameters F_c, F_a, ${}^bF_i$, and C_d, with their associated definitions are also summarized in Table 4.4.2a and Table 4.4.2b. Particularly noteworthy is the low value of ${}^bF_i$ for the thorium fuel, case m. This is due to the fact that natural thorium fuels do not contain any fissile fuel inventory. The depleter subsystem inventory requirement of about 2% uranium-233 has to be produced first by the breeder subsystem and considerably reduces the breeder support capacity. This inventory penalty is not present during the second breed-burn cycle, case n. The two cycle average, case o, however, shows only a slightly increased value of ${}^bF_i$ as compared to case m. Detailed depletion calculations of this work show that the effective fuel burn fraction ${}^bF_i$ is relatively close to unity, for cases p to s. Here the relatively small fuel burnup loss associated with fissile fuel inventory requirements is due to reactivity losses produced by fission product buildup. The increased fissile fuel inventory requirement with burnup, however, considerably decreases the depleter subsystem conversion ratio, C_d, defined by

Eq. 4.3.6, making high fuel burnup less desirable.

The system effective conversion ratio, C_{eff}, defined by Eq. 4.3.15, summarizes all fuel related fissile isotope loss fractions, and is shown in Table 4.4.2b together with the corresponding breeder based fissile fuel utilization, N_{fi}, defined by Eq. 4.3.16. In Fig. 4.4.1 the relationship between neutron multiplication factor, M_b, effective fissile fuel conversion ratio, C_{eff}, and fissile atom consumption, N_{fi}, are shown. As discussed earlier in this section, M_b, is underestimated for cases a to l. From Fig. 4.4.1 and Table 4.4.2b it can therefore be concluded that the spectral choice, described in Sec. 4.2, used in the determination of cross section data for this work, produces system parameters typical for D_2O-H_2O moderated breeder blankets.

The fuel supported breeder power, P_{tbb}, and depleter power, P_{td}, are summarized in Table 4.4.2c. These powers are based on effective fission energies presented by Duderstadt[75]. These fission energies are conservative, considering that effective values up to 5% higher have been used[71]. Noteworthy are the potentially high depleter support powers obtained for thorium fuels. The errors indicated for cases p to s are obtained from comparison with detailed support power calculation results presented in Sec. 4.6. It should also be noted that the breeder blanket Q-value, Q_{tbb}, listed in Table 4.4.2c, falls between 1.0 and

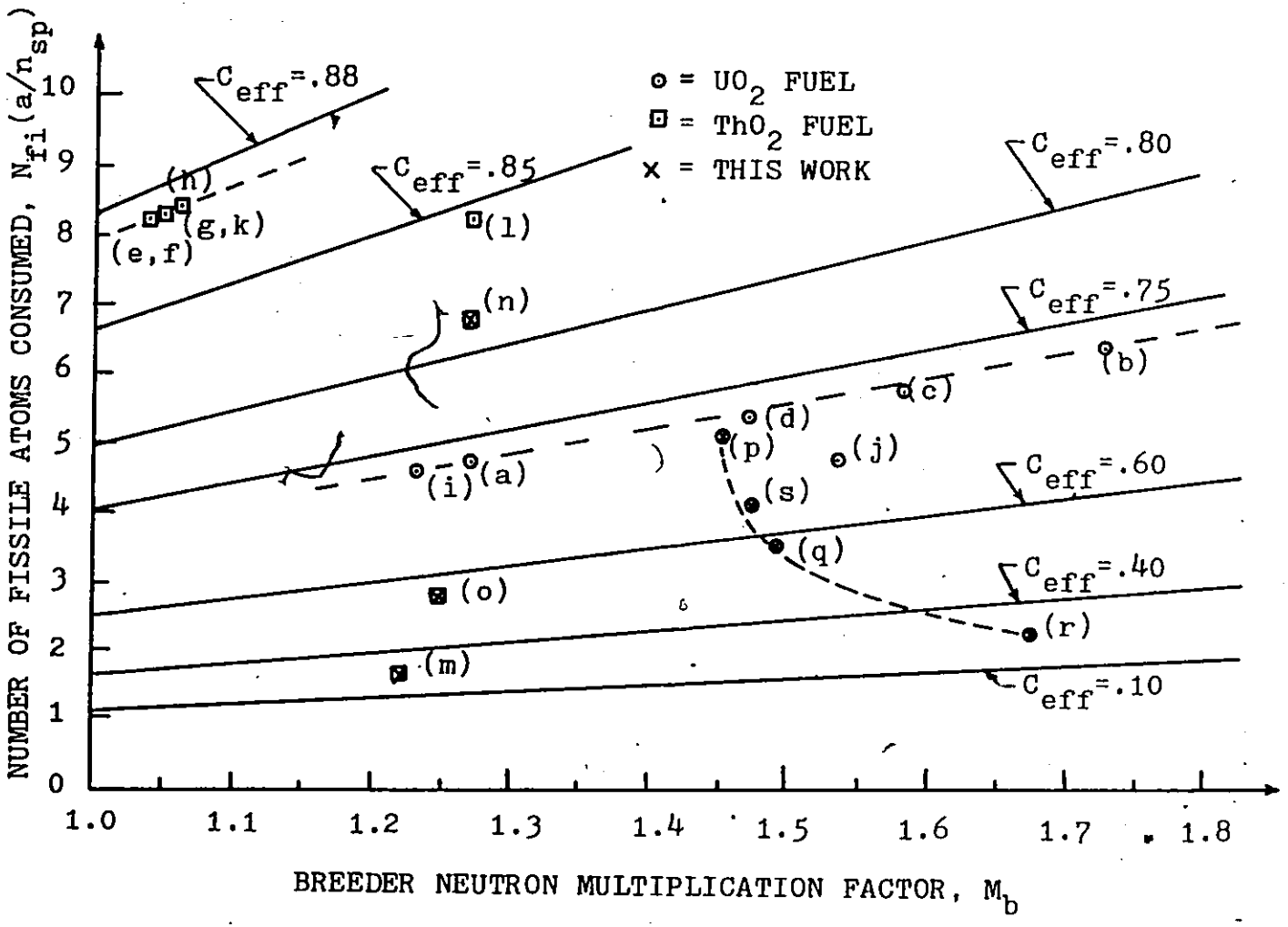

Fig. 4.4.1 Breeder-converter symbiotic system comparison.

2.0, typical for low power fissile fuel breeder blankets based on the uranium-plutonium chain.

4.5 Conservation of Mass-Energy Flow

The dynamic properties of a symbiotic reactor system can be described by its' mass-energy flow rates and inventory change rates. These rates are generally defined by Eq. 4.1.2 to Eq. 4.1.4 and can be expressed in terms of their components as

$$R_s(t) = R_{sh}(t) + R_{se}(t) + R_{sp}(t) + R_{sw}(t) \qquad (4.5.1)$$

and

$$I_s(t) = I_{sh}(t) + I_{se}(t) + I_{sp}(t) + I_{sw}(t) \qquad (4.5.2)$$

respectively. Here the subscript s denotes the subsystem and the subscripts h, e, p, and w stand for heavy element fuel mass, fuel rest mass converted to energy, mobile atomic particle mass such as the neutron mass, and nuclear fuel waste mass respectively. Figure 4.5.1 shows a typical symbiotic system. The solid path in Fig. 4.5.1 indicates the general mass-energy flow although each subsystem can be bypassed as indicated by the broken line. For each subsystem the fundamental law of conservation of mass-energy yields

$$R_{is}(t) = I_s(t) + R_{fs}(t), \qquad (4.5.3)$$

where the subscripts i and f denote initial and final flow rates respectively. Evidently, it is required that

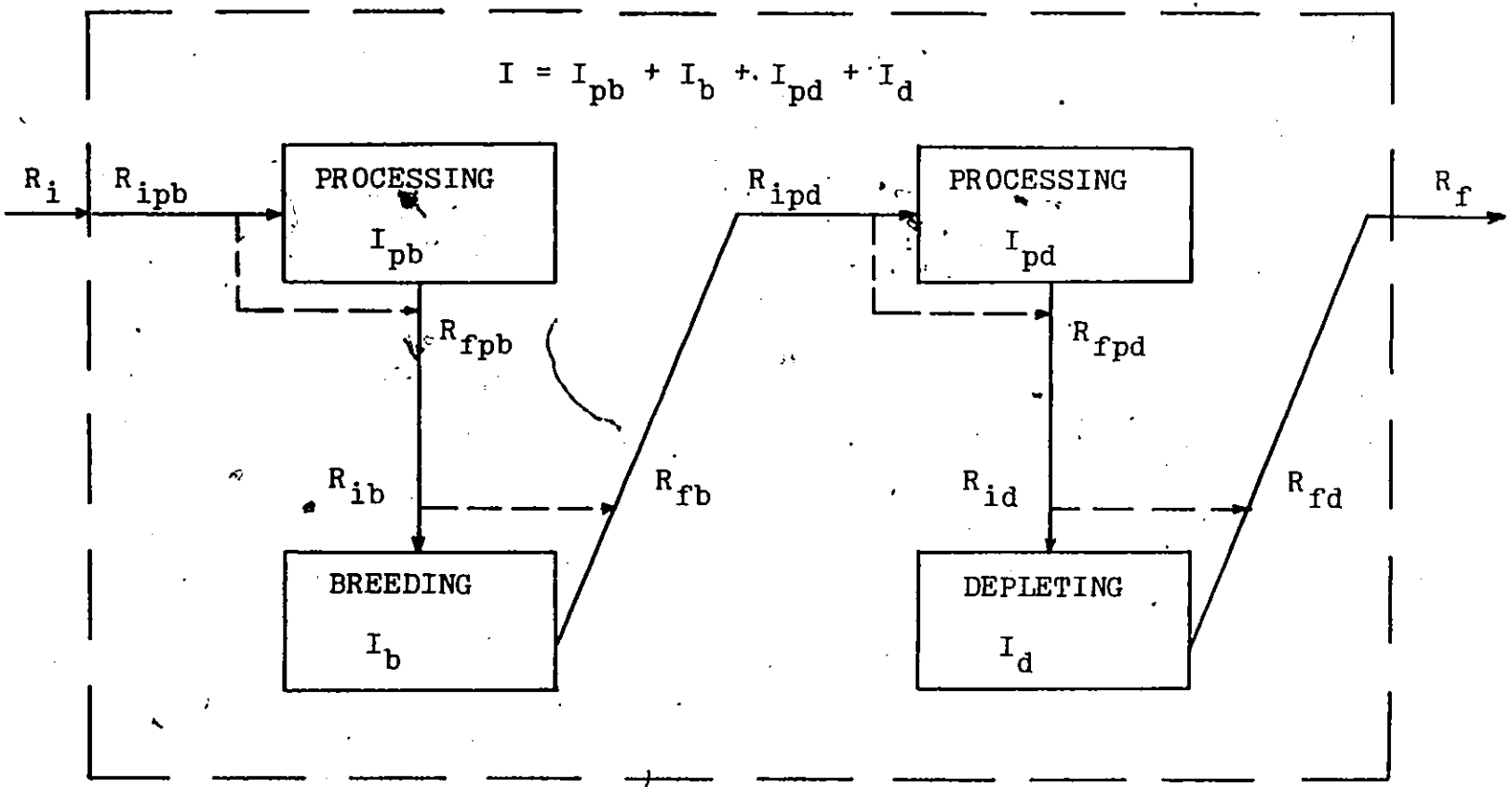

Fig. 4.5.1 Cycle mass-energy flow rates of a symbiotic system.

$$R_{fs}(t) \equiv R_{i(s+1)}(t) \quad (4.5.4)$$

As shown in Fig. 4.5.1 the subsystem s or its adjacent subsystem s+1 can define the subsystems pb, b, pd, and d symbolizing pre breeder processing, breeding, pre depletion processing, and depletion respectively.

For the system shown in Fig. 4.5.1, the total rate of inventory change is given by

$$I(t) = I_{pb}(t) + I_b(t) \text{ or } I_{pd}(t) + I_d(t) , \quad (4.5.5)$$

with the corresponding conservation of mass-energy requirement

$$R_i(t) = I(t) + R_f(t) . \quad (4.5.6)$$

Here it is understood that

$$R_i(t) \equiv R_{ipb}(t) \quad (4.5.7)$$

and

$$R_f(t) \equiv R_{fd}(t) . \quad (4.5.8)$$

Equation 4.5.1 to Eq. 4.5.8 completely describe the time dependent mass-energy flow of the symbiotic reactor system. A special case of the system model is a standard depletion reactor for which Eq. 4.5.3 yields

$$R_{idh} = R_{fdh} + R_{fde} + R_{fdp} + R_{fdw} . \quad (4.5.9)$$

Assuming equilibrium steady state operation requires

$$I_d(t) = 0 . \quad (4.5.10)$$

For a conventional reactor system one typically obtains

$$R_{fde}/R_{fdh} \simeq 10^{-5} . \quad (4.5.11)$$

and

$$R_{fdp}/R_{fdh} \simeq 10^{-5} , \qquad (4.5.12)$$

yielding to a very good approximation

$$R_{ih} = R_{fh} + R_{fw} , \qquad (4.5.13)$$

which states that for a conventional reactor system the fuel mass flow is conserved.

Basic reactor system properties can best be obtained for system steady state operation. This is also the normal mode of operation and is therefore considered next. Equilibrium conditions require

$$I_s(t) = 0 . \qquad (4.5.14)$$

Substituting Eq. 4.5.14 into Eq. 4.5.3 yields

$$R_i = R_{is} = R_{fs} = R_f , \qquad (4.5.15)$$

as the principle of conservation of the mass-energy flow rate for each subsystem and the entire system.

A symbiotic system as shown in Fig. 4.5.1 can be expanded to form a sequence of such systems as schematically shown in Fig. 4.5.2, to describe a symbiotic system with fuel recycling. Each fuel cycle of this dynamic symbiotic system is identified by the superscript order number n. After each cycle a system defined fraction of the mass-energy flow rate is removed from the system. This cycle loss fraction is given by

$$n_\delta = \frac{(n_{\delta_h}\, n_{R_{fh}} + n_{\delta_e}\, n_{R_{fe}} + n_{\delta_p}\, n_{R_{fp}} + n_{\delta_w}\, n_{R_{fw}})}{n_{R_f}} , \qquad (4.5.16)$$

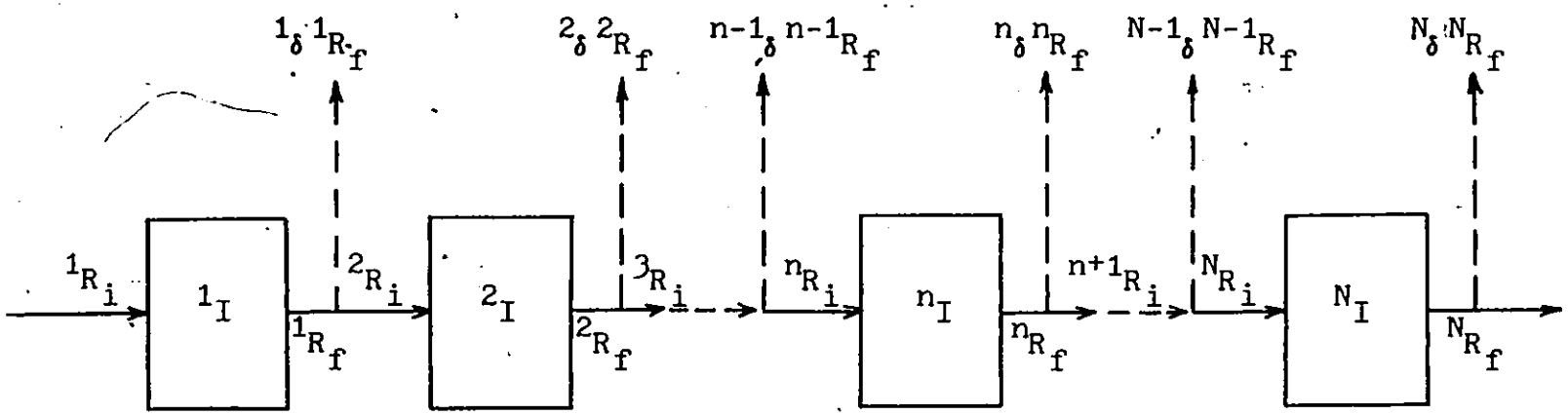

Fig. 4.5.2 Multicycle mass-energy flow rates of a symbiotic system.

where δ_h, δ_e, δ_p, and δ_w are the fractional mass-energy removal rates for heavy element fuel, energy, mobile atomic particle, and fuel waste respectively. Since the mass-energy flow rate between cycles is conserved, we obtain the recursive relationship

$$ {}^{n+1}R_i = {}^{n}R_f \, (1 - {}^{n}\delta) \, . \qquad (4.5.17) $$

Combining Eq. 4.5.17 with Eq. 4.5.6 yields

$$ {}^{n+1}R_i = ({}^{n}R_i - {}^{n}I) \, (1 - {}^{n}\delta) \, , \qquad (4.5.18) $$

which reduces to

$$ {}^{n+1}R_i = {}^{n}R_i \, (1 - {}^{n}\delta) \, , \qquad (4.5.19) $$

or

$$ {}^{n+1}R_i = \left[\prod_{m=1}^{n} (1 - {}^{m}\delta) \right] {}^{1}R_i \qquad (4.5.20) $$

for equilibrium operation.

4.5 Mass-Energy Supported Power Based on Fuel Recycling without Reprocessing

Section 4.2 described selected physics aspects of nuclear reactor systems while Sec. 4.4 compares typical symbiotic reactor systems using oxide nuclear fuel with low fissile fuel concentrations by employing a lumped parameter analysis. The cases discussed, a to s, as summarized in Table 4.4.1, all use lead targets producing neutron yields, ν_{ssp}, of approximately 30 n/p. This neutron yield can be increased by replacing some or all of the lead target by

uranium or thorium. The increased neutron yield is basically due to fission neutron multiplication resulting in a corresponding increase in the target Q-value. The increase per target unit-Q is between 8 n/Q and 10 n/Q[41,48] for a 1 GeV proton beam. In this and the following sections, systems with different target-Q and neutron yields are analyzed. These cases are summarized in Table 4.6.1. Here, a target neutron yield increase of 9 n/Q has been used which corresponds to an effective fission energy yield of 200 MeV and a net neutron yield of 1.8 neutrons per fission. With the introduction of uranium or thorium as targets, the parasitic neutron capture in the target is also increased, attributable largely to moderated blanket neutrons leaking back into the target from the blanket. This effect is practically negligible for small lead targets but for small uranium targets reduction of up to 50% in the fissile fuel breeding capacity can be expected for systems with low fissile fuel inventories[30]. As discussed in Sec. 3.3, the neutron blanket-to-target leakage effects can be incorporated in the loss fraction γ_{be} defined by Eq. 3.3.25. As shown in Table 4.6.1, in addition to five cases with γ_{be} equal to unity, five cases with γ_{be} equal to 0.8 are also included in the analysis. It should be noted here that blanket-to-target neutron leakage produces fissile fuel breeding in uranium or thorium targets.

Table 4.6.1 Reference breeder subsystem parameters

Case Number	S_n Eq. 4.3.1 (n/s)	γ_{be} Eq. 3.3.25	ν_{ssp} Eq. 4.3.2 (n/p)	Q_{tcb} Eq. 4.3.24
1	5.62×10^{19}	1.0	30.0	1
2	7.30×10^{19}	1.0	39.0	2
3	8.99×10^{19}	1.0	48.0	3
4	10.67×10^{19}	1.0	57.0	4
5	12.36×10^{19}	1.0	66.0	5
5	4.49×10^{19}	0.8	30.0	1
7	5.84×10^{19}	0.8	39.0	2
8	7.19×10^{19}	0.8	48.0	3
9	8.54×10^{19}	0.8	57.0	4
10	9.89×10^{19}	0.8	66.0	5

The listed parameters correspond to a proton breeder target beam with the properties:

I_p = 0.300 A (proton beam current)

E_p = 1.000 GeV (proton energies of the beam)

q = 1.602×10^{-19} C (proton charge)

In Sec. 4.5 a symbiotic system with fuel recycling is modelled for a homogeneous system with cycle order number n. The isotopic composition of the fuel will however differ from cycle to cycle, resulting in a heterogeneous system. The principle of conservation of mass-energy flow, as given by Eq. 4.5.15 for steady state operation, is still valid for each cycle, yielding a breeder supported depletion subsystem power,

$$^{n}P_{td} = {}^{n}P_{tbb}({}^{n}S_{n})\ {}^{n}\beta_{d}({}^{n}k_{efd}(\tau_{d}))\ /\ {}^{n}\beta_{b}({}^{n}k_{efd}(0)) \quad (4.6.1)$$

obtained by substituting Eq. 4.2.24 into Eq. 4.2.23. As indicated, the fuel produced breeder blanket power, $^{n}P_{tbb}$, is constrained mainly by the neutron drive source, $^{n}S_{n}$, while the breeder and depleter subsystem burnups, $^{n}\beta_{b}$ and $^{n}\beta_{d}$ are respectively constrained by initial and final fuel reactivity requirements of the depleter subsystem, as discussed in Sec. 4.2. For a symbiotic system based on burning natural uranium, such as a CANDU-converter reactor symbiotic system, fuel supported breeder blanket powers, $^{n}P_{tbb}$, and fuel supported depleter powers, $^{n}P_{td}$, are shown in Fig. 4.6.1 and Fig. 4.6.2 respectively as a function of breeder-converter cycle order number n for different neutron drive sources. The cycle associated breeder and depleter fuel burnups are summarized in Fig. 4.6.3, while relevant system parameters are given in Table 4.6.1. Here the first cycle burnup corresponds to the conventional reactor

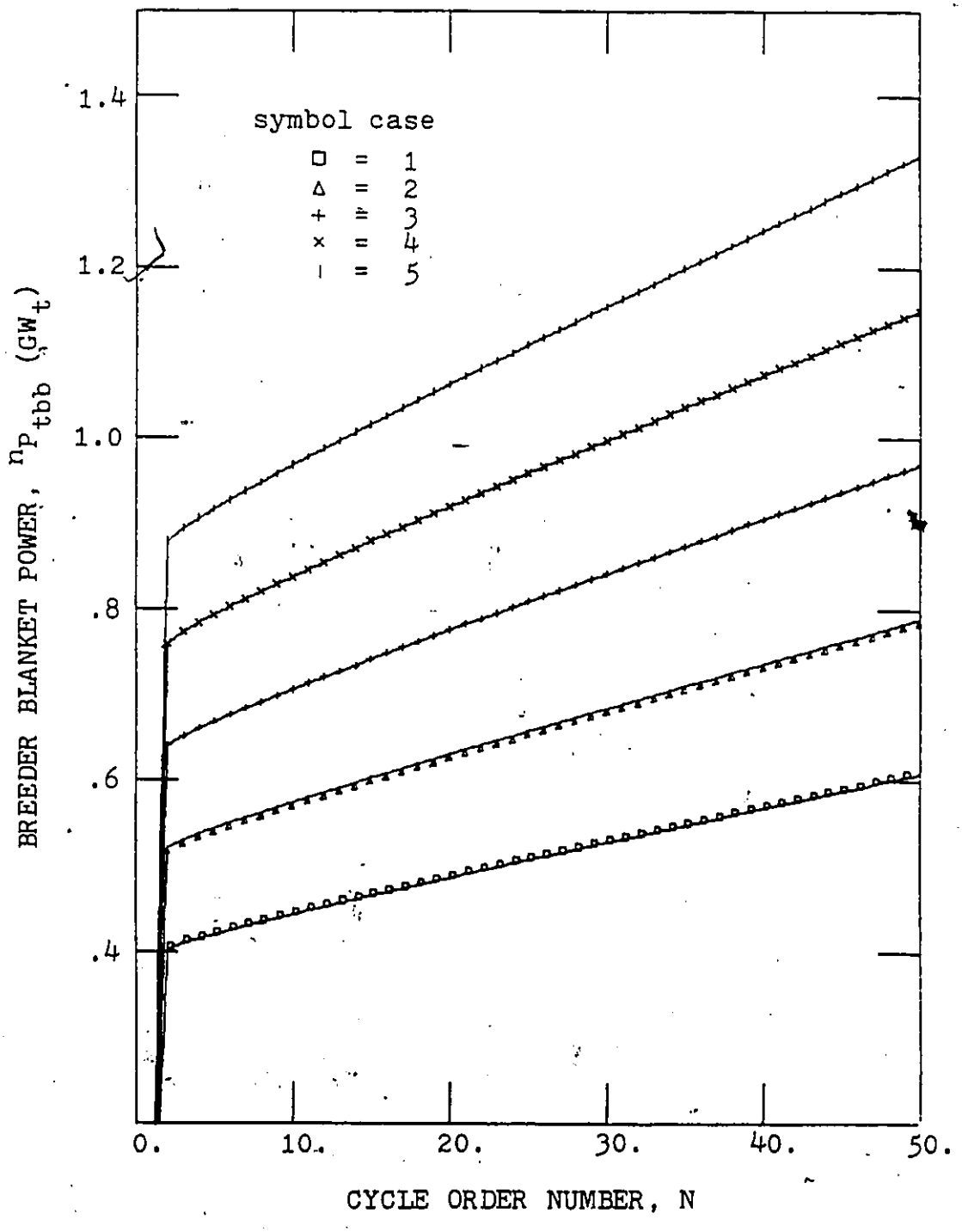

Fig. 4.6.1a Fuel cycle supported breeder blanket power without fuel reprocessing; cases 1 to 5 of Table 4.6.1.

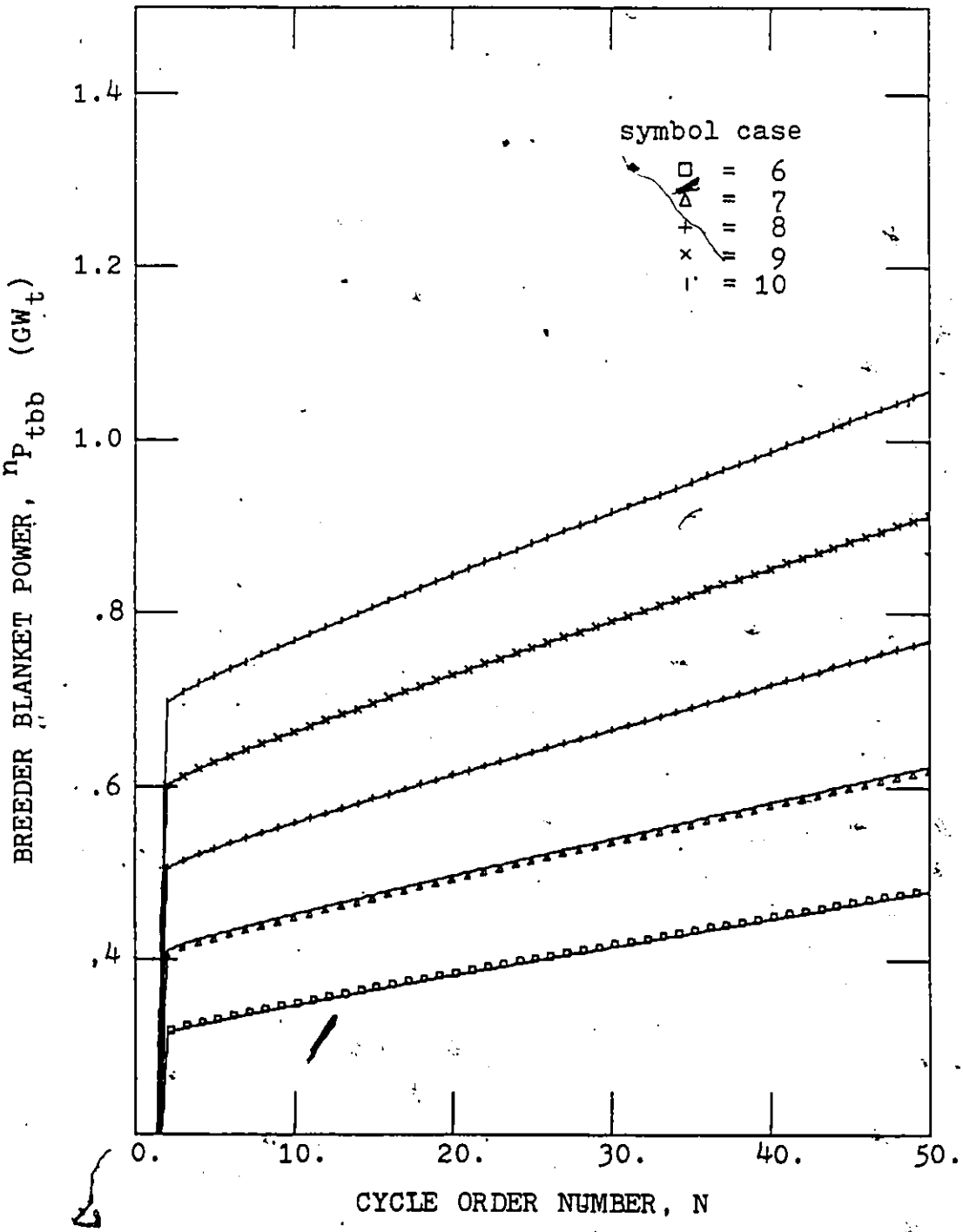

Fig. 4.6.1b Fuel cycle supported breeder blanket power without fuel reprocessing; cases 6 to 10 of Table 4.6.1.

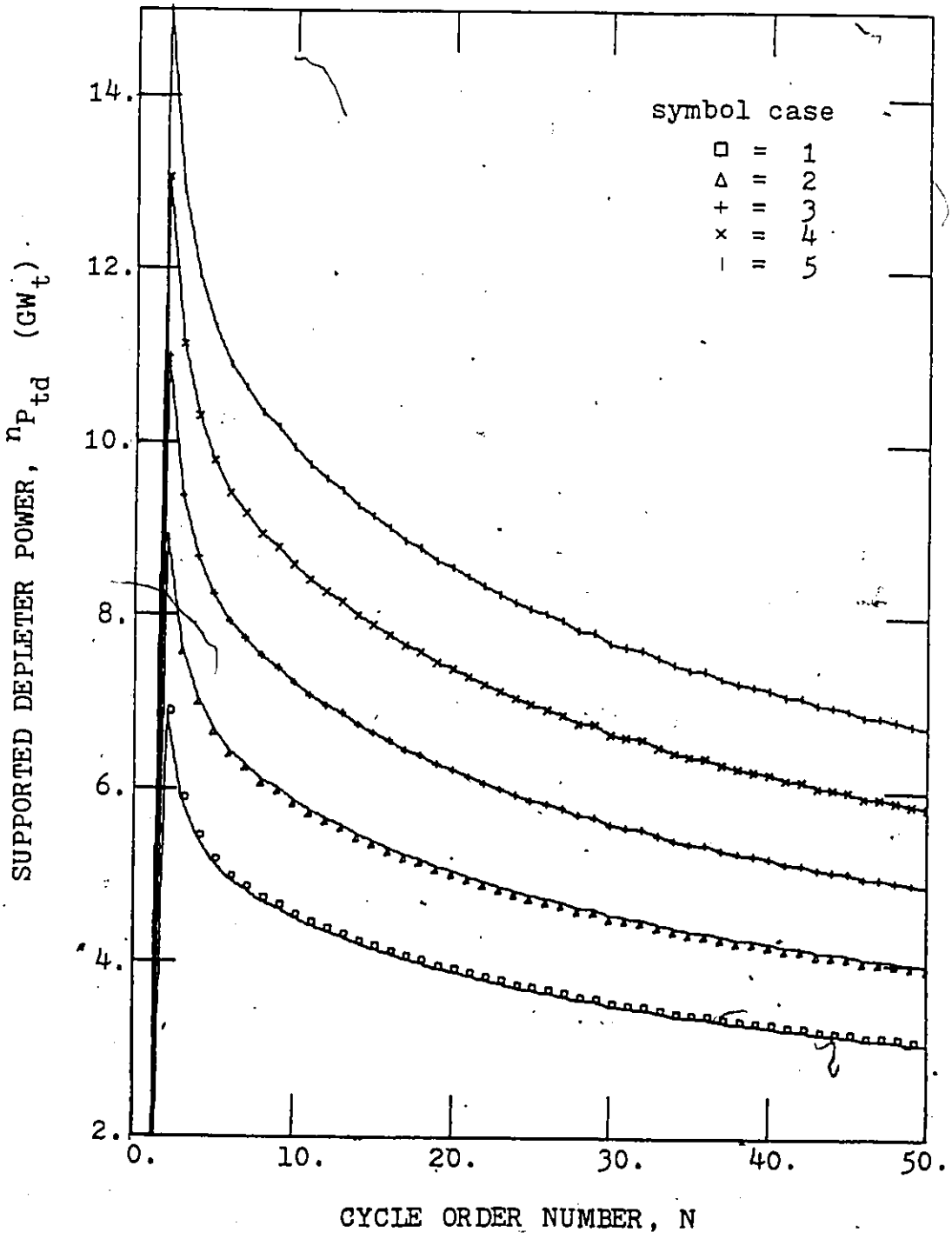

Fig. 4.6.2a Fuel cycle supported depleter power without fuel reprocessing; cases 1 to 5 of Table 4.6.1.

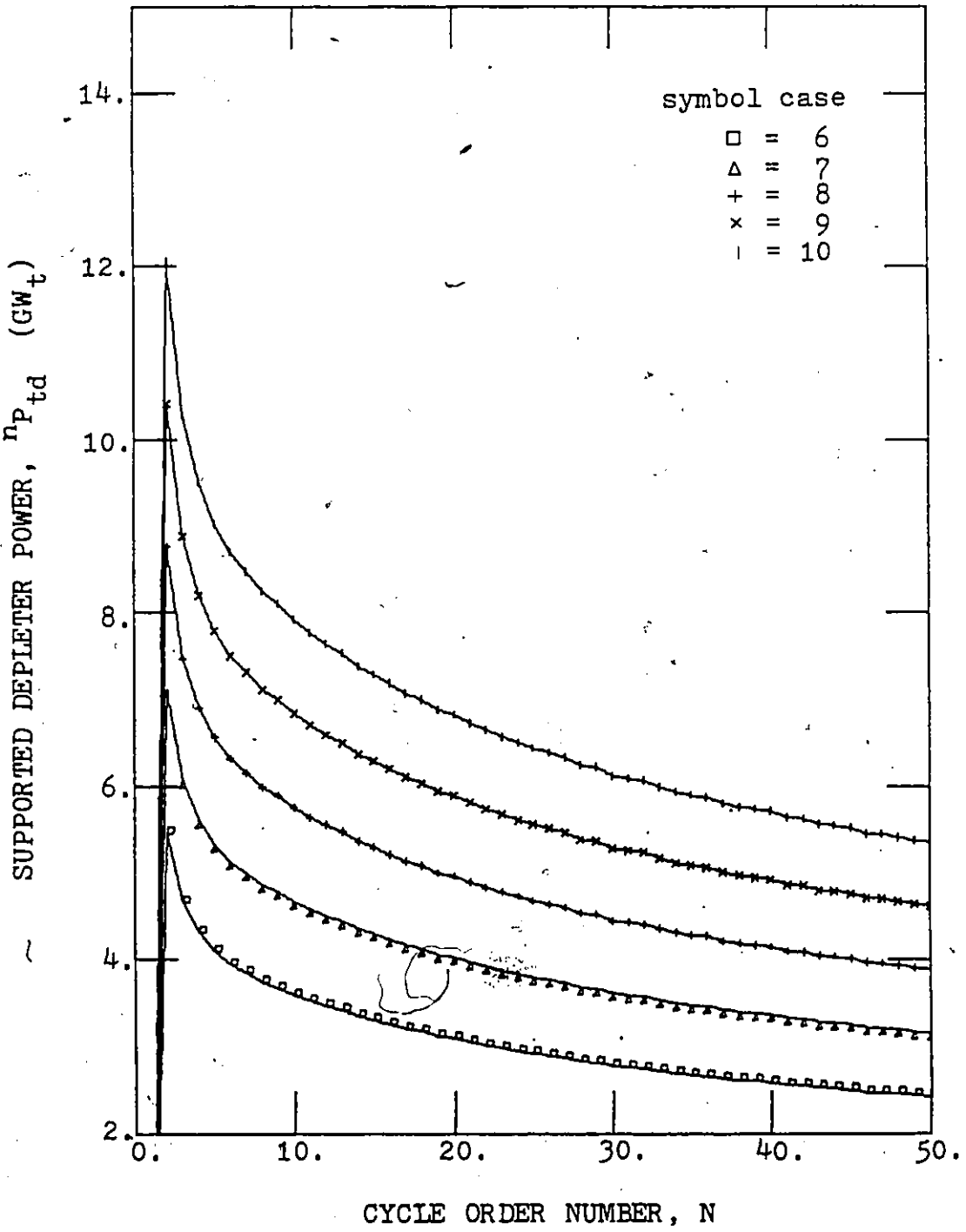

Fig. 4.6.2b Fuel supported depleter power without fuel reprocessing; cases 6 to 10 of Table 4.6.1.

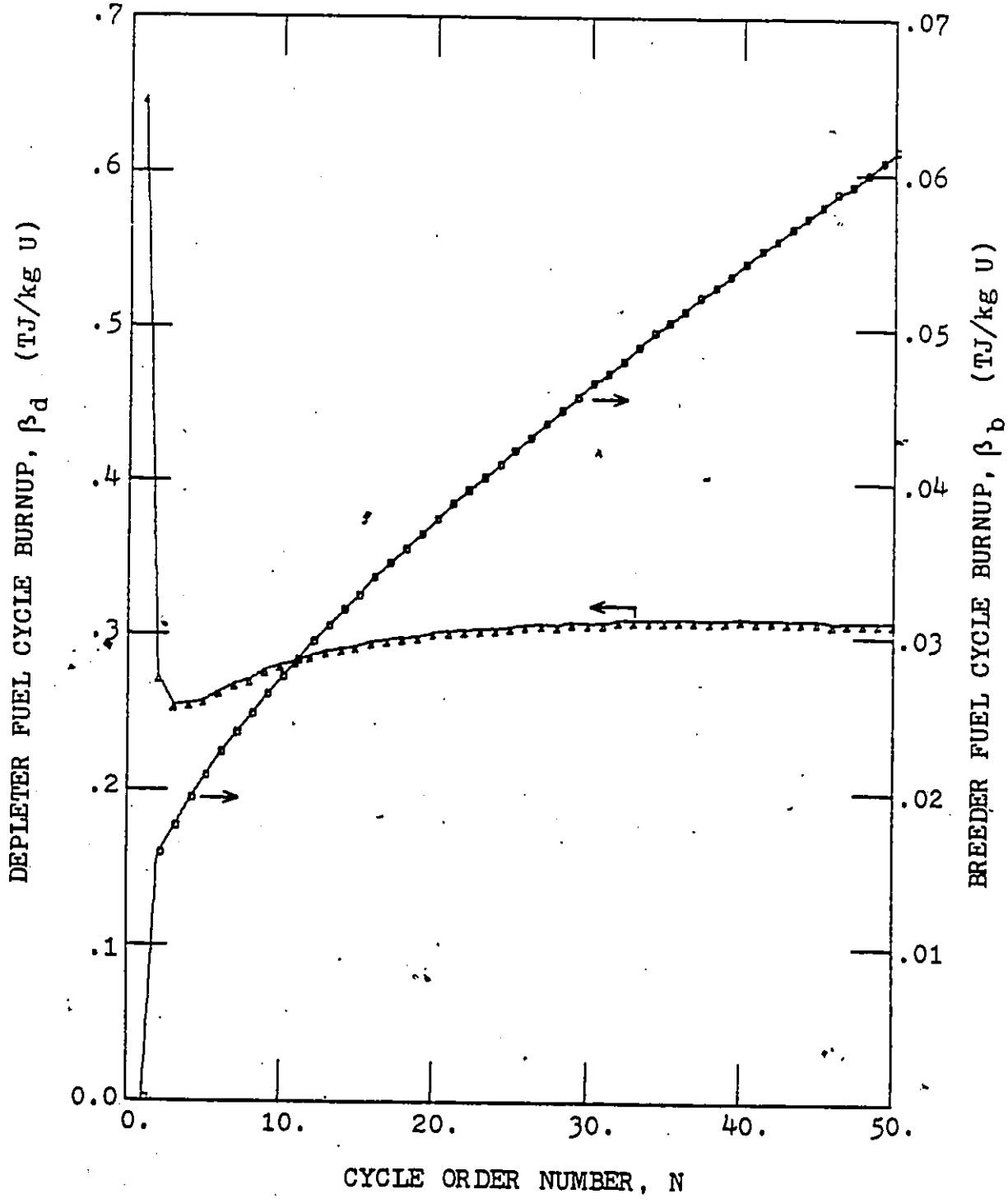

Fig. 4.6.3 Breeder and depleter fuel cycle burnup without fuel reprocessing; cases 1 to 10 of Table 4.6.1.

once-through fuel burnup of 7500 MWd/TU. Although Fig. 4.6.1 to Fig. 4.6.3 consist of discrete sets of points, for reason of clarity also lines joining them are shown. Figure 4.6.1 shows that the fuel produced breeder blanket power, $^{n}P_{tbb}$, increases steadily with increasing cycle number due to the increase in fissile fuel in the blanket. The supported thermal converter power however initially decreases rapidly with increasing cycle-number but levels out for high cycle-numbers. This effect is mainly due to the decrease in converter conversion ratio as can readily be seen in the system analysis of Sec. 4.3 and Sec. 4.4, particularly in Table 4.4.2, cases p to r.

The blanket and depleter powers, $^{n}P_{tbb}$ and $^{n}P_{td}$, for the system of fuel recycling with periodic chemical reprocessing including fission product removal are summarized in Fig. 4.6.4 and Fig. 4.6.5 with the corresponding fuel burnups given in Fig. 4.6.6. A solid line is again used to join the discrete case points. The high n performance, as expected, is greatly increased and power operation ranges are considerably reduced. The isolated points in Fig. 4.6.6 are the fuel burnups following fission product removal. In these cases reactivity is gained from fission product removal and a breeder subsystem is not required.

In the system formulation of supported power as

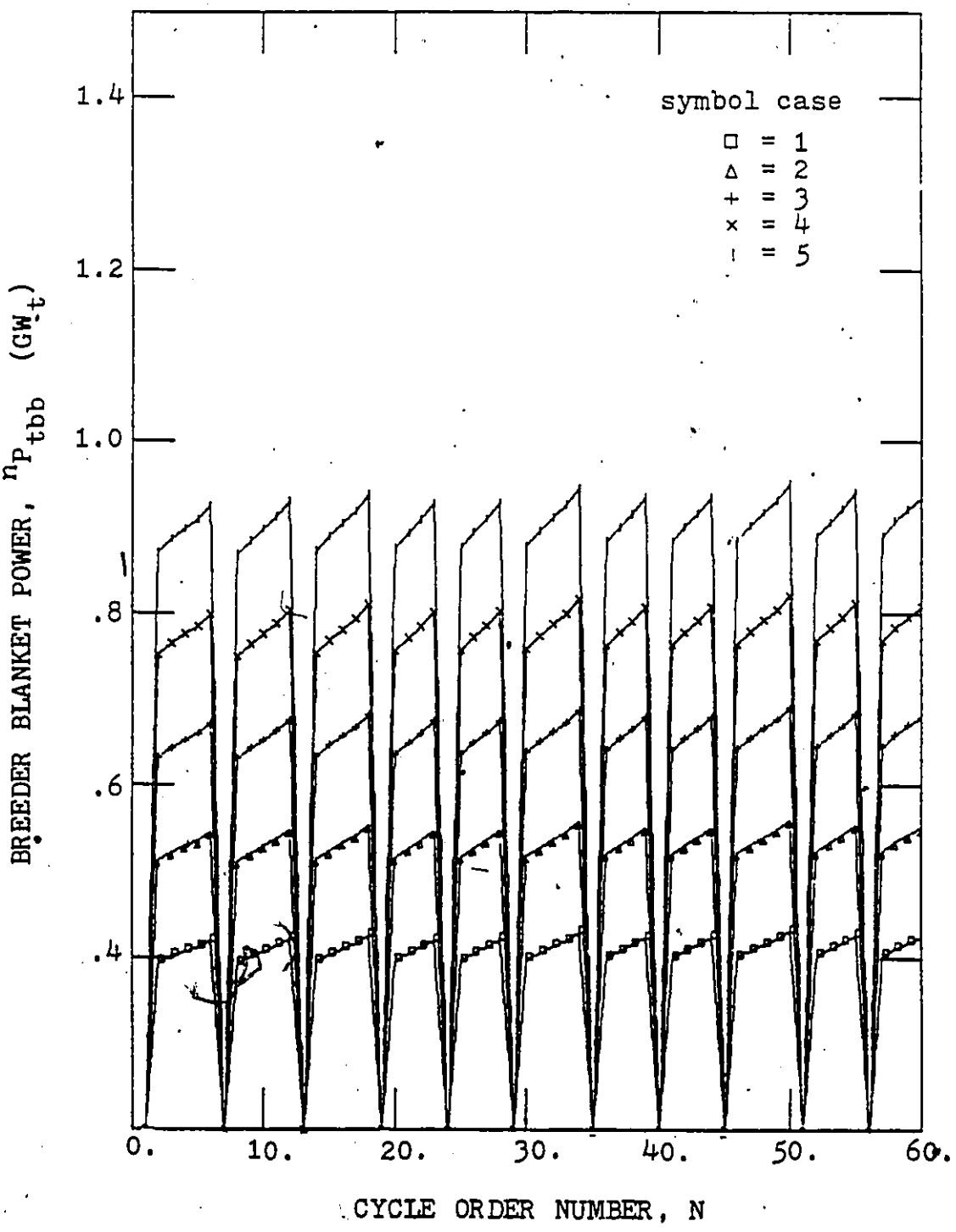

Fig. 4.6.4a Fuel cycle supported breeder blanket power with periodic fuel reprocessing; cases 1 to 5 of Table 4.6.1.

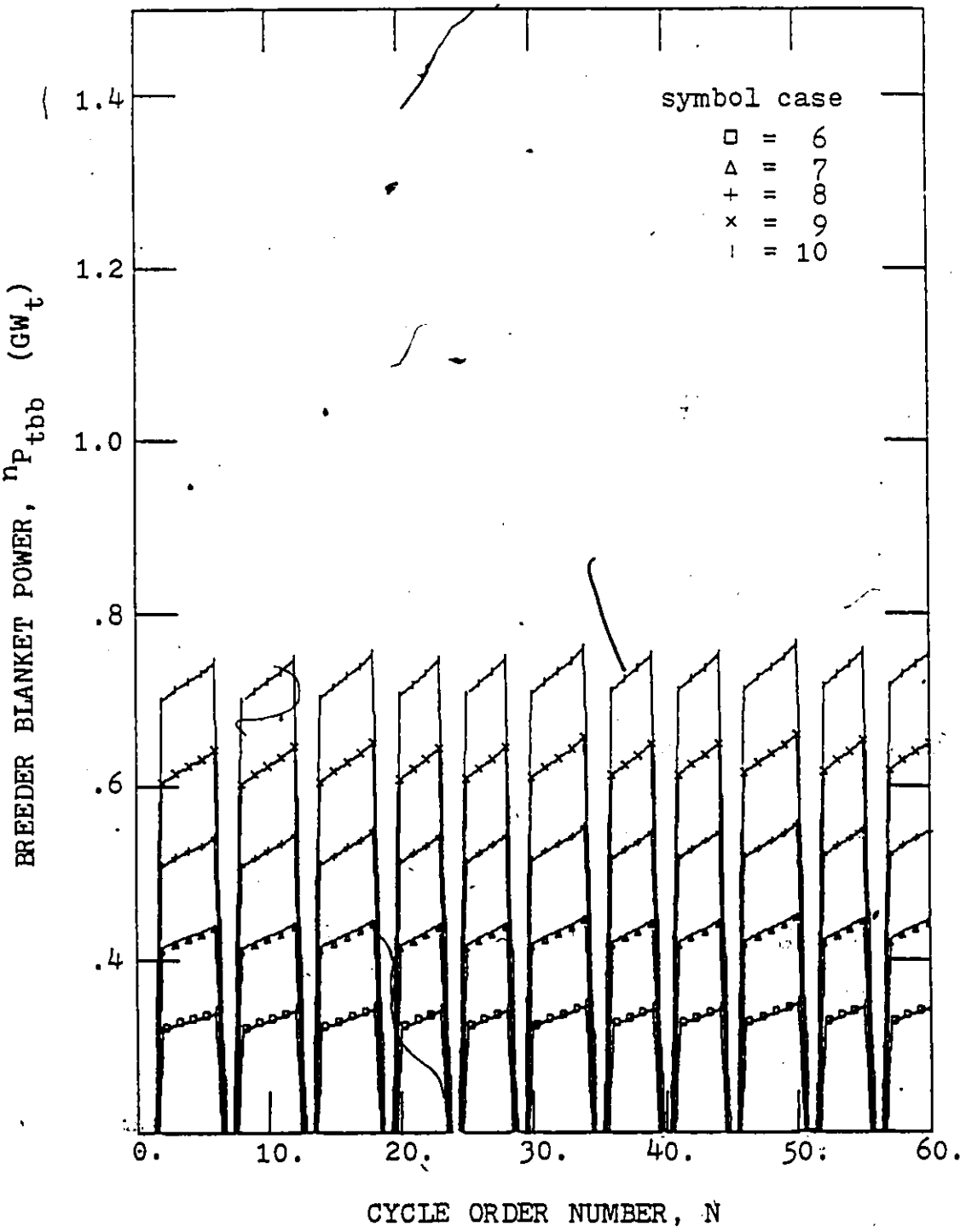

Fig. 4.6.4b Fuel cycle supported breeder blanket power with periodic fuel reprocessing; cases 6 to 10 of Table 4.6.1.

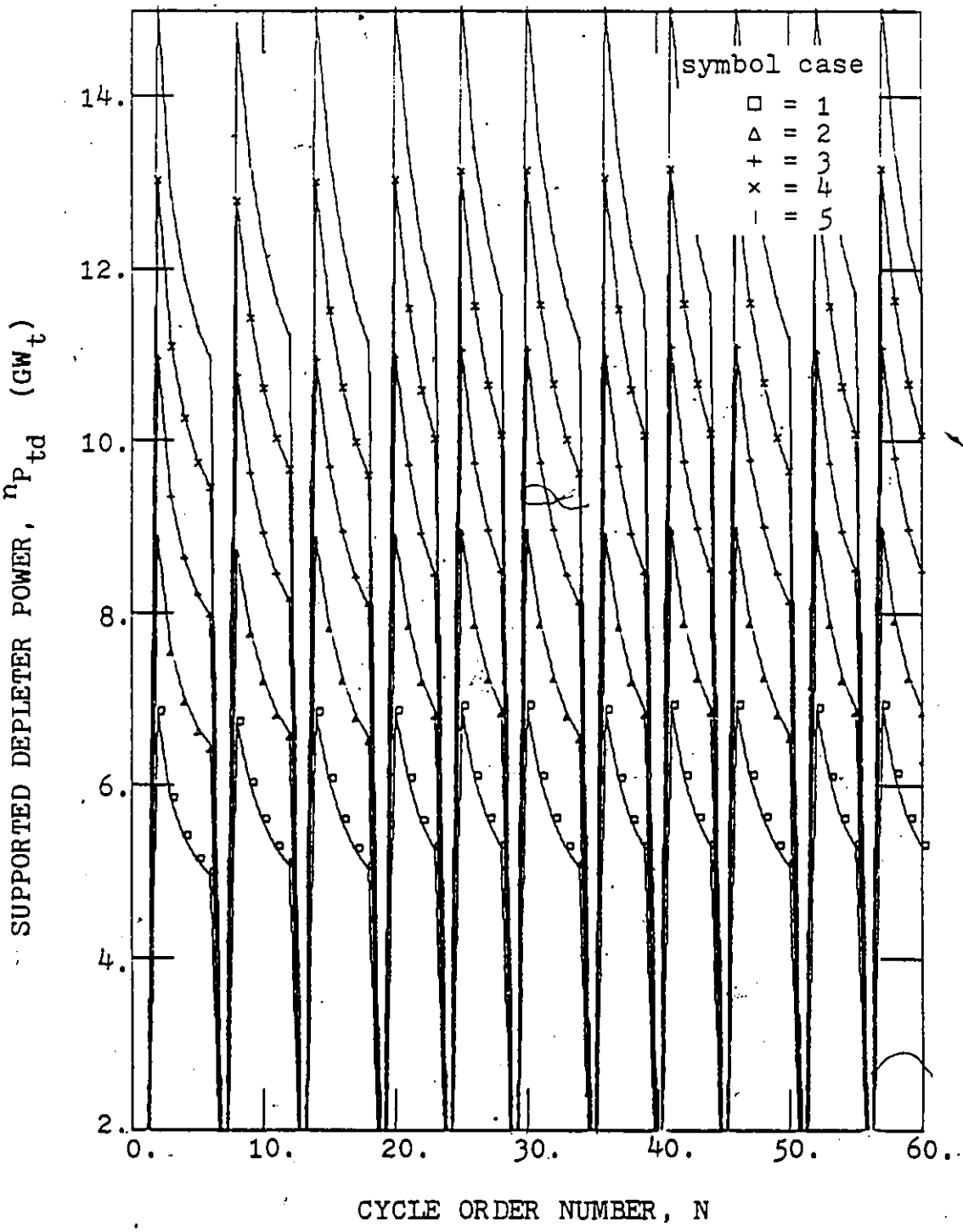

Fig. 4.6.5a Fuel cycle supported depleter power with periodic fuel reprocessing; cases 1 to 5 of Table 4.6.1.

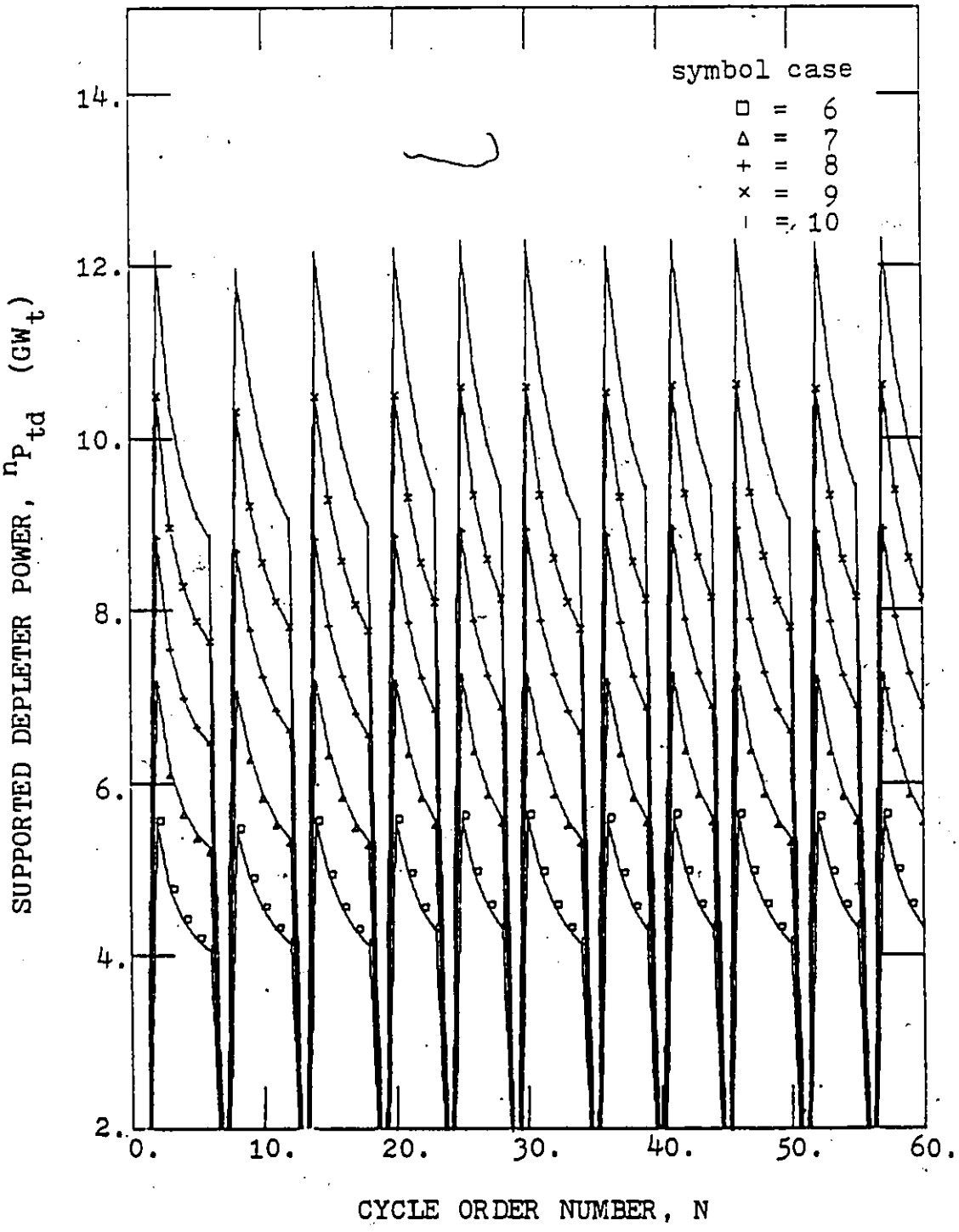

Fig. 4.6.5b Fuel cycle supported depleter power with periodic fuel reprocessing; cases 6 to 10 of Table 4.6.1.

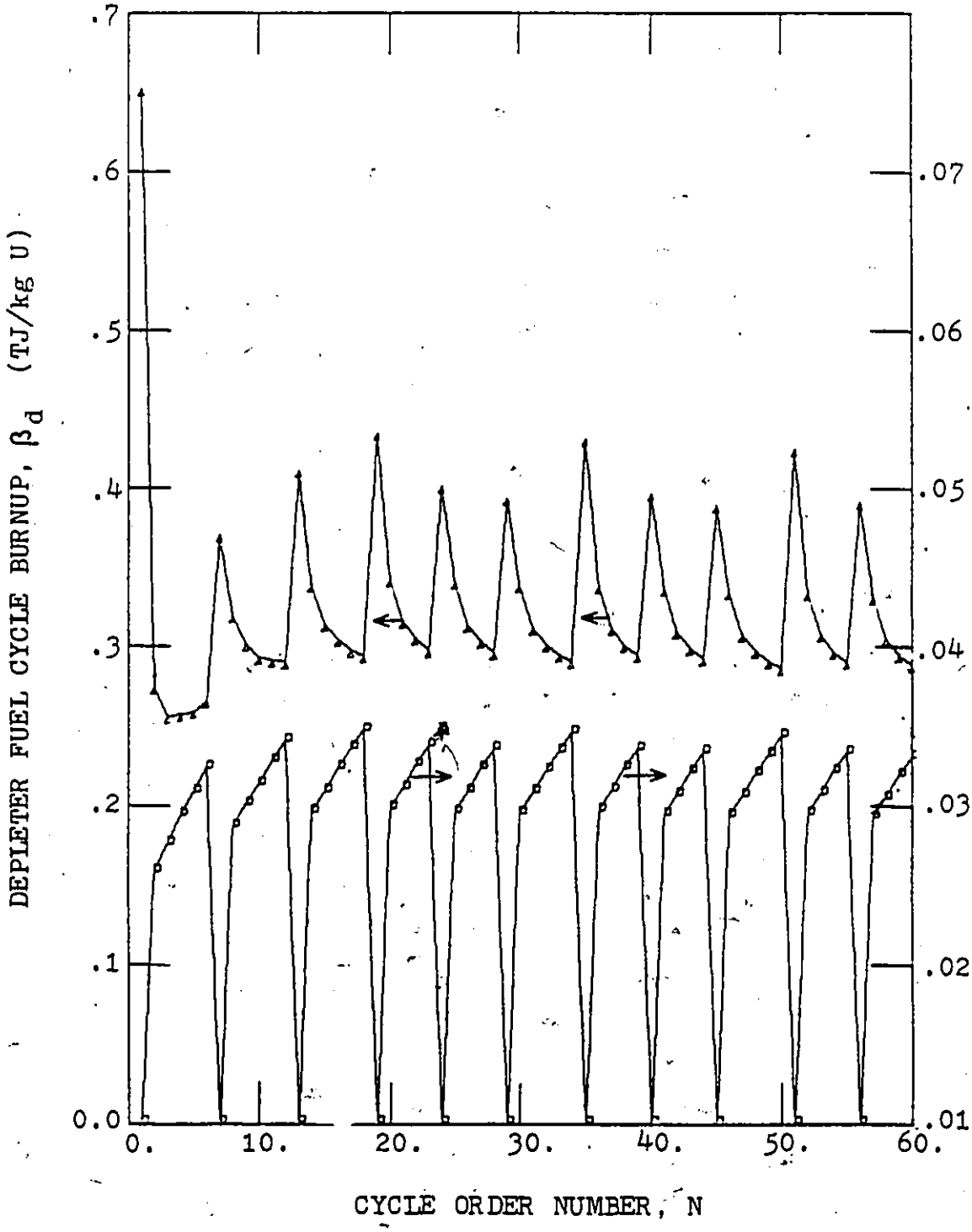

Fig. 4.6.6 Breeder and depleter fuel cycle burnup with periodic fuel reprocessing; cases 1 to 10 of Table 4.6.1.

defined by Eq. 4.6.1, each fuel cycle n is supported by the entire reference breeder subsystem. For a symbiotic system with fuel recycling, as shown in Fig. 4.5.2, Eq. 4.5.20 has to be satisfied for equilibrium steady state operation. Furthermore, to ease comparisons, it is generally required that the reference driving power of the breeder subsystem remains constant. The initial mass-energy flow of such a system, ${}^{1}R_{ic}$, is now derived. For a multicycle system a breeder subsystem can only devote a fraction, ${}^{n}x$, of its' total breeding capacity for breeding in each cycle n. This fraction is defined by

$$ {}^{n}x = {}^{n}R_{ic} / {}^{n}R_{i}, \tag{4.6.2} $$

where ${}^{n}R_{i}$ is the isolated cycle initial mass-energy flow rate. ${}^{n}R_{i}$ can be obtained from Eq. 4.5.1 to yield

$$ {}^{n}R_{i} = {}^{n}R_{oh} \tag{4.6.3} $$

since the initial conditions

$$ {}^{n}R_{oe} = {}^{n}R_{op} = {}^{n}R_{ow} = 0 \tag{4.6.4} $$

do not eliminate the generality of the formulation. The entire reference breeder is therefore supporting fuel-mass feed rate ${}^{n}R_{oh}$, defined by Eq. 4.2.18, where use is made of Eq. 4.5.15. Employing the recursive relation Eq. 4.5.20, Eq. 4.6.2 can be rewritten to yield

$$ {}^{n}x = \prod_{m=1}^{n} (1 - {}^{m}\delta') \, {}^{1}R_{ic} / {}^{n}R_{i} , \tag{4.6.5} $$

where, for convenience, one defines

$$ {}^{m+1}\delta' = {}^{m}\delta \qquad (4.6.6) $$

and

$$ {}^{1}\delta' = 0 \ . \qquad (4.6.7) $$

For individual fuel cycles ℓ which do not require a breeder subsystem it follows that

$$ {}^{\ell}x = 0 \ . \qquad (4.6.8) $$

The sum of all breeder fractions, ${}^{n}x$, has to yield unity, or by using Eq. 4.6.8 one obtains

$$ \sum_{n \neq \ell}^{N} {}^{n}x = 1 \ , \qquad (4.6.9) $$

where N is the highest fuel cycle. Substituting Eq. 4.6.5 into Eq. 4.6.9 and solving for ${}^{1}R_{ic}$ yields

$$ {}^{1}R_{ic} = \left(\sum_{n \neq \ell}^{N} \prod_{m=1}^{n} (1 - {}^{m}\delta') \ / \ {}^{n}R_{i} \right)^{-1} \ . \qquad (4.6.10) $$

By using the general system definition Eq. 4.2.21, the average supported fuel powers for an N-cycle system is given by

$$ P_{td} = {}^{1}R_{ic} \ \beta_{d} \qquad (4.6.11) $$

and

$$ P_{tbb} = {}^{1}R_{ic} \ \beta_{b} \qquad (4.6.12) $$

for depleter and breeder subsystems respectively. An alternative formulation is

$$ P_{td} = \sum_{n=1}^{N} {}^{n}R_{ic} \ {}^{n}\beta_{d} \qquad (4.6.13) $$

and

$$P_{tbb} = \sum_{n=1}^{N} {}^{n}R_{ic}\, {}^{n}\beta_{b} \,. \qquad (4.6.14)$$

By using the recursive relation Eq. 4.5.20 as well as Eq. 4.6.6 and Eq. 4.6.7, Eq. 4.6.13 and Eq. 4.6.14 can be rewritten to yield

$$P_{td} = {}^{1}R_{ic} \left(\sum_{n=1}^{N} \prod_{m=1}^{n} (1 - {}^{m}\delta') \, {}^{n}\beta_{d} \right) \qquad (4.6.15)$$

and

$$P_{tbb} = {}^{1}R_{ic} \left(\sum_{n=1}^{N} \prod_{m=1}^{n} (1 - {}^{m}\delta') \, {}^{n}\beta_{b} \right) . \qquad (4.6.16)$$

Comparing Eq. 4.6.11 with Eq. 4.6.15 and Eq. 4.6.12 with Eq. 4.6.16 the total depleter and breeder burnups emerge as

$$\beta_{d} = \sum_{n=1}^{N} \prod_{m=1}^{n} (1 - {}^{m}\delta') \, {}^{n}\beta_{d} \qquad (4.6.17)$$

and

$$\beta_{b} = \sum_{n=1}^{N} \prod_{m=1}^{n} (1 - {}^{m}\delta') \, {}^{n}\beta_{b} \,. \qquad (4.6.18)$$

A total system fuel burnup can be defined as

$$\beta_{t} = \beta_{d} + \beta_{b} \,, \qquad (4.6.19)$$

the sum of depleter and breeder fuel burnups.

The symbiotic system parameters discussed so far have been expressed as a function of the fuel cycle n or the total number of fuel cycles N. An alternative is to express system parameters as a function of total fuel burnup, β_{t}, at the end of the associated cycle n. The isolated cycle mass-energy flow rate, ${}^{n}R_{i}$, is therefore

$$^{n}R_i = R_i(\beta_t), \tag{4.6.20}$$

while

$$^{1}R_{ic} = {}^{1}R_{ic}(\beta_t), \tag{4.6.21}$$

and dependent on the final burnup of the system's highest cycle N. Figure 4.6.7 shows the isolated cycle mass-energy flow rate, $R_i(\beta_t)$, and the multicycle mass-energy flow rate, $^{1}R_{ic}(\beta_t)$, for the system without reprocessing. For convenience, the multicycle model as shown in Fig. 4.5.2 has been chosen such that

$$^{n}\delta = 0. \tag{4.6.22}$$

Similar to Fig. 4.6.7, the mass-energy flow rates of the symbiotic system with periodic fission product removal is shown in Fig. 4.6.8. For fuel cycles without reprocessing, Eq. 4.6.22 is still valid, however after reprocessing only the heavy element fuel is retained in the mass-energy flow of the system. The associated mass-energy loss fraction, as defined by Eq. 4.5.16, of such cycles is summarized in Table 4.6.2 with its' corresponding total fuel burnup as defined by Eq. 4.6.19. The average supported fuel powers, P_{td} and P_{tbb} as given by Eq. 4.6.11 and Eq. 4.6.12 for a multicycle system, are shown in Fig. 4.6.9 and Fig. 4.6.10 respectively. For comparison the powers with the reprocessing scheme are shown in Fig. 4.6.11 and Fig. 4.6.12. It can be seen that the converter and breeder fuel powers are more uniform for a scheme with periodic fission product removal.

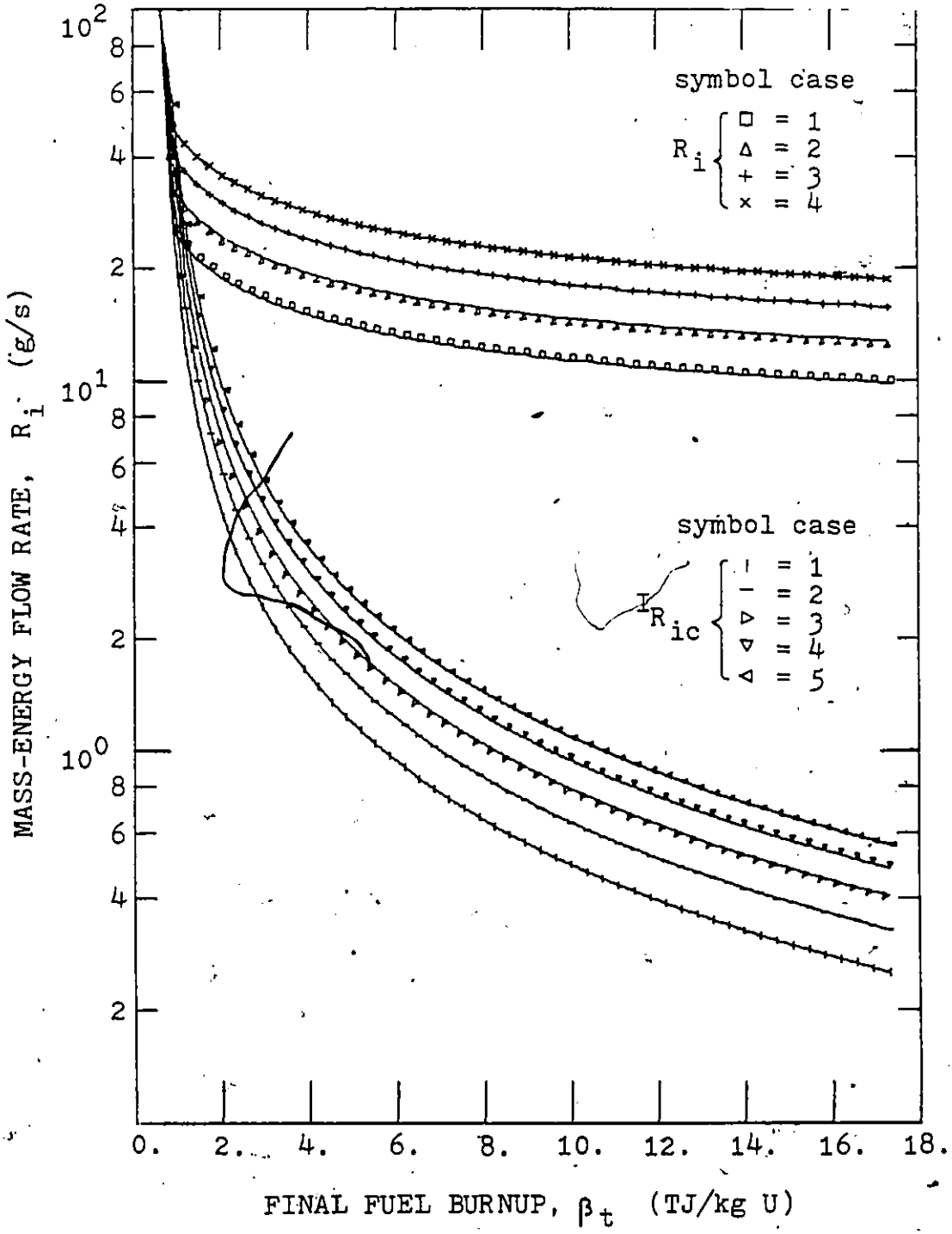

Fig. 4.6.7a Symbiotic system mass-energy flow rates without fuel reprocessing; cases 1 to 5 of Table 4.6.1.

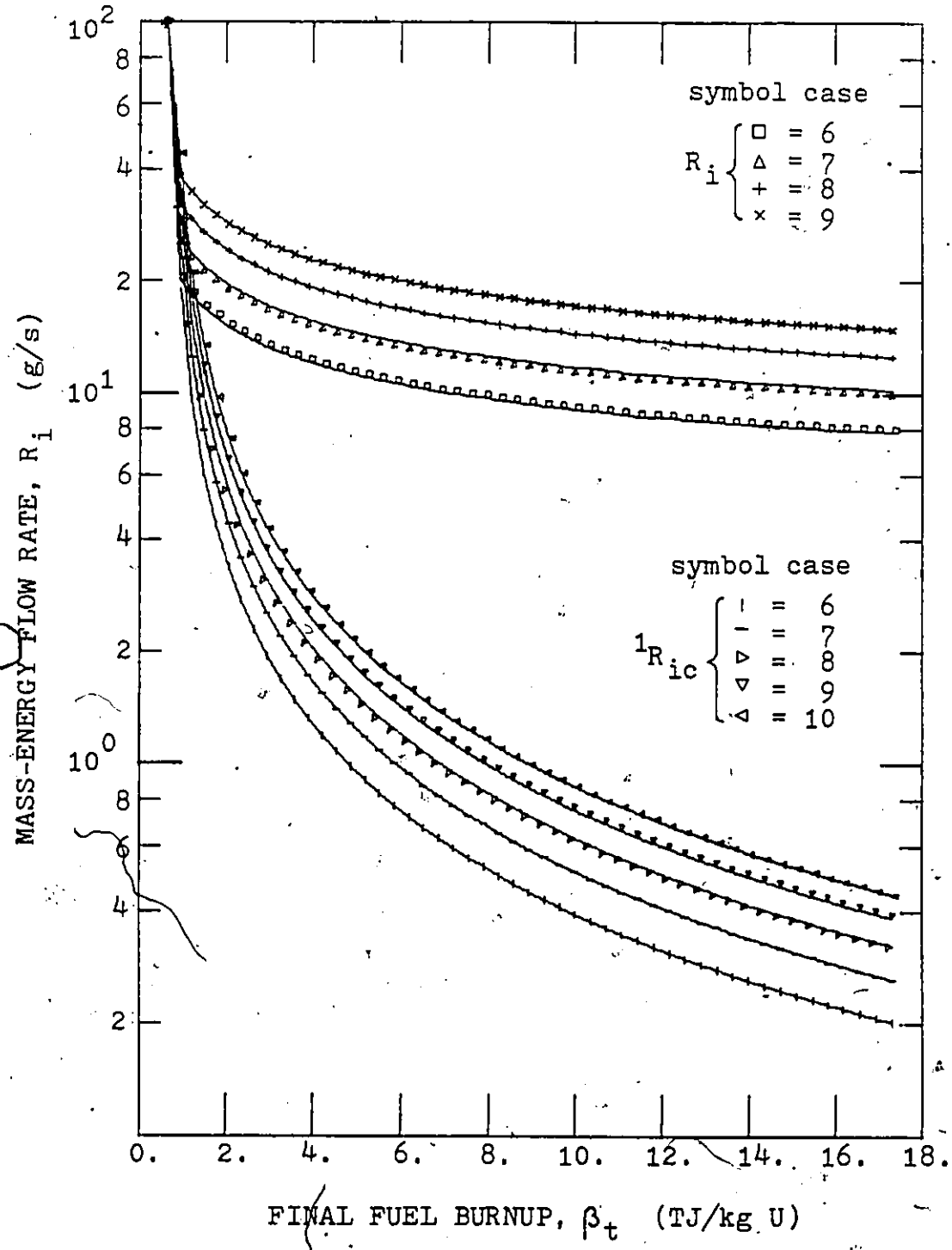

Fig. 4.6.7b Symbiotic system mass-energy flow rates without fuel reprocessing; cases 6 to 10 of Table 4.6.1.

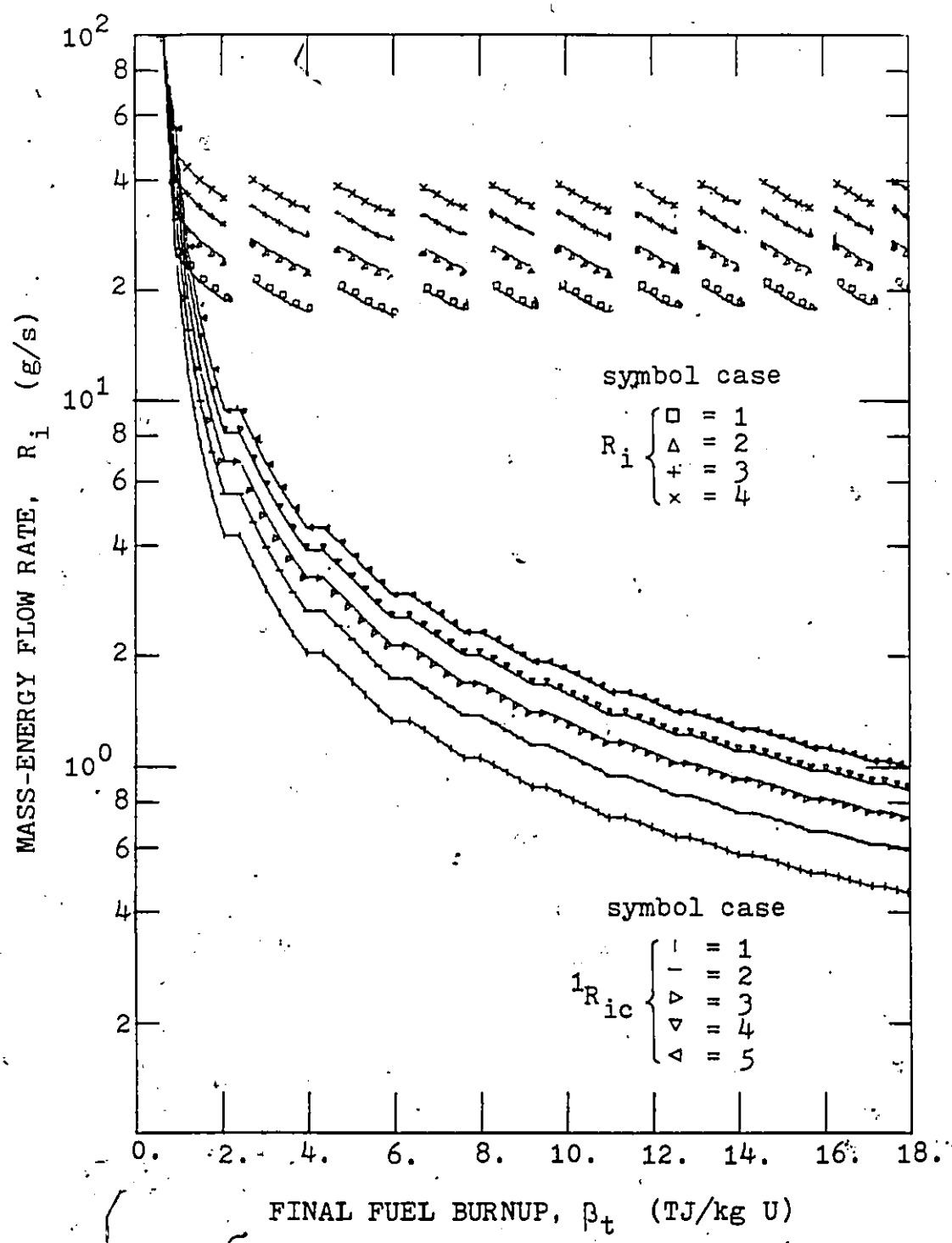

Fig. 4.6.8a Symbiotic system mass-energy flow rates with periodic fuel reprocessing; cases 1 to 5 of Table 4.6.1.

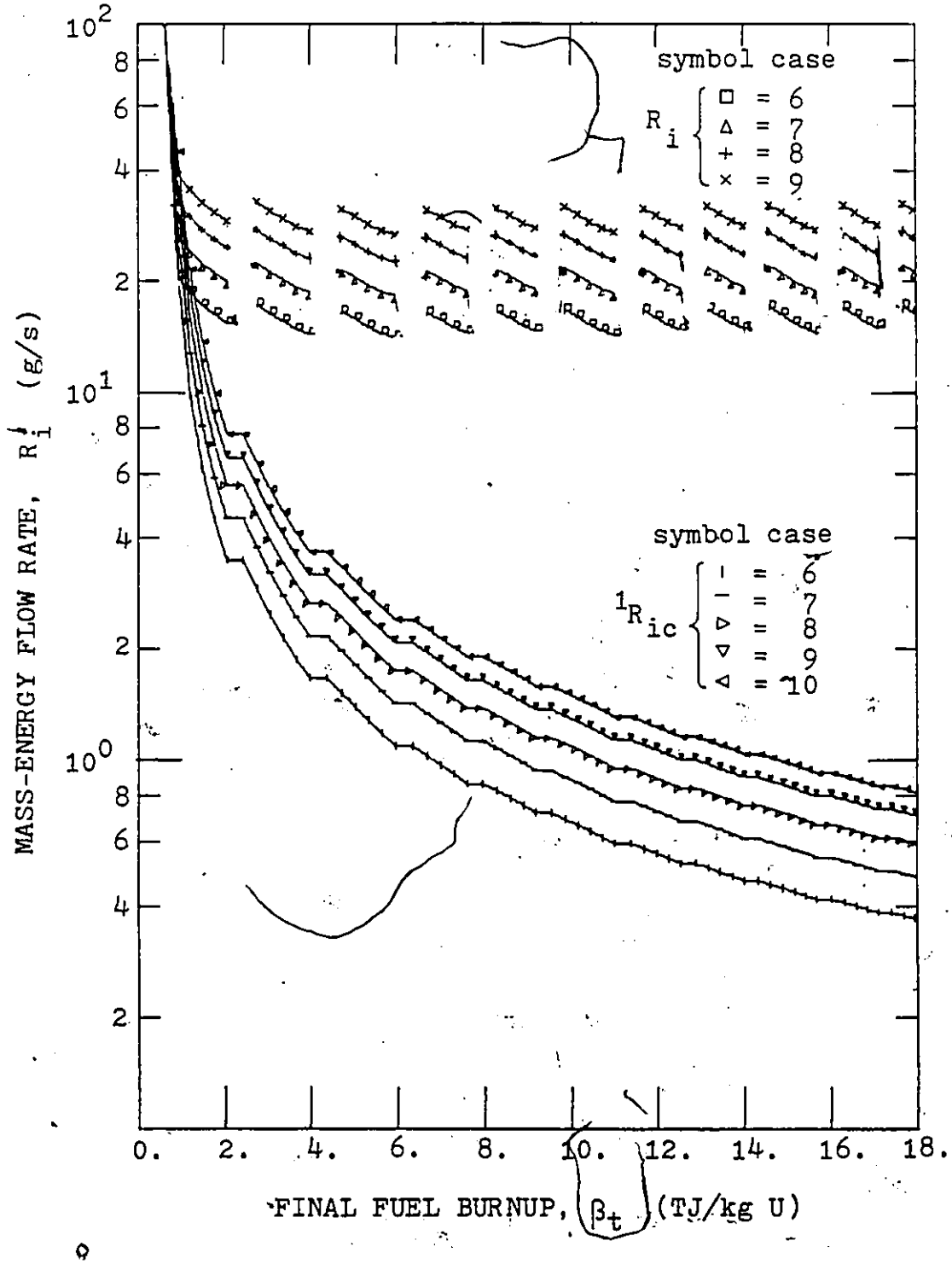

Fig. 4.6.8b Symbiotic system mass-energy flow rates with periodic fuel reprocessing; cases 6 to 10 of Table 4.6.1.

Table 4.6.2 Fractional mass-energy loss for system cycles with reprocessing

Cycle Order Number 'n'	β_t Eq. 4.6.19 (TJ/kgU)	n_δ Eq. 4.5.16
6	2.051	0.0241
12	3.972	0.0230
18	5.943	0.0241
23	7.599	0.0207
28	9.182	0.0203
34	11.001	0.0237
39	12.534	0.0205
44	14.000	0.0200
50	15.683	0.0234
55	17.101	0.0202

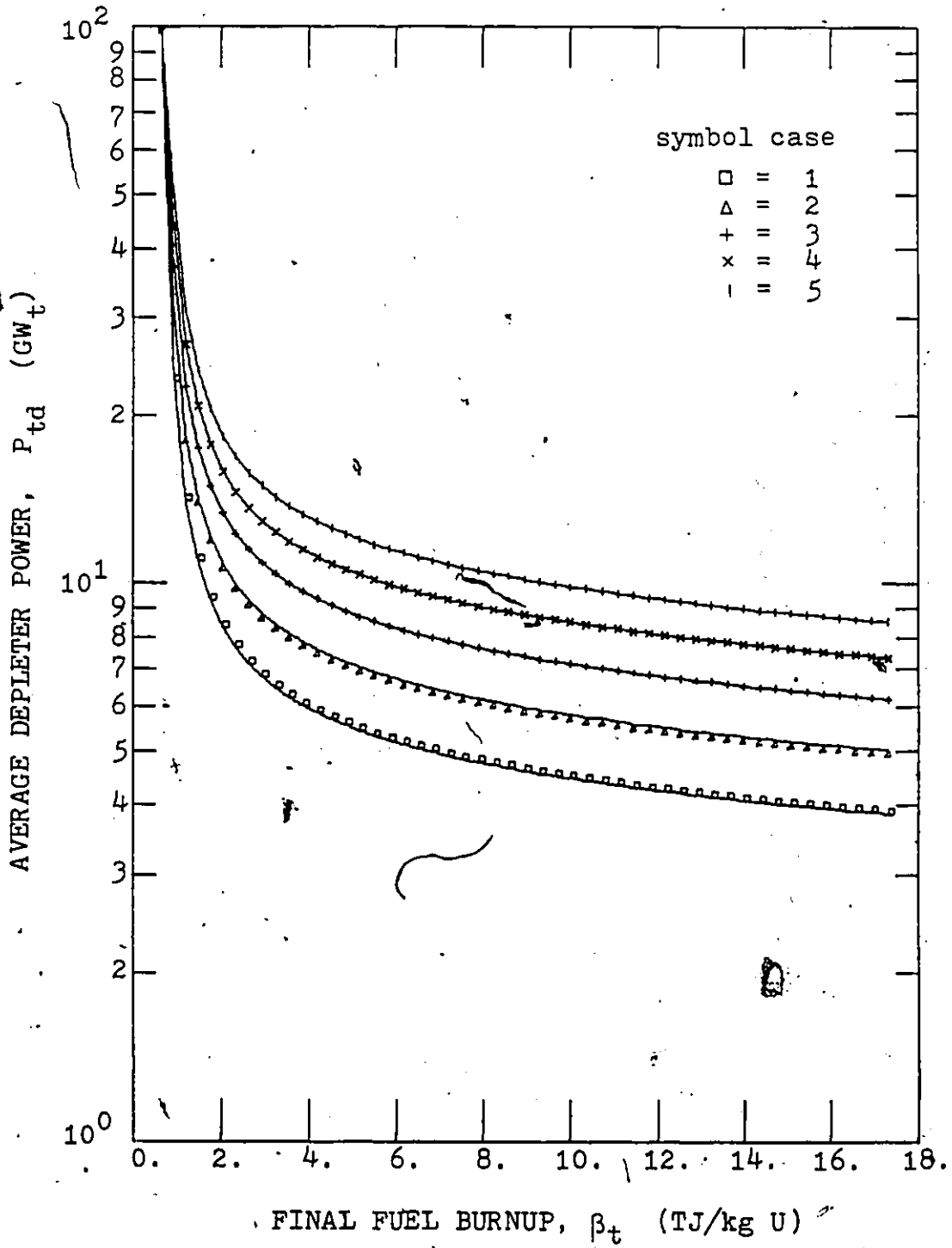

Fig. 4.6.9a System supported average depleter power without fuel reprocessing; cases 1 to 5 of Table 4.6.1.

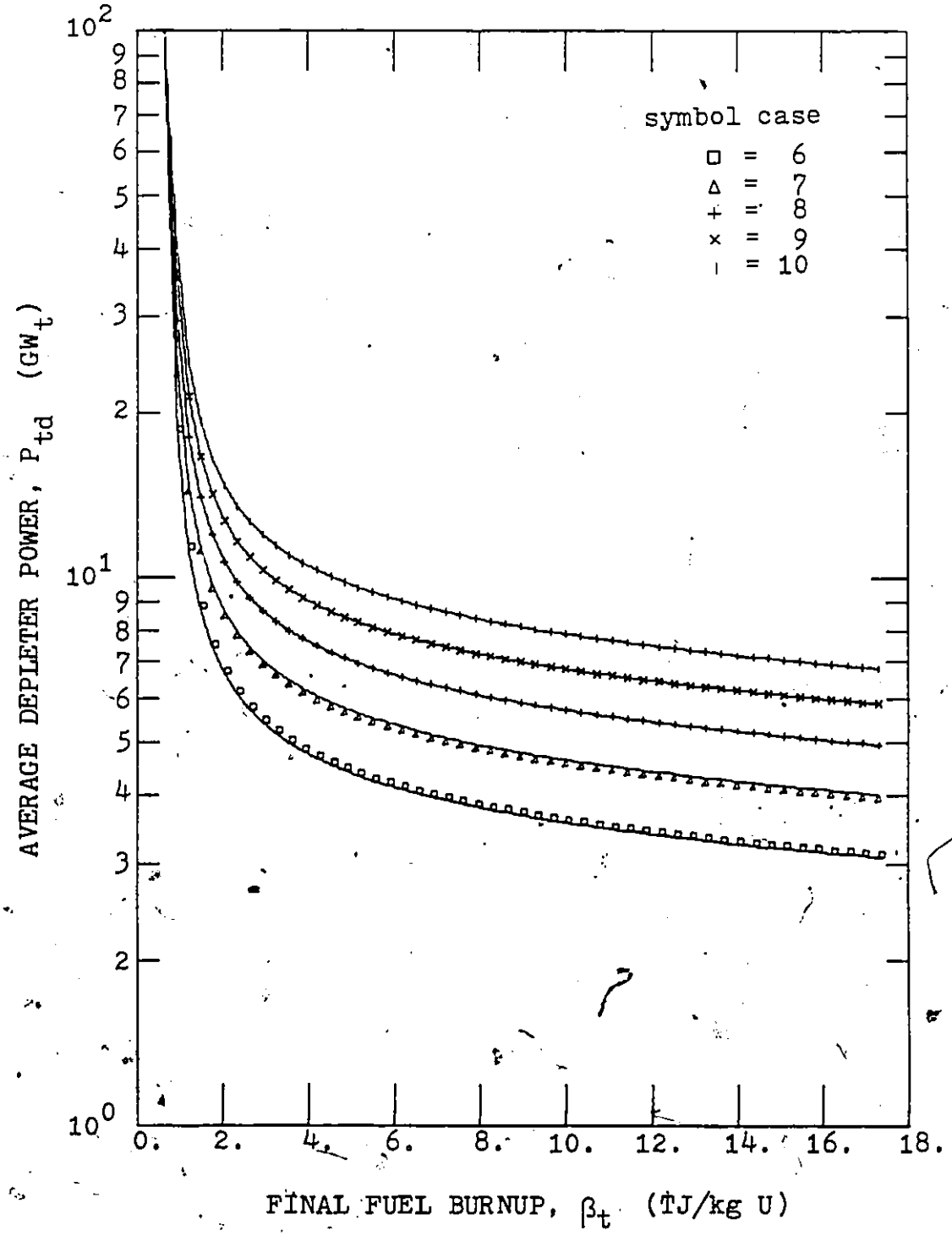

Fig. 4.6.9b System supported average depleter power without fuel reprocessing; cases 6 to 10 of Table 4.6.1.

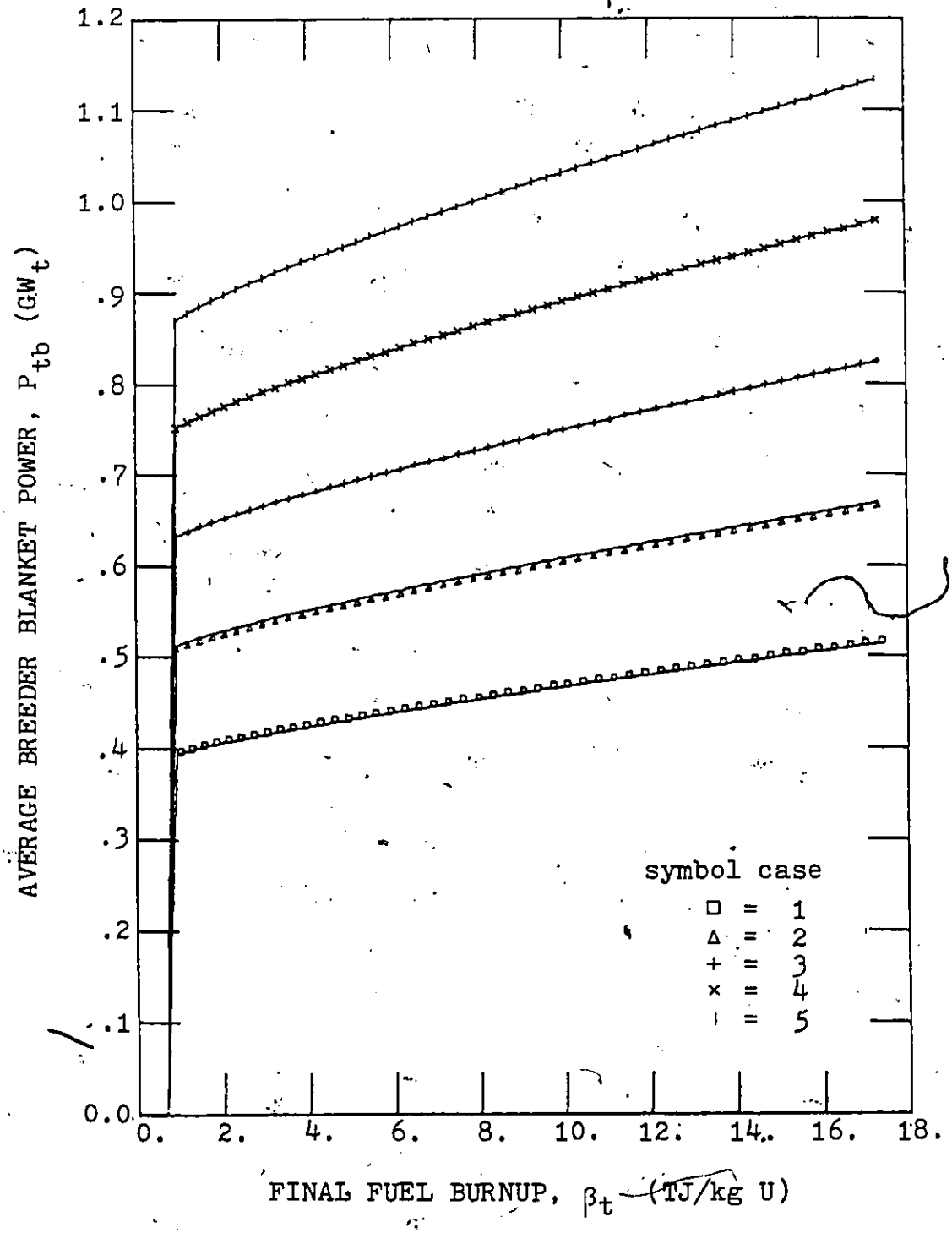

Fig. 4.6.10a Average fuel supported breeder blanket power without fuel reprocessing; cases 1 to 5 of Table 4.6.1.

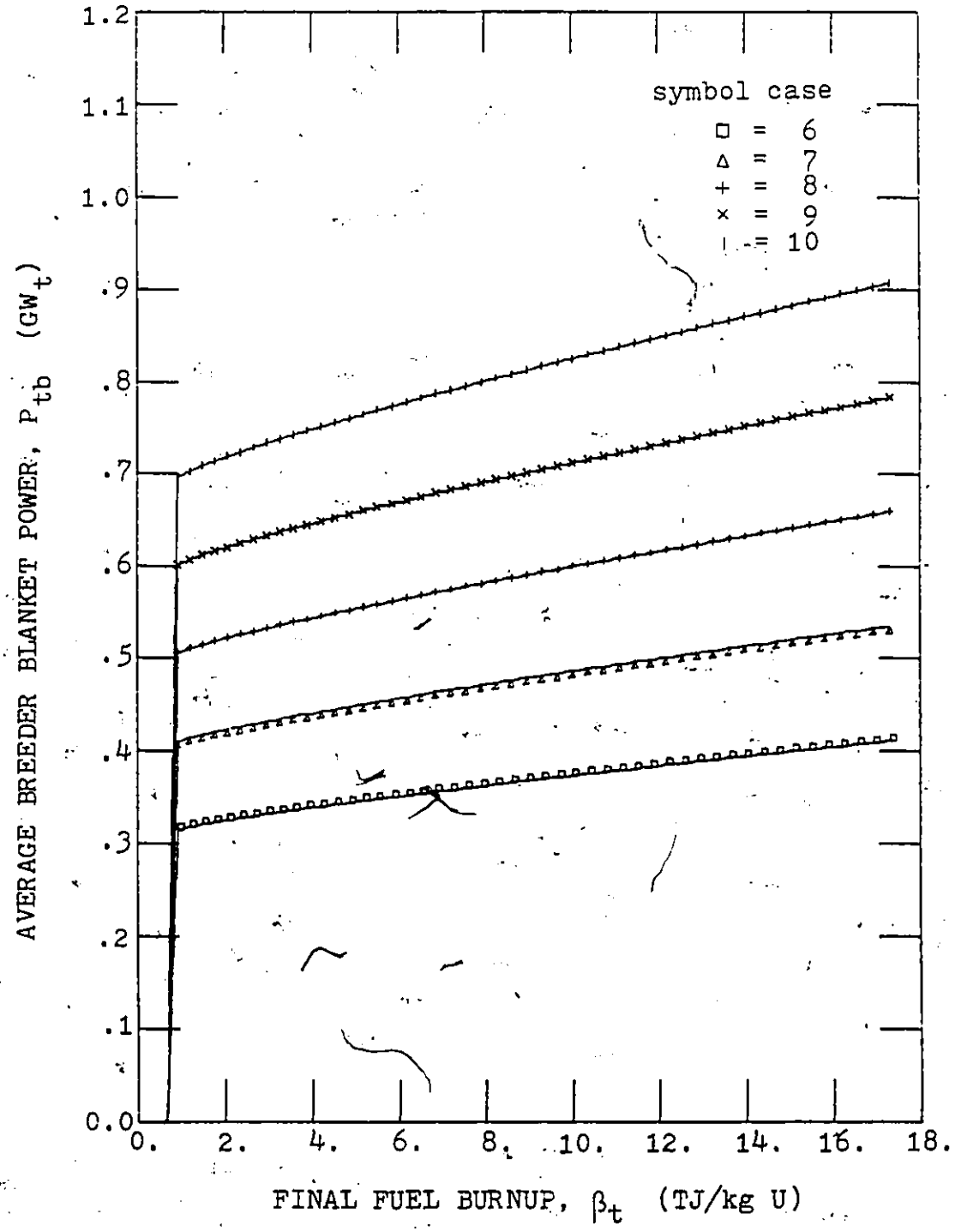

Fig. 4.6.10b Average fuel supported breeder blanket power without fuel reprocessing; cases 6 to 10 of Table 4.6.1.

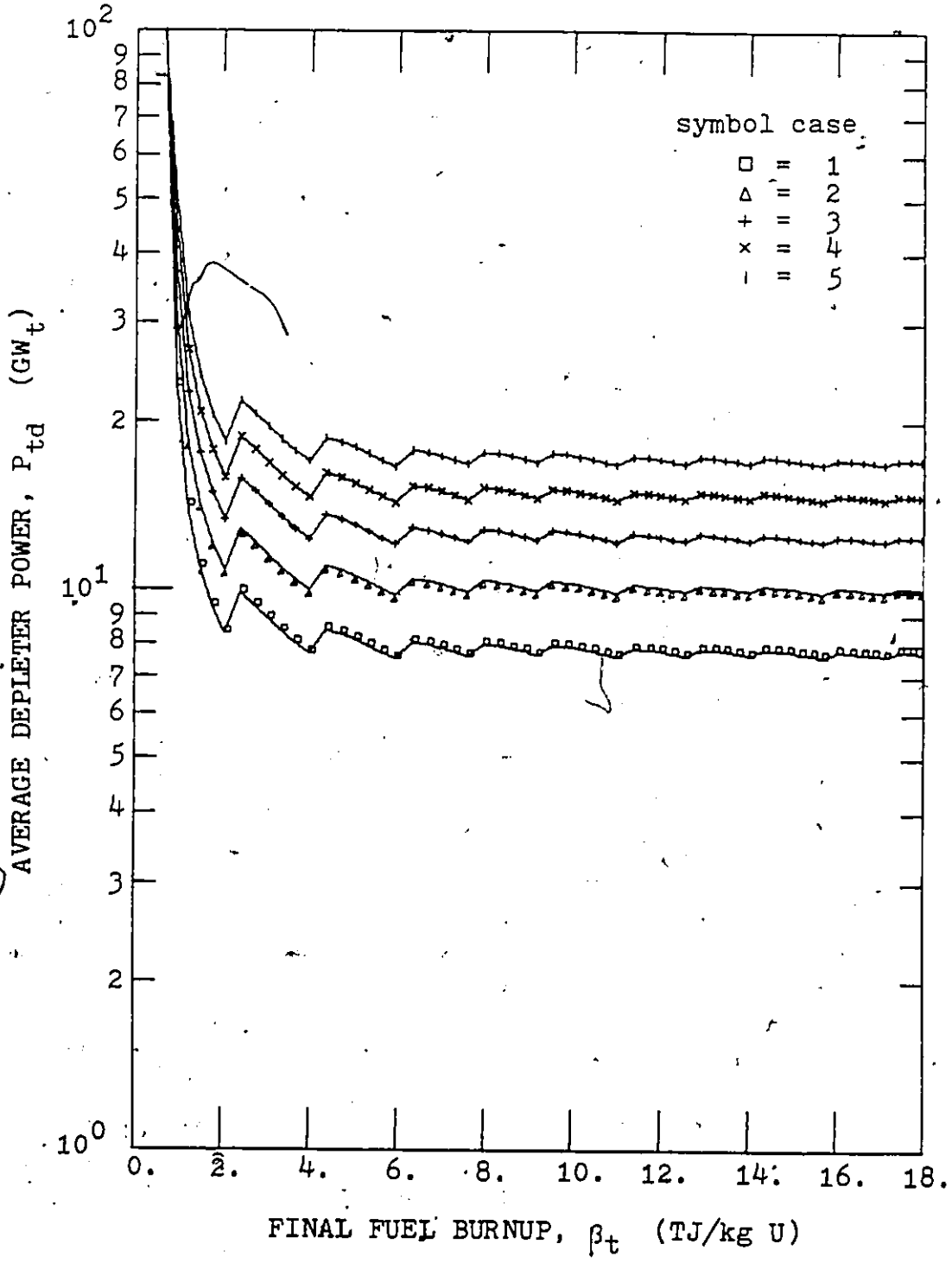

Fig. 4.6.11a System supported average depleter power with periodic fuel reprocessing; cases 1 to 5 of Table 4.6.1.

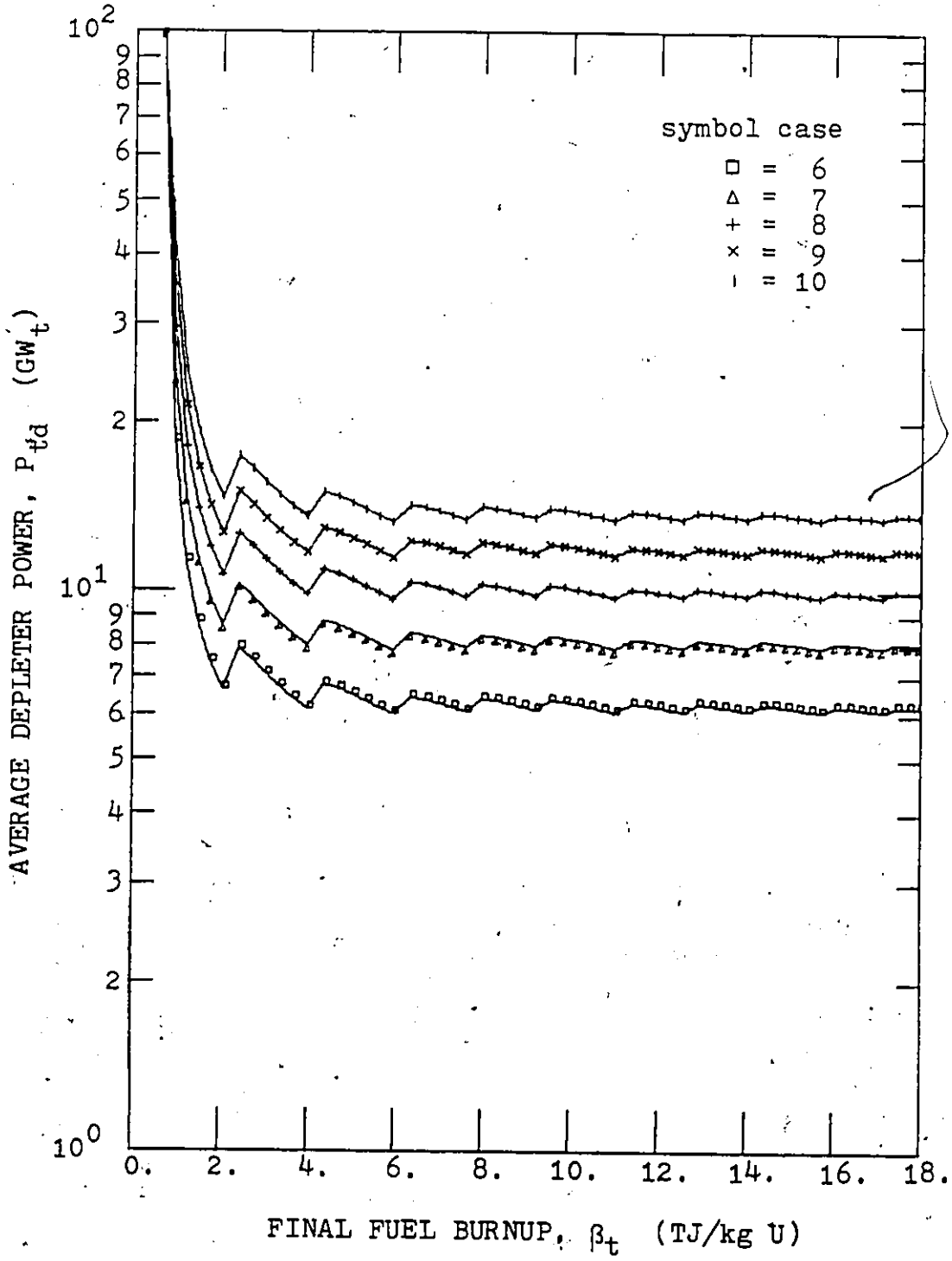

Fig. 4.6.11b System supported average depleter power with periodic fuel reprocessing; cases 6 to 10 of Table 4.6.1.

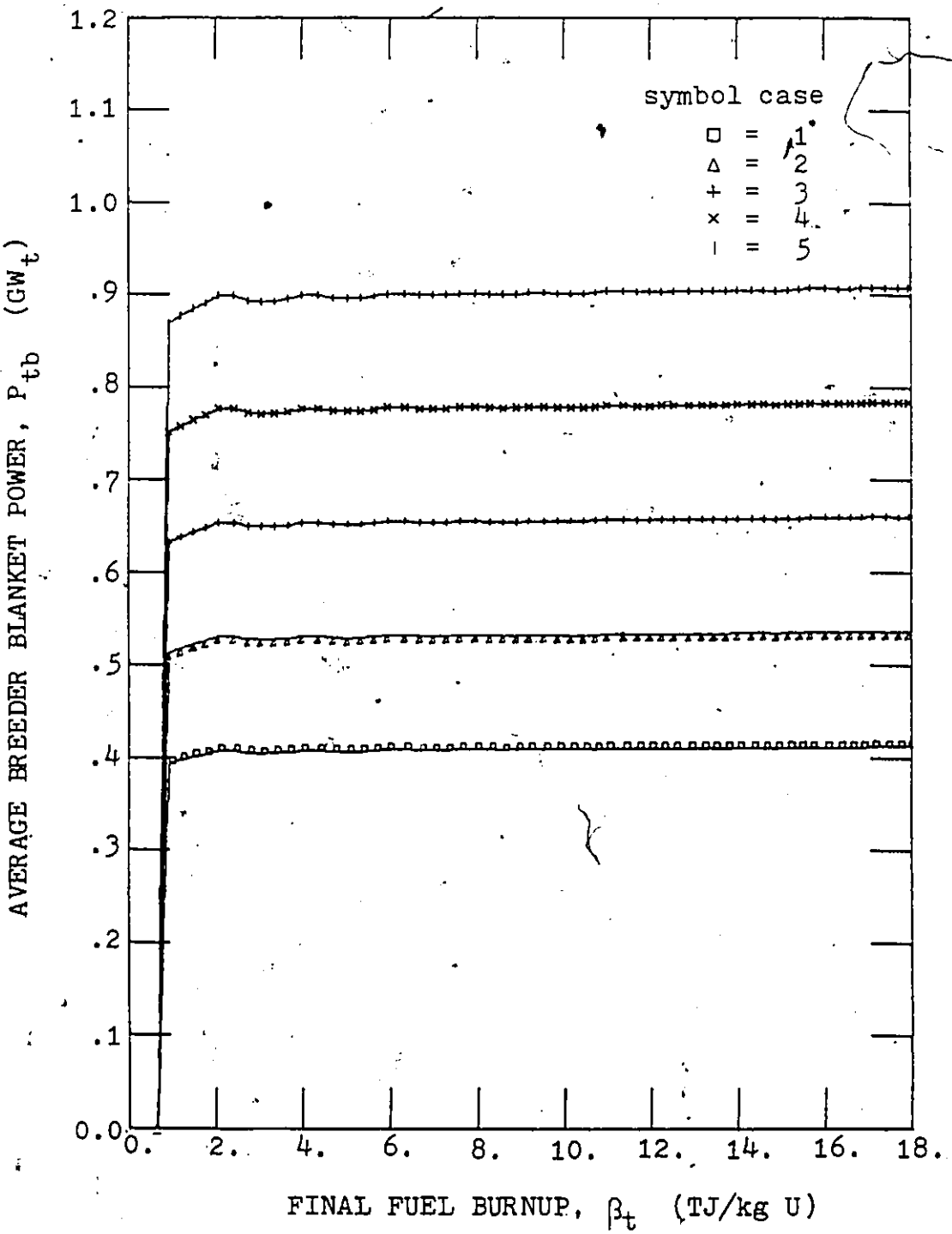

Fig. 4.6.12a Average fuel supported breeder blanket power with periodic fuel reprocessing; cases 1 to 5 of Table 4.6.1.

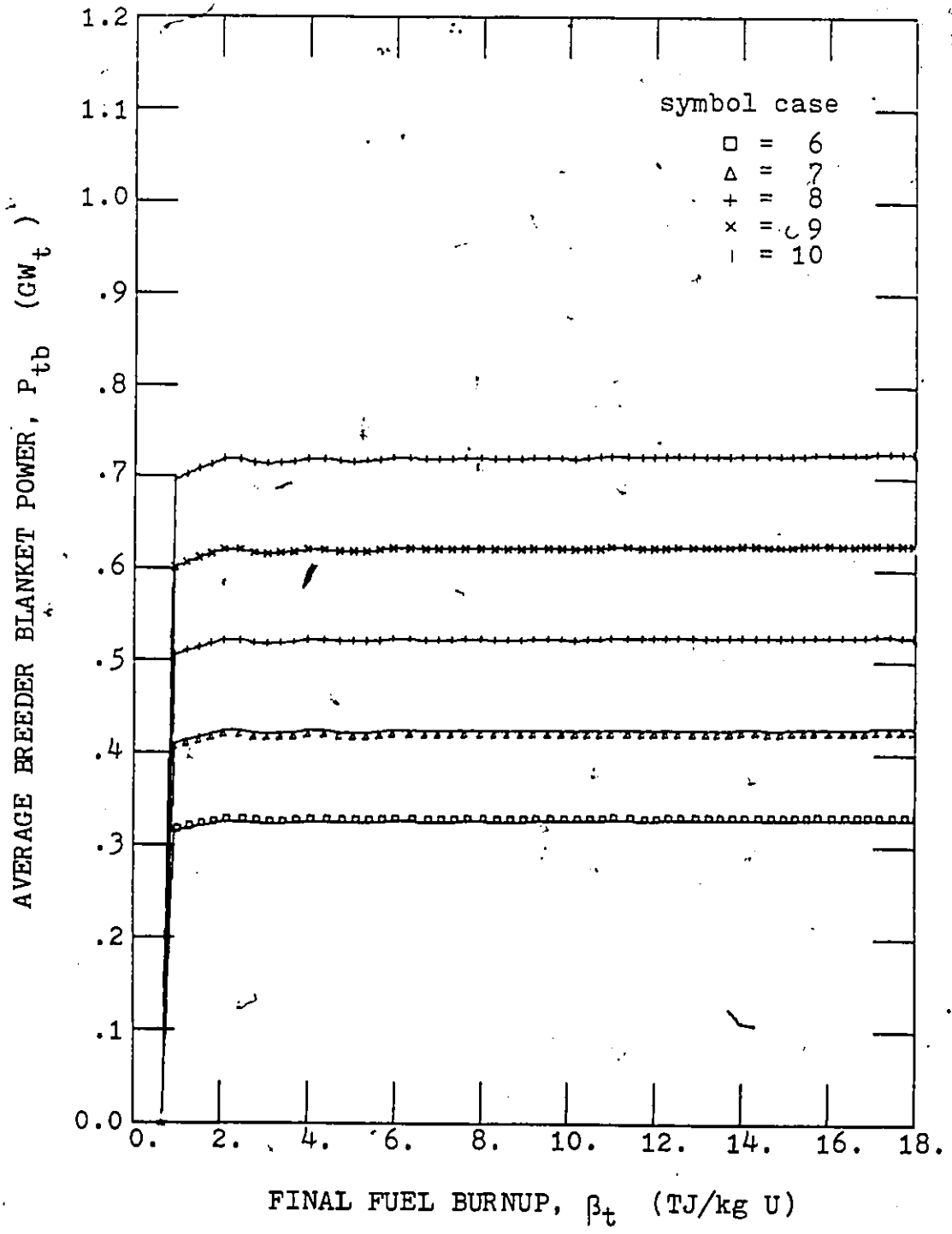

Fig. 4.6.12b Average fuel supported breeder blanket power with periodic fuel reprocessing; cases 6 to 10 of Table 4.6.1..

A homogenized subcritical multiplication factor for a multicycle system can be obtained from Eq. 4.2.13 to yield

$$k_{\infty b} = \frac{\sum_{n \neq \ell}^{N} n_x \, n_{R_{pn}}}{\sum_{n \neq \ell}^{N} n_x \, n_{R_{an}}} , \qquad (4.6.23)$$

where n_x is the cycle breeder fraction of Eq. 4.6.9 and the cycle averaged neutron production and absorption rates are defined respectively by

$$n_{R_{pn}} = \int_{\tau} dt \; n_{R_{pn}}(t) \; / \; n_{\tau_b} \qquad (4.6.24)$$

and

$$n_{R_{an}} = \int_{\tau} dt \; n_{R_{an}}(t) \; / \; n_{\tau_b} . \qquad (4.6.25)$$

The cycle and time dependent production and absorption rates, $n_{R_{pn}}(t)$ and $n_{R_{an}}(t)$, used here, are generally defined by Eq. 4.2.10 and Eq. 4.2.7 respectively. The subcritical multiplication constants of the breeder blanket, $k_{\infty b}$, are compared in Fig. 4.6.13 and Fig. 4.6.14 for multicycle systems without and with periodic reprocessing. Isolated cycle subcritical multiplication constants, given by

$$n_{k_{\infty b}} = n_{R_{pn}} \; / \; n_{R_{an}} , \qquad (4.6.26)$$

are also shown in Fig. 4.6.13 and Fig. 4.6.14. As expected, the system with periodic reprocessing yields a neutron multiplication constant practically independent of the final fuel burnup, β_t, defined by Eq. 4.6.19, while the system without any fuel reprocessing shows a steady increase in the multiplication constant as fuel burnup progresses.

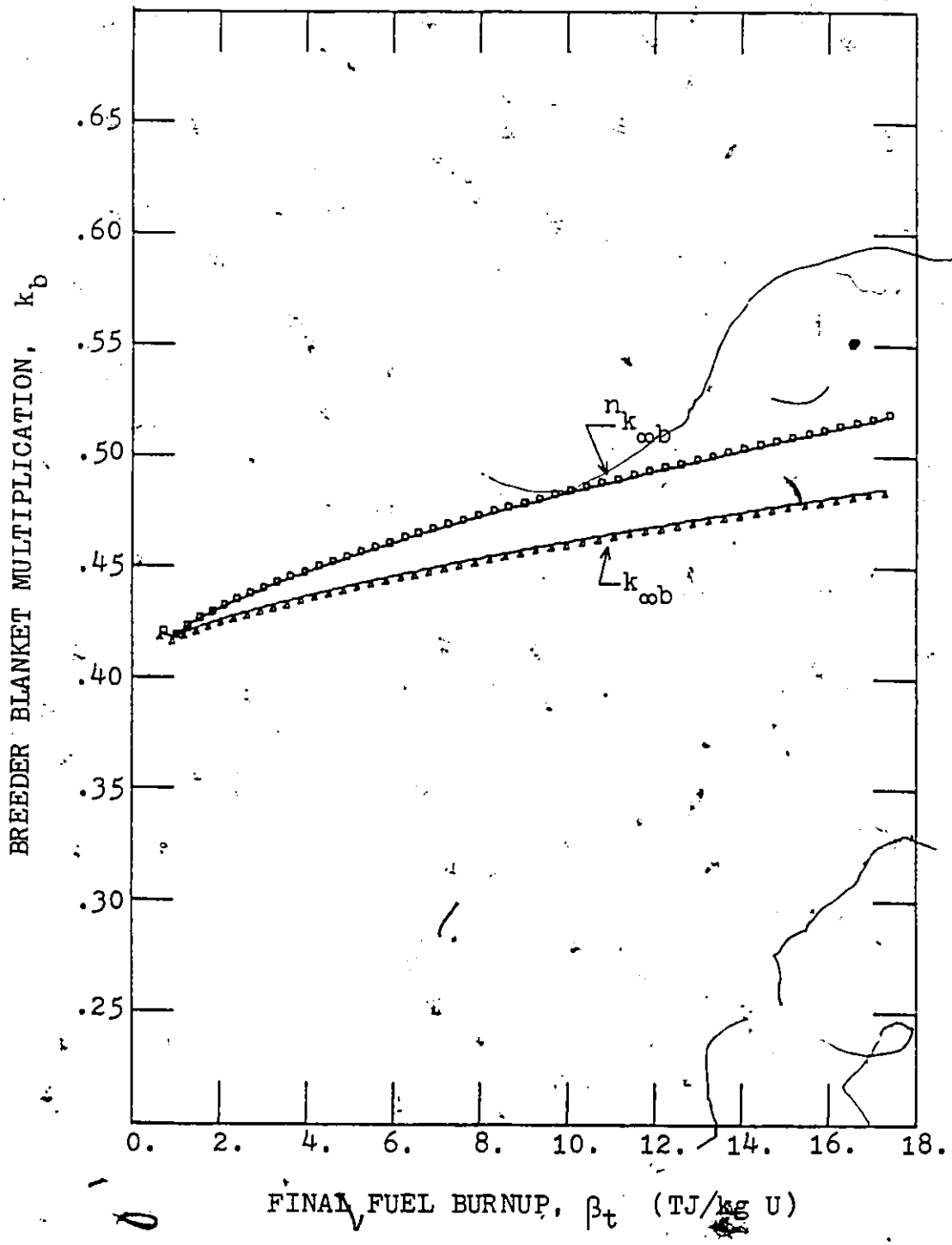

Fig. 4.6.13 Subcritical breeder blanket multiplication without fuel reprocessing; cases 1 to 10 of Table 4.6.1.

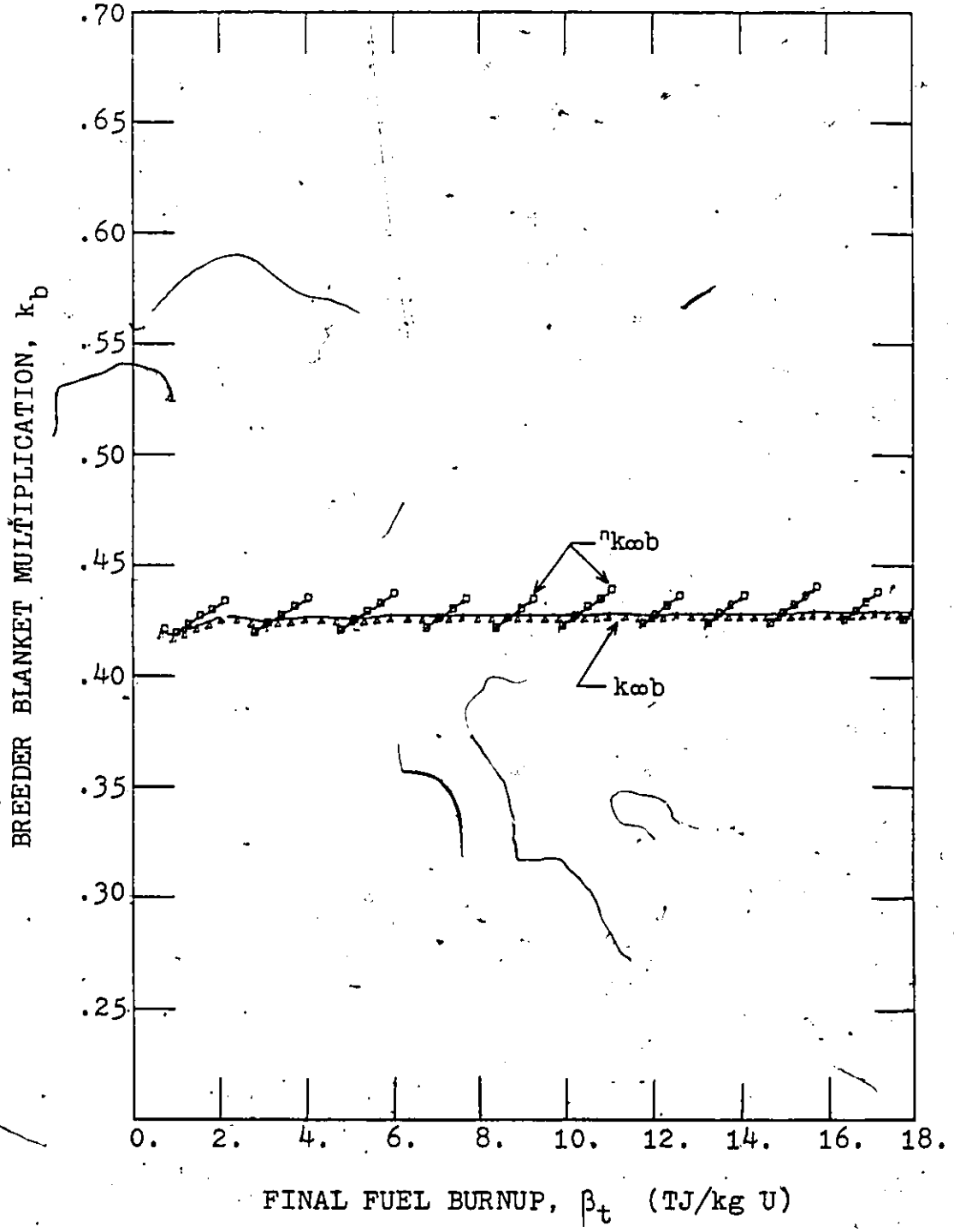

Fig. 4.6.14 Subcritical breeder blanket multiplication with periodic fuel reprocessing; cases 1 to 10 of Table 4.6.1.

4.7 Fuel Utilization

Approximately 1% of potential fissionable material is consumed in a conventional reactor system. In a breeder-converter symbiotic reactor system, this remaining 99% of the fissionable fuel can potentially be utilized. The degree of fissionable fuel utilization can be expressed by the fuel utilization factor, f_u, defined as

$$f_u = \beta_t / {}^{o}\beta_d, \tag{4.7.1}$$

where β_t is the total system fuel burnup defined by Eq. 4.6.19, while ${}^{o}\beta_d$ is the fuel burnup of an associated, unassisted reference converter reactor. For a converter reactor capable of burning natural fuel, Eq. 4.7.1 yields

$$f_u = \beta_t / {}^{1}\beta_d . \tag{4.7.2}$$

Similar to Eq. 4.7.1, a fuel stretching factor can be defined as

$$f_s = \beta_d / {}^{o}\beta_d \tag{4.7.3}$$

or

$$f_s = \beta_d / {}^{1}\beta_d \tag{4.7.4}$$

for a converter reactor capable of burning natural nuclear fuel. Using Eq. 4.6.11, Eq. 4.7.3 and Eq. 4.7.4 can be written to yield

$$f_s = P_{td} / {}^{1}R_{ic}\, {}^{o}\beta_d \tag{4.7.5}$$

and

$$f_s = P_{td} / {}^{1}R_{ic}\, {}^{1}\beta_d . \tag{4.7.6}$$

Making use of Eq. 4.2.21, the mass flow rates of an

associated reference reactor of thermal power P_{td}, become

$$ {}^{o}R_i = P_{td} \,/\, {}^{o}\beta_d \qquad (4.7.7) $$

and

$$ {}^{1}R_i = P_{td} \,/\, {}^{1}\beta_d \,. \qquad (4.7.8) $$

Substituting Eq. 4.7.7 into Eq. 4.7.5 and Eq. 4.7.8 into Eq. 4.7.6 yields

$$ f_s = {}^{o}R_i \,/\, {}^{1}R_{ic} \qquad (4.7.9) $$

and

$$ f_s = {}^{1}R_i \,/\, {}^{1}R_{ic} \,. \qquad (4.7.10) $$

The fresh fuel supply rates ${}^{o}R_i$, ${}^{1}R_i$, and ${}^{1}R_{ic}$ are directly proportional to the lifetime system fuel cost. The fuel stretching factor, f_s, therefore becomes a measure of relative fuel costs of conventional and symbiotic systems which is of great importance in a relative cost analysis. In Fig. 4.7.1 and Fig. 4.7.2 the fuel utilization factor, f_u, and the fuel stretching factor, f_s, are shown for the systems with and without fuel reprocessing. The fuel utilization factor is generally larger than the fuel stretching factor since some fuel burnup takes place in the breeder blanket. The fuel stretching factor for the symbiotic system without reprocessing is lower than the fuel stretching factor of the system with periodic reprocessing. This is due to higher breeder blanket fuel burnup in the system without reprocessing associated with higher fissile isotope content in the fuel.

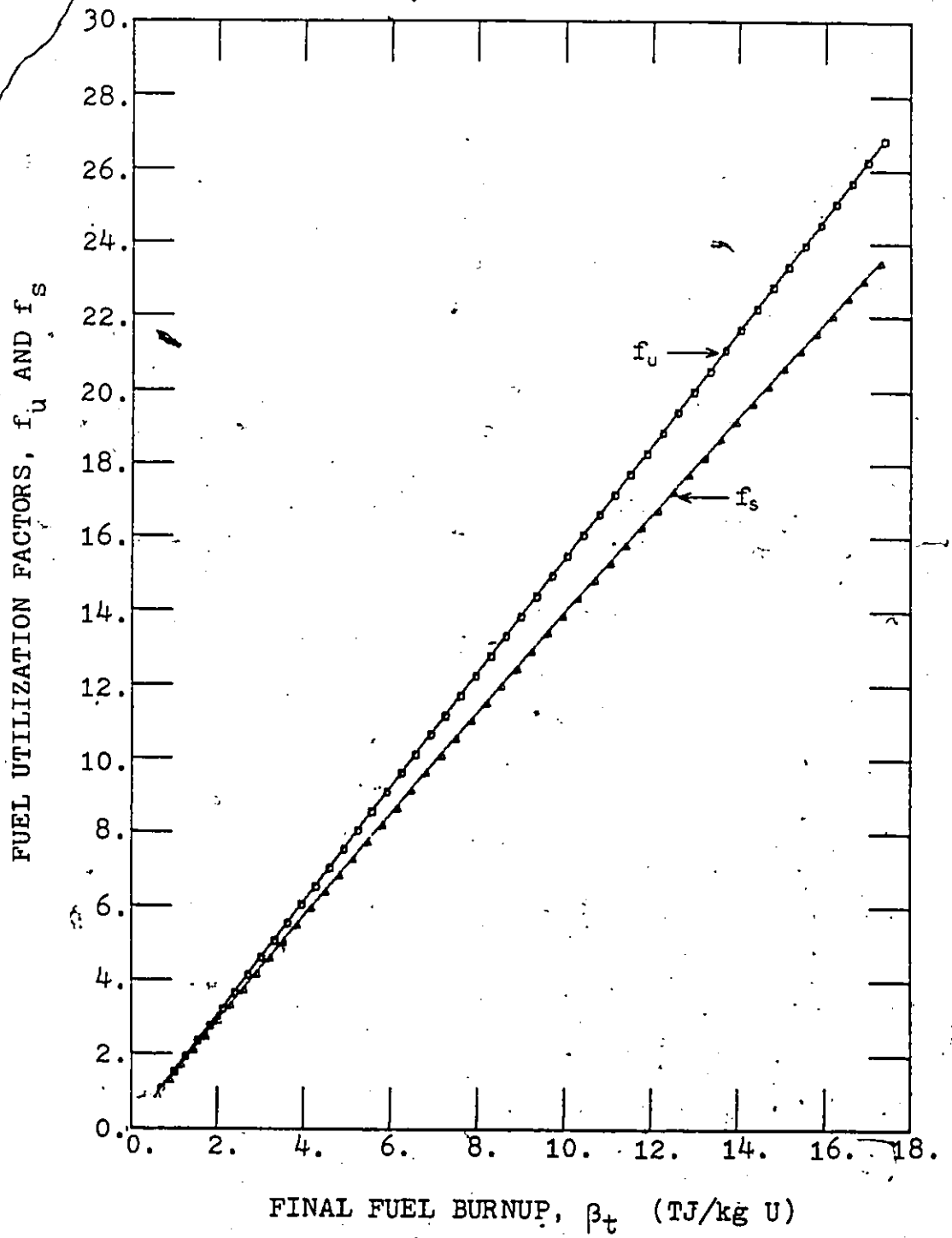

Fig. 4.7.1 Fuel utilization of the symbiotic systems without fuel reprocessing; cases 1 to 10 of Table 4.6.1.

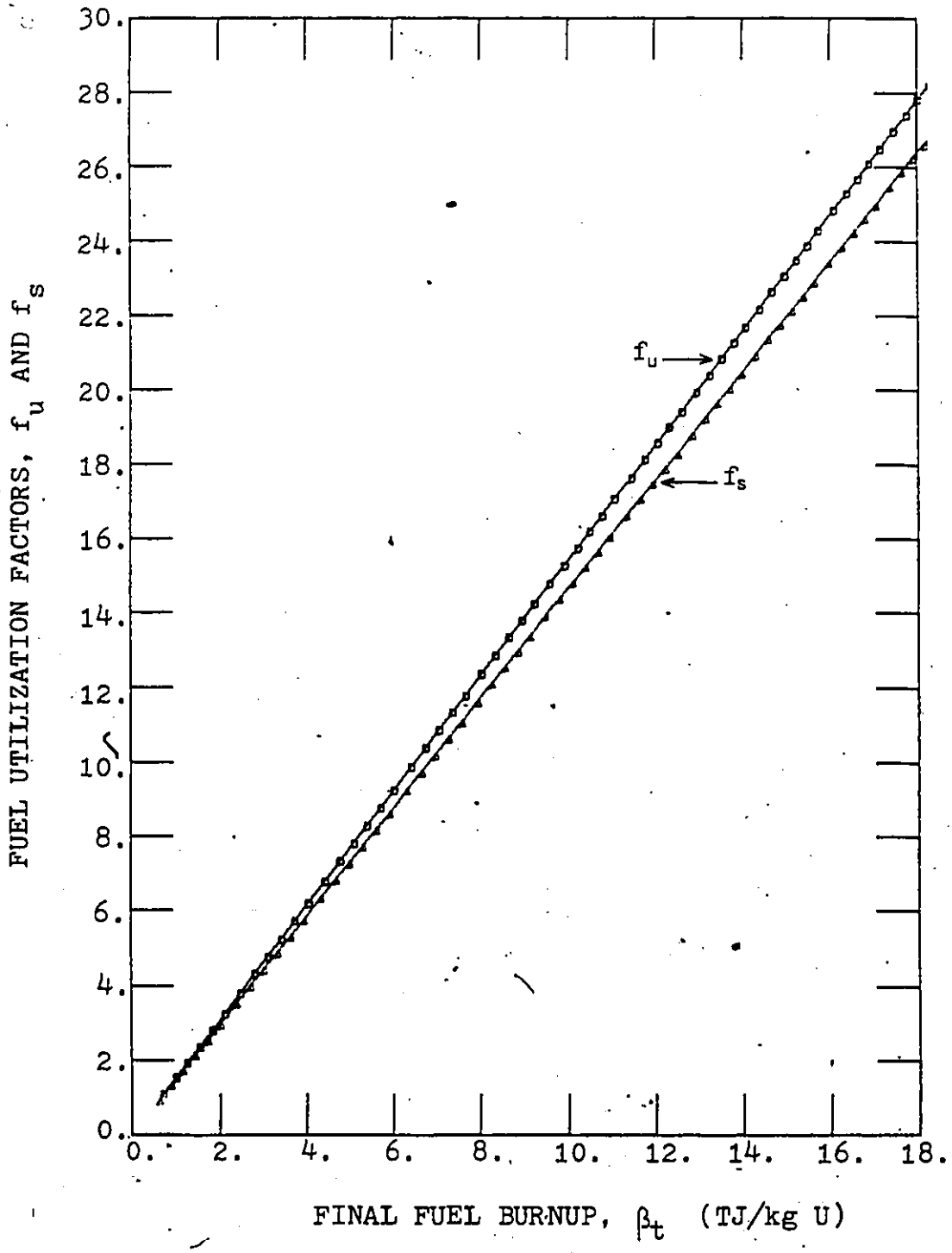

Fig. 4.7.2 Fuel utilization of the symbiotic systems with periodic fuel reprocessing; cases 1 to 10 of Table 4.6.1.

CHAPTER 5

POWER DYNAMICS WITH LIMITED REPROCESSING

5.1 System Power Balance

Chapter 4 dealt with the fuel dynamics of the symbiotic reactor systems. The analysis included the derivation of the power produced by the fuel elements of the conventional reactor subsystem and the breeder subsystem. For a conventional reactor system, the fuel produced power is the only power source while for a symbiotic system other power sources as well as power sinks have to be accounted for. Here, typical energy sources are fusion, fission, and spallation reactions with associated power sinks and the subsystem drive powers. Since the symbiotic system eventually will be analysed in terms of the associated net electrical power output, an overall power balance will now be developed.

For a driven breeder reactor, an external electrical power source, P_{ee}, is required to operate the breeder subsystem. The power, P_{ee}, is delivered to the actively neutron producing breeder core with an efficiency, ε_{ee}, yielding a direct breeder core drive power

$$P_{te} = \varepsilon_{ee} P_{ee} . \qquad (5.1.1)$$

The average internal breeder core power, $\bar{P}_{tcb}$, is defined by

$$\bar{P}_{tcb} = \sum_k \sum_j \sum_i \int_\tau dt \int_E dE \int_{V_c} d\vec{r}\, U_{kji}(E)\sigma_{kji}(E)n_i(\vec{r},t)\psi_j(\vec{r},E,t)/\tau \qquad (5.1.2)$$

where a representative time interval, τ, is chosen and the spatial integration is performed over the core volume, V_c. The average core-to-blanket leakage power, $\bar{P}_{tc\ell}$, is given by

$$\bar{P}_{tc\ell} = \sum_j \int_\tau dt \int_E dE \int_{S_{cb}} d\vec{s}\, E_j \vec{J}(\vec{r},E,t) \cdot \hat{n}/\tau, \qquad (5.1.3)$$

where the surface integral is carried out over the target-blanket interface, S_{cb}, and $\hat{n}$ is the target unit surface vector. Further, a core thermal Q-value is defined as

$$Q_{tcb} = (\bar{P}_{tcb} + P_{te})/P_{te} \qquad (5.1.4)$$

yielding a total thermal core power

$$P_{tci} = Q_{tcb} P_{te} - \bar{P}_{tc\ell} . \qquad (5.1.5)$$

A blanket thermal Q-value is similarly defined as

$$Q_{tbb} = P_{tbb}/P_{te} , \qquad (5.1.6)$$

where P_{tbb} is defined by Eq. 4.6.12, yielding a total thermal blanket power

$$P_{tbi} = Q_{tbb} P_{te} + \bar{P}_{tc\ell} . \qquad (5.1.7)$$

Also, an overall breeder Q-value can be defined by

$$Q_{tb} = Q_{tcb} + Q_{tbb} . \qquad (5.1.8)$$

Using consistent notation, a thermal breeder utilization factor, Q_{td}, is formulated to yield

$$Q_{td} = P_{td}/P_{te} , \qquad (5.1.9)$$

with P_{td} given by Eq. 4.6.11. Rearranging Eq. 5.1.9 gives

$$P_{td} = Q_{td} P_{te} . \qquad (5.1.10)$$

The equations derived above can be used to define the total

thermal power of the symbiotic system to yield

$$P_{ts} = Q_{ts} P_{te} , \qquad (5.1.11)$$

where the total thermal system Q-value is given by

$$Q_{ts} = (Q_{tcb} + Q_{tbb} + Q_{td} + (1/\varepsilon_{ee} - 1)). \qquad (5.1.12)$$

The net electrical power produced by the symbiotic system can be obtained by multiplying each power component of Eq. 5.1.11 by its associated thermal-to-electrical conversion efficiency, η, yielding

$$P_{es} = \eta_c P_{tci} + \eta_b P_{tbi} + (\eta_d Q_{td} - 1/\varepsilon_{ee}) P_{te} . \qquad (5.1.13)$$

The last term of Eq. 5.1.13 is the electrical power required to drive the breeder subsystem. The system net thermal-to-electrical conversion efficiency, η_s, is defined by

$$\eta_s = P_{es}/P_{ts} \qquad (5.1.14)$$

and shown in Fig. 5.1.1. and Fig. 5.1.2 as a function of fuel end burnup, β_t, for the symbiotic systems of interest here. As expected, the system net efficiency increases with increasing neutron yield, with generally better performance being achieved for cases with limited reprocessing. This is a result of increased system Q-values. The system thermal Q-values, Q_{tbb} and Q_{td}, used in obtaining η_s, are both proportional to the blanket neutron source S_{nb} defined generally by Eq. 4.2.2. It is also known that an increase in S_{nb}, for a constant accelerator beam drive power, is obtained by increasing the atomic mass and fission cross sections of the target isotopes. The target Q-value con-

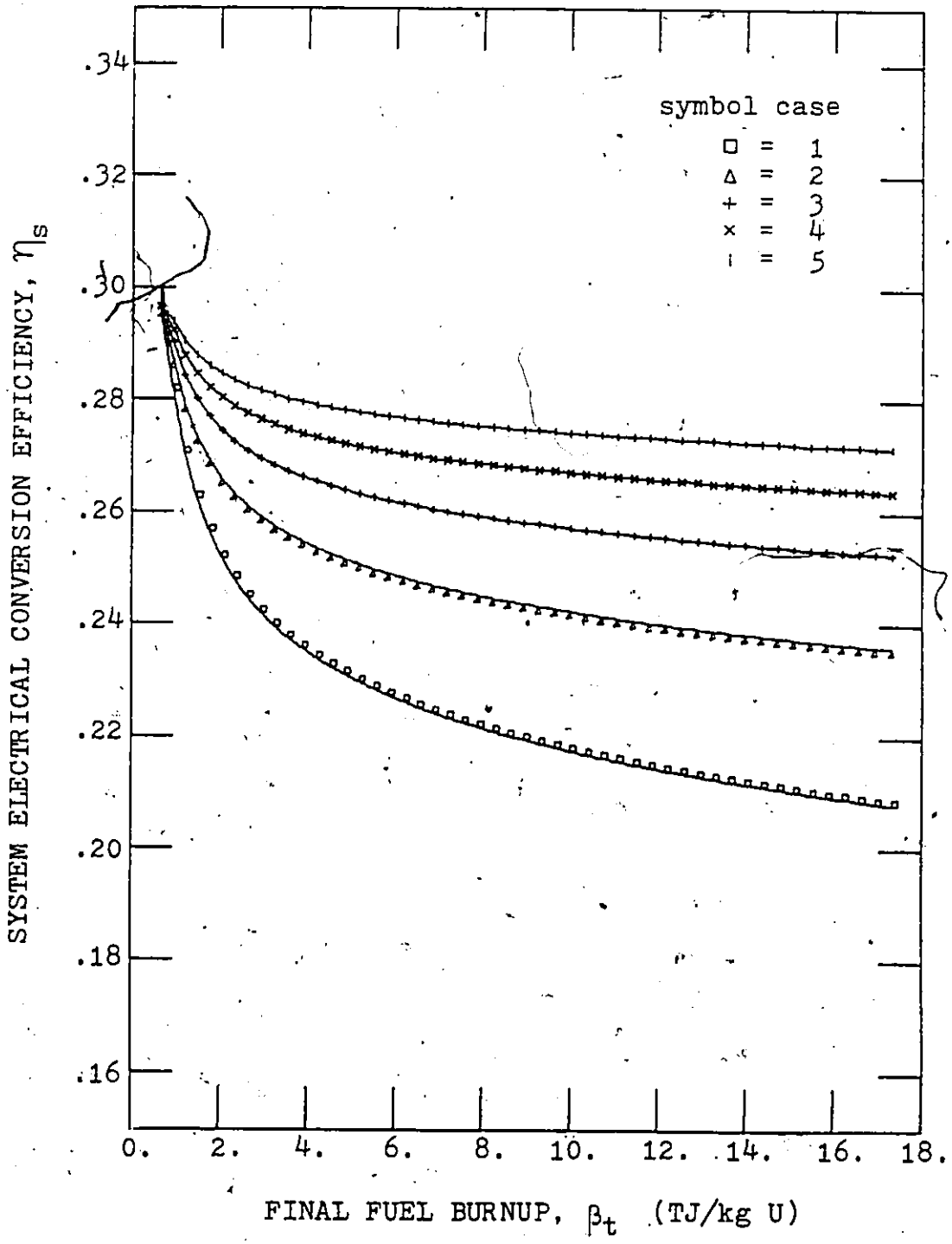

Fig. 5.1.1a System electrical conversion efficiency without fuel reprocessing; cases 1 to 5 of Table 4.6.1.

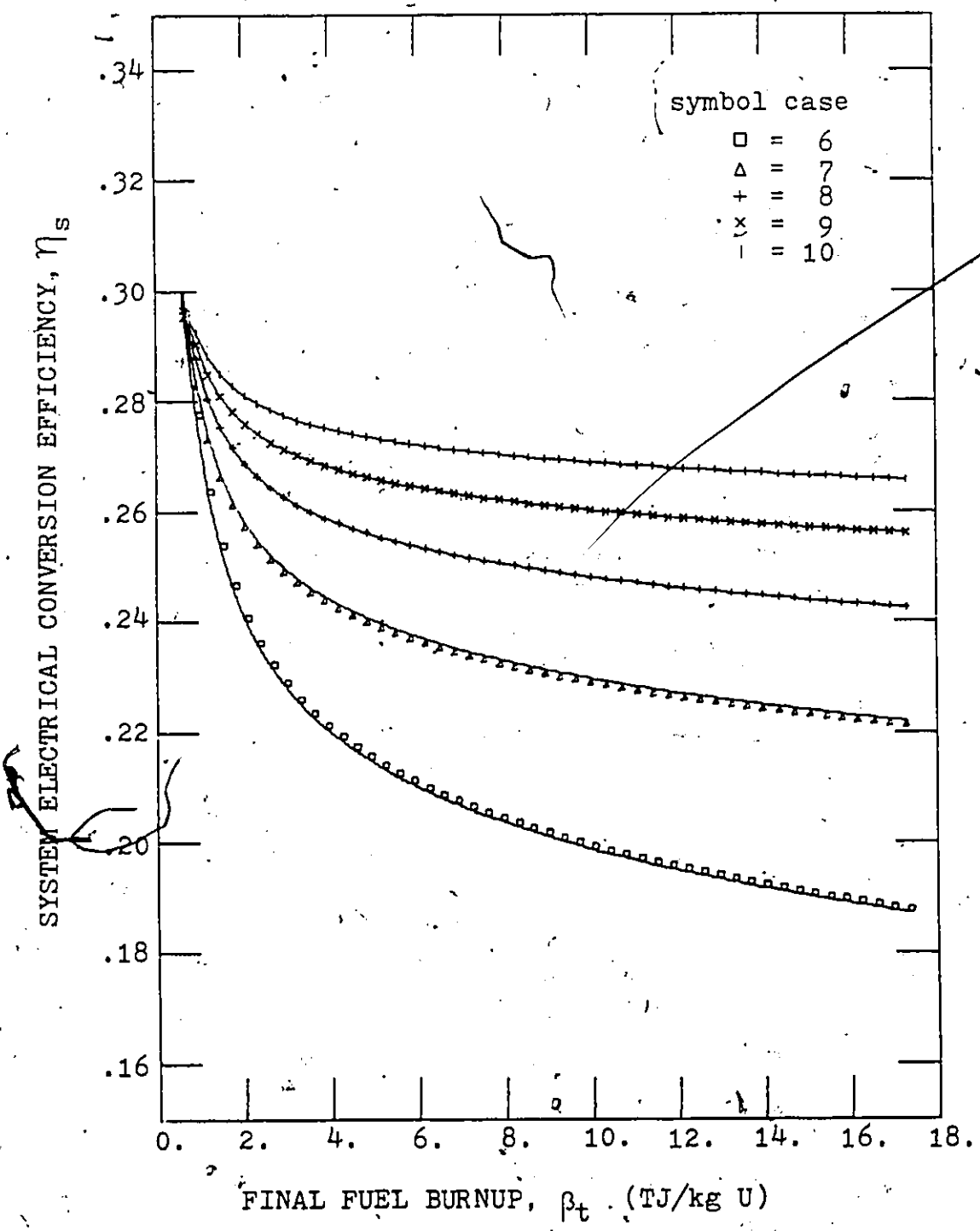

Fig. 5.1.1b System electrical conversion efficiency without fuel reprocessing; cases 6 to 10 of Table 4.6.1.

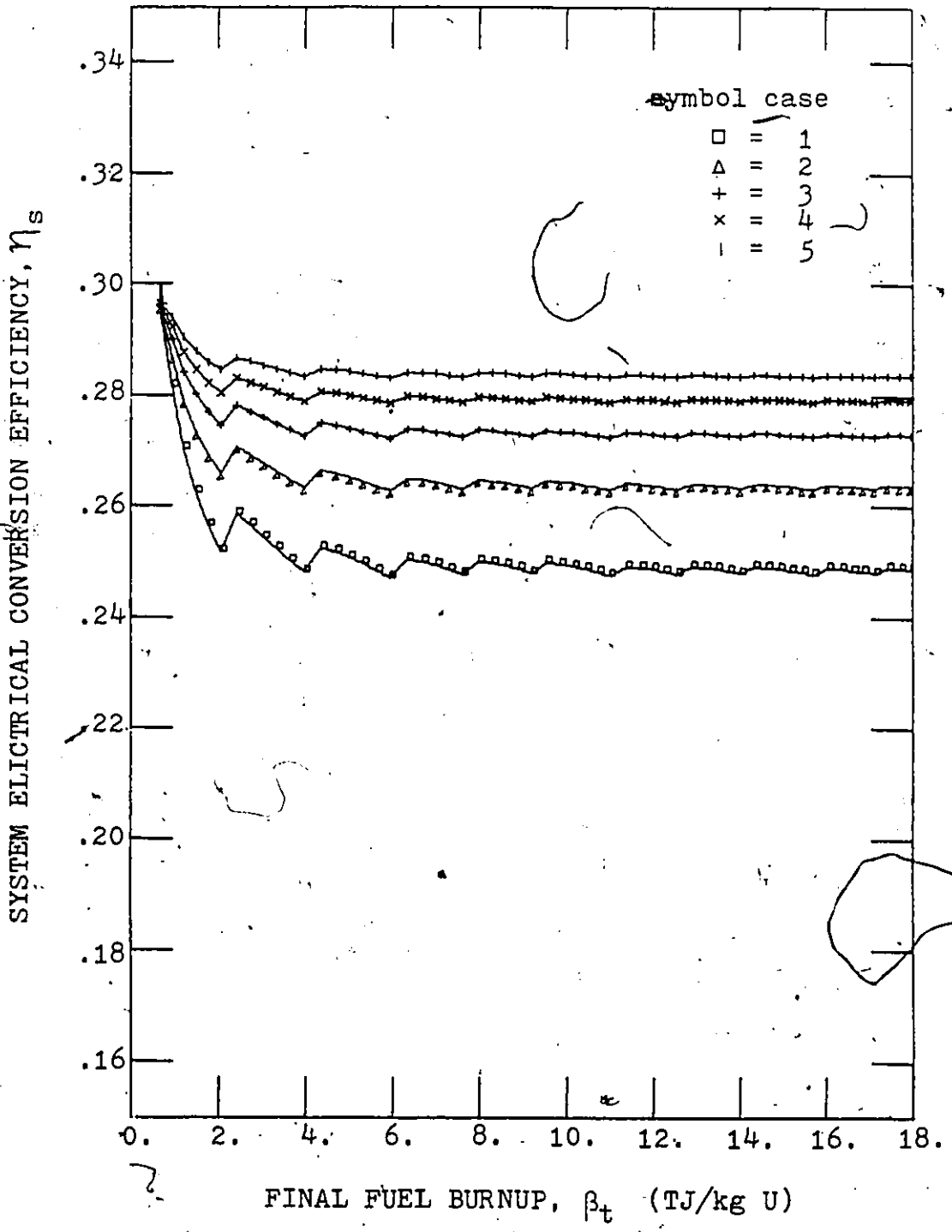

Fig. 5.1.2a System electrical conversion efficiency with periodic fuel reprocessing; cases 1 to 5 of Table 4.6.1.

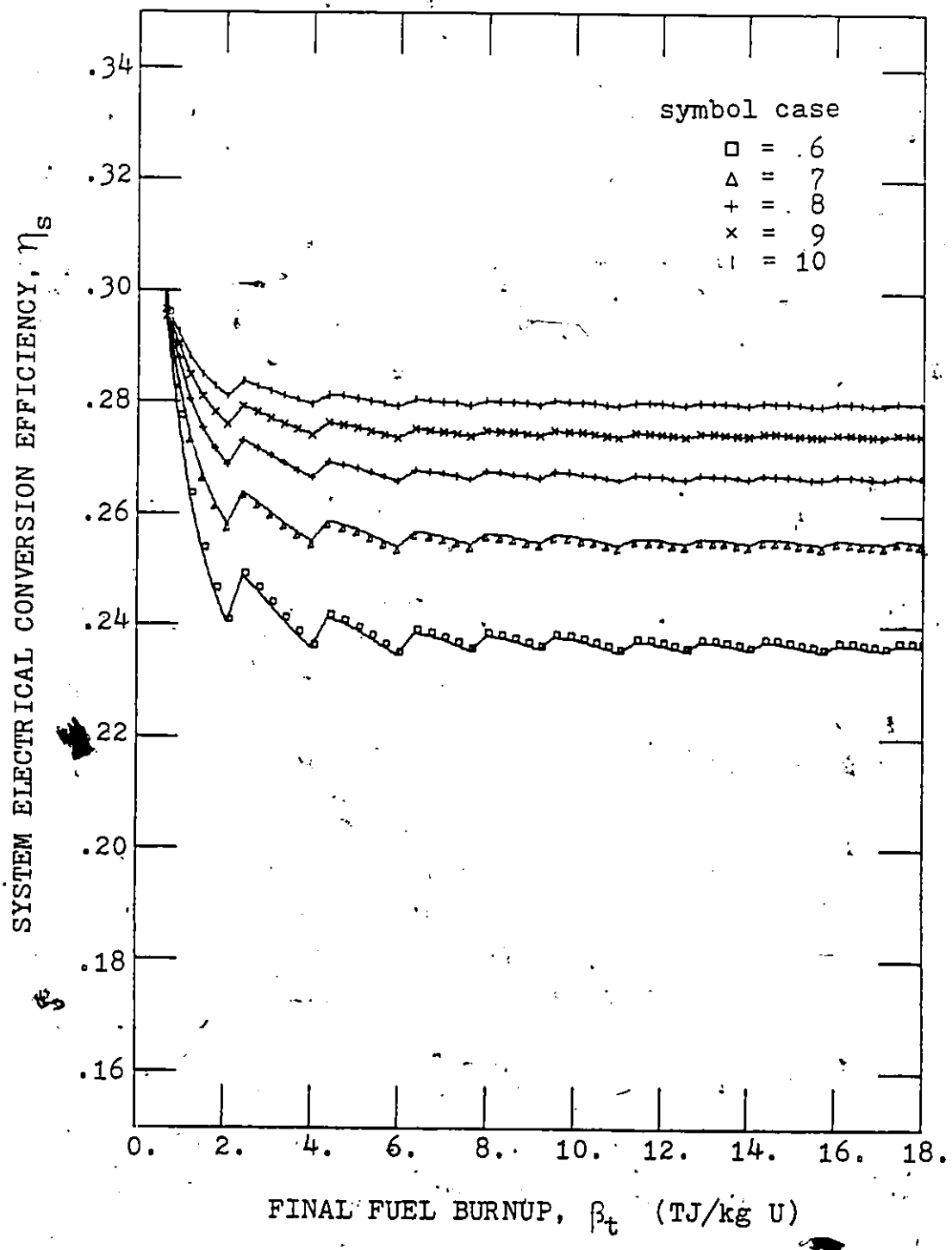

Fig. 5.1.2b System electrical conversion efficiency with periodic fuel reprocessing; cases 6 to 10 of Table 4.6.1.

sequently also increases. Table 4.6.1 shows the appropriate values for Q_{tcb} for depleted uranium-lead mixtures as target material. Thus with increasing neutron yield, the first three terms of Eq. 5.1.12 and Eq. 5.1.13 become more dominant when compared to the last term defining the accelerator drive power loss and contribute to an overall efficiency, η_s, closer to the efficiencies, η_c, η_b, and η_d.

5.2 Power Utilization

In Chapter 4, the breeder supported nuclear fuel powers were derived for an arbitrarily chosen but constant breeder drive power to yield Eq. 4.6.11 and Eq. 4.6.12 for converter power and breeder power respectively. It is, however, desirable to obtain drive power independent system parameters. The breeder-depleter power utilization, Q_{td}, already defined by Eq. 5.1.9 is such a parameter, and is shown in Fig. 5.2.1 and Fig. 5.2.2 as a function of recycled fuel burnup for several breeder neutron sources given in Table 4.6.1. The low burnup Q-value is exceptionally high. This is due to high conversion ratios and low fission product absorption rates in breeder and converter subsystems for fuels with low burnup, as well as the use of a nuclear fuel which initially does not need a breeder subsystem. The power utilization factor, Q_{td}, can be used to determine breeder requirements for symbiotic systems of arbitrary

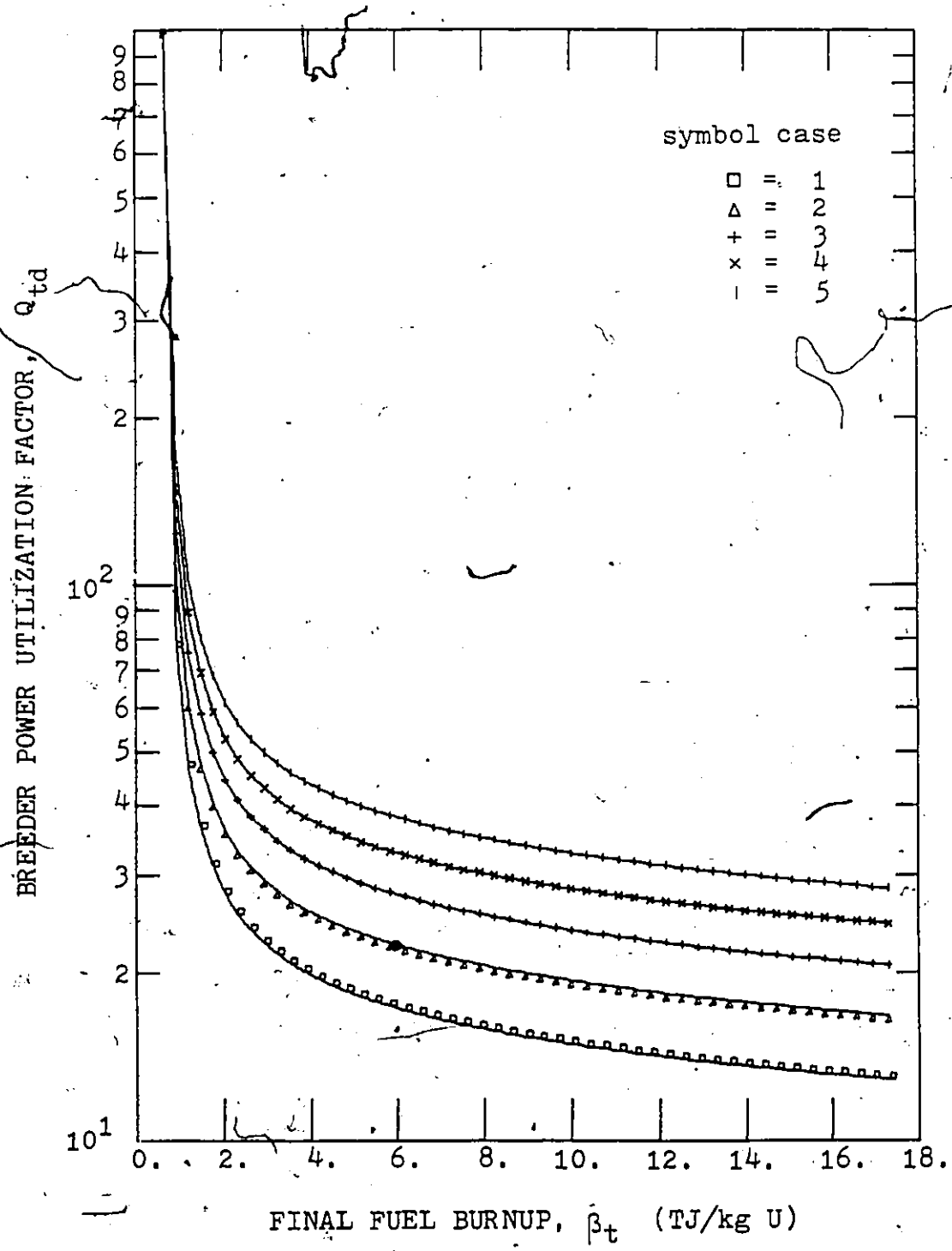

Fig. 5.2.1a Symbiotic system breeder power utilization without fuel reprocessing; cases 1 to 5 of Table 4.6.1.

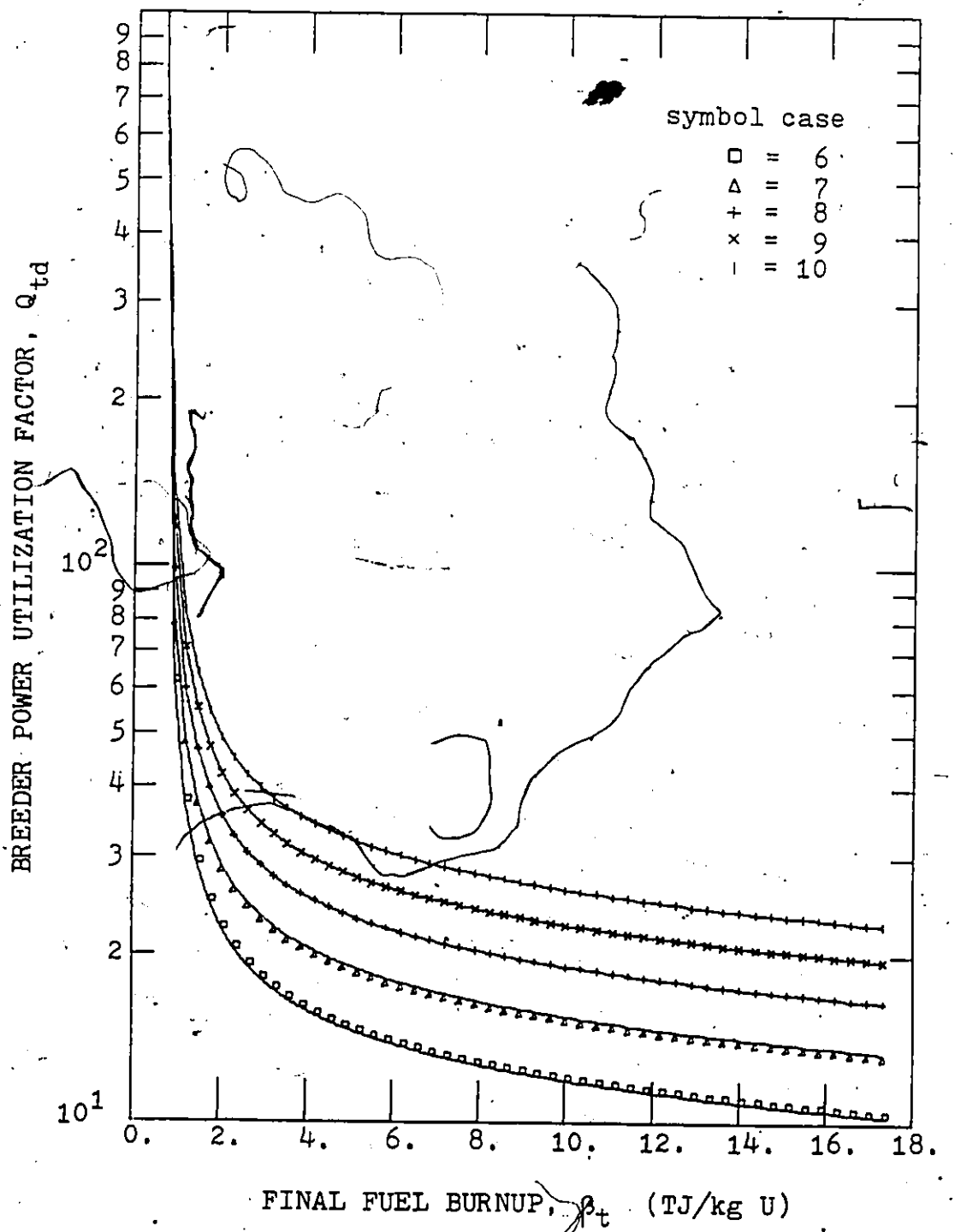

Fig. 5.2.1b Symbiotic system breeder power utilization without fuel reprocessing; cases 6 to 10 of Table 4.6.1.

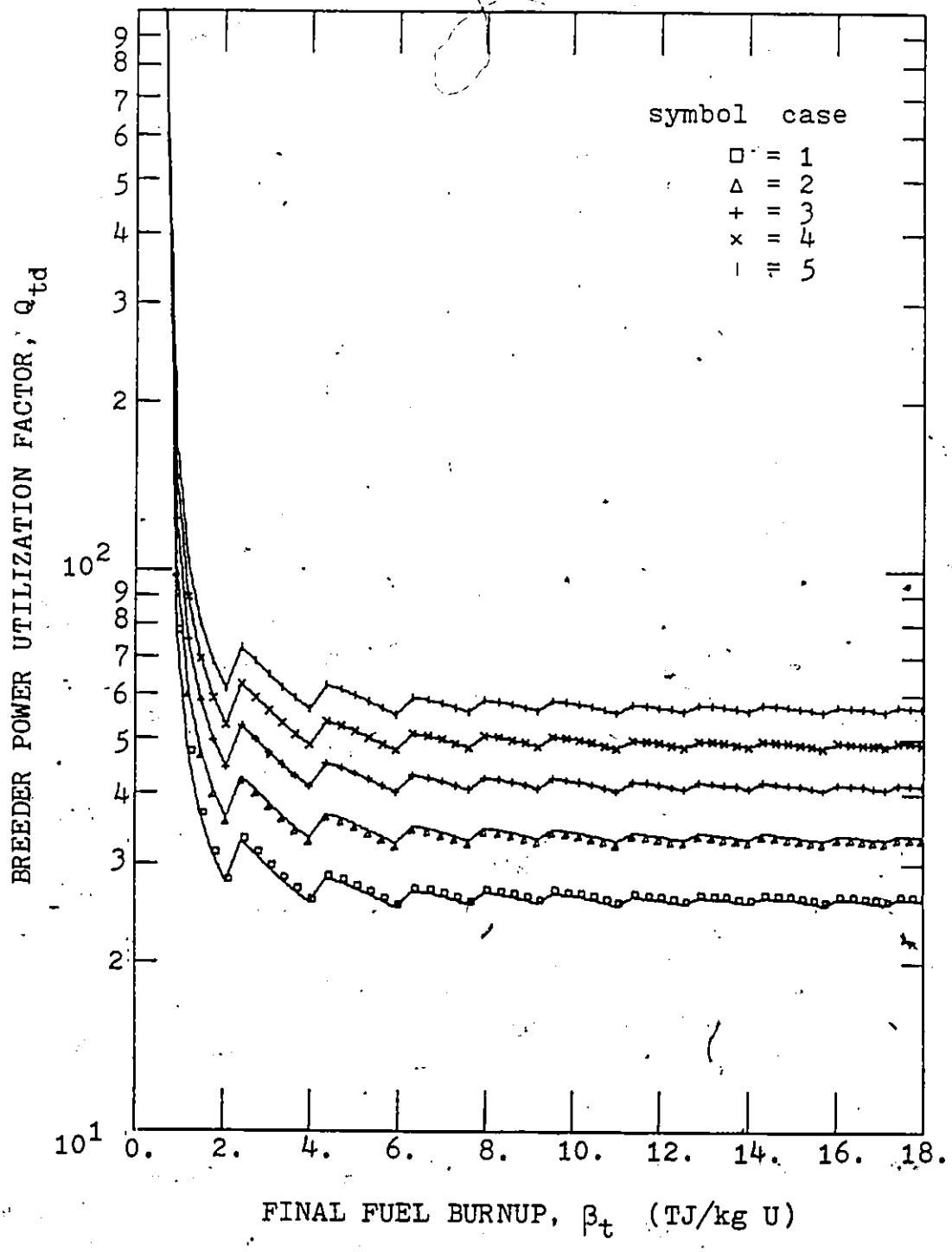

Fig. 5.2.2a Symbiotic system breeder power utilization with periodic fuel reprocessing; cases 1 to 5 of Table 4.6.1.

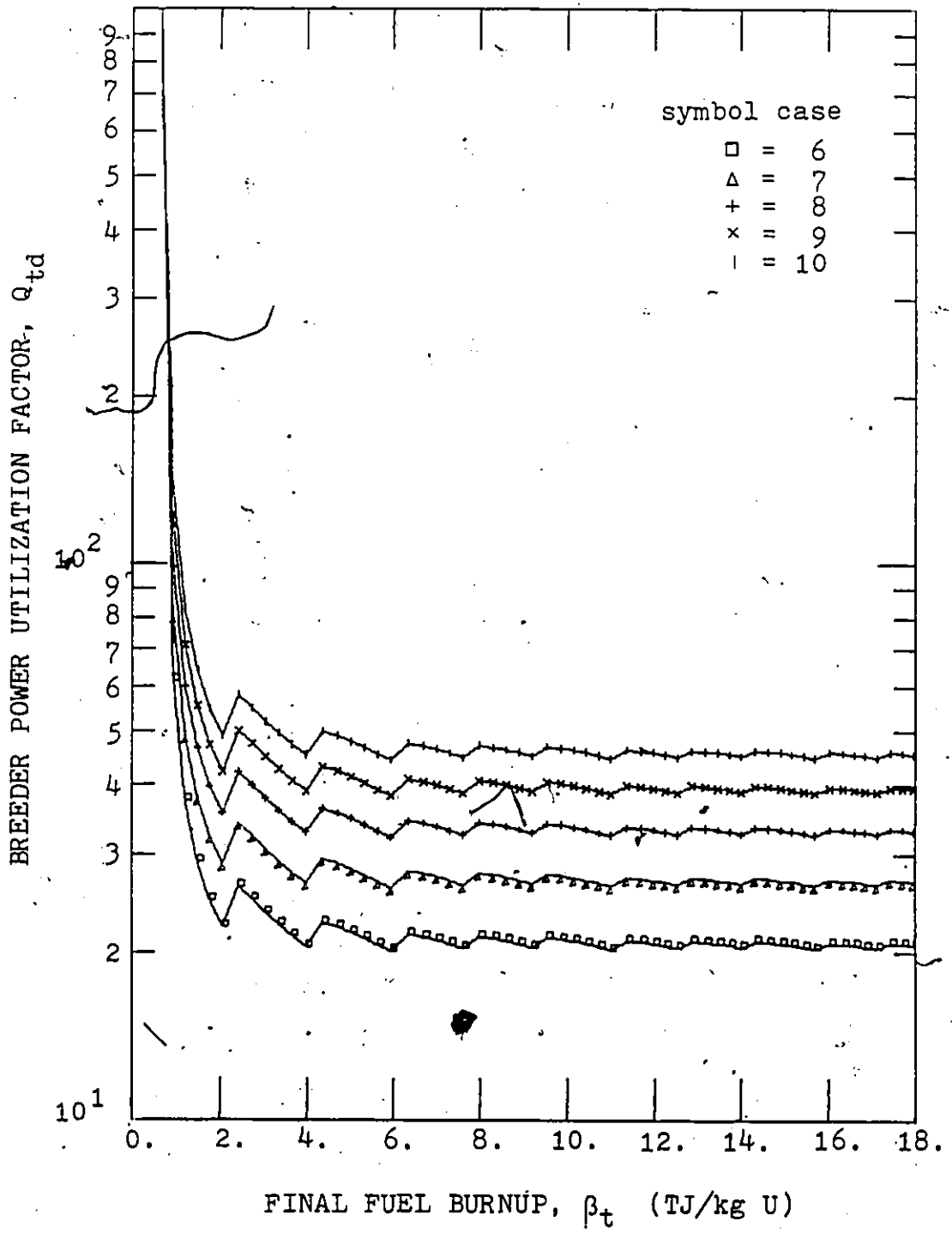

Fig. 5.2.2b Symbiotic system breeder power utilization with periodic fuel reprocessing; cases 6 to 10 of Table 4.6.1.

power and is evidently of major importance for economic analyses of symbiotic systems. In Fig. 5.2.2, it can be noted that for high fuel burnups, the utilization factor for cases with periodic reprocessing is about twice as large as the factor for cases without reprocessing. This reduces associated breeder costs though the required reprocessing costs reduce this advantage.

Similar to the breeder-depleter power utilization factor, Q_{td}, an internal breeder power utilization factor, Q_{tb}, can be defined

$$Q_{tb} = Q_{tcb} + Q_{tbb}, \qquad (5.2.1)$$

where Q_{tcb} and Q_{tbb} are defined by Eq. 5.1.4 and Eq. 5.1.6 respectively. The internal breeder power utilization, Q_{tb}, is shown in Fig. 5.2.3 and Fig. 5.2.4 for the two fuel recycle systems and the breeder neutron sources given in Table 4.6.1. It can be seen that Q_{tb} is relatively insensitive to fuel neutron source, S_{nb}, defined by Eq. 4.2.2. The target-blanket power is generally proportional to the target-blanket cost, consequently Q_{tb} becomes an important parameter in the breeder cost estimate as well as in the system overall power balance.

5.3 Net Power Advantage

Evaluating system operating characteristics, it is important to determine the extent of breeder subsystem self-

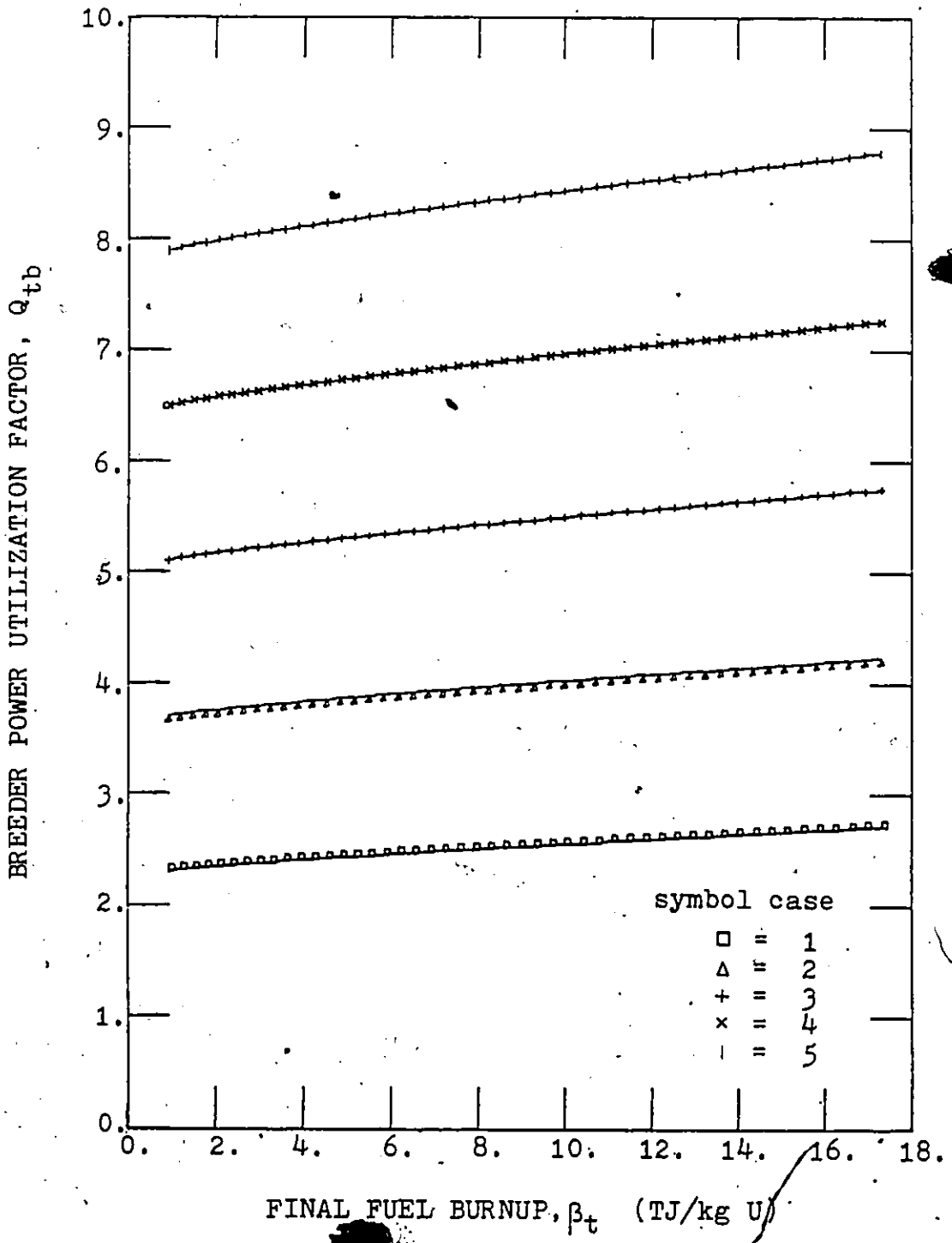

Fig. 5.2.3a System thermal breeder power utilization without fuel reprocessing; cases 1 to 5 of Table 4.6.1.

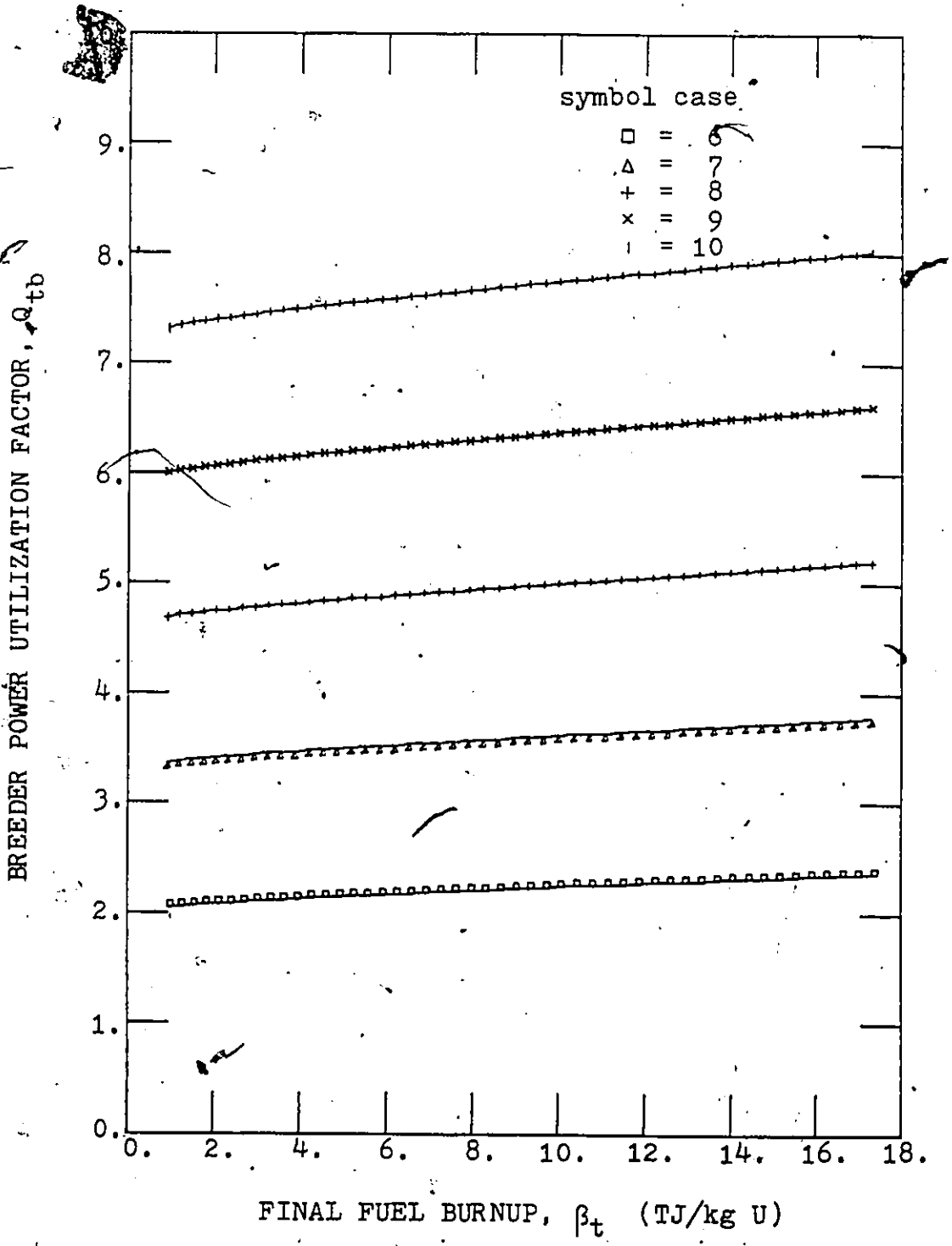

Fig. 5.2.3b System internal breeder power utilization without fuel reprocessing; cases 6 to 10 of Table 4.6.1.

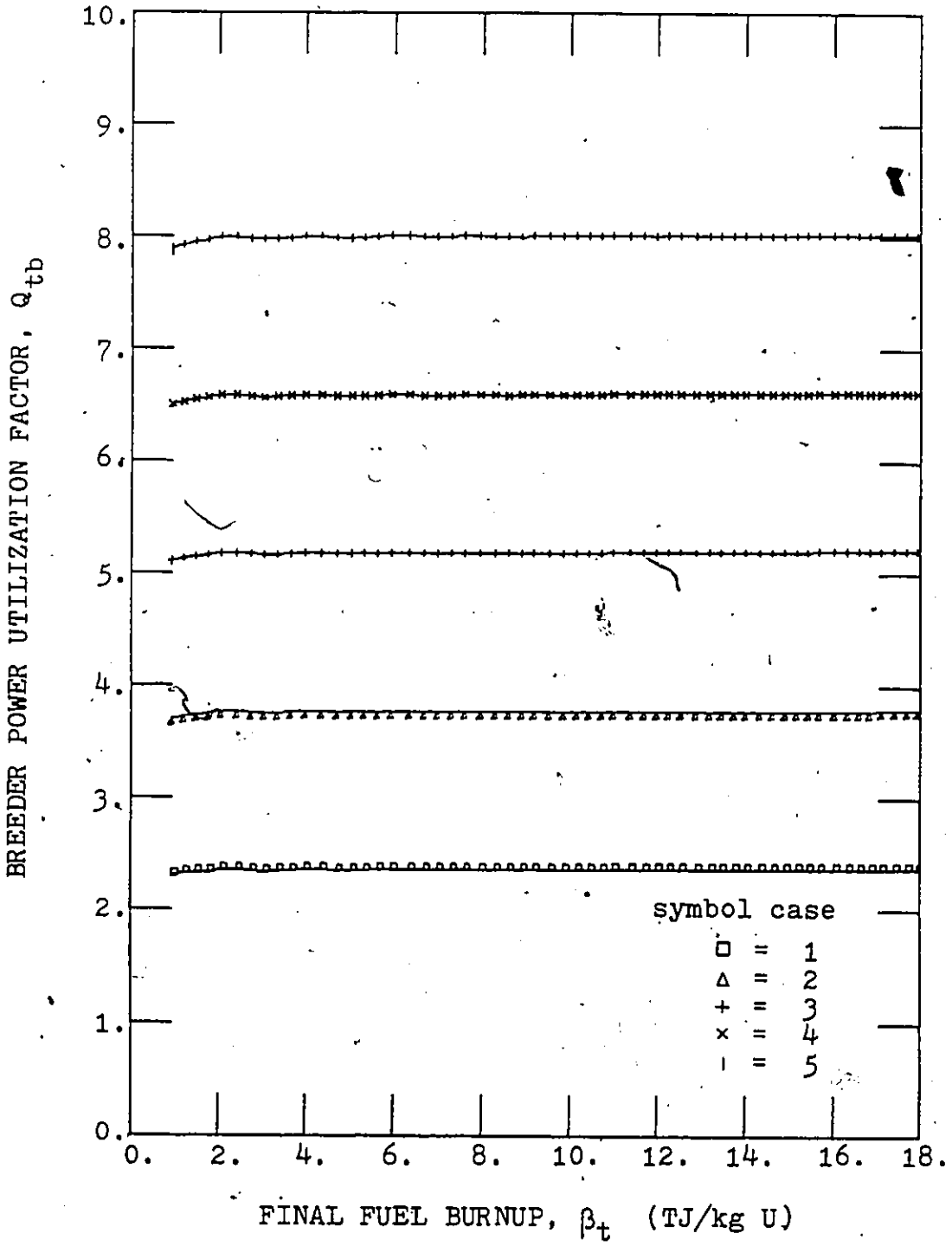

Fig. 5.2.4a System internal breeder power utilization with periodic fuel reprocessing; cases 1 to 5 of Table 4.6.1.

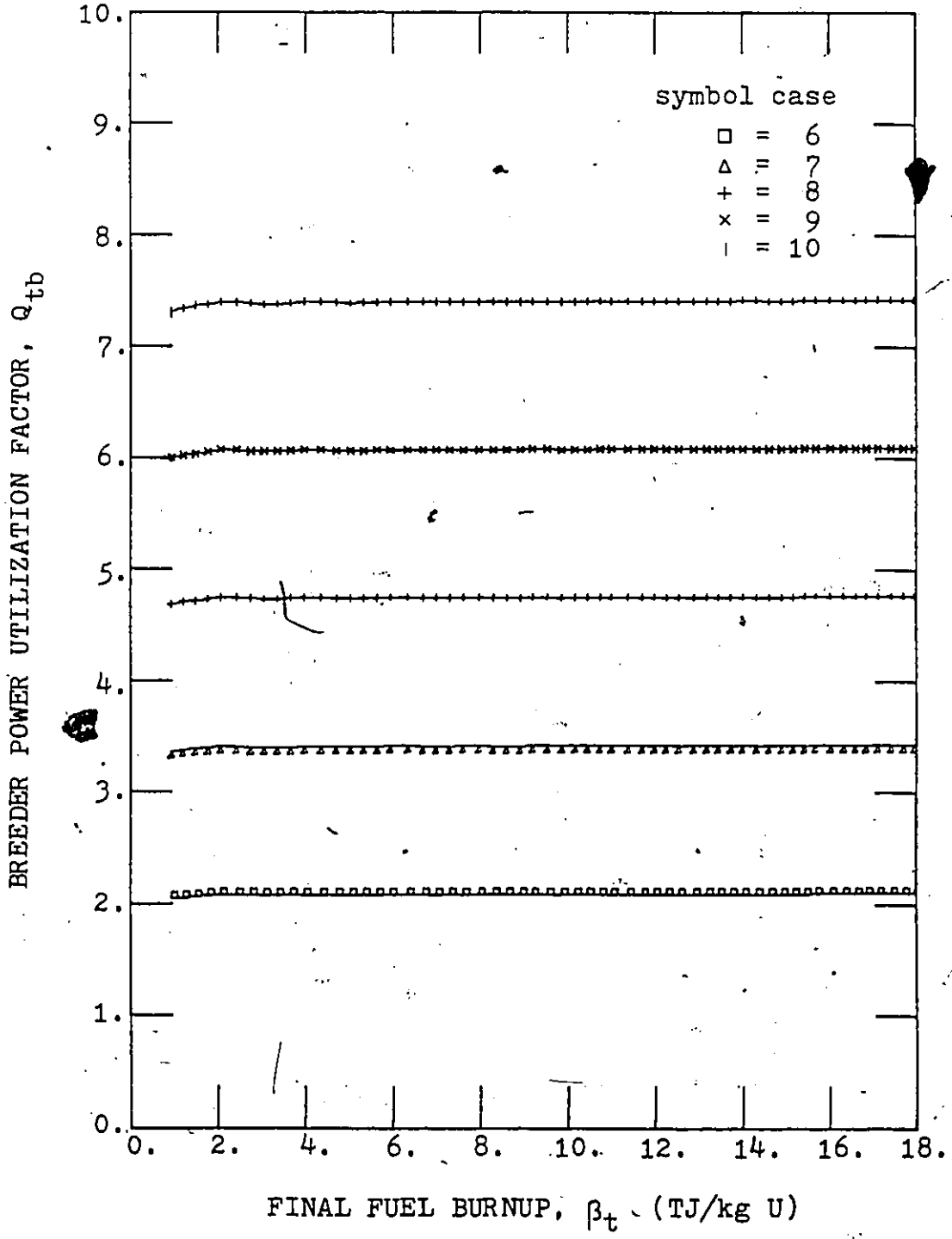

Fig. 5.2.4b System internal breeder power utilization with periodic fuel reprocessing; cases 6 to 10 of Table 4.6.1.

sufficiency, or even net electrical power production. A system net power advantage ratio can therefore be defined as

$$F_{es} = P_{es}/P_{ed} , \qquad (5.3.1)$$

where P_{es} is the ratio of net system electrical power output, defined by Eq. 5.1.13, and P_{ed} is the net electrical power produced by the depleter subsystem. Here

$$P_{ed} = \eta_d P_{td} , \qquad (5.3.2)$$

with P_{td} defined by Eq. 4.6.11. The breeder subsystem is electrical power self-sufficient for an advantage ratio equal to unity. The net power advantage ratio is shown in Fig. 5.3.1 and Fig. 5.3.2 for systems with and without limited reprocessing for different operating conditions. The breeder subsystem is power self-sufficient for a total thermal target-blanket breeder Q-value, Q_{tb}, Eq. 5.2.1, of about 4 corresponding to case 2 given in Table 4.6.1. The cases with limited reprocessing show an increased advantage ratio only when F_{es} is less than unity.

5.4 Parameter Correlation

In Chapter 4 and this chapter, a number of system parameters have been investigated. Of special importance, however, are parameters directly affecting the economic characteristics of the system. Several such parameters can be identified. A system fuel stretching factor, f_s, as defined by Eq. 4.7.3, quantifies the fresh fuel savings

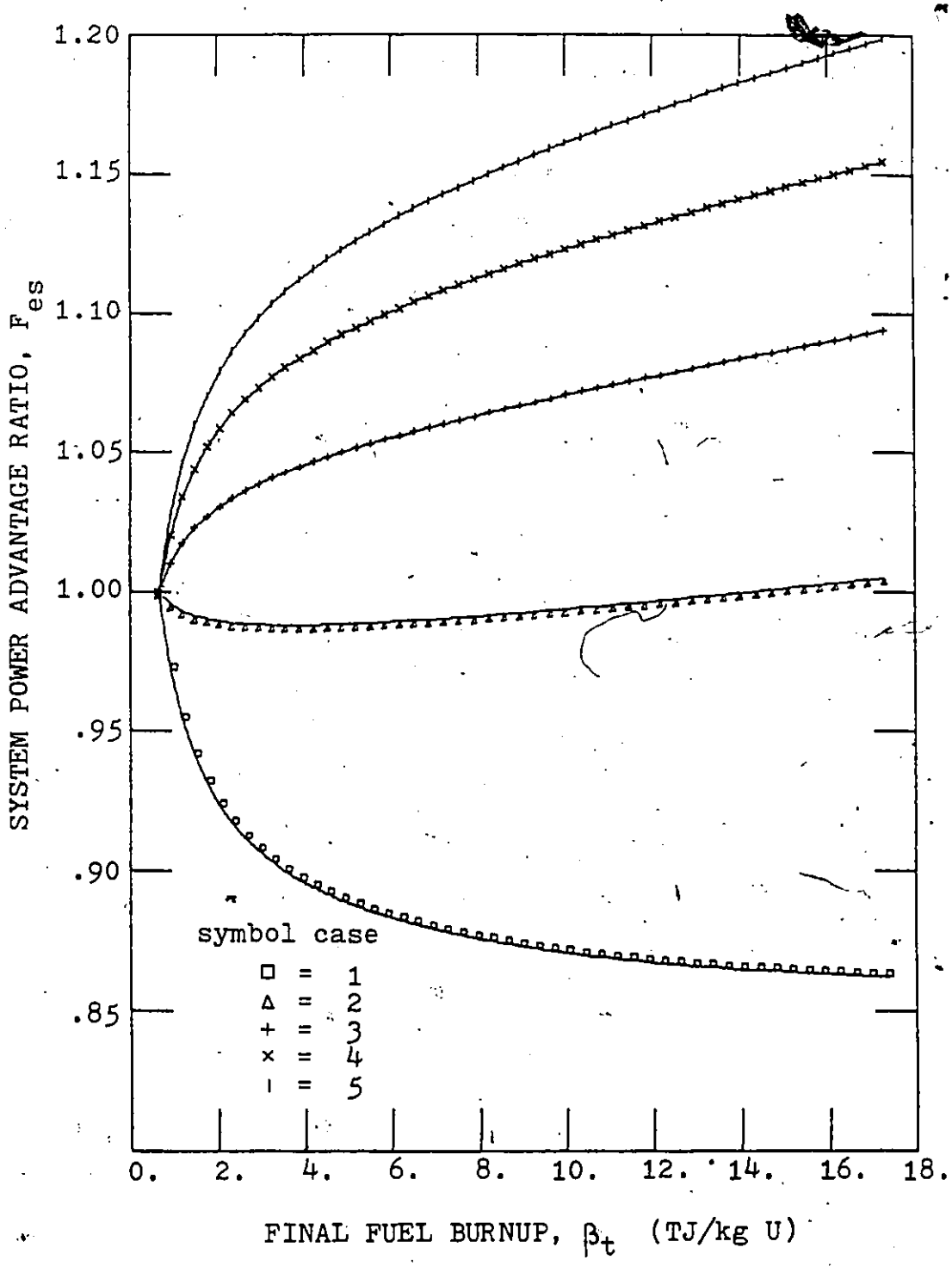

Fig. 5.3.1a System net electrical power advantage without fuel reprocessing; cases 1 to 5 of Table 4.6.1.

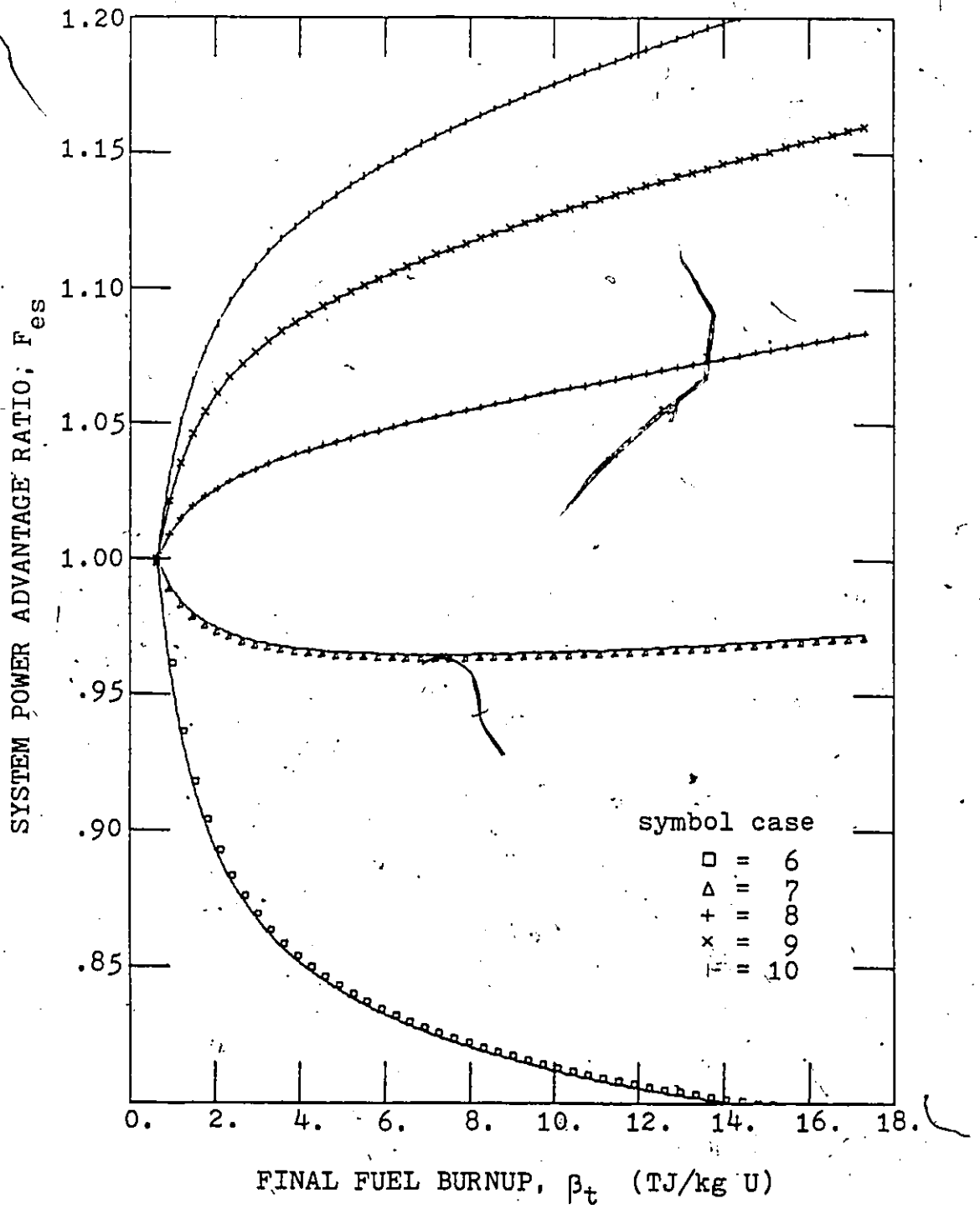

Fig. 5.3.1b System net electrical power advantage without fuel reprocessing; cases 6 to 10 of Table 4.6.1.

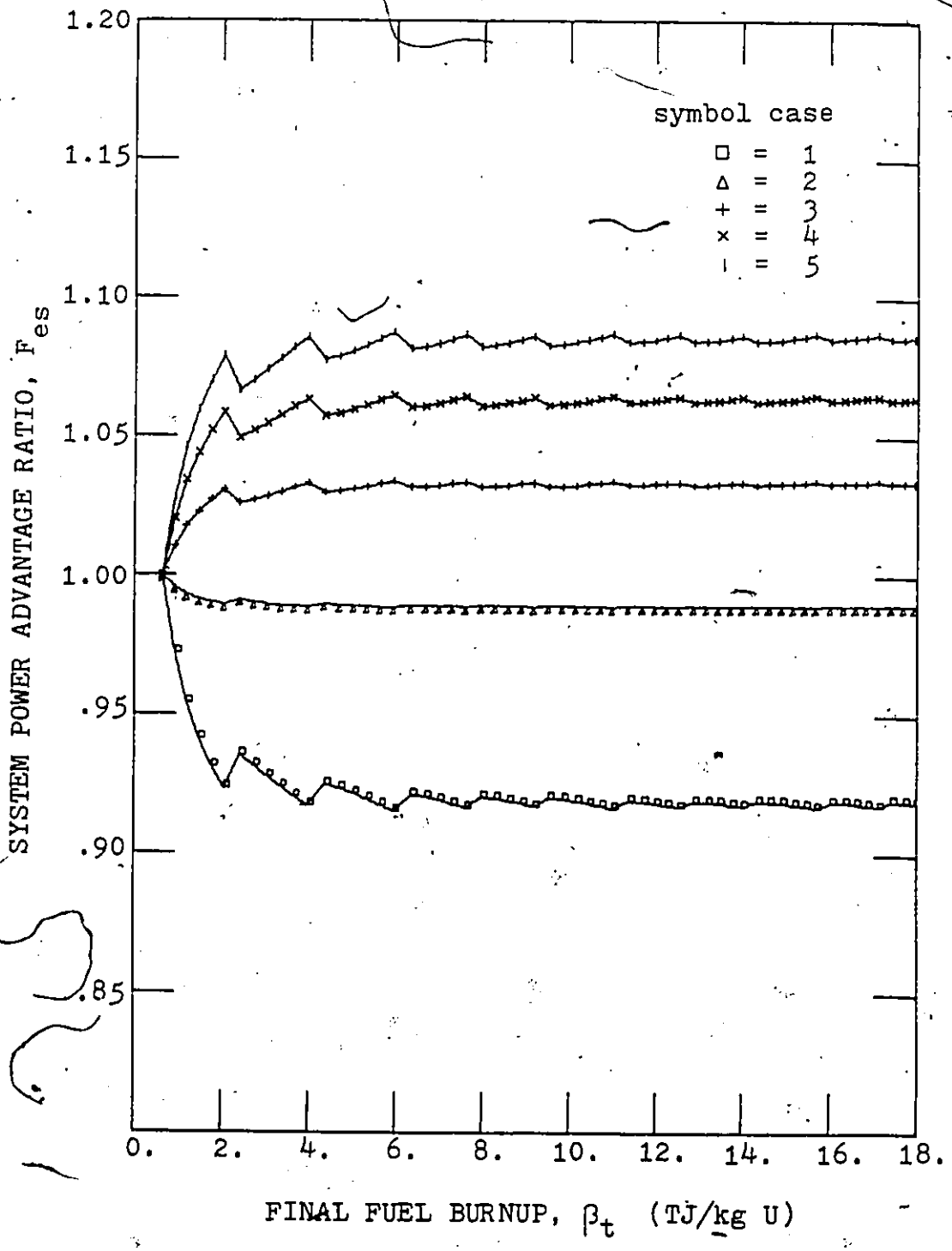

Fig. 5.3.2a System net electrical power advantage with periodic fuel reprocessing; cases 1 to 5 of Table 4.6.1.

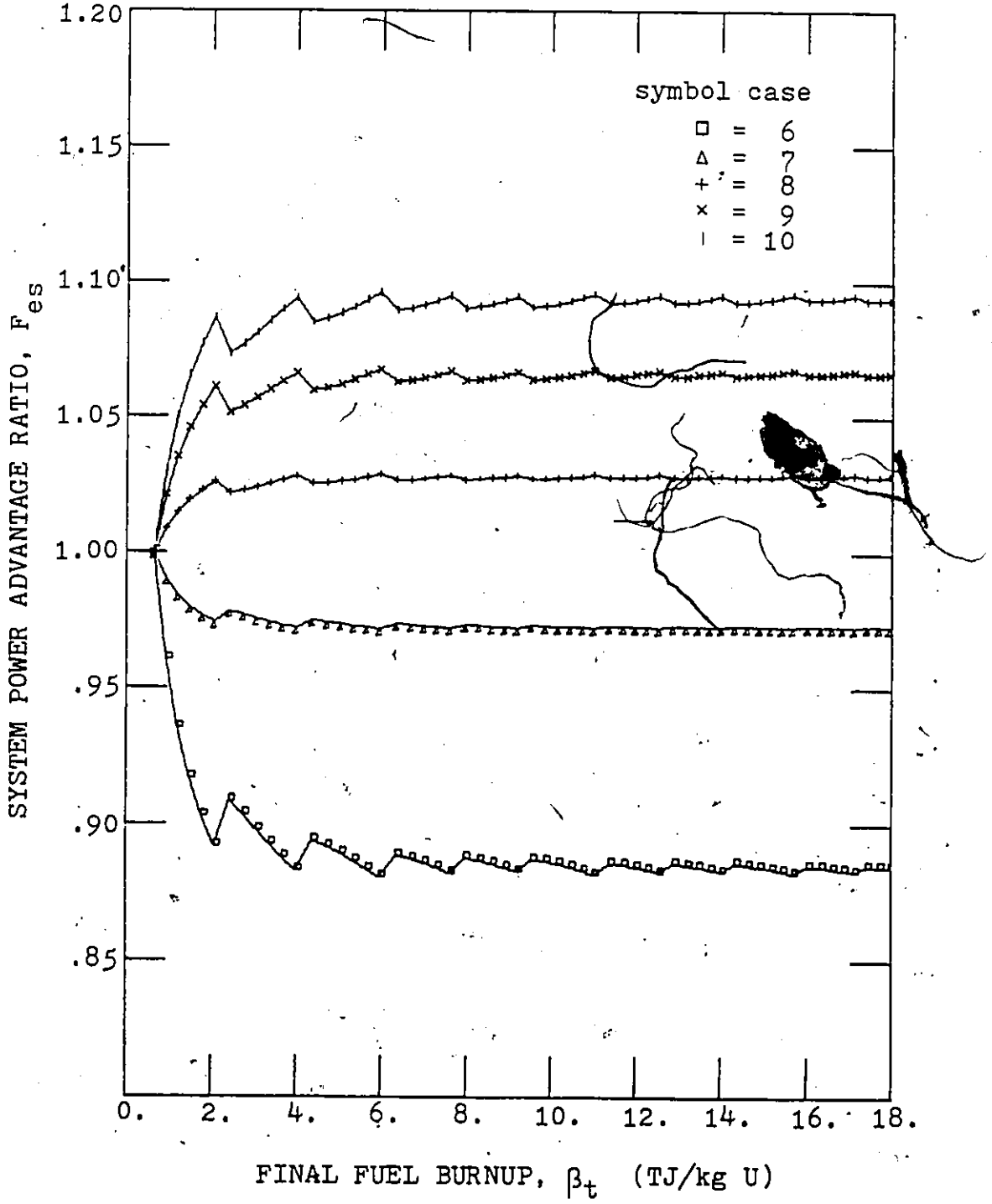

Fig. 5.3.2b System net electrical power advantage with periodic fuel reprocessing; cases 6 to 10 of Table 4.6.1.

through the introduction of a breeder subsystem. Similarly, the breeder-depleter power utilization, Q_{td}, defined by Eq. 5.1.9 and discussed in Sec. 5.2, defines the relative size of the breeder subsystem. For fuel recycling without reprocessing, f_s and Q_{td} have opposing effects since, as f_s is increased through higher fuel burnup, the magnitude of Q_{td} decreases. As the fuel cost decreases, the breeder cost therefore increases. A similar trade-off situation exists in association with the internal power utilization, Q_{tb}, defined by Eq. 5.2.1. Increasing Q_{tb} improves the power balance of the symbiotic system reflected by F_{es}, defined by Eq. 5.3.1. The same increase, however, also increases the breeder subsystem cost. Since f_s, Q_{td}, Q_{tb} and F_{es} are highly interdependent, an optimization of these parameters is only possible through an appropriate correlation function which expresses the relationship between these parameters.

In most analyses, a nuclear power system has to be evaluated in terms of the electrical energy produced per unit cost, E'_{ec}. The energy production advantage of a symbiotic system over a conventional reactor system can therefore be expressed by the ratio

$$A_{sd} = E'_{ecs}/E'_{ecd} , \qquad (5.4.1)$$

where the subscripts s and d stand for symbiotic system and depleter system respectively. Equation 5.4.1 defines a realistic correlation function for system parameter

optimization, while at the same time assessing the relative economic performance of the system. It is evident that an energy production advantage factor greater than unity has to be obtained to make the symbiotic system economically feasible. The energy per unit cost, E'_{ec}, is defined by

$$E'_{ec} = P_e \, t/C \qquad (5.4.2)$$

where P_e is the average electrical power produced by the system during its effective operation time t and C is the associated total system cost. The energy production advantage factor, defined by Eq. 5.4.1, from now on referred to as the advantage factor, can be expressed in terms of the system net power advantage ratio, F_{es}, defined by Eq. 5.3.1 to yield

$$A_{sd} = F_{es}/F_{ec} \, , \qquad (5.4.3)$$

where a cost correlation factor can be defined by

$$F_{ec} = c_s/c_d \, . \qquad (5.4.4)$$

Here, consistent with Eq. 5.4.2, the cost per unit time c for each system is defined by

$$c_s = C_s/t_s \qquad (5.4.5)$$

and

$$c_d = C_d/t_d \, .$$

In determining c_s and c_d, the system lifetime as well as the system load factor have to be taken into account. From Eq. 5.4.3, it can be concluded that in order to obtain an economically improved system, the breeder subsystem does not

necessarily have to be power self-sufficient. The only requirement is that the power advantage ratio, F_{es}, is larger than the cost correlation factor, F_{ec}.

5.5 Cost Correlation

The general definition of the cost correlation factor, F_{ec}, is given by Eq. 5.4.4 and its' cost assessment is now considered as

$$F_{ec} = \frac{1 + c_{bc}/c_{dc} + c_{sf}/c_{dc}}{1 + c_{df}/c_{dc}} \qquad (5.5.1)$$

where the subscripts c and f stand for capital-operational cost and fuel costs respectively. The cost is broken up into subsystem capital-operational costs and system fuel costs.

The breeder-converter subsystem capital-operational cost ratio, expressed in terms of the breeder-depleter power utilization, Q_{td}, defined by Eq. 5.1.9, and the internal breeder power utilization, Q_{tb}, defined by Eq. 5.2.1, yields

$$\frac{c_{bc}}{c_{dc}} = \frac{1}{Q_{td}} \left(\frac{c_{tac}}{c_{tdc}} + Q_{tb} \frac{c_{tbc}}{c_{tdc}}\right) , \qquad (5.5.2)$$

where

$$c_{tdc} = c_{dc}/P_{td} , \qquad (5.5.3)$$

$$c_{tac} = c_{ac}/P_{te} , \qquad (5.5.4)$$

and

$$c_{tbc} = c_{bc}/(P_{tcb} + P_{tbb} + P_{te}) . \qquad (5.5.5)$$

The ratio of symbiotic system fuel cost to converter capital-operational cost can be expressed in terms of the fuel stretching factor, f_s, defined by Eq. 4.7.3, to yield

$$\frac{c_{sf}}{c_{dc}} = \frac{F_{cfc}}{f_s} F_{cr} , \qquad (5.5.6)$$

where the conventional reactor fractional fuel cost, F_{cfc}, is defined by

$$F_{cfc} = c_{df}/c_{dc} \qquad (5.5.7)$$

and F_{cr} is the relative fuel cost increase due to reprocessing charges. For the system without reprocessing

$$F_{cr} \equiv 1 , \qquad (5.5.8)$$

while for a system with periodic reprocessing, one obtains

$$F_{cr} = F_{cff}(1 + s_{rsd}) + F_{cmf} . \qquad (5.5.9)$$

Here, F_{cff} and F_{cmf} are the relative fuel fabrication and mill-grade fuel costs of the conventional depleter reactor with their sum being equal to unity; s_{rsd} is the relative reprocessing cost fraction. For no reprocessing charges

$$s_{rsd} \equiv 0 . \qquad (5.5.10)$$

The relative reprocessing cost fraction can generally be written as

$$s_{rsd} = w_{rsd} M_r/M_{oh} \qquad (5.5.11)$$

where w_{rsd} is the cost ratio of active fuel reprocessing and fabrication to fresh fuel fabrication. The total reprocessed fuel mass, M_r, per initial fuel mass, M_{oh}, Eq. 4.4.9, becomes

$$\frac{M_r}{M_{oh}} = \sum_{p=1}^{P} \prod_{\ell=1}^{p} (1 - {}^{\ell}\delta'_m) \qquad (5.5.12)$$

where p defines the non-reprocessing period and ℓ stands for fuel cycles after reprocessing. ${}^{\ell}\delta'_m$ is defined as cycle ℓ-1 fuel mass removal fraction. ${}^{1}\delta'_m$ is defined as being equal to zero. In Eq. 5.5.12, P stands for the total number of reprocessing cycles.

5.6 Energy Production Advantage with and without Limited Reprocessing

In the cost correlation function, F_{ec}, derived in the previous section, the system cost parameters have all been expressed as ratios relative to conventional depleter reactors. The cost parameters obtained are thus related to an existing technology. The capital-operational cost ratios can, however, fluctuate considerably since substantial uncertainty exists in actual reactor lifetimes, load factors, interest rates on capital expenditures, and relative mill-grade fuel costs. In this analysis, the relative fuel cost, F_{cfc}, Eq. 5.5.7, is therefore considered the major cost variable. During the time from 1977 to 1982, several independent system component cost estimates have been made yielding the following results.

The ratio of accelerator capital-operational cost per unit beam power to depleter capital-operational cost per

unit thermal power were estimated by several sources[32,37,48,50,56] to yield

$$\frac{c_{tac}}{c_{tdc}} = 2.8 \pm 5\% , \qquad (5.6.1)$$

while the ratio of breeder subsystem target-blanket capital-operational cost per unit thermal power to depleter capital-operational cost per unit thermal power is generally taken as

$$\frac{c_{tbc}}{c_{tdc}} = 1.0 . \qquad (5.6.2)$$

This estimate is felt to be reasonable since relative to a conventional critical reactor, the increased cost of a more complex target system is balanced by a decrease in cost due to a less complex blanket system and subcritical subsystem operation.

From recent estimates[76], the relative fuel component costs are

$$F_{cff} = 0.38 \qquad (5.6.3)$$

and

$$F_{cmf} = 0.62 , \qquad (5.6.4)$$

while the cost ratio of active fuel reprocessing and fabrication to fresh fuel fabrication [74] is

$$w_{rsd} = 3.0 . \qquad (5.6.5)$$

The cycle mass removal fraction, $^{\ell}\delta'_{m}$, used in Eq. 5.5.12 is taken to be equal to the mass-energy removal fraction, $^{m}\delta'$,

defined by Eq. 4.6.6 and its' numerical values for the analyzed system are summarized in Table 4.6.2.

Substituting Eq. 5.6.1 to Eq. 5.6.5 into the expression for the system energy production advantage factor, Eq. 5.4.3, yields

$$A_{sd} = F_{es}/F_{ec} \quad , \tag{5.6.6}$$

where

$$F_{es} = \left(\eta_c Q_{tcb} + \eta_b Q_{tbb} + \frac{\bar{P}_{tc\ell}}{P_{te}} (\eta_b - \eta_c) + \eta_d Q_{td} - \frac{1}{\varepsilon_{ee}}\right)/\eta_d Q_{td} \tag{5.6.7}$$

and

$$F_{ec} = \left(1 + \frac{1}{Q_{td}} (2.8 + Q_{tcb} + Q_{tbb}) + \frac{F_{cfc}}{f_s} (0.38(1 + 3.0 \frac{M_r}{M_{oh}}) + 0.62)\right)/(1 + F_{cfc}). \tag{5.6.8}$$

The general system parameters are summarized in Table 5.6.1.

The cost correlation factor, F_{ec}, is shown in Fig. 5.6.1. and Fig. 5.6.2 for the symbiotic systems without reprocessing and with periodic reprocessing respectively. Here, the dominant feature is the insensitivity of the cost correlation factor to changes in the target produced fission neutron source. Even a 20% reduction in the effective neutron source S_n, as shown in Fig. 5.6.1f to Fig. 5.6.1j, and Fig. 5.6.2f to Fig. 5.6.2j, shows only a small increase in the system cost correlation factor. It should be noted

Table 5.6.1 General symbiotic system parameters.

parameter	values used	most recent values	references	description
η_c	0.40	0.35-0.40	48,75	conversion efficiency of spallation targets
η_b	0.30	0.30-0.40	40,48,75	conversion efficiency of breeder blankets
η_d	0.30	0.29-0.35	40,48, 75,76	conversion efficiency of depleter reactors
ϵ_{ee}	0.70	0.50-0.70	40,48,49, 50,56	conversion efficiency of accelerators
F_{cff}	0.38	0.38	76	fuel fabrication cost fraction
F_{cmf}	0.62	0.62	76	fuel mill-grade cost fraction
w_{rsd}	3.00	2.5-3.5	74	fuel relative reprocessing cost fraction
c_{tac}/c_{tdc}	2.80	2.6-3.0	32,37,48 50,56	relative accelerator cost fraction
c_{tbc}/c_{tdc}	1.00	1.0	32,37,48 50,56	relative breeder cost fraction
F_{cfc}	0.20 0.40 0.60 0.80 1.00	0.43	76	total fuel cost fraction

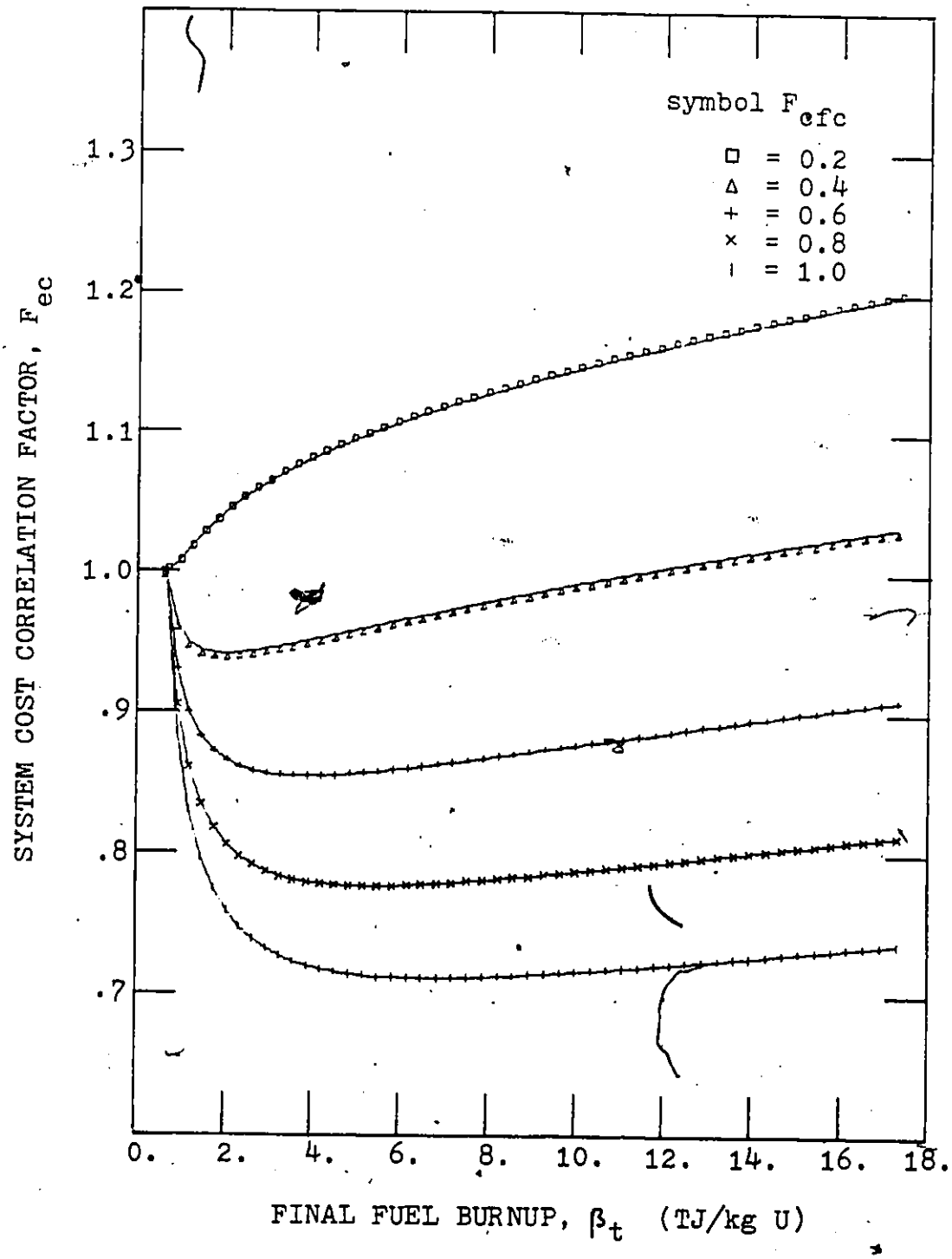

Fig. 5.6.1a Symbiotic system cost correlation factor without fuel reprocessing; case 1 of Table 4.6.1.

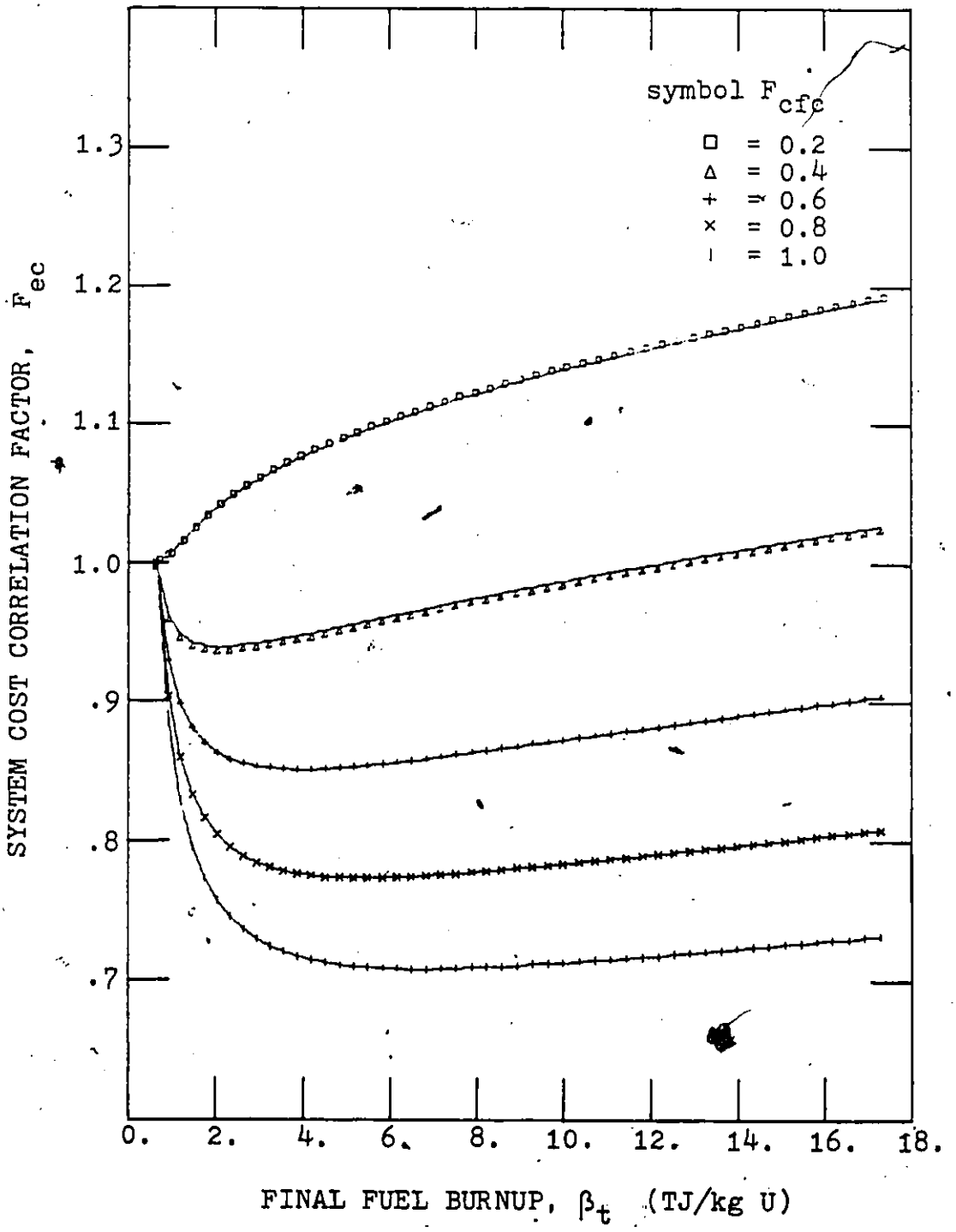

Fig. 5.6.1b Symbiotic system cost correlation factor without fuel reprocessing; case 2 of Table 4.6.1.

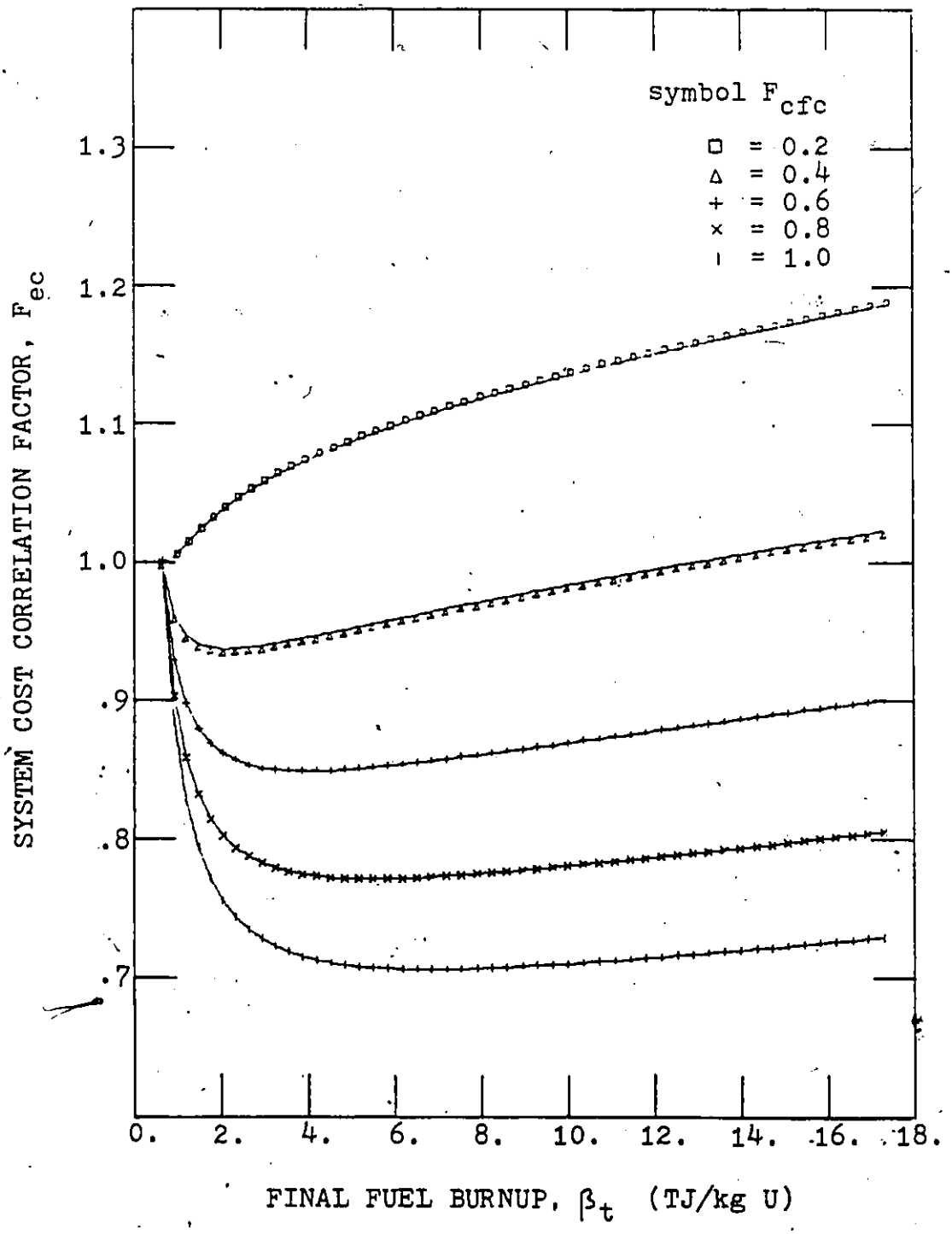

Fig. 5.6.1c Symbiotic system cost correlation factor without fuel reprocessing; case 3 of Table 4.6.1.

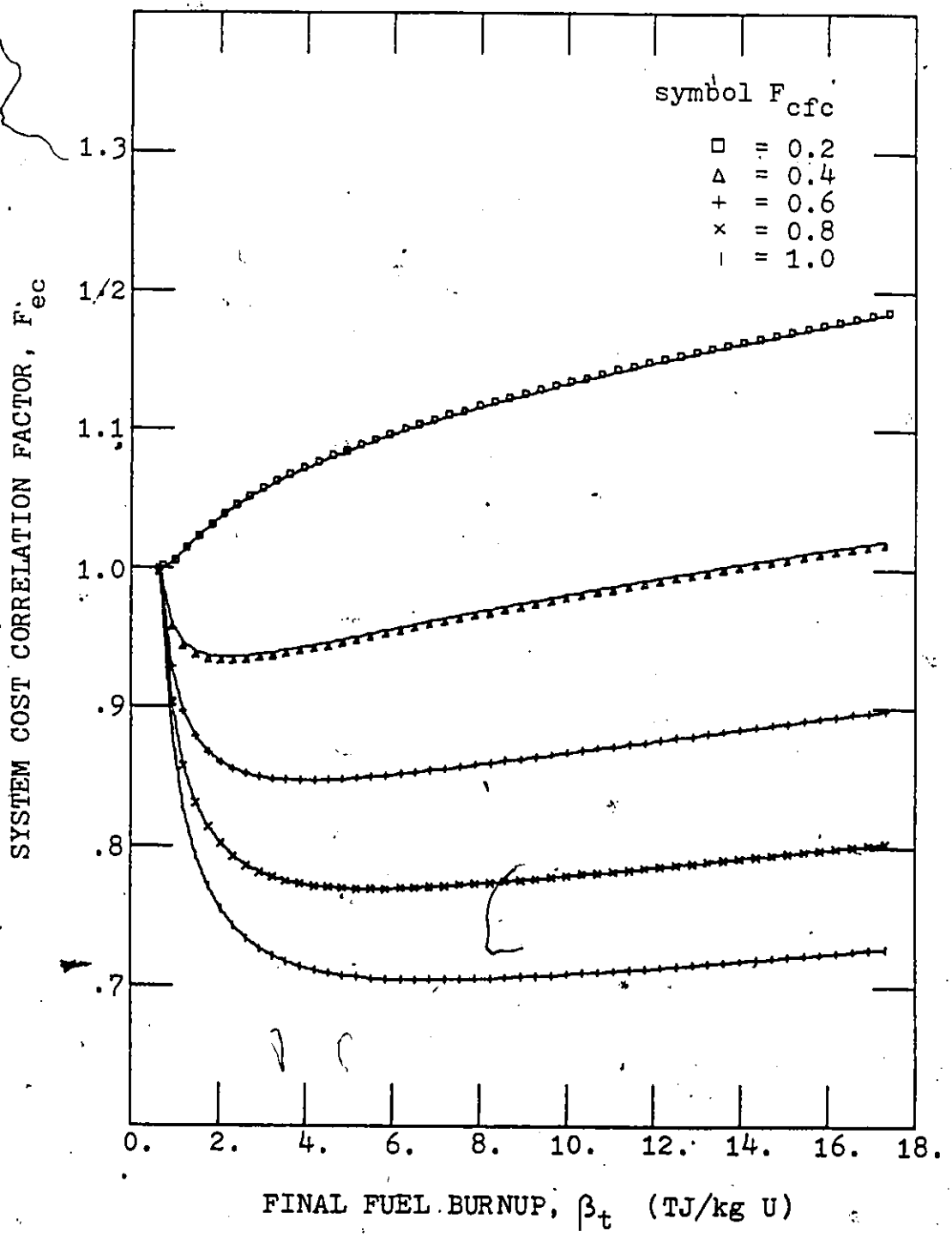

Fig. 5.6.1d Symbiotic system cost correlation factor without fuel reprocessing; case 4 of Table 4.6.1.

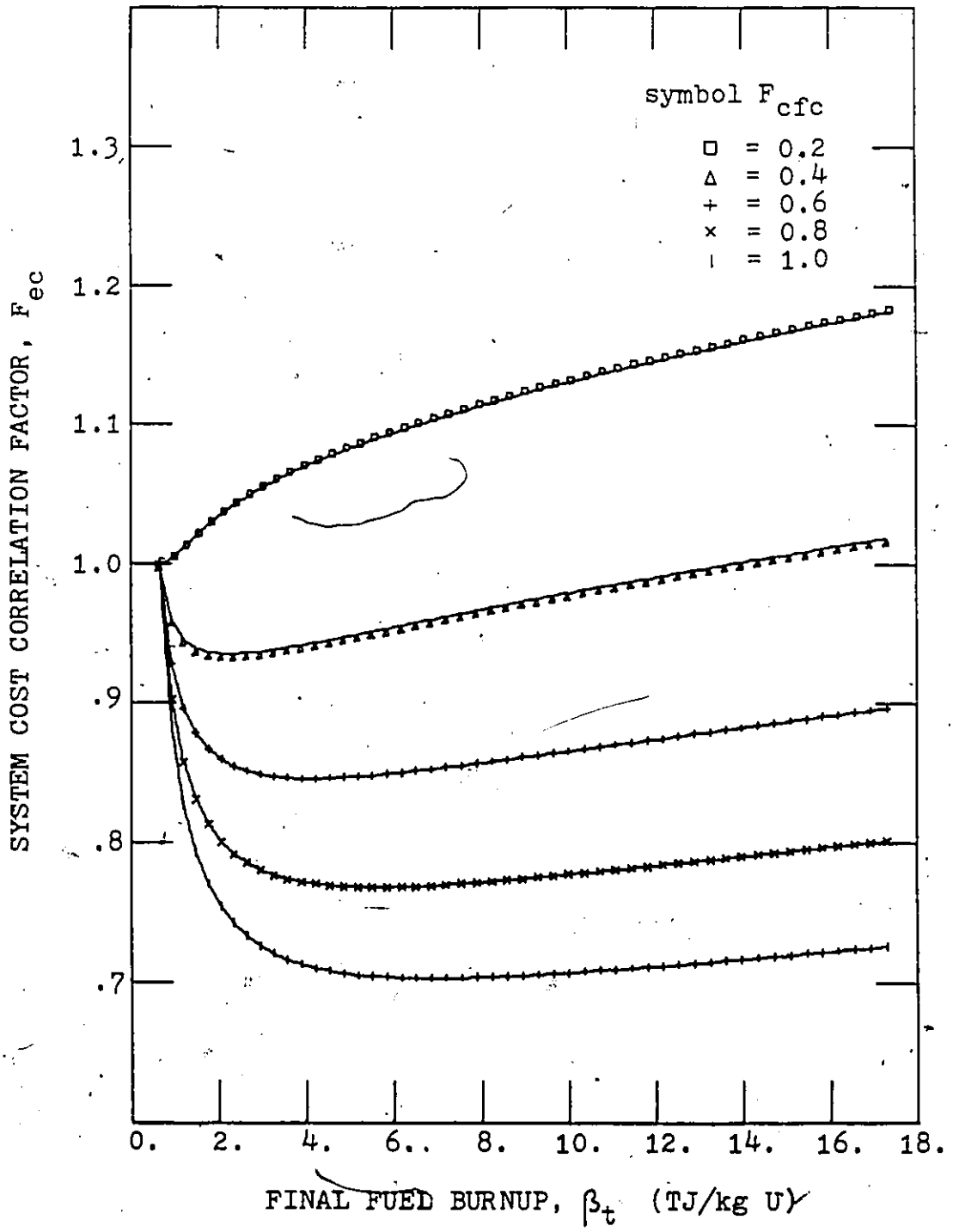

Fig. 5.6.1e Symbiotic system cost correlation factor without fuel reprocessing; case 5 of Table 4.6.1.

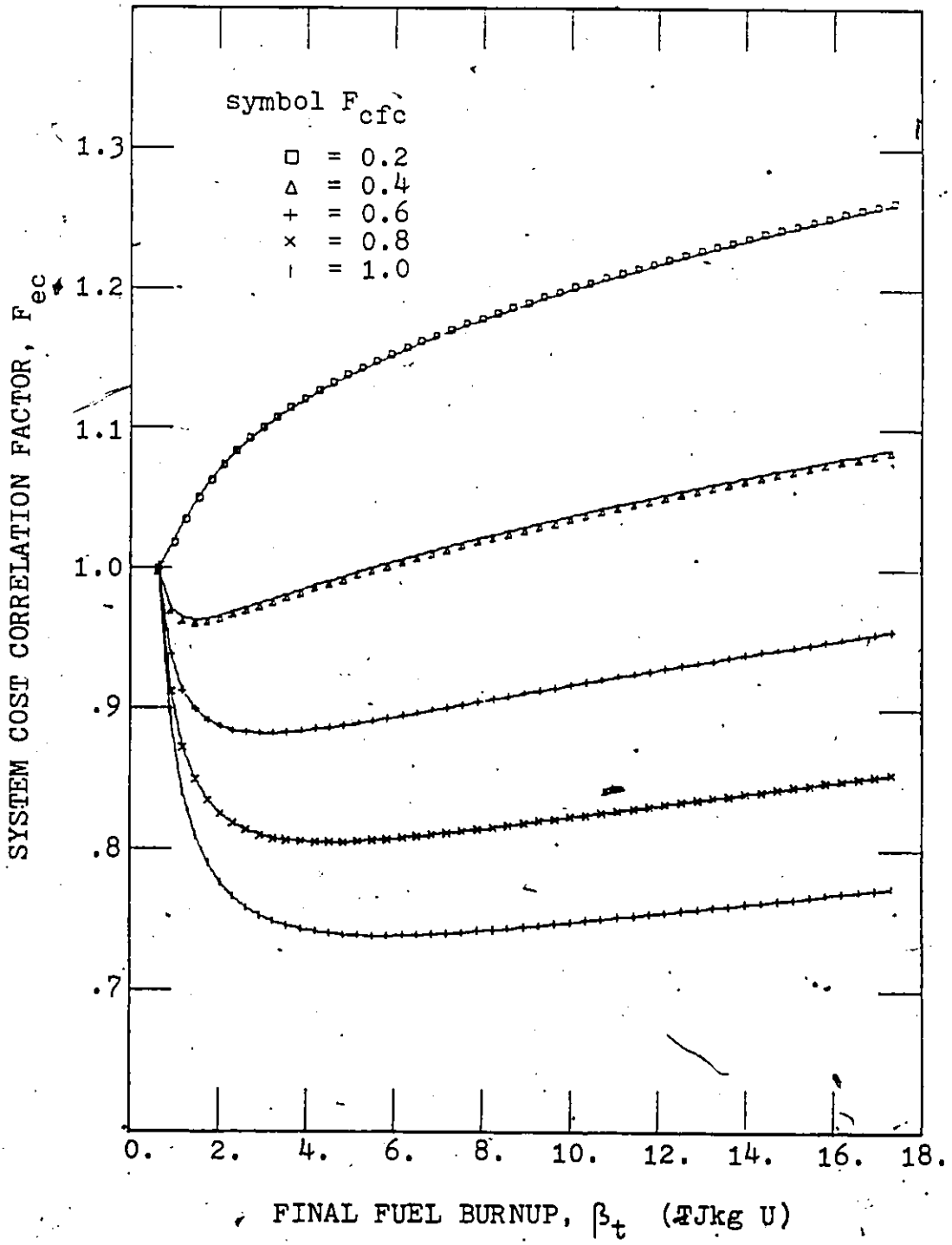

Fig. 5.6.1f Symbiotic system cost correlation factor without fuel reprocessing; case 6 of Table 4.6.1.

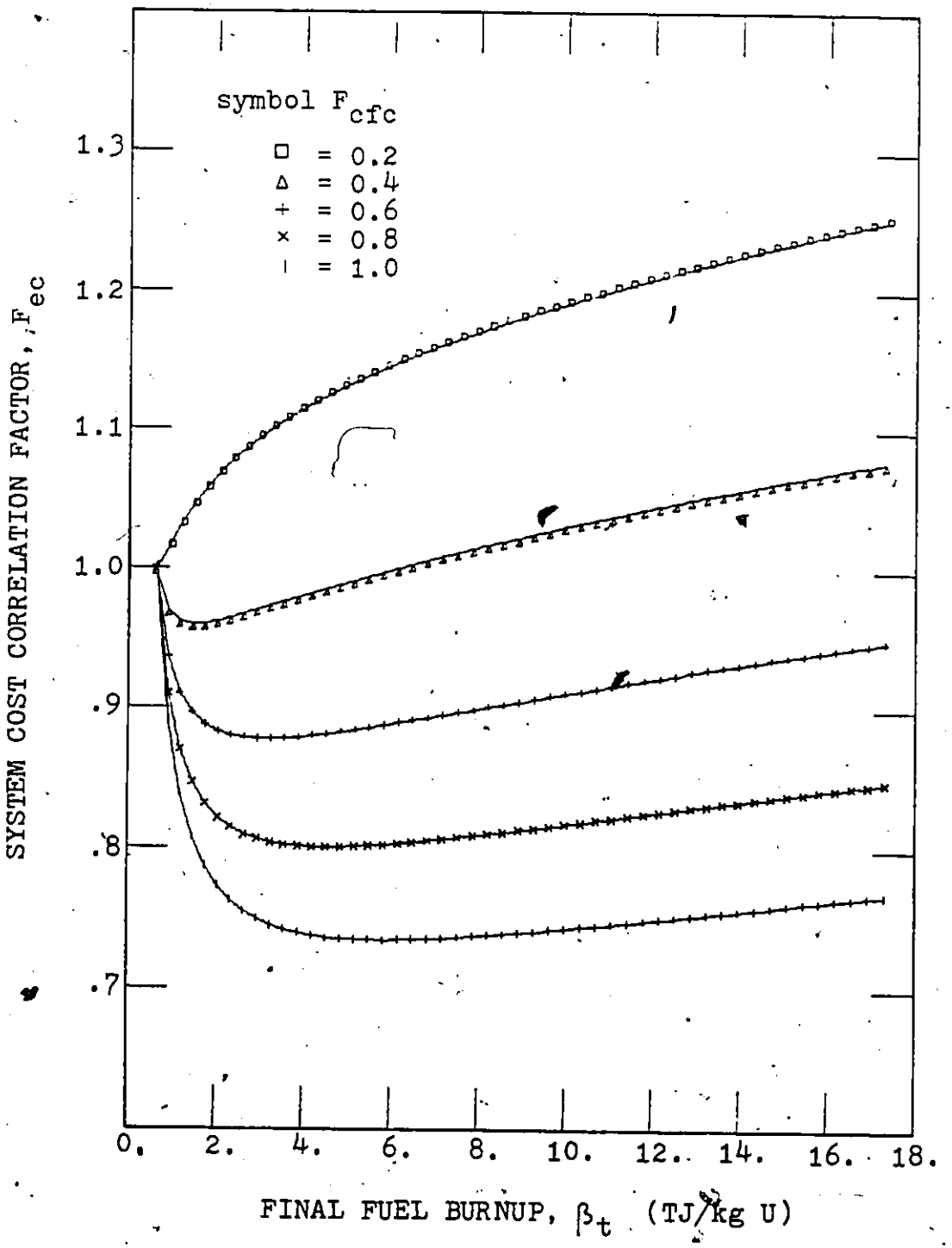

Fig. 5.6.1g Symbiotic system cost correlation factor without fuel reprocessing; case 7 of Table 4.6.1.

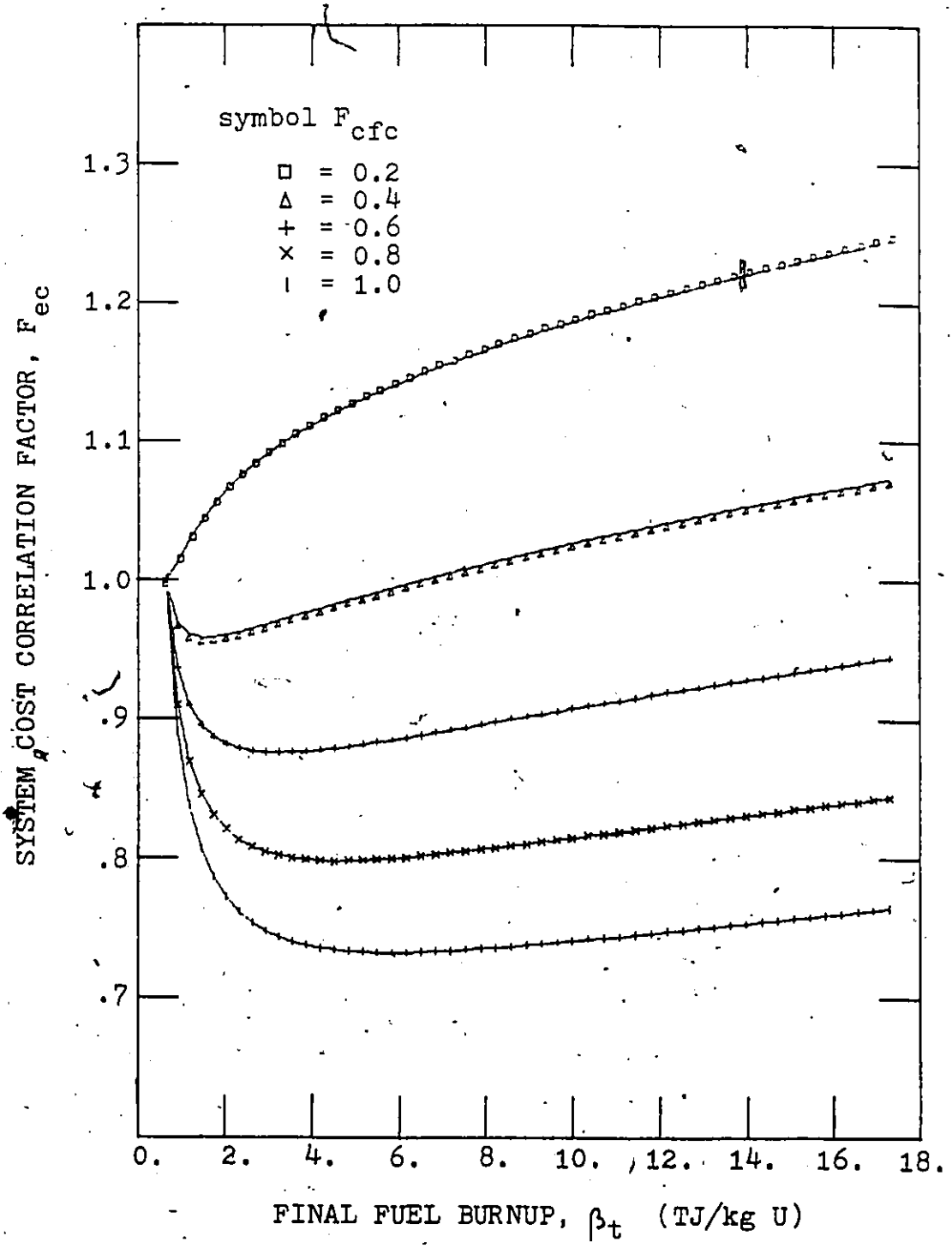

Fig. 5.6.1h Symbiotic system cost correlation factor without fuel reprocessing; case 8 of Table 4.6.1.

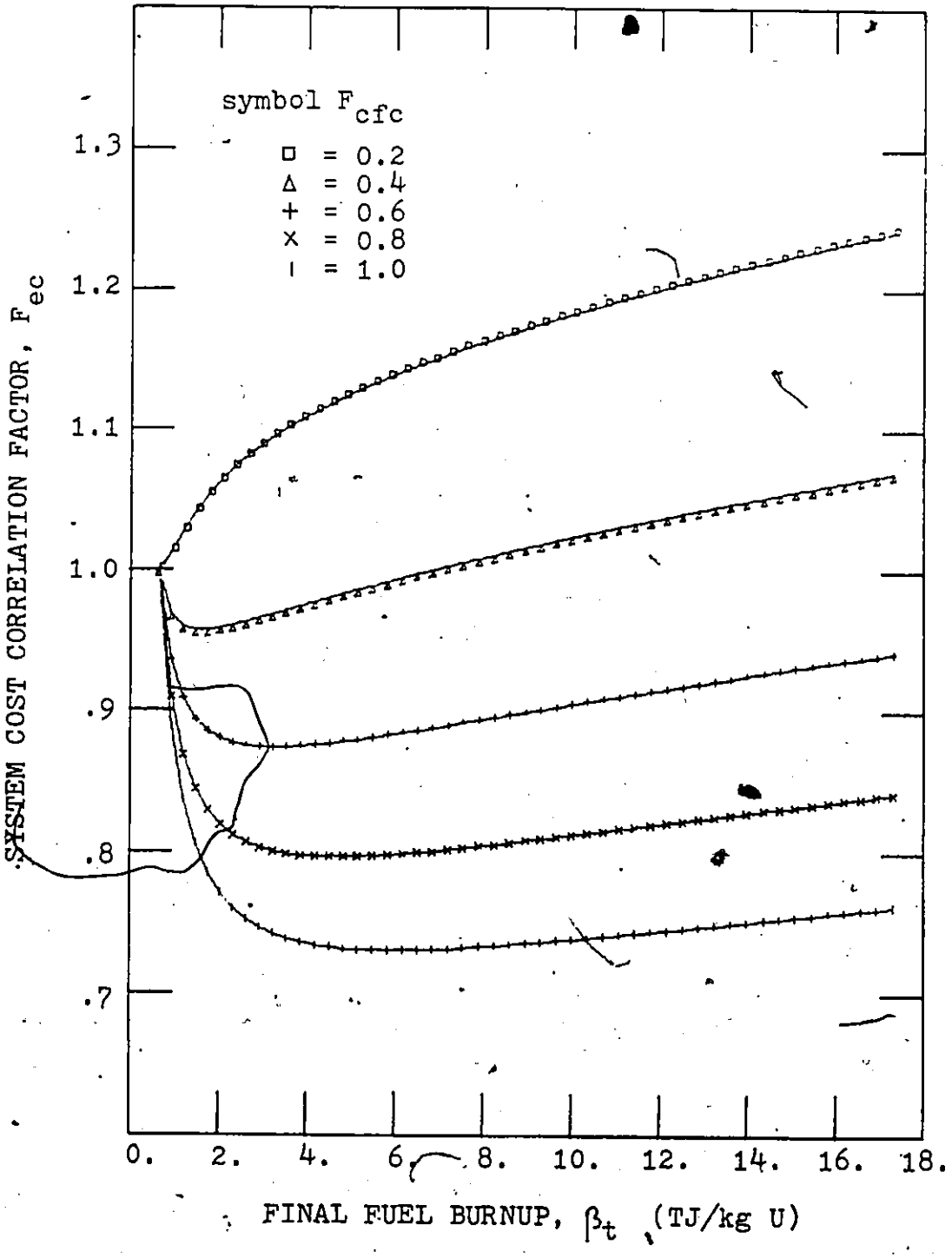

Fig. 5.6.1i Symbiotic system cost correlation factor without fuel reprocessing; case 9 of Table 4.6.1.

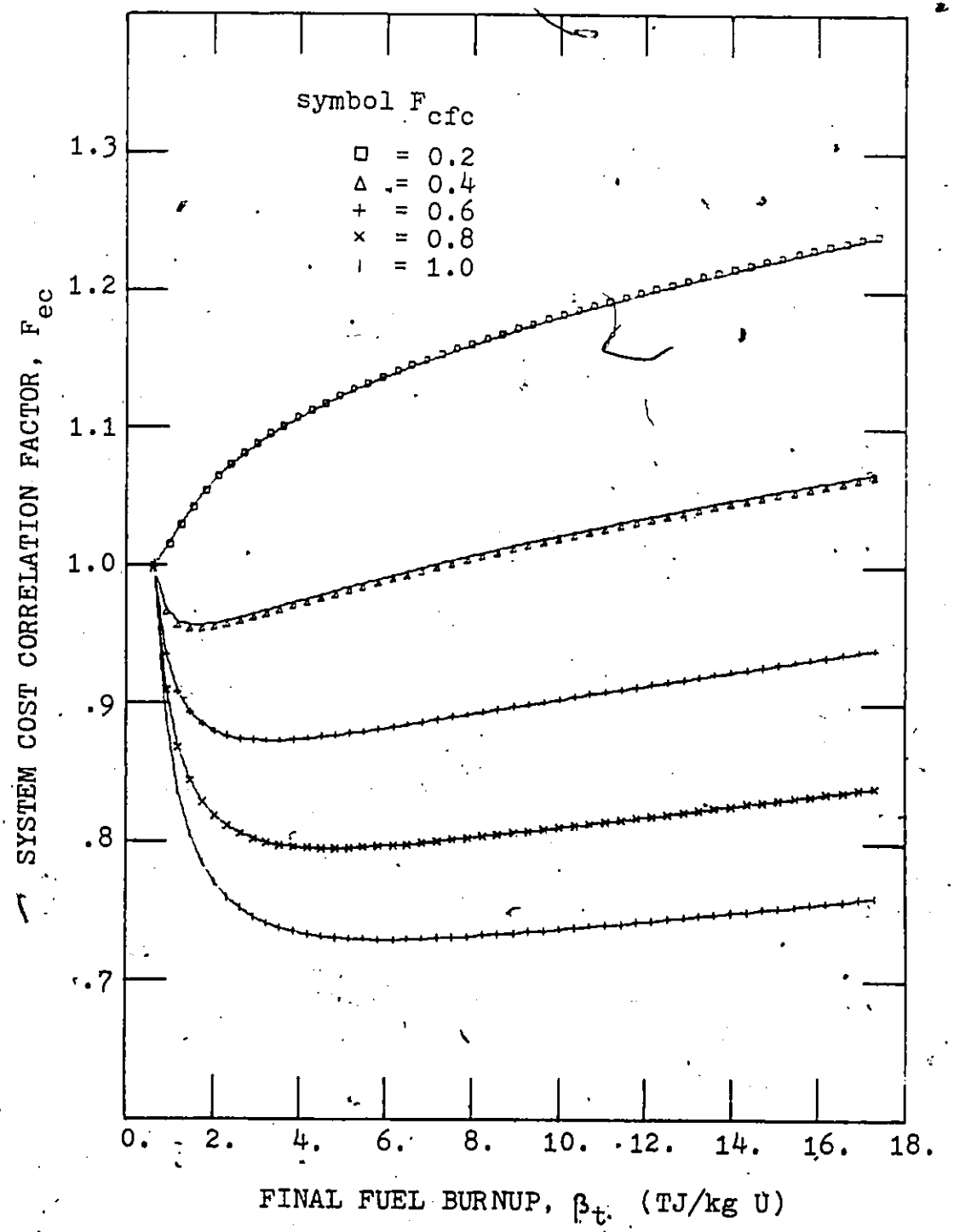

Fig. 5.6.1j Symbiotic system cost correlation factor without fuel reprocessing; case 10 of Table 4.6.1.

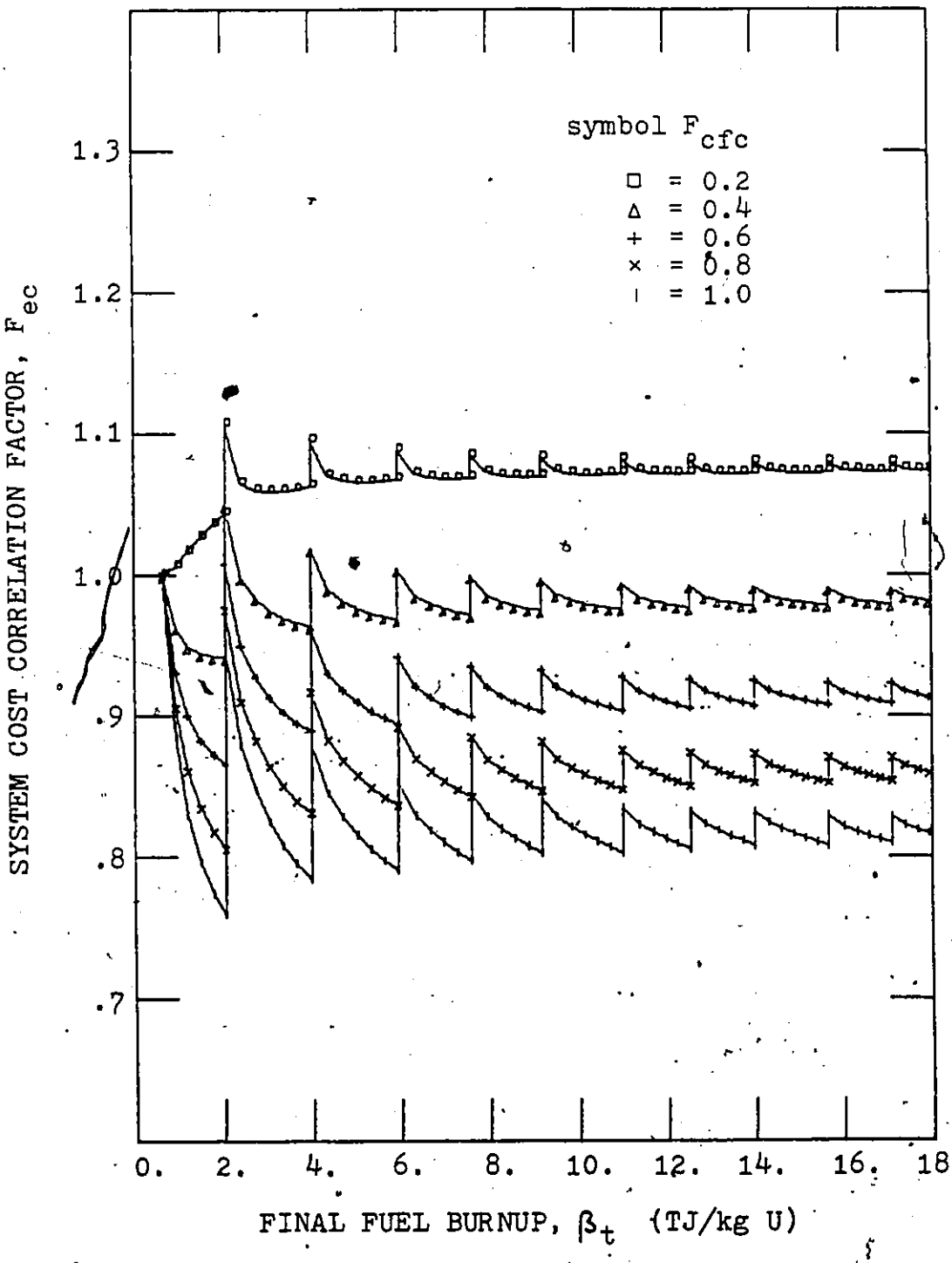

Fig. 5.6.2a Symbiotic system cost correlation factor with periodic reprocessing; case 1 of Table 4.6.1.

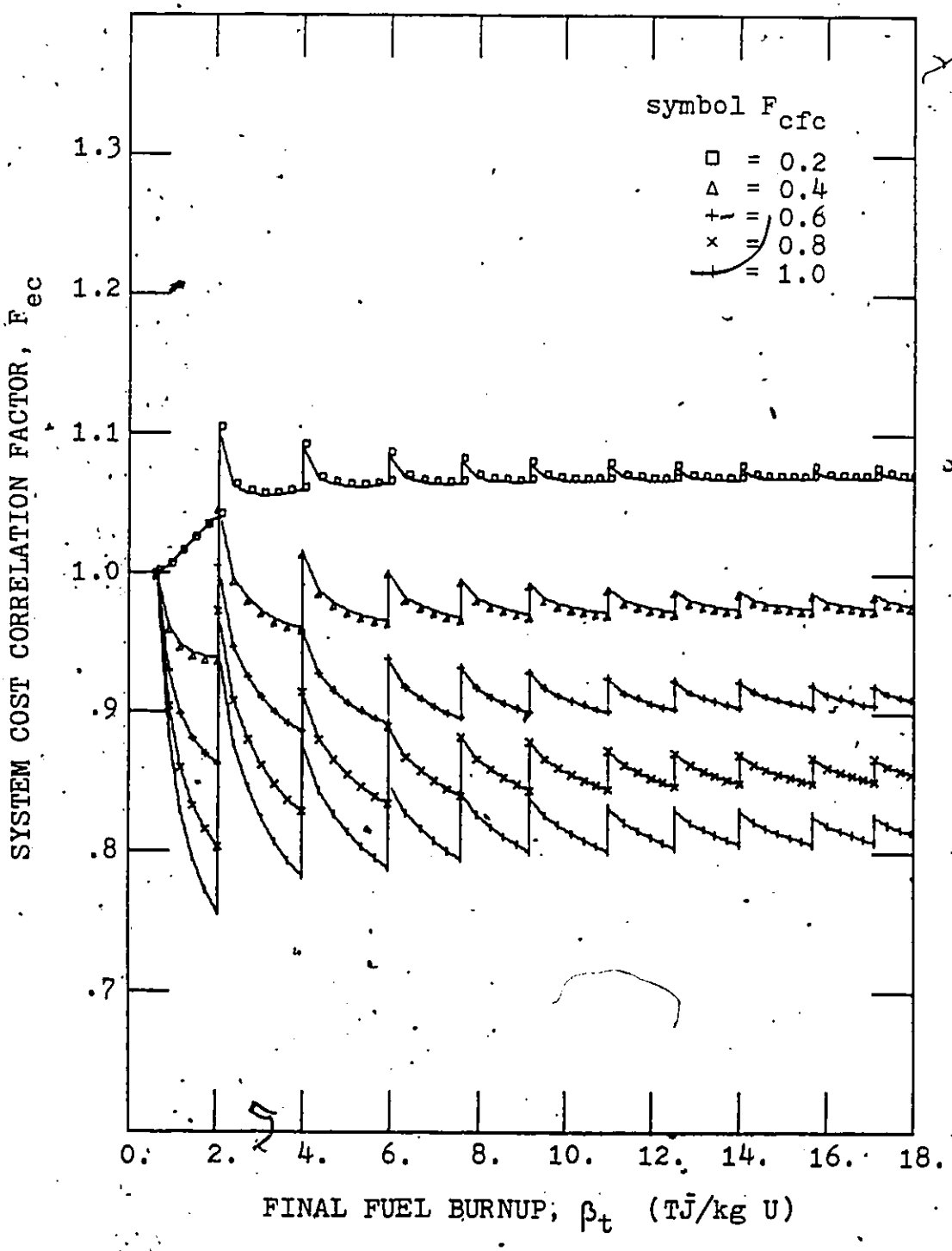

Fig. 5.6.2b Symbiotic system cost correlation factor with periodic reprocessing; case 2 of Table 4.6.1.

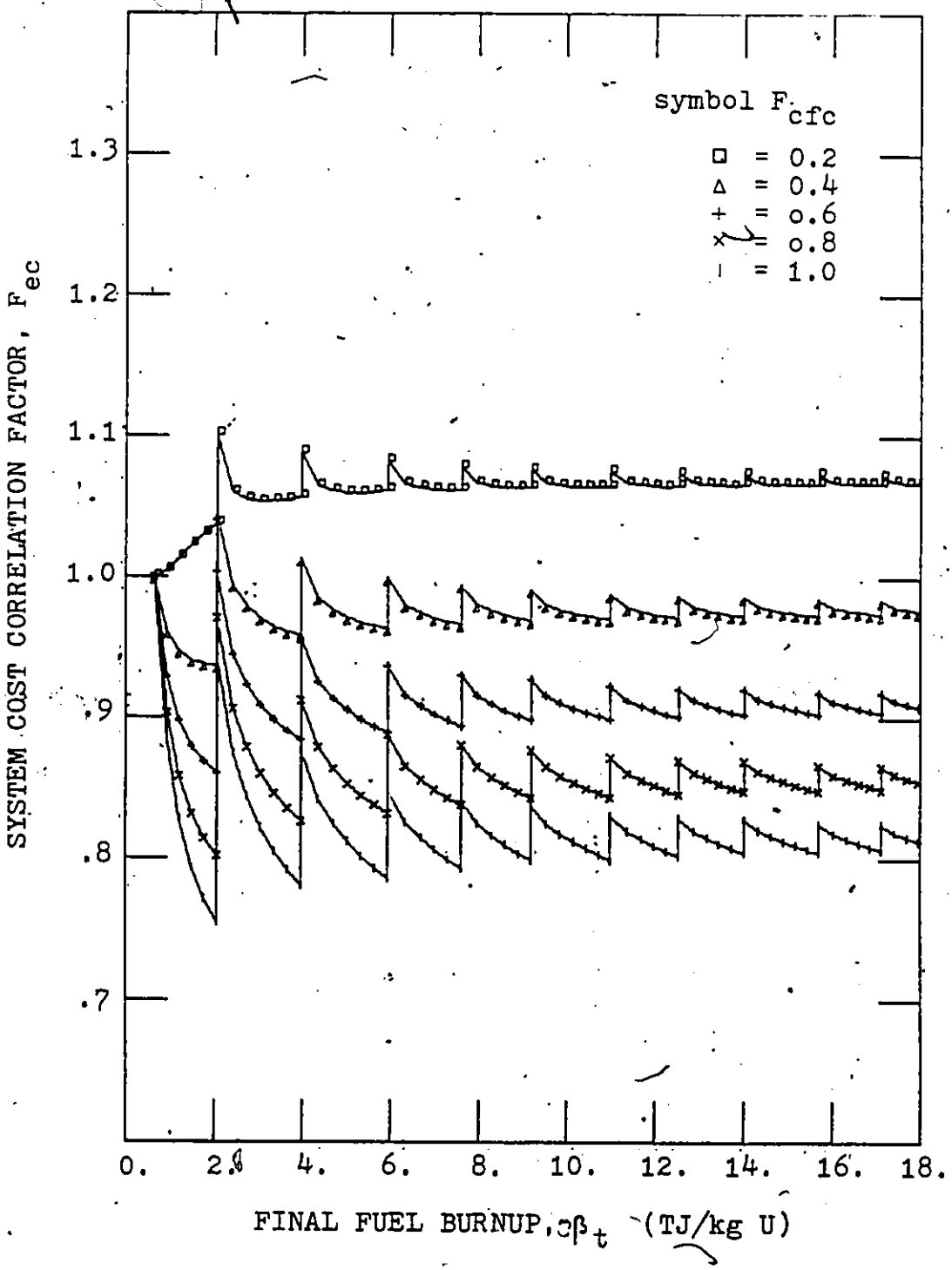

Fig. 5.6.2c Symbiotic system cost correlation factor with periodic reprocessing; case 3 of Table 4.6.1.

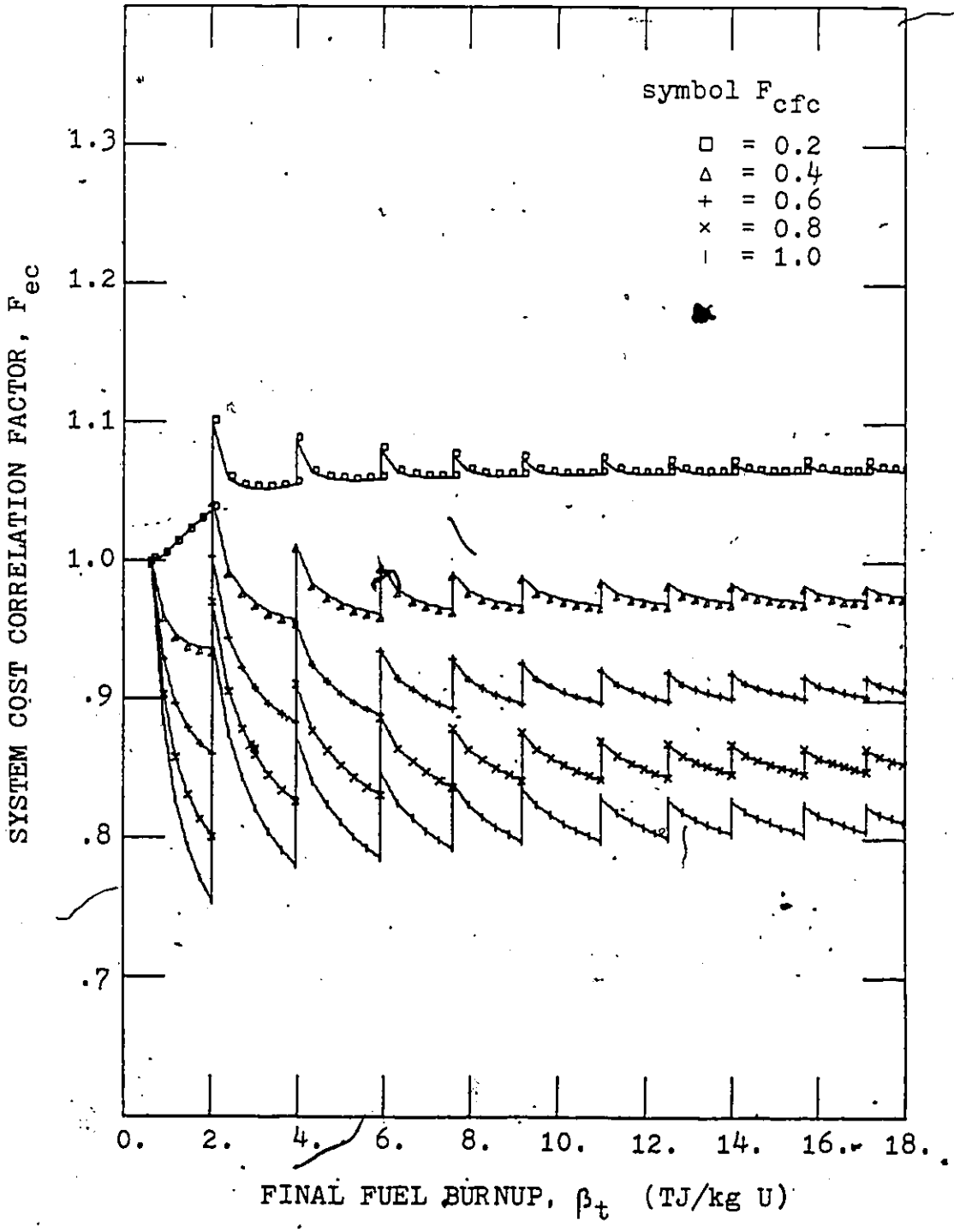

Fig. 5.6.2d Symbiotic system cost correlation factor with periodic reprocessing; case 4 of Table 4.6.1.

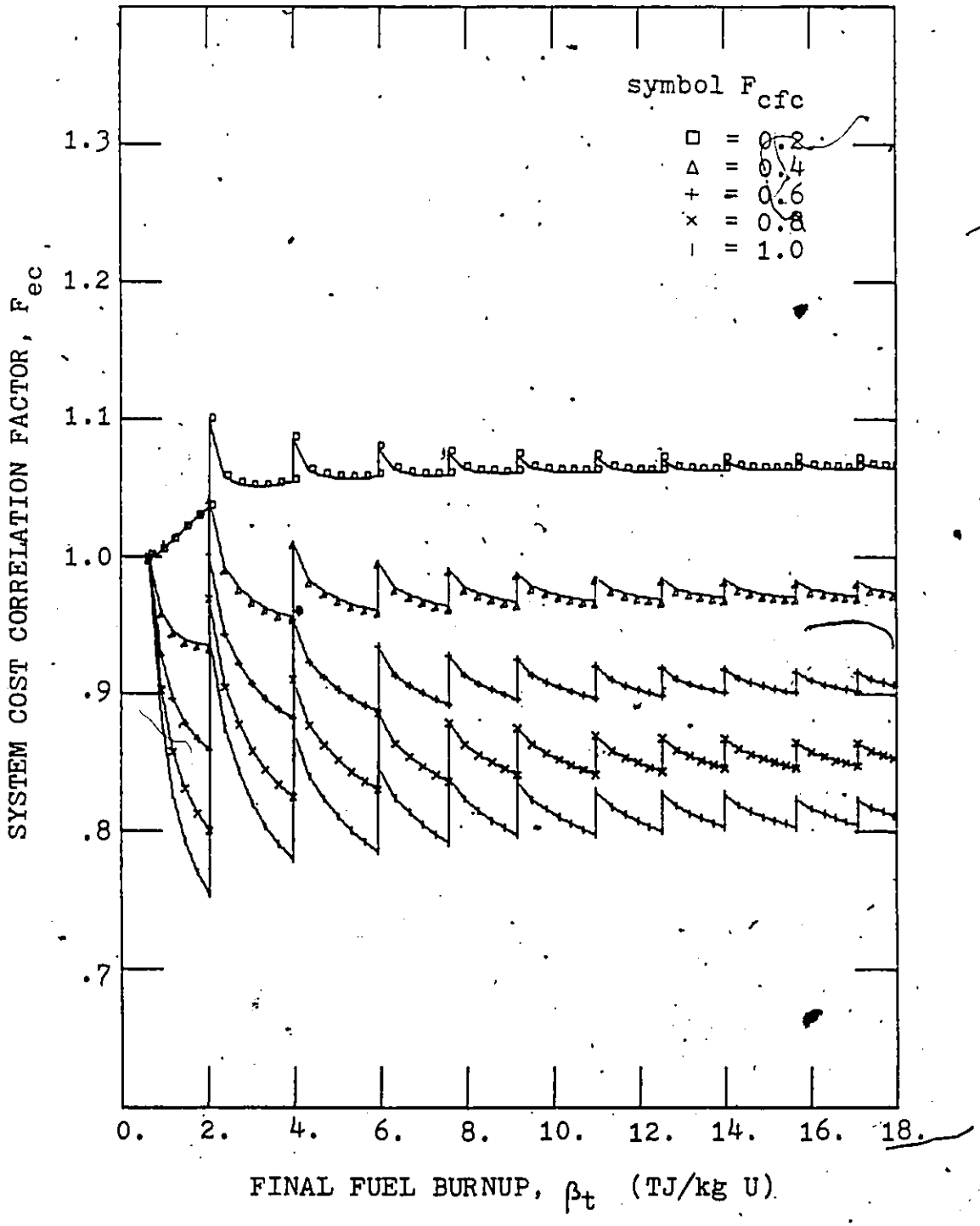

Fig. 5.6.2e Symbiotic system cost correlation factor with periodic reprocessing; case 5 of Table 4.6.1.

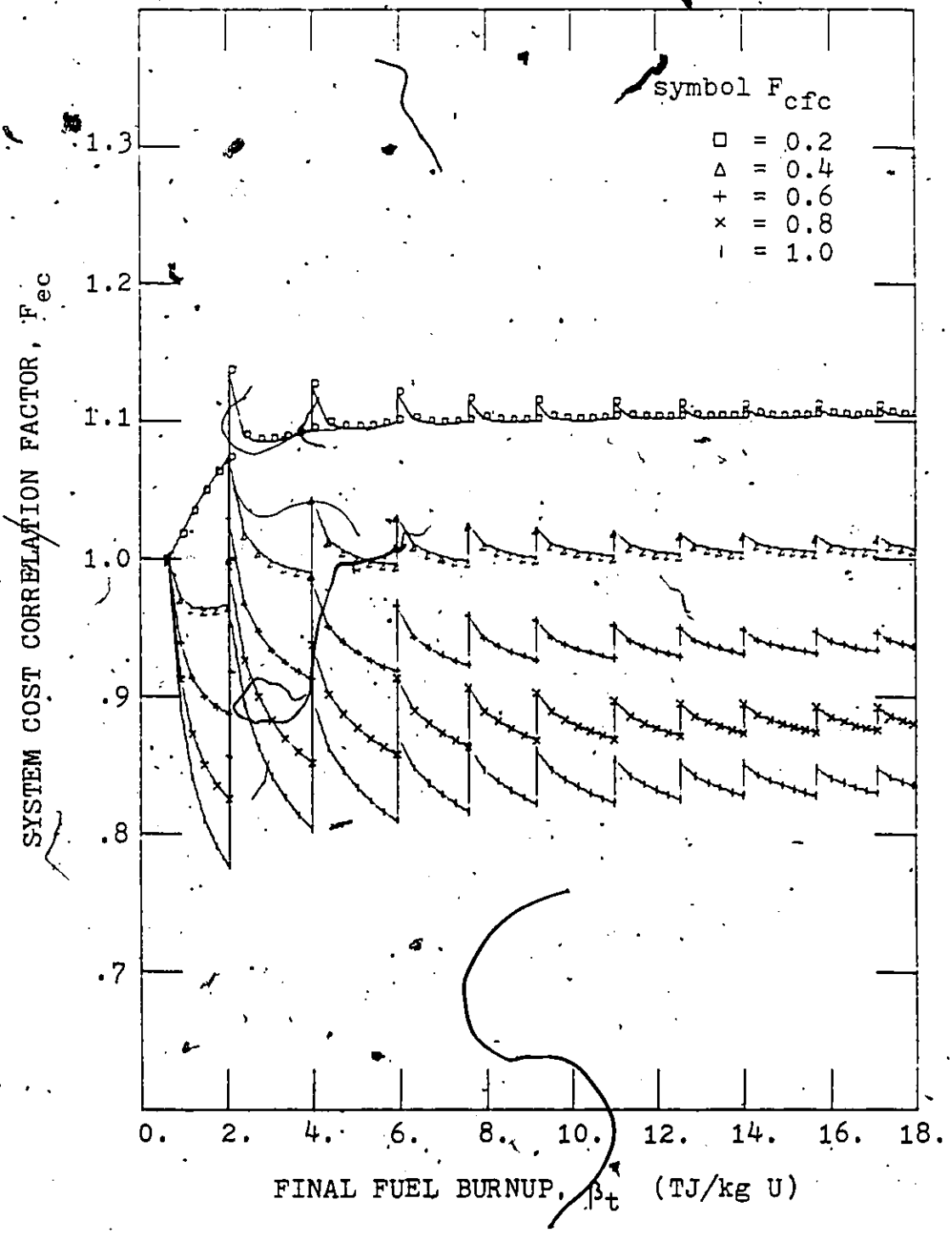

Fig. 5.6.2f Symbiotic system cost correlation factor with periodic reprocessing; case 6 of Table 4.6.1.

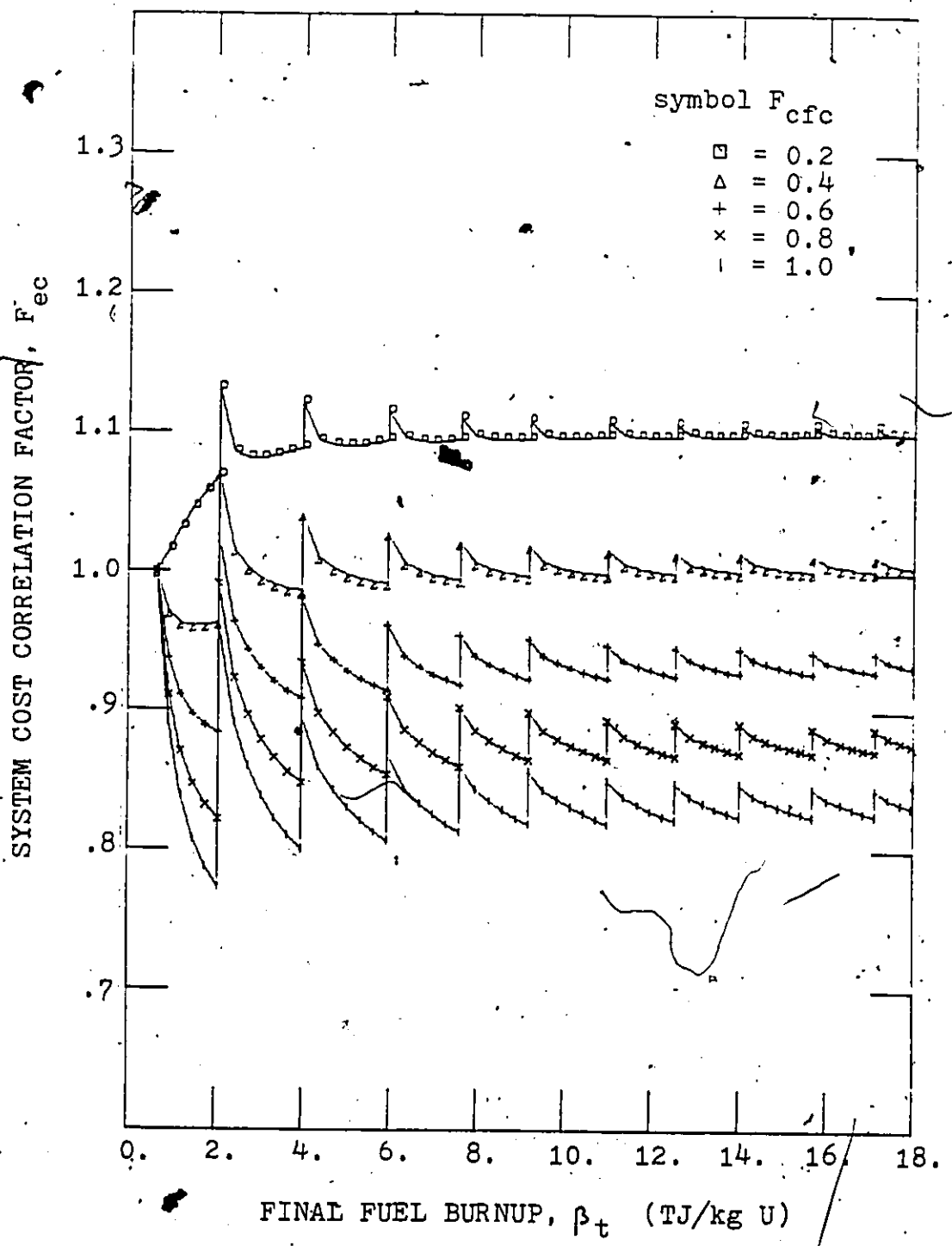

Fig. 5.6.2g Symbiotic system cost correlation factor with periodic reprocessing; case 7 of Table 4.6.1.

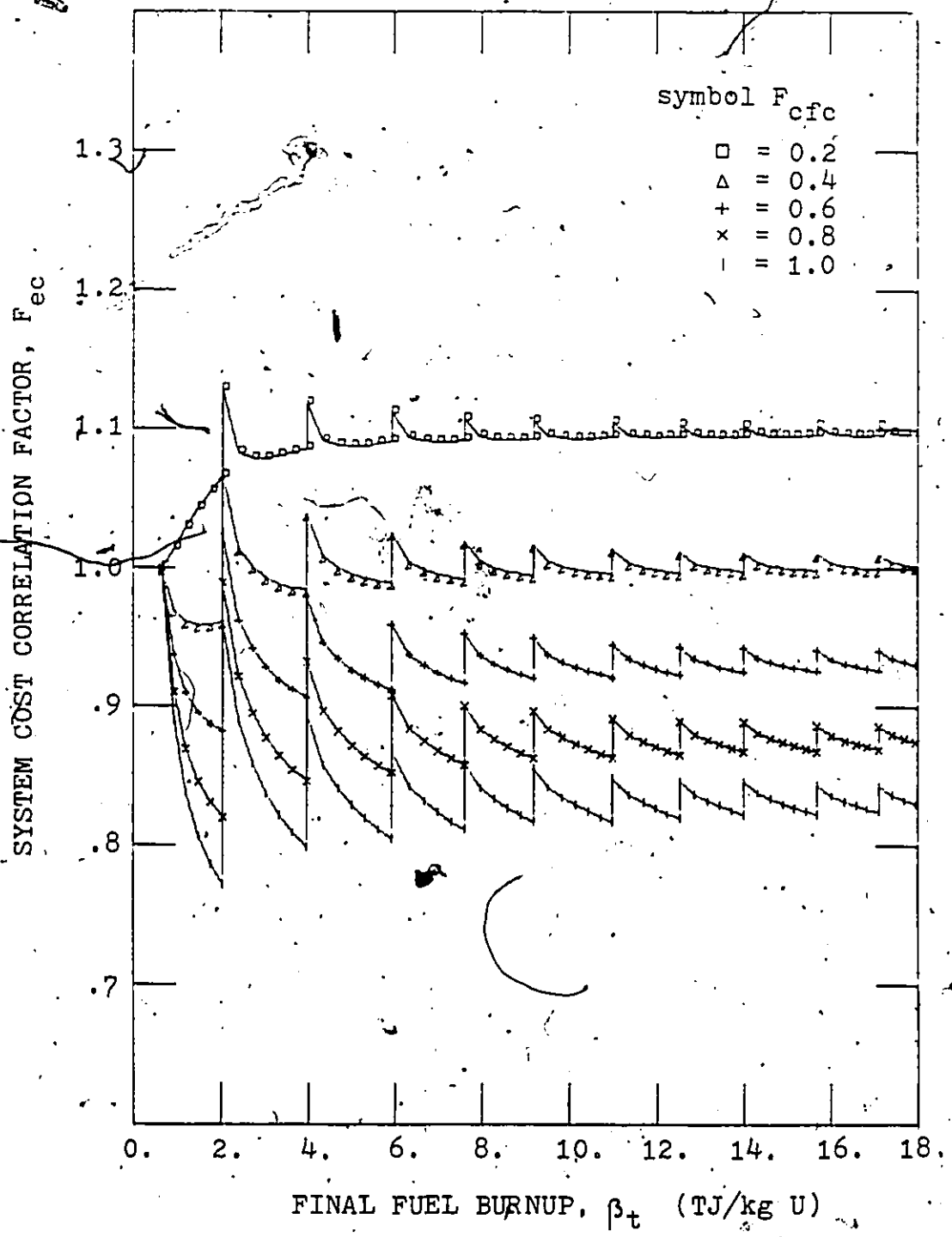

Fig. 5.6.2h Symbiotic system cost correlation factor with periodic reprocessing; case 8 of Table 4.6.1.

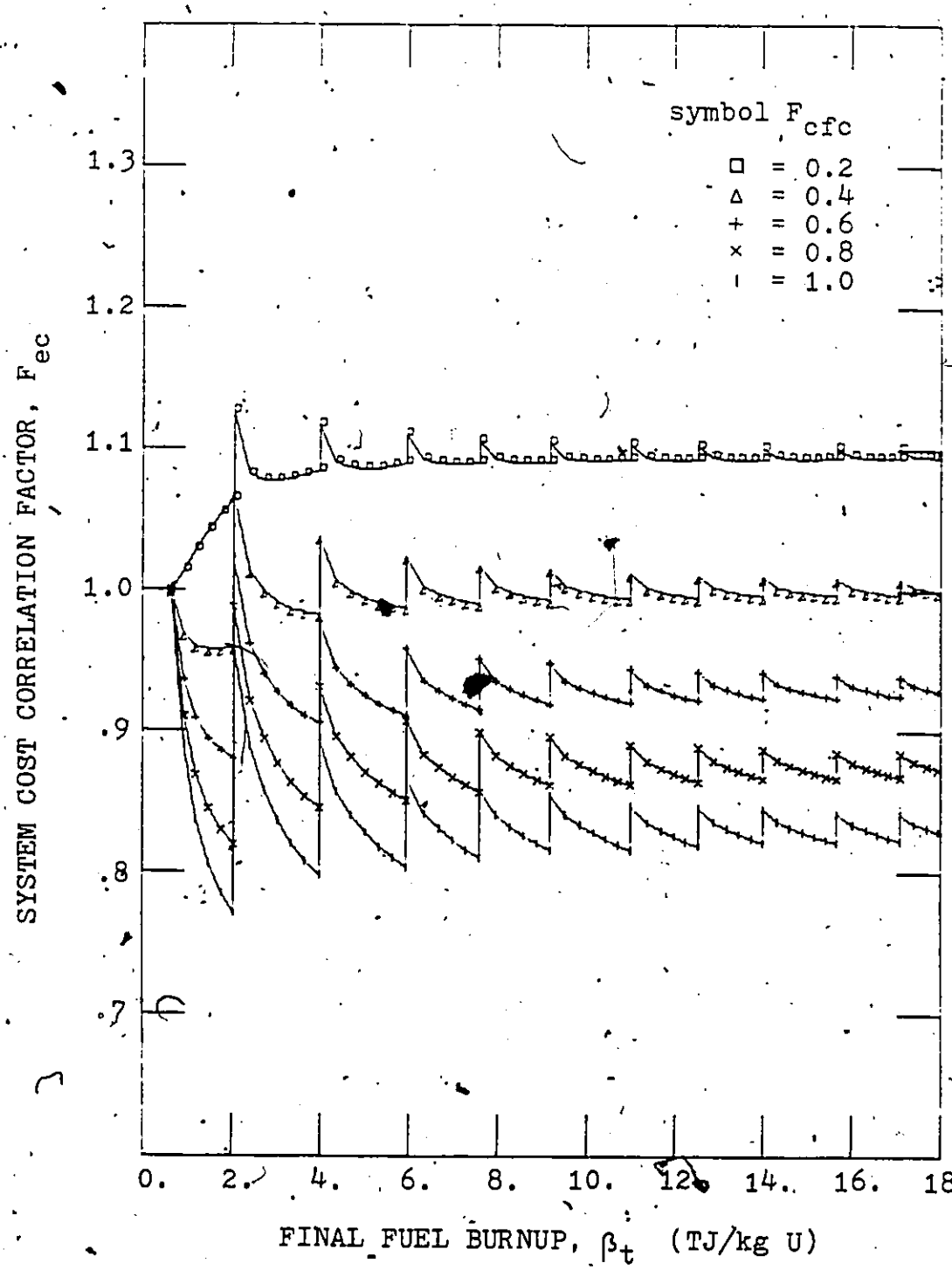

Fig. 5.6.2i Symbiotic system cost correlation factor with periodic reprocessing; case 9 of Table 4.6.1.

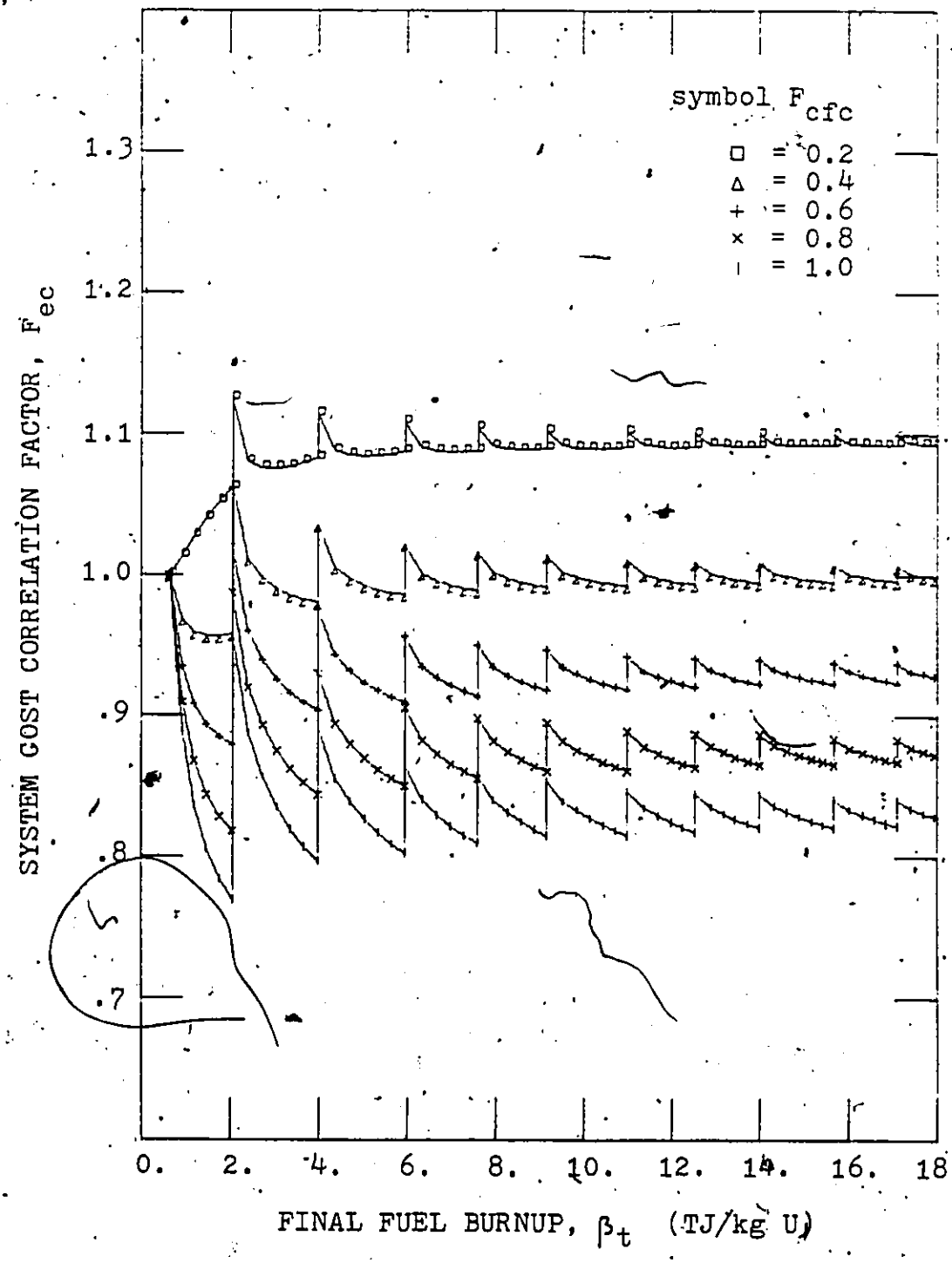

Fig. 5.6.2j Symbiotic system cost correlation factor with periodic reprocessing; case 10 of Table 4.6.1.

here that for a fuel to capital-operational cost fraction, F_{cfc}, greater than approximately 0.3, the cost correlation factor is less than unity. As a direct consequence, the system power advantage ratio, F_{es}, can be less than unity for a system energy advantage factor, A_{sd}, greater than unity. The accelerator breeder, therefore, can be a net power consumer.

The system energy advantage factor, A_{sd}, defined by Eq. 5.6.6, is shown in Fig. 5.6.3 and Fig. 5.6.4 for the two systems. It should be noted here that, in the worst case, with an effective neutron source of 24 n/p, case 6 of Table 4.6.1, an advantage factor greater than unity is achieved for a fuel cost fraction, F_{cfc}, greater than 0.5 for cases without reprocessing, and greater than 0.8 for cases with periodic reprocessing. This is in spite of the feature that the symbiotic system produces generally more than 10% less electrical power than the equivalent conventional depleter reactor, case 6 of Fig. 5.3.1. As discussed in Sec. 5.3, breeder subsystem power self-sufficiency is realized for Q_{tb} approximately equal to 4, corresponding to cases 2 and 7, as shown in Fig. 5.3.1 and Fig. 5.3.2. The system energy advantage factor for these cases is greater than unity for fractional fuel costs, F_{cfc}, of approximately 0.45 and 0.40 for schemes with and without fuel reprocessing respectively. This puts the symbiotic

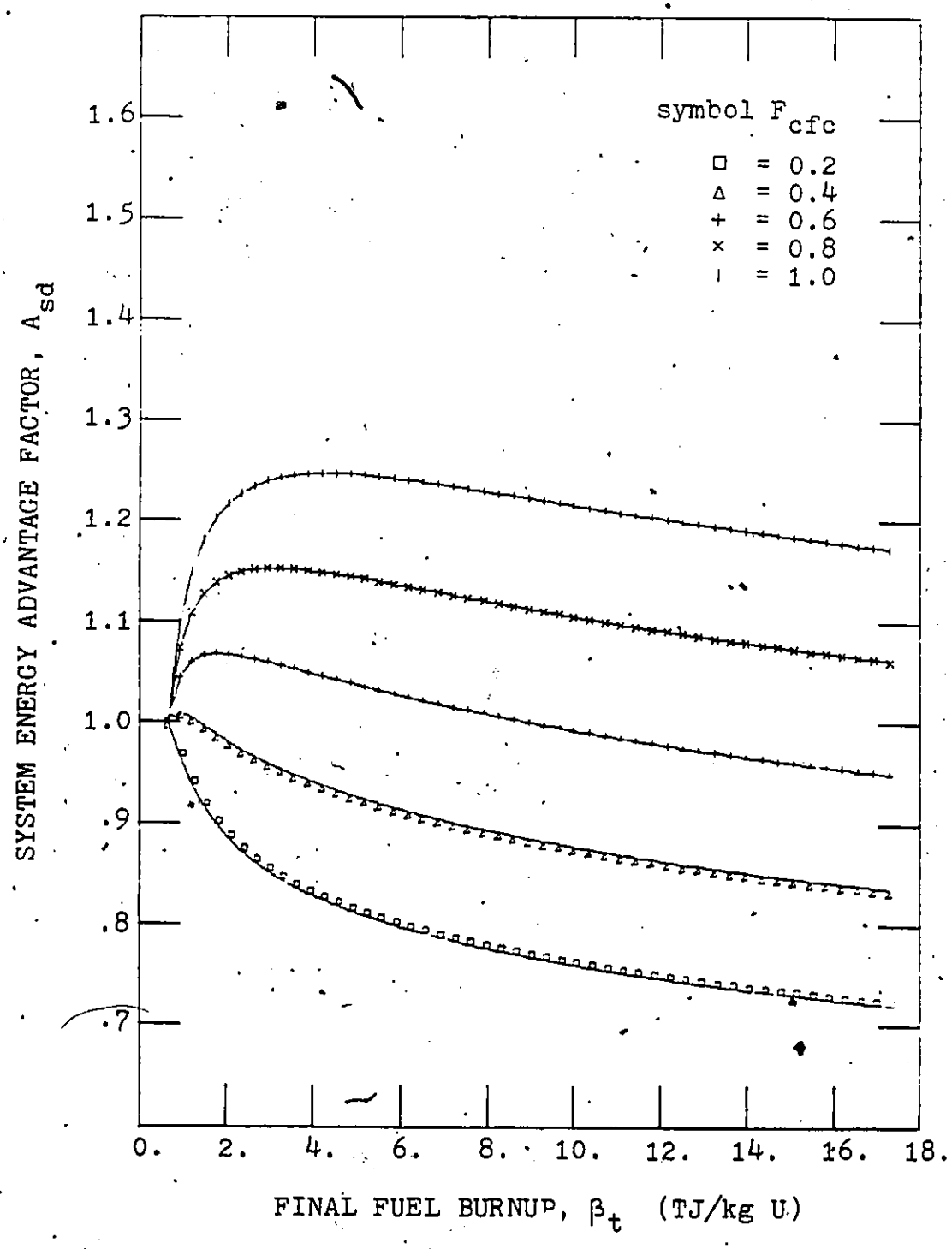

Fig. 5.6.3a Symbiotic system energy advantage factor without fuel reprocessing; case 1 of Table 4.6.1.

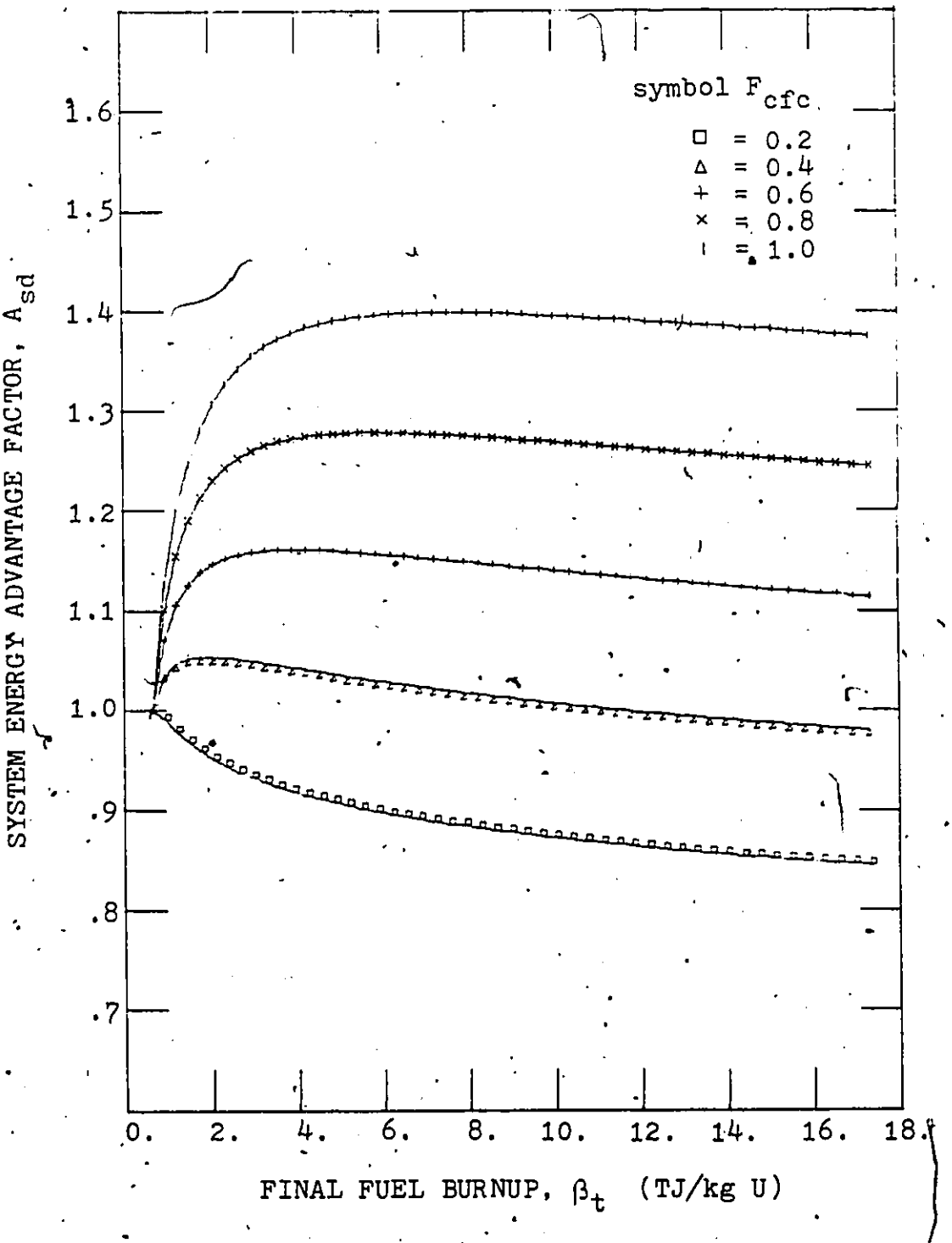

Fig. 5.6.3b Symbiotic system energy advantage factor without fuel reprocessing; case 2 of Table 4.6.1.

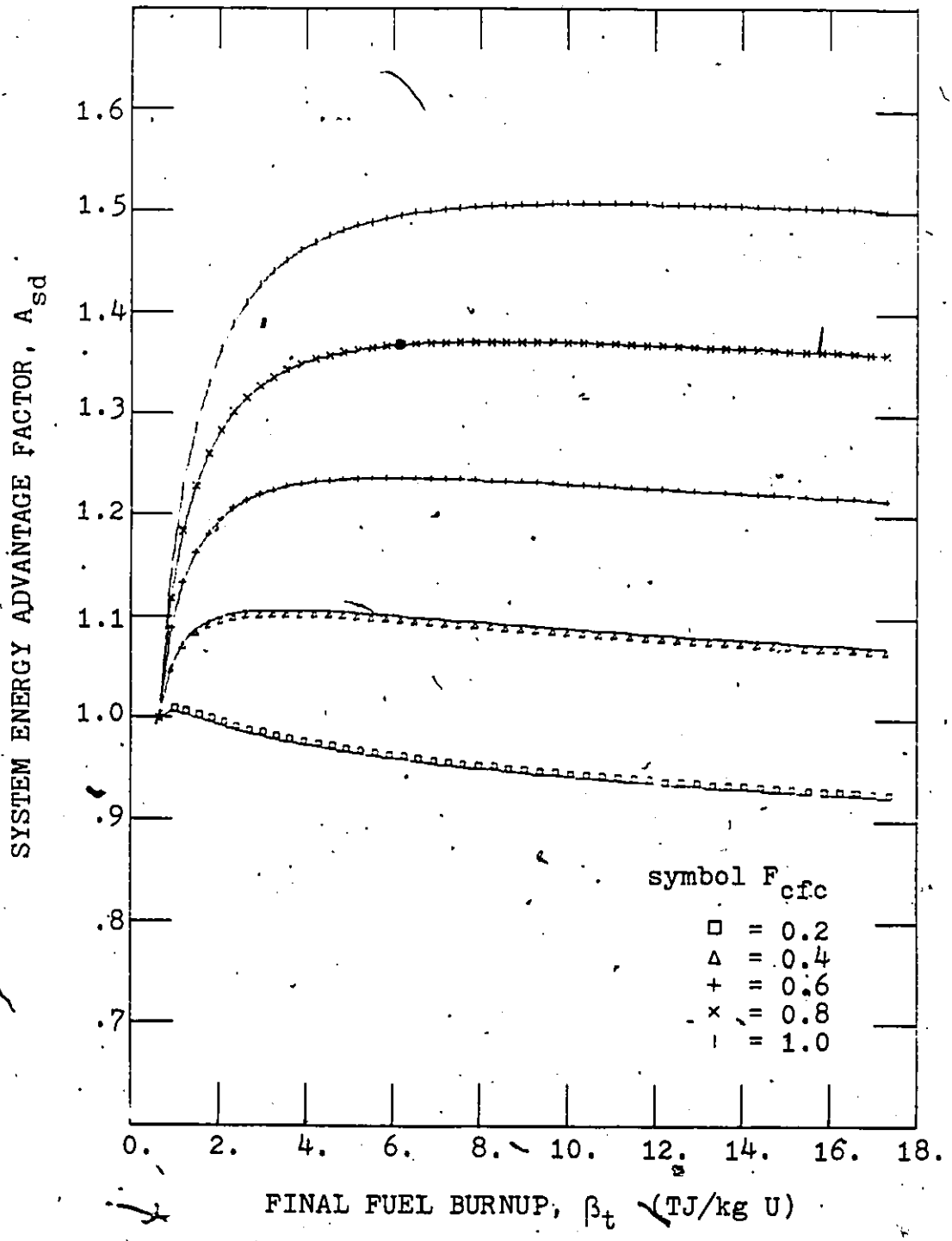

Fig. 5.6.3c Symbiotic system energy advantage factor without fuel reprocessing; case 3 of Table 4.6.1.

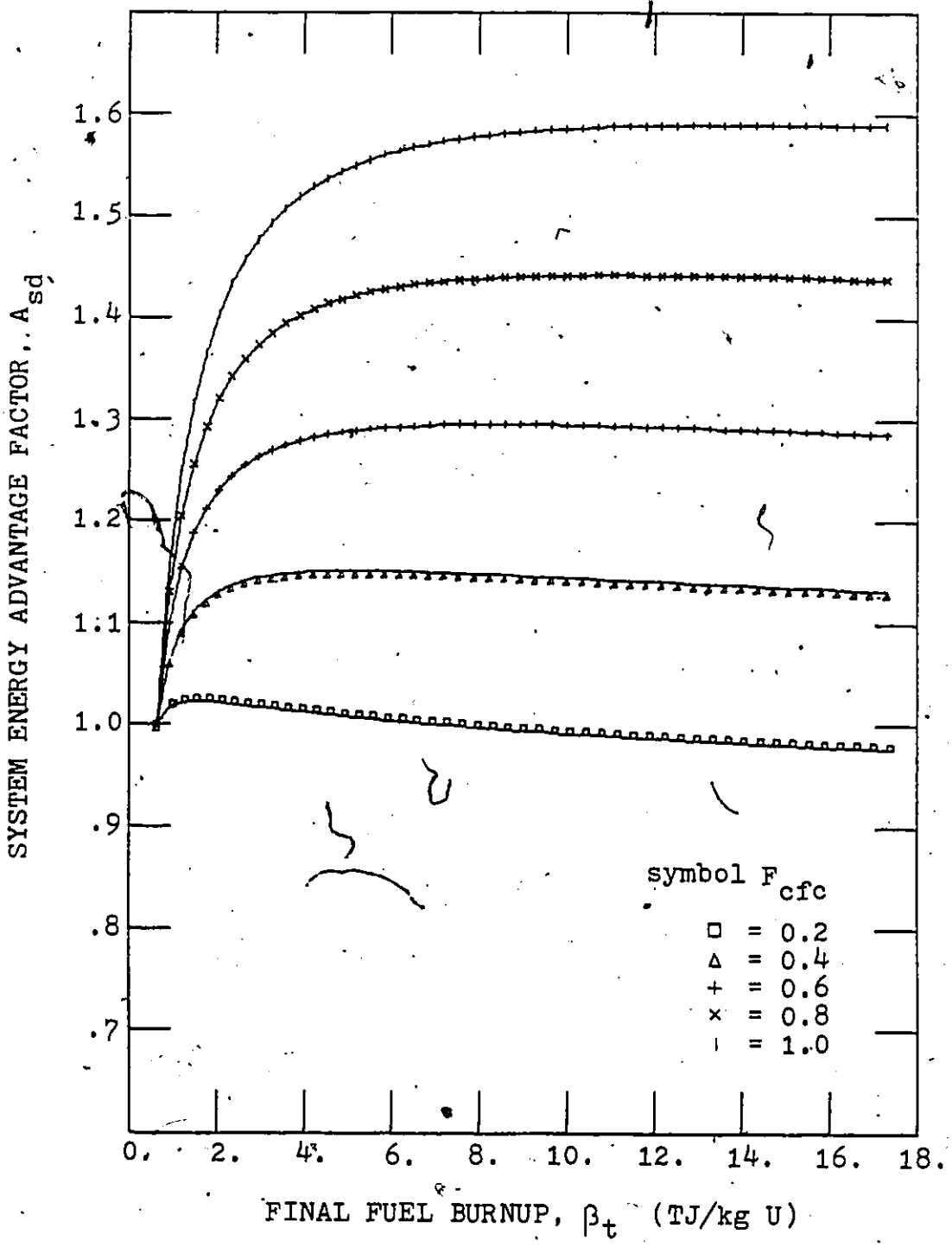

Fig. 5.6.3d Symbiotic system energy advantage factor without fuel reprocessing; case 4 of Table 4.6.1.

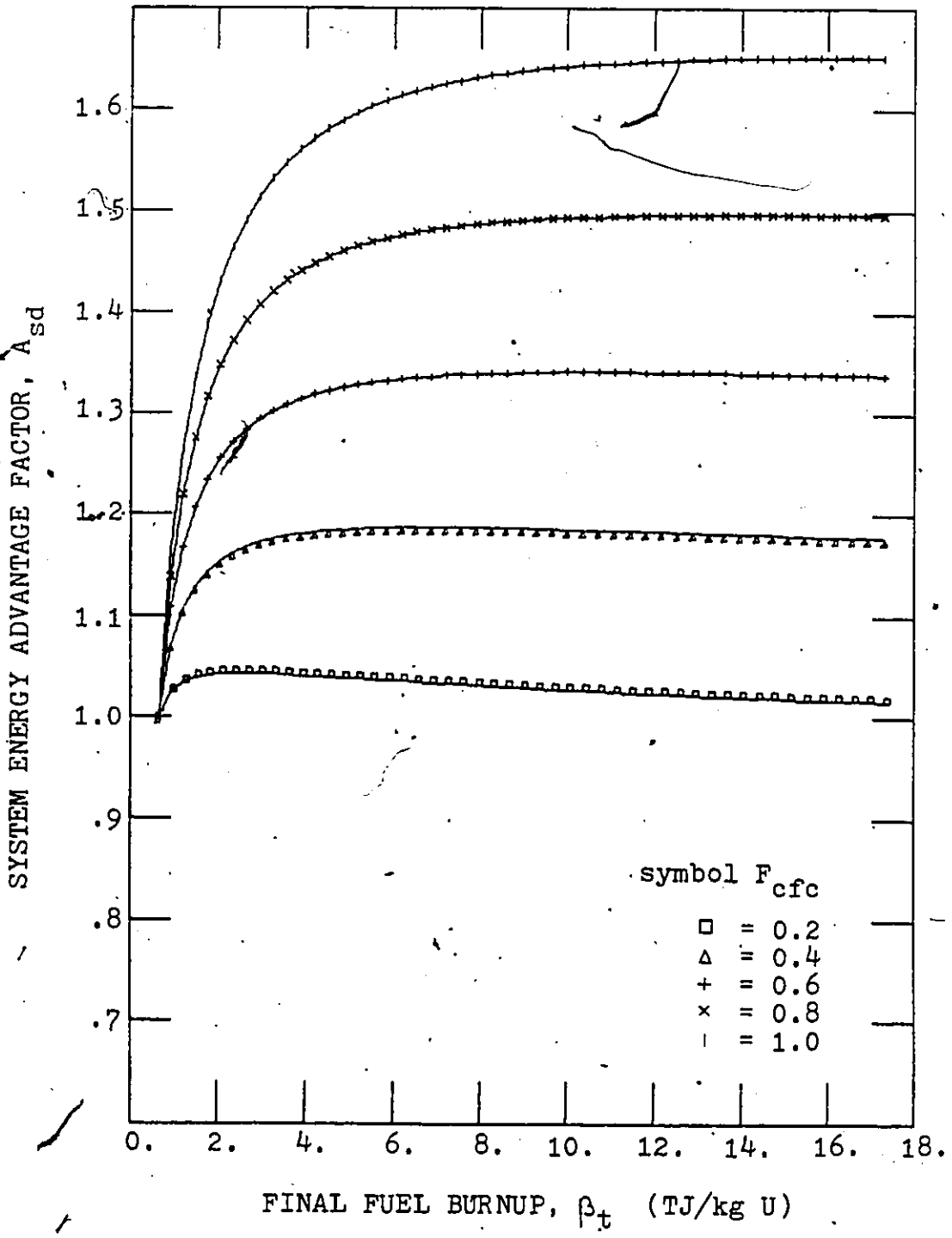

Fig. 5.6.3e Symbiotic system energy advantage factor without fuel reprocessing; case 5 of Table 4.6.1.

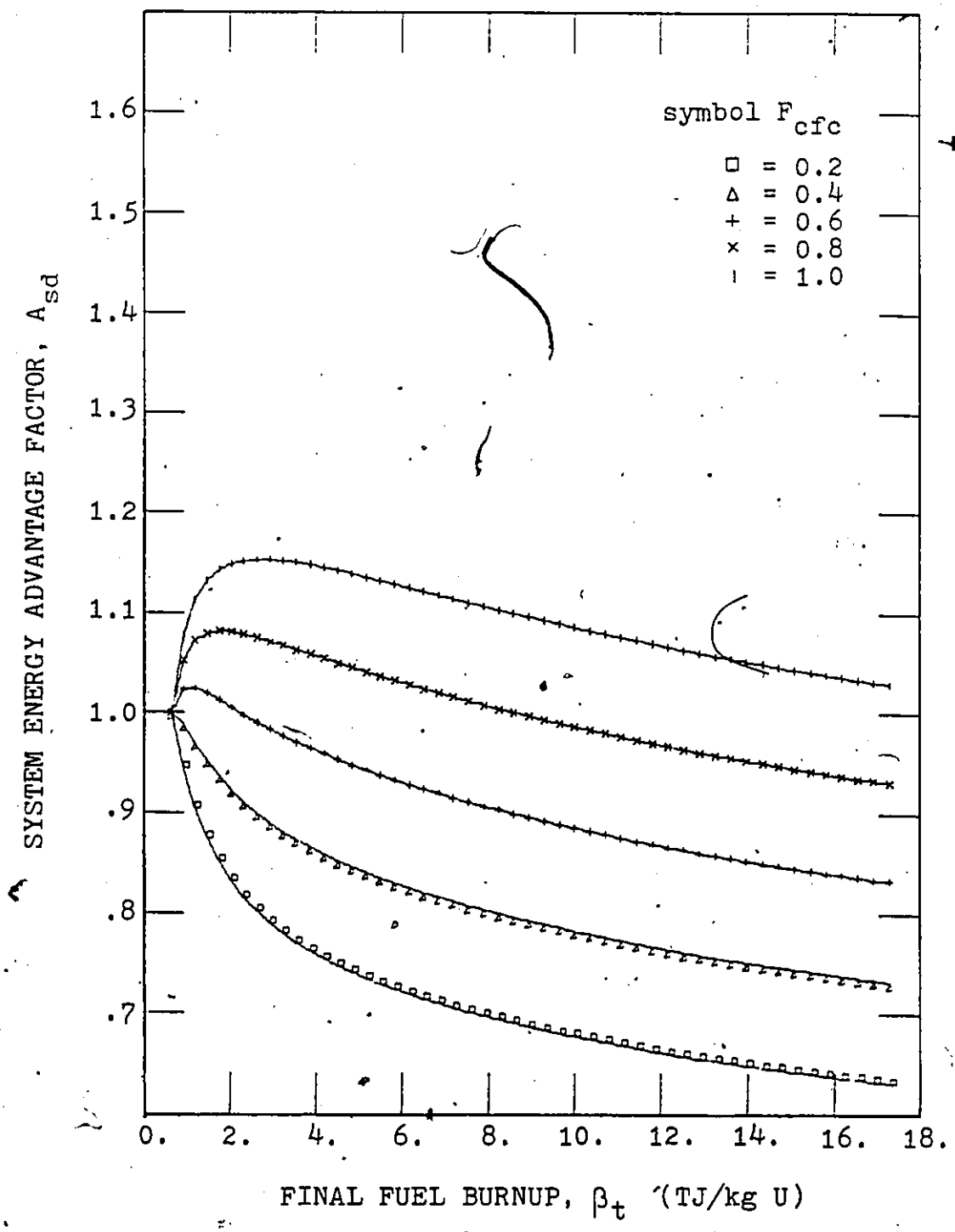

Fig. 5.6.3f Symbiotic system energy advantage factor without fuel reprocessing; case 6 of Table 4.6.1.

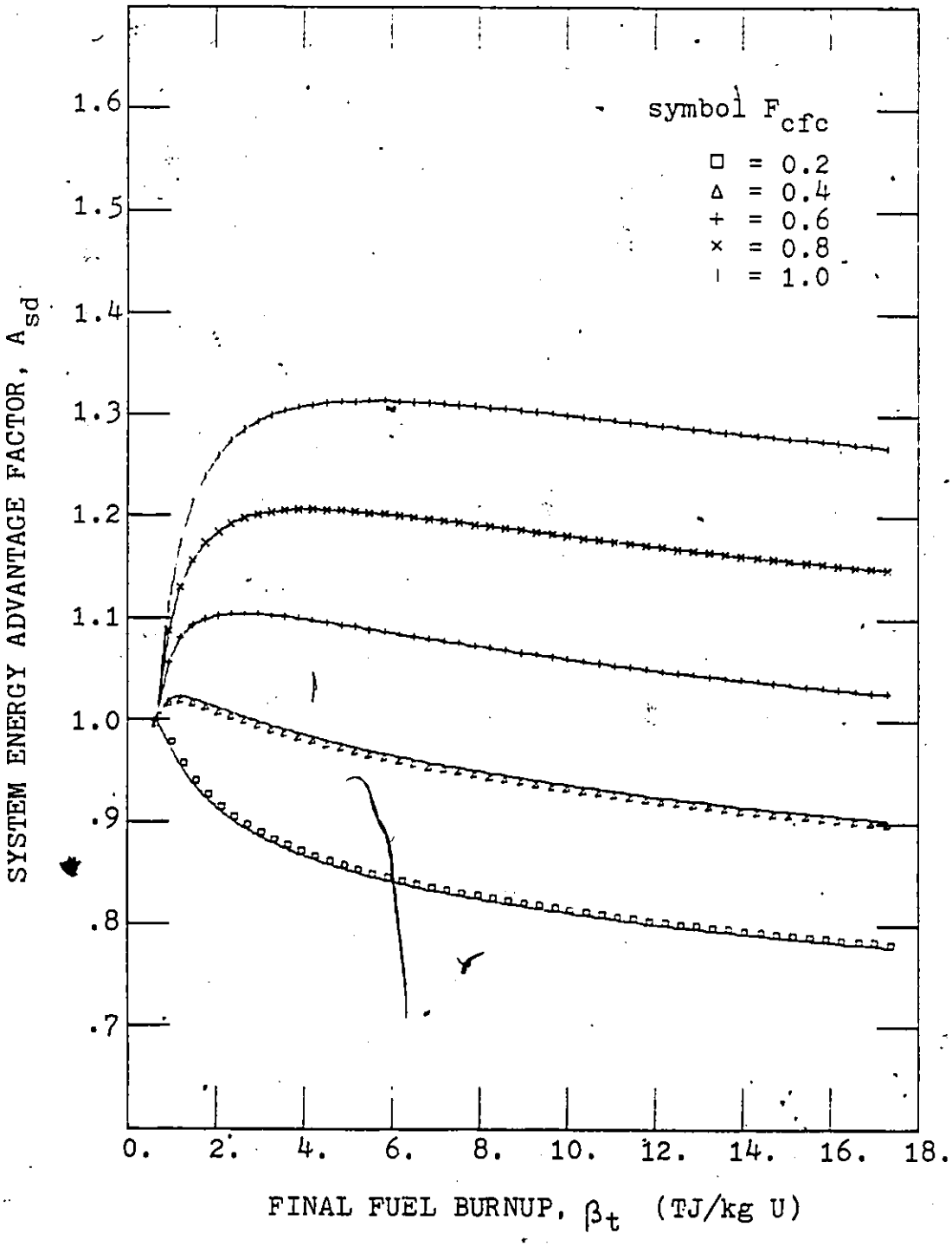

Fig. 5.6.3g: Symbiotic system energy advantage factor without fuel reprocessing; case 7 of Table 4.6.1.

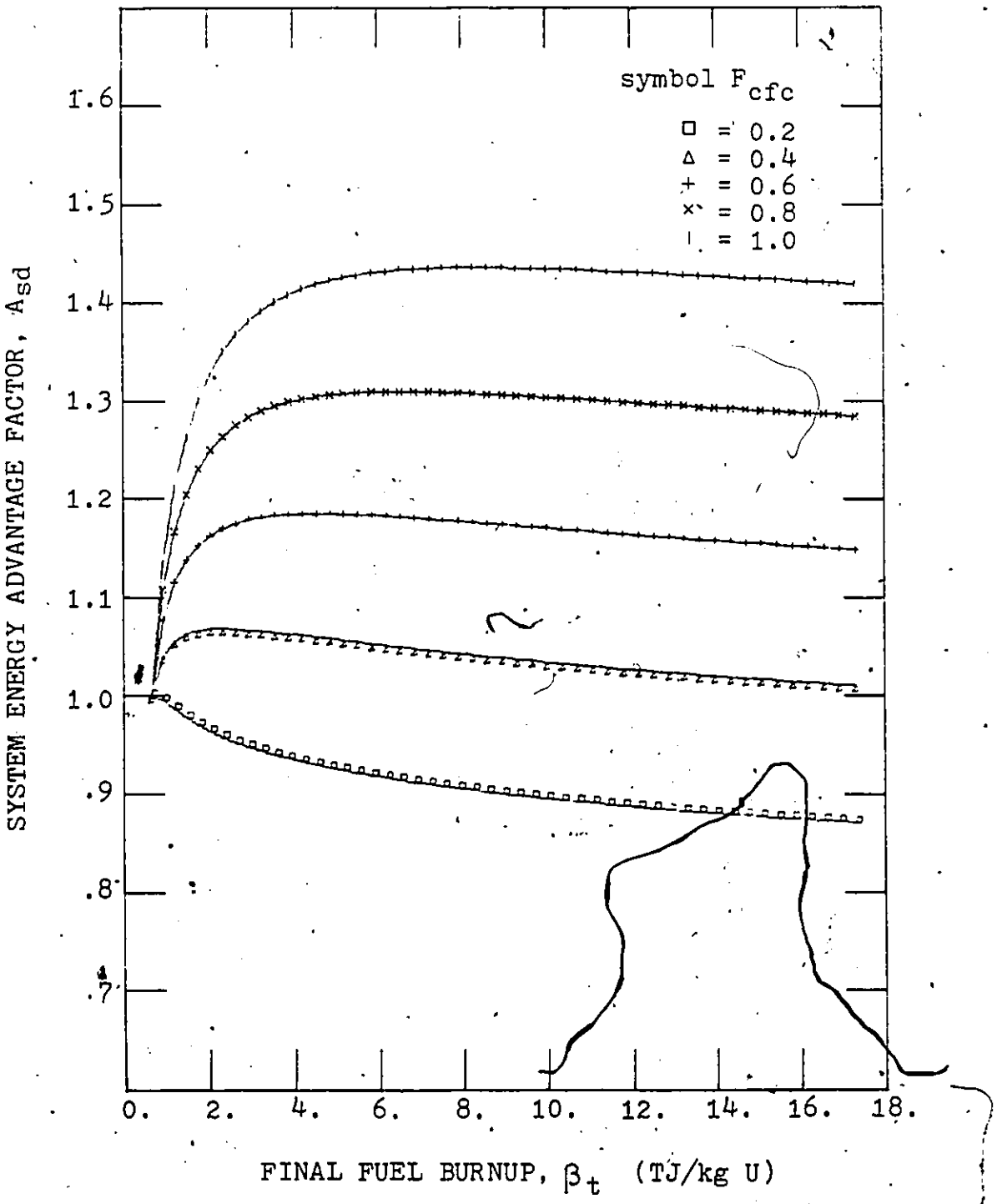

Fig. 5.6.3h Symbiotic system energy advantage factor without fuel reprocessing; case 8 of Table 4.6.1.

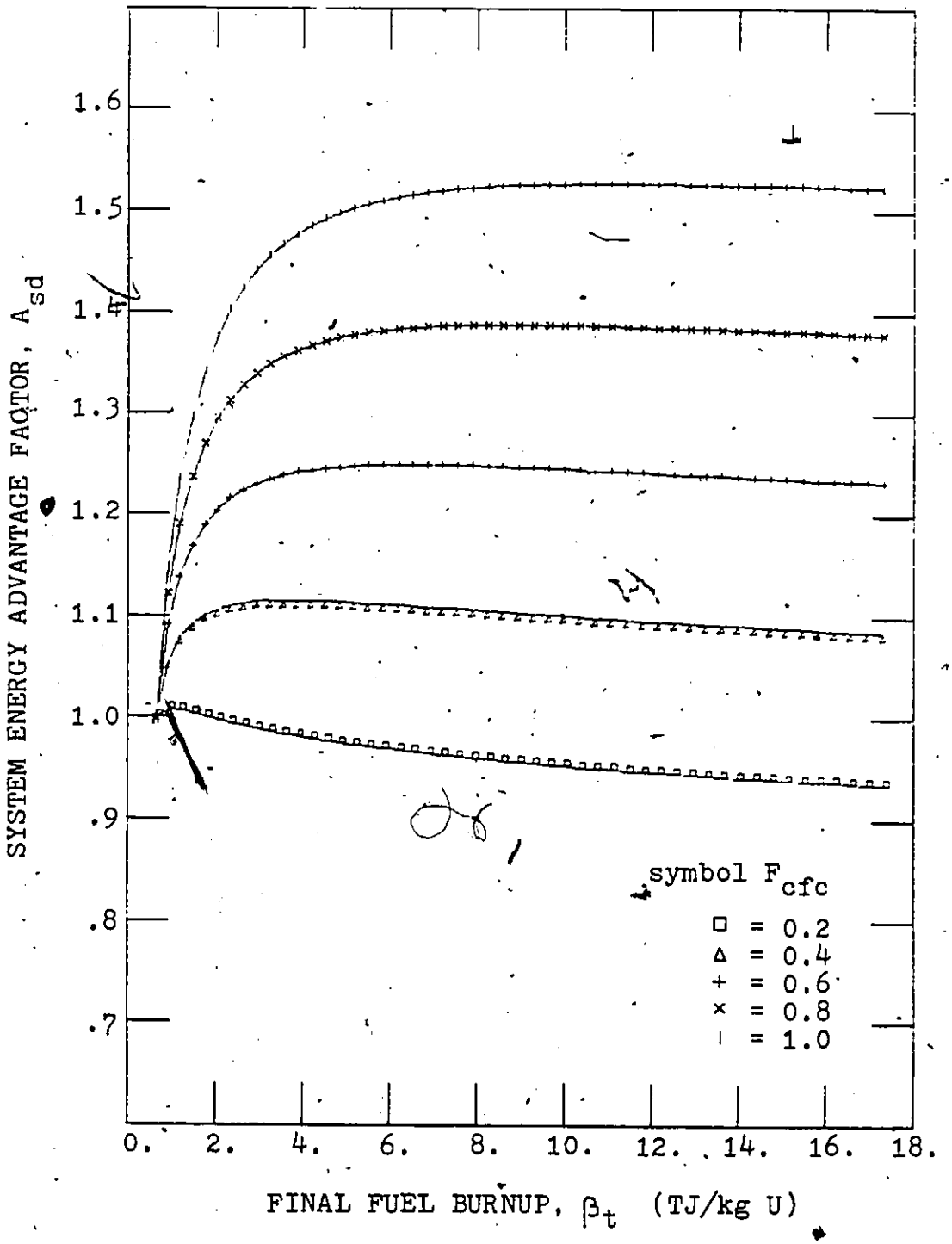

Fig. 5.6.3i Symbiotic system energy advantage factor without fuel reprocessing; case 9 of Table 4.6.1.

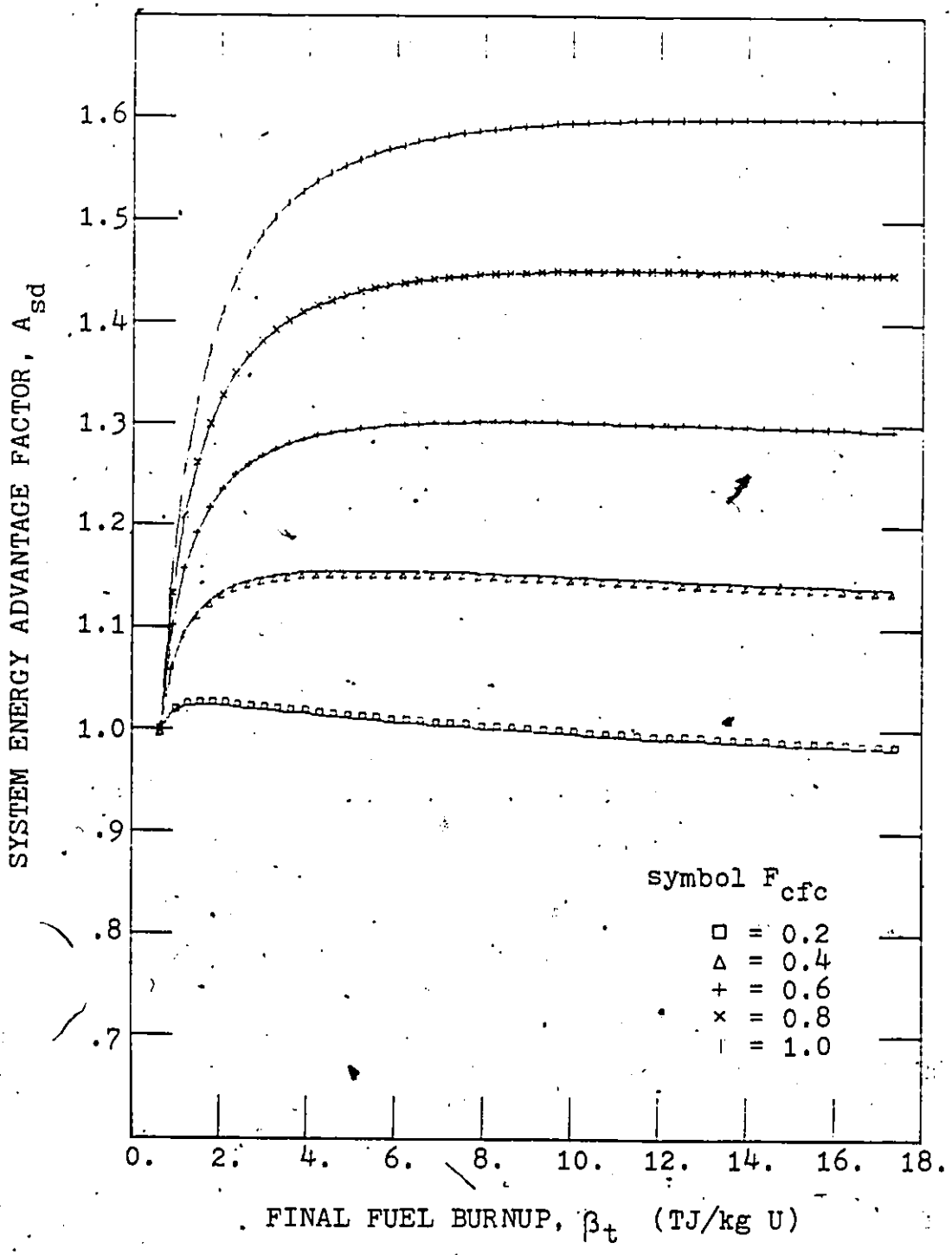

Fig. 5.6.3j Symbiotic system energy advantage factor without fuel reprocessing; case 10 of Table 4.6.1.

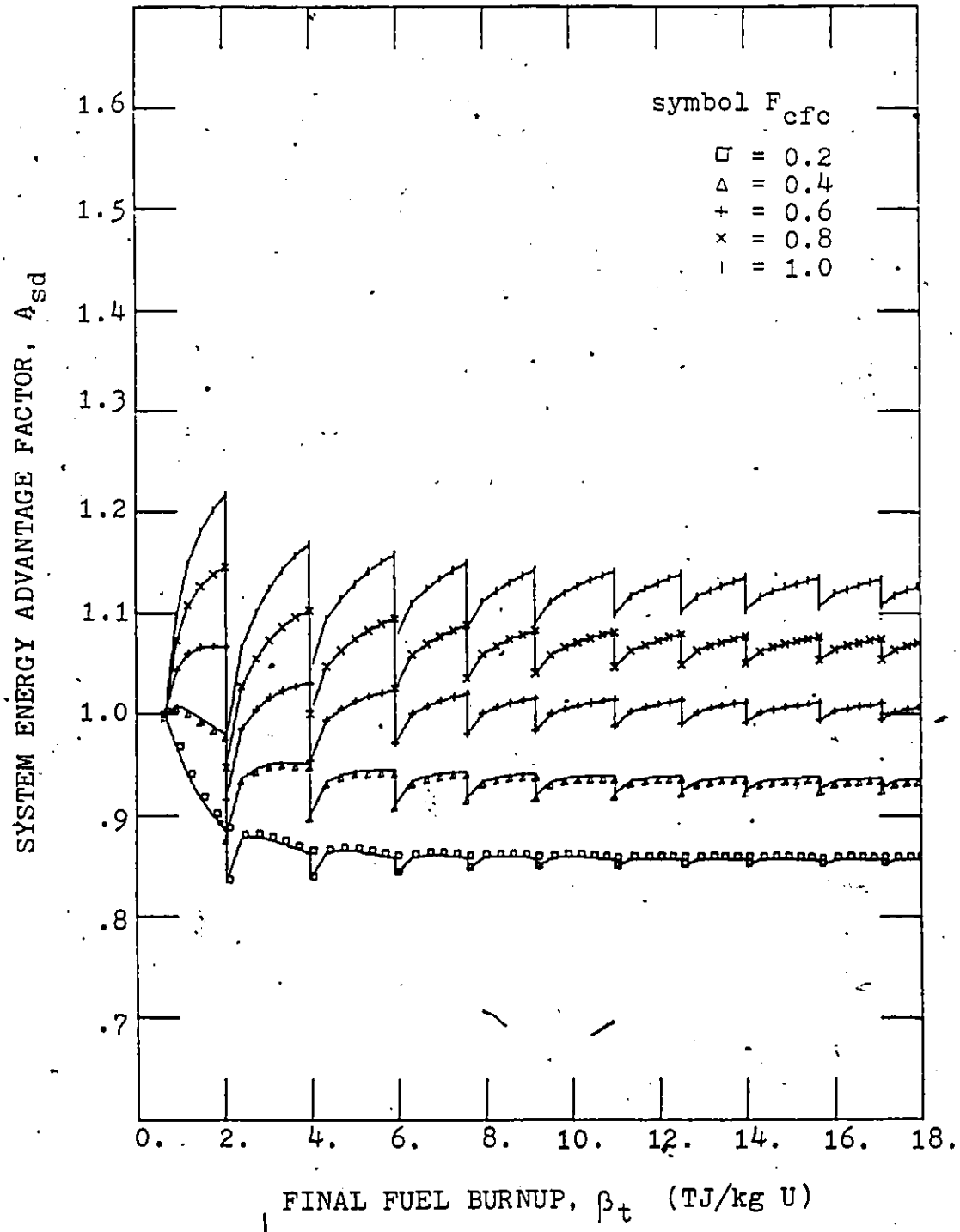

Fig. 5.6.4a Symbiotic system energy advantage factor, with periodic reprocessing; case 1 of Table 4.6.1.

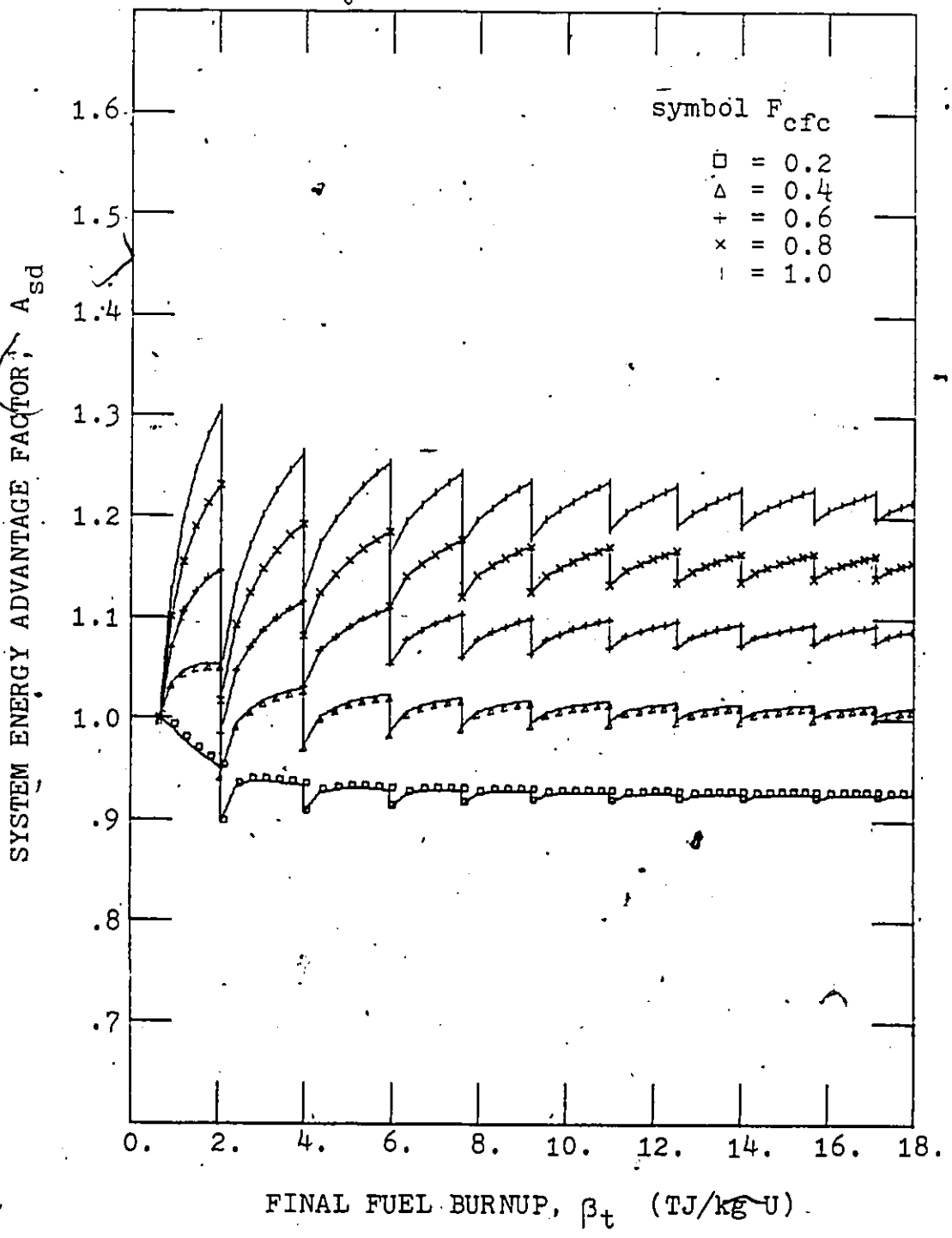

Fig. 5.6.4b Symbiotic system energy advantage factor with periodic reprocessing; case 2 of Table 4.6.1.

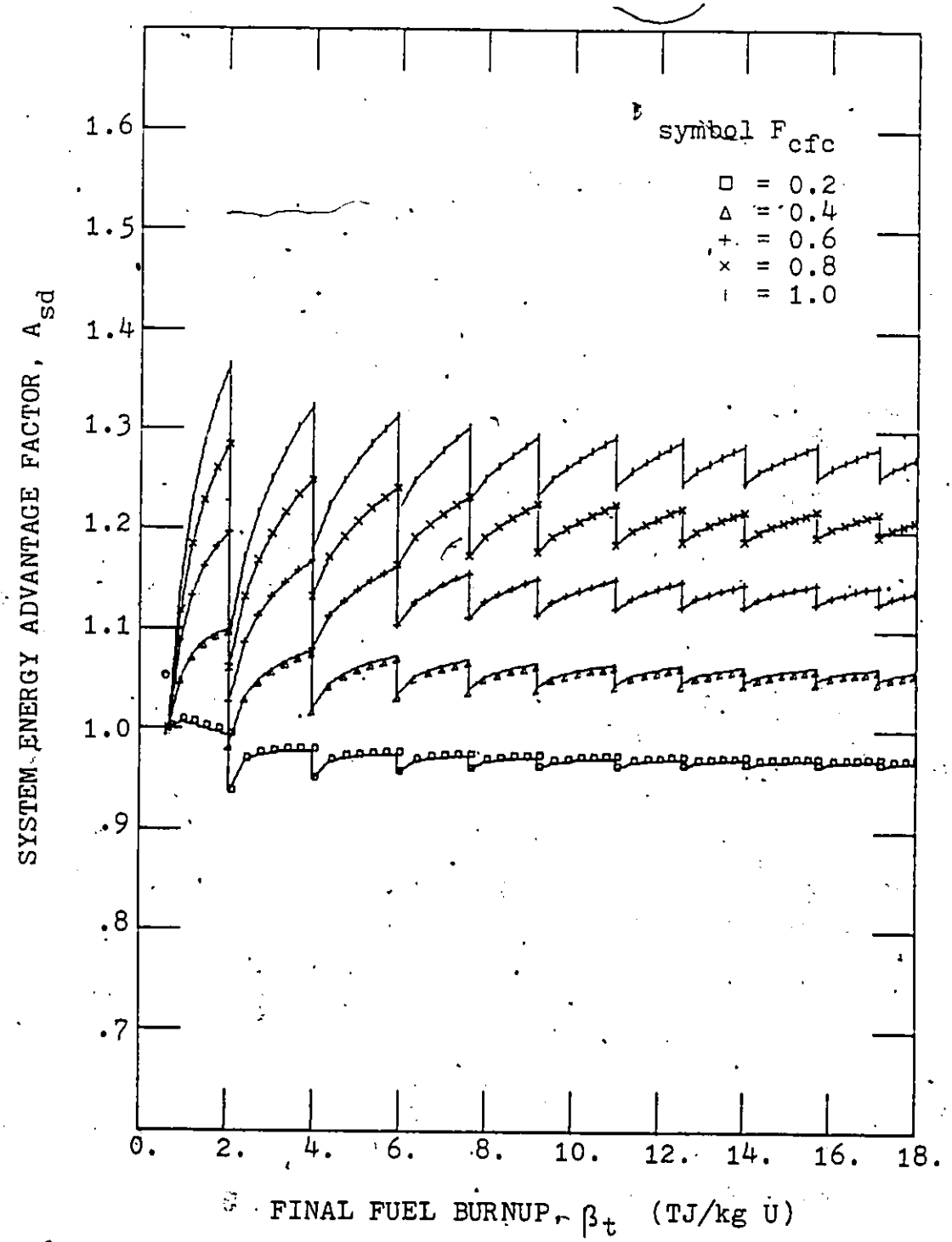

Fig. 5.6.4c Symbiotic system energy advantage factor with periodic reprocessing; case 3 of Table 4.6.1.

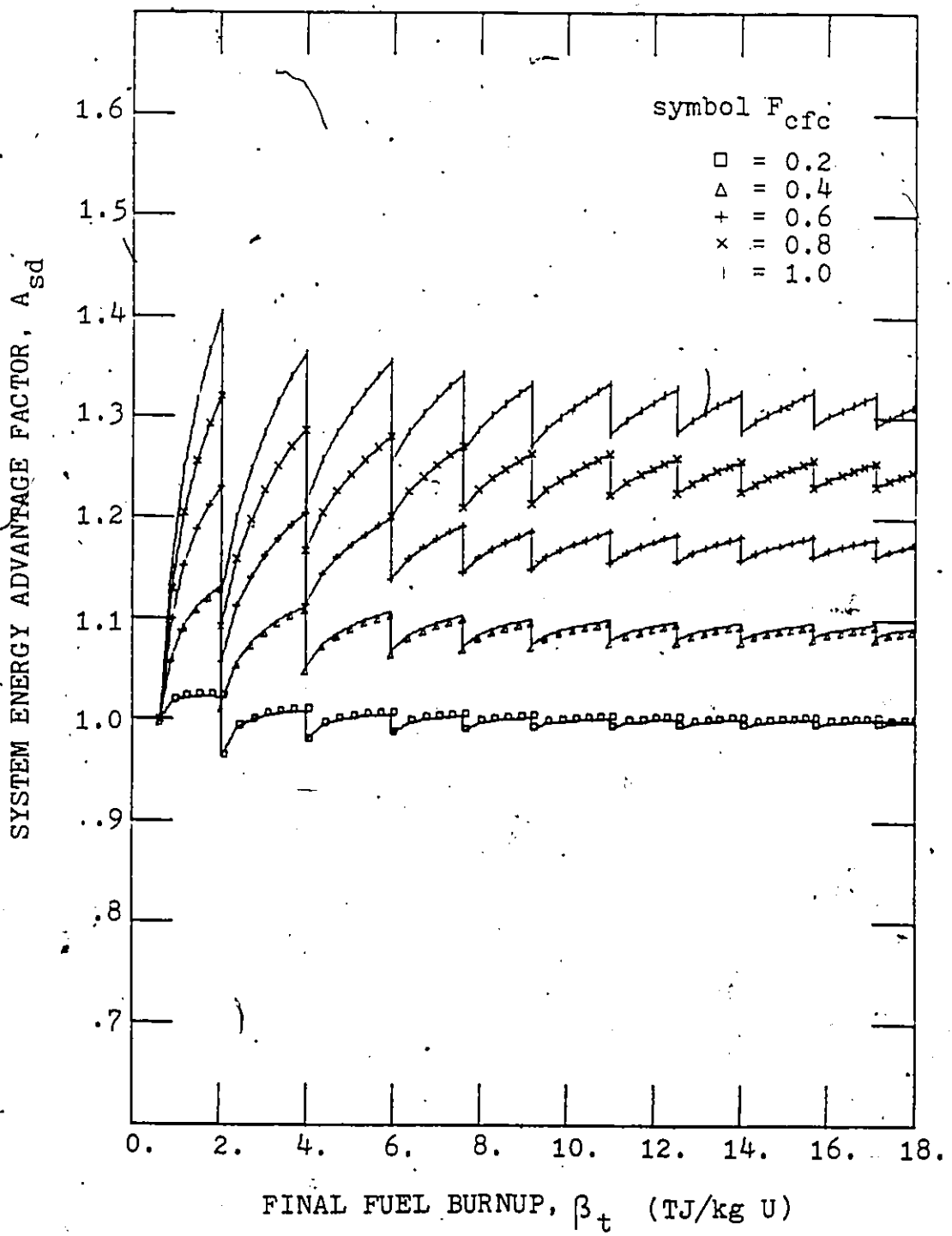

Fig. 5.6.4d Symbiotic system energy advantage factor with periodic reprocessing; case 4 of Table 4.6.1.

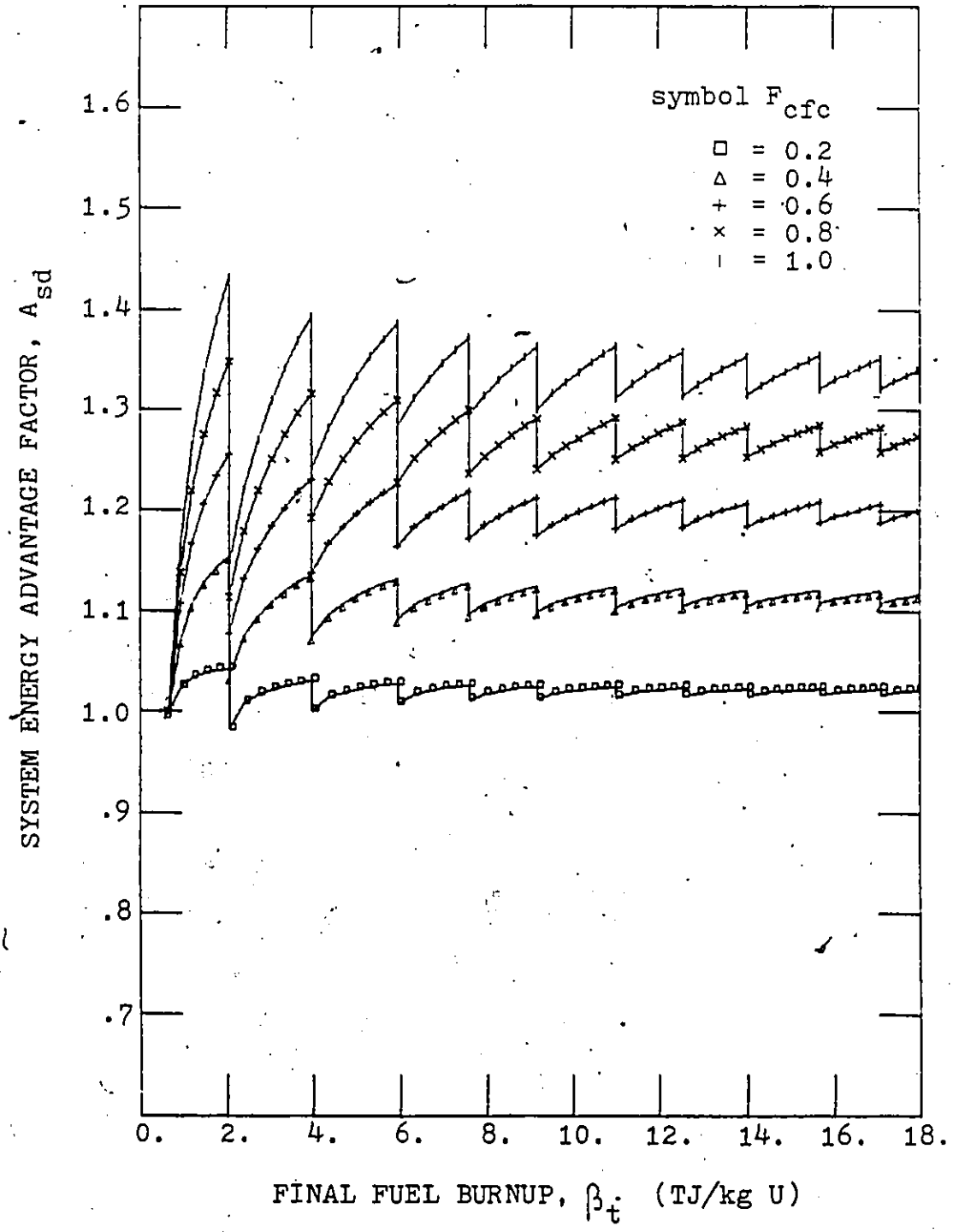

Fig. 5.6.4e Symbiotic system energy advantage factor with periodic reprocessing; case 5 of Table 4.6.1.

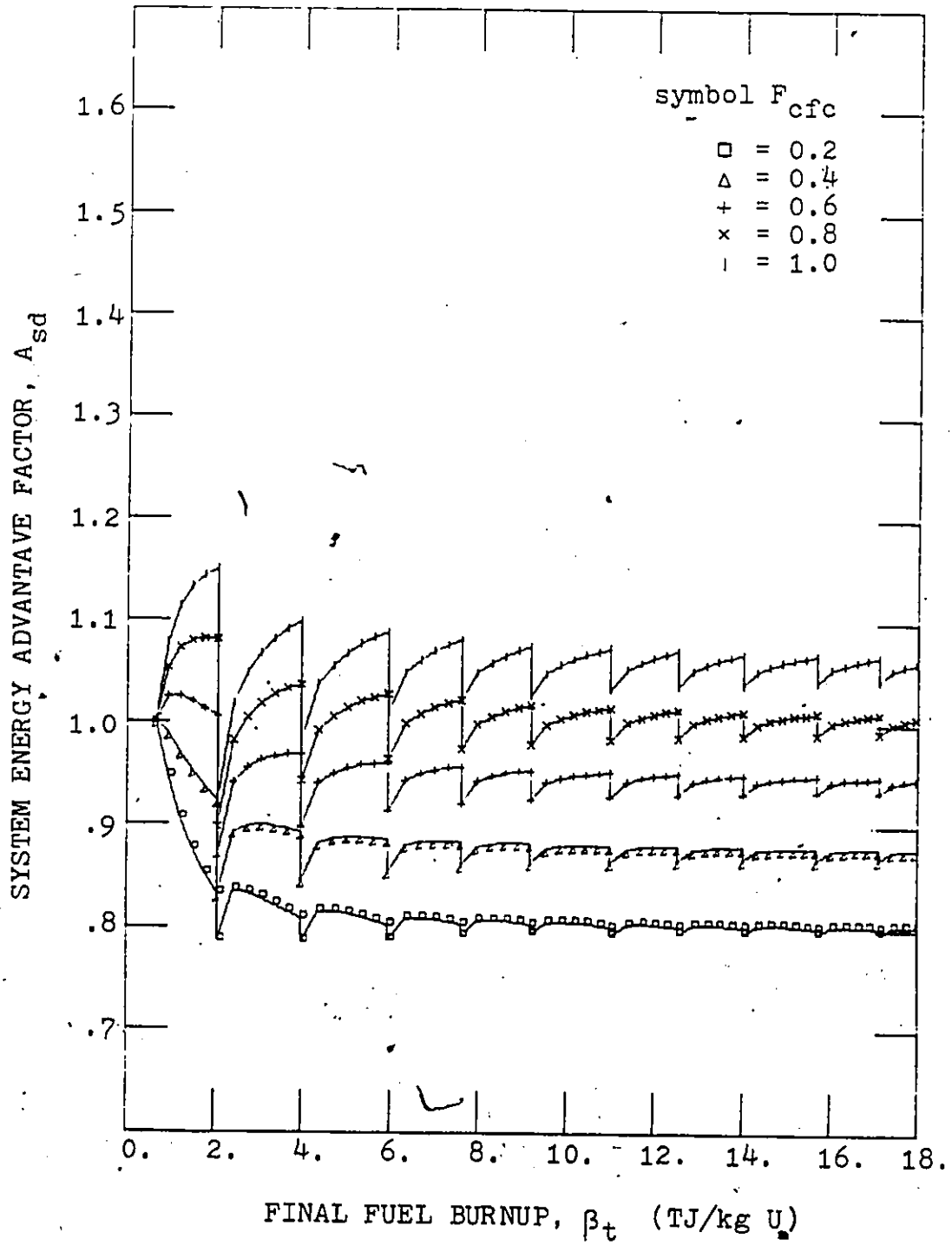

Fig. 5.6.4f Symbiotic system energy advantage factor with periodic reprocessing; case 6 of Table 4.6.1.

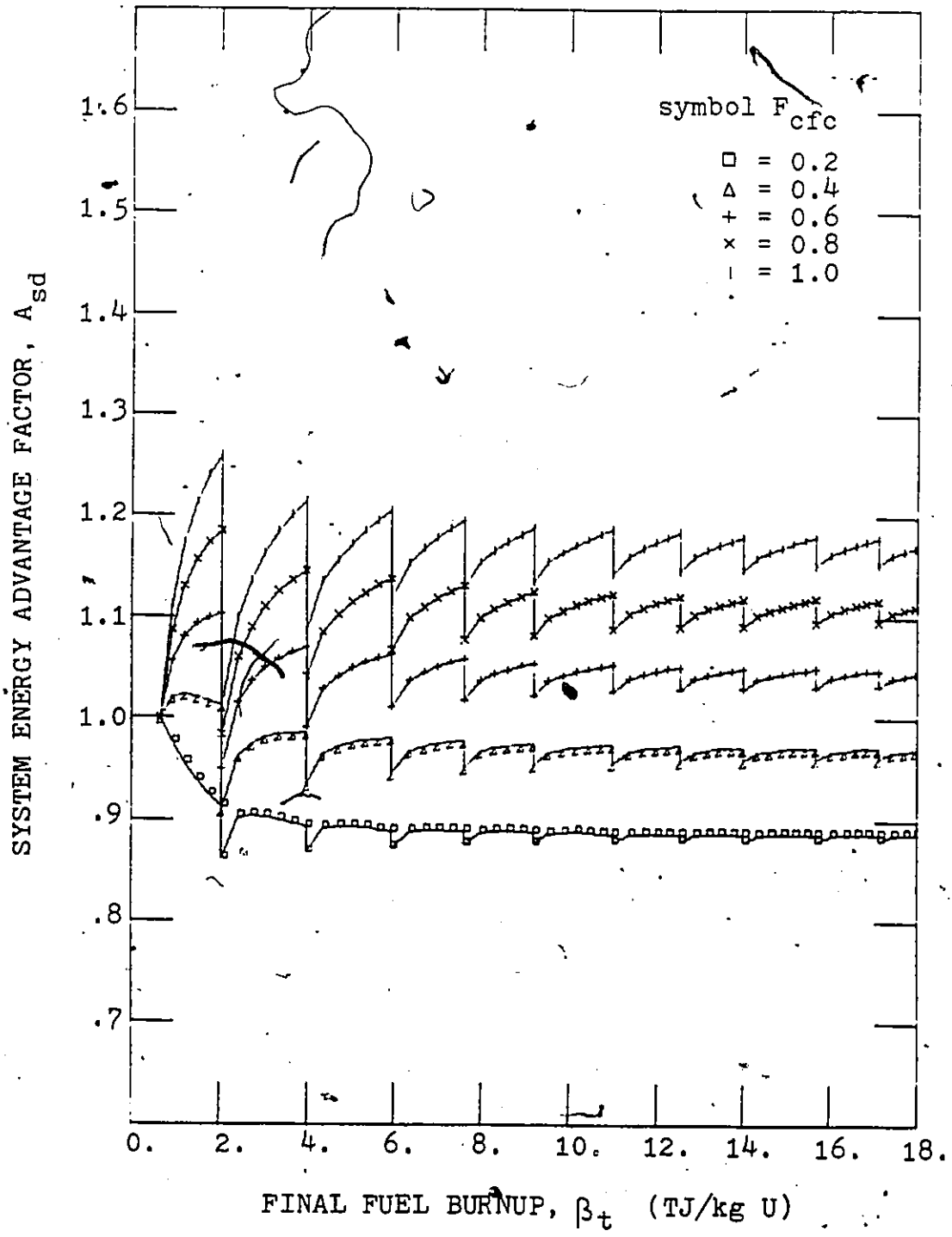

Fig. 5.6.4g Symbiotic system energy advantage factor with periodic reprocessing; case 7 of Table 4.6.1.

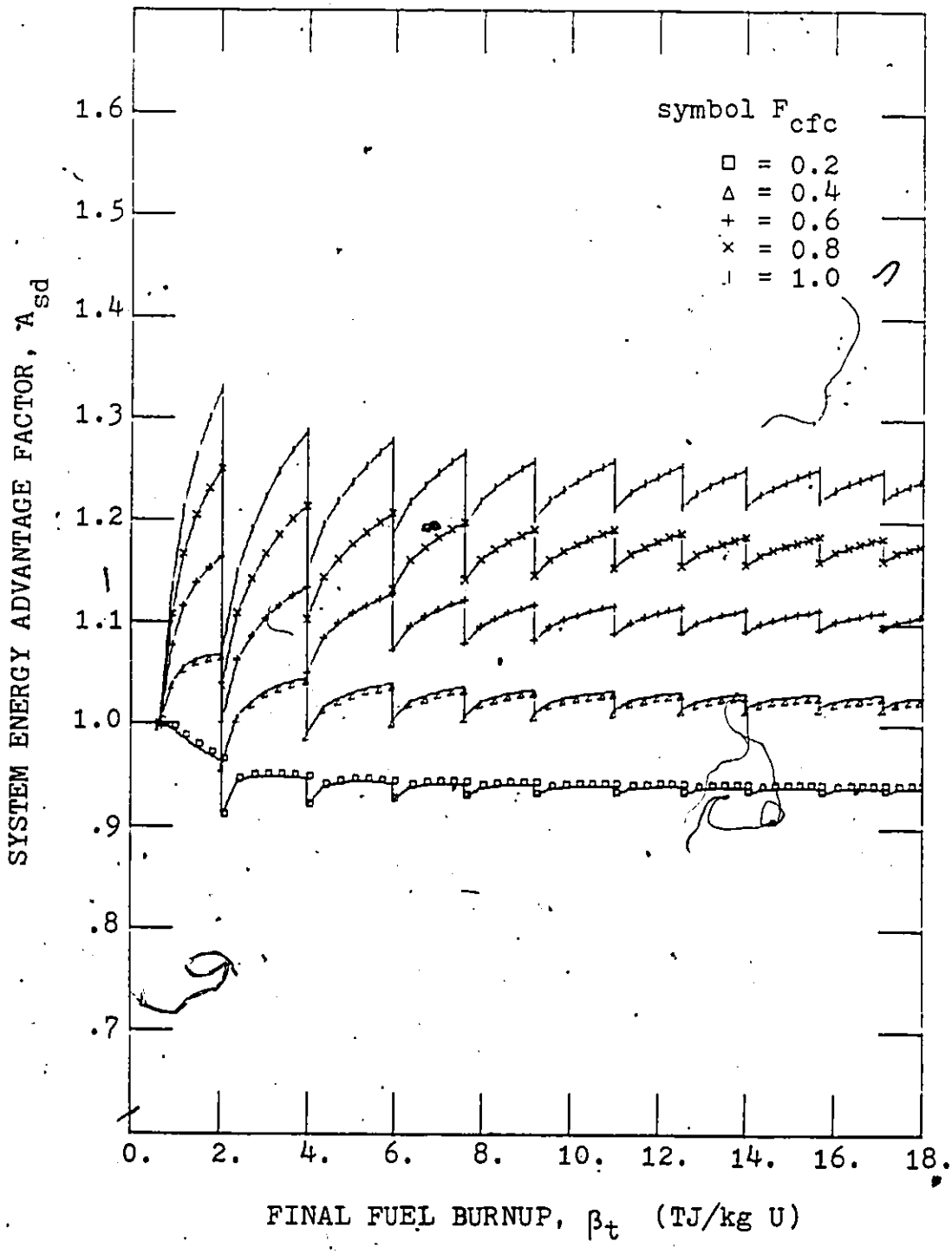

Fig. 5.6.4h Symbiotic system energy advantage factor with periodic reprocessing; case 8 of Table 4.6.1.

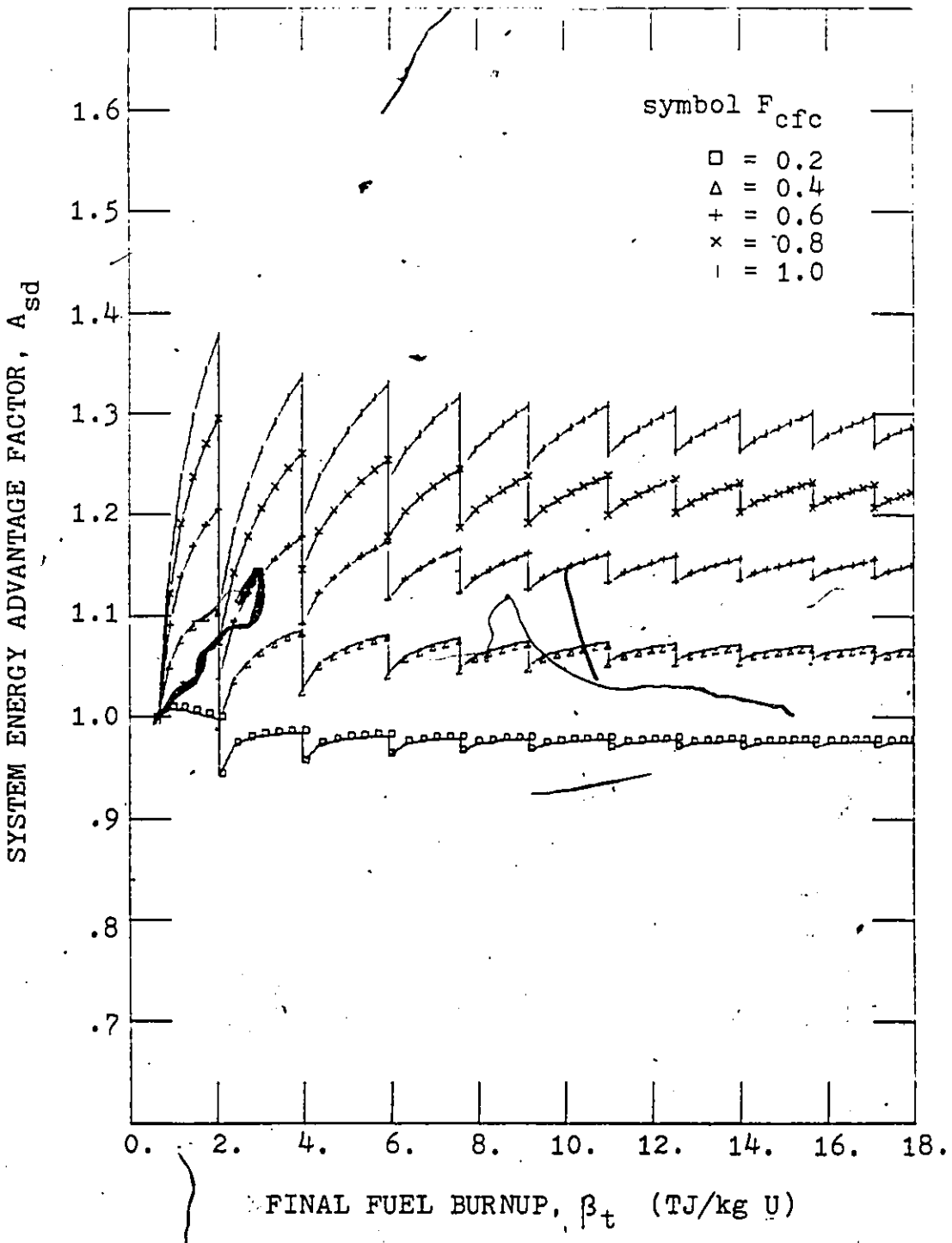

Fig. 5.6.4i Symbiotic system energy advantage factor with periodic reprocessing; case 9 of Table 4.6.1.

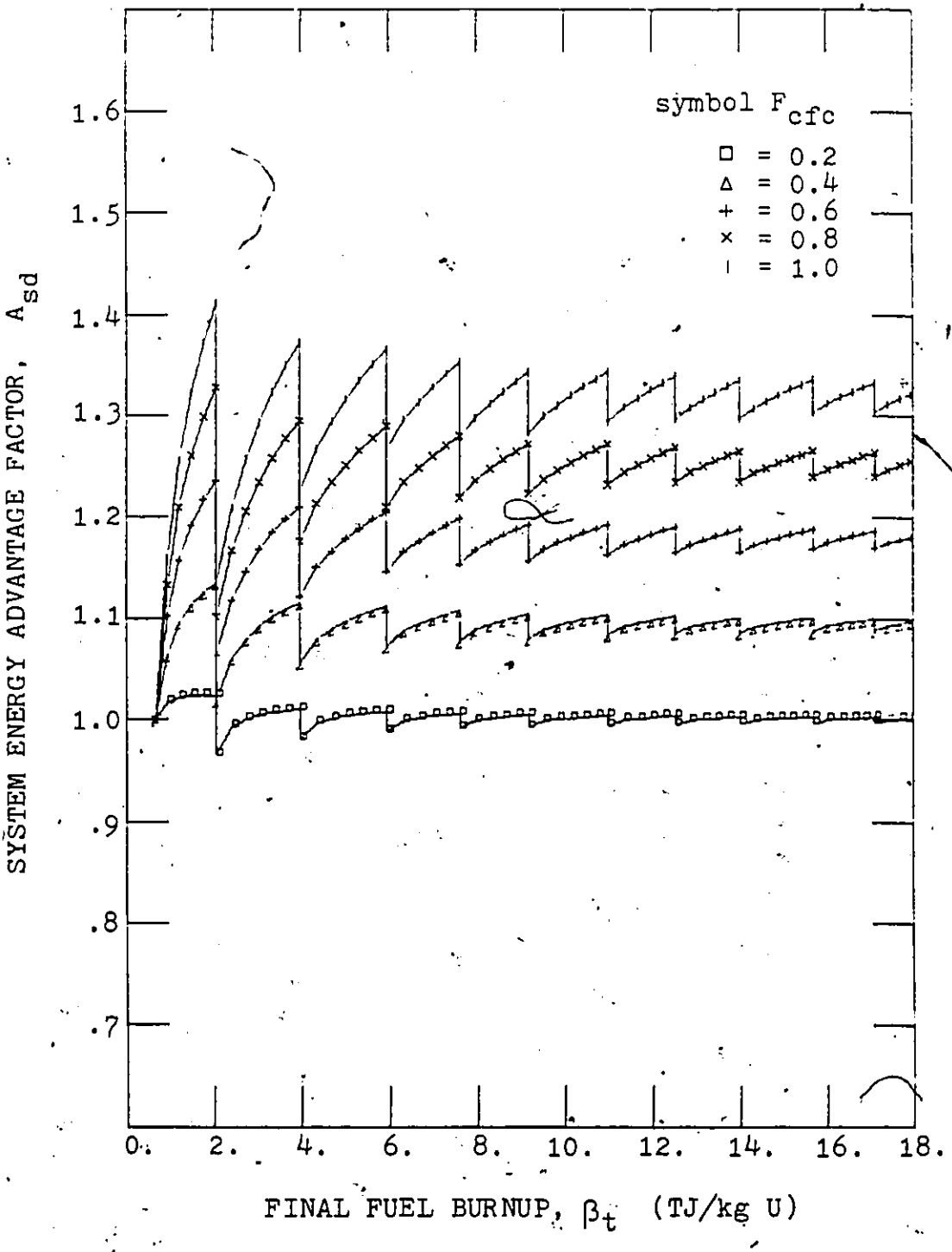

Fig. 5.6.4j Symbiotic system energy advantage factor with periodic reprocessing; case 10 of Table 4.6.1.

system breakeven condition in the range of the present fuel cost fraction estimate of 0.43[76]. The cases 2 to 5, and 7 to 10, which can be described as fission target systems, show impressive system advantage factors. The high target power densities of such breeder subsystems, however, will put severe restrictions on their practicability.

The dominant feature of the system energy advantage factor as shown in Fig. 5.6.3 is that it peaks at relatively low fuel burnups. This maximum results from two competing major effects: one effect produces increased energy advantage factors with increased burnup due to an increasing fuel stretching factor, f_s, Eq. 4.7.10, as shown in Fig. 4.7.1 and Fig. 4.7.2, reducing the fuel cost of the symbiotic system, while the other effect decreases the energy advantage factor with increased burnups due to increases in the breeder subsystem cost. The increased breeder cost in turn is due to a decreasing breeder power utilization factor, Q_{td}, Eq. 5.1.9, shown in Fig. 5.2.1 and Fig. 5.2.2. The decrease in Q_{td} with increasing burnup is mainly due to the decrease of the conversion ratio, C_d, Eq. 4.3.6, as discussed in Sec. 4.4 and shown in Table 4.4.2b, cases p to r. The low burnup advantage factor peak is not undesirable since the fuel does not have to be irradiated to levels where material integrity limitations become a burnup restriction. Figure 5.6.5 shows the maximum energy

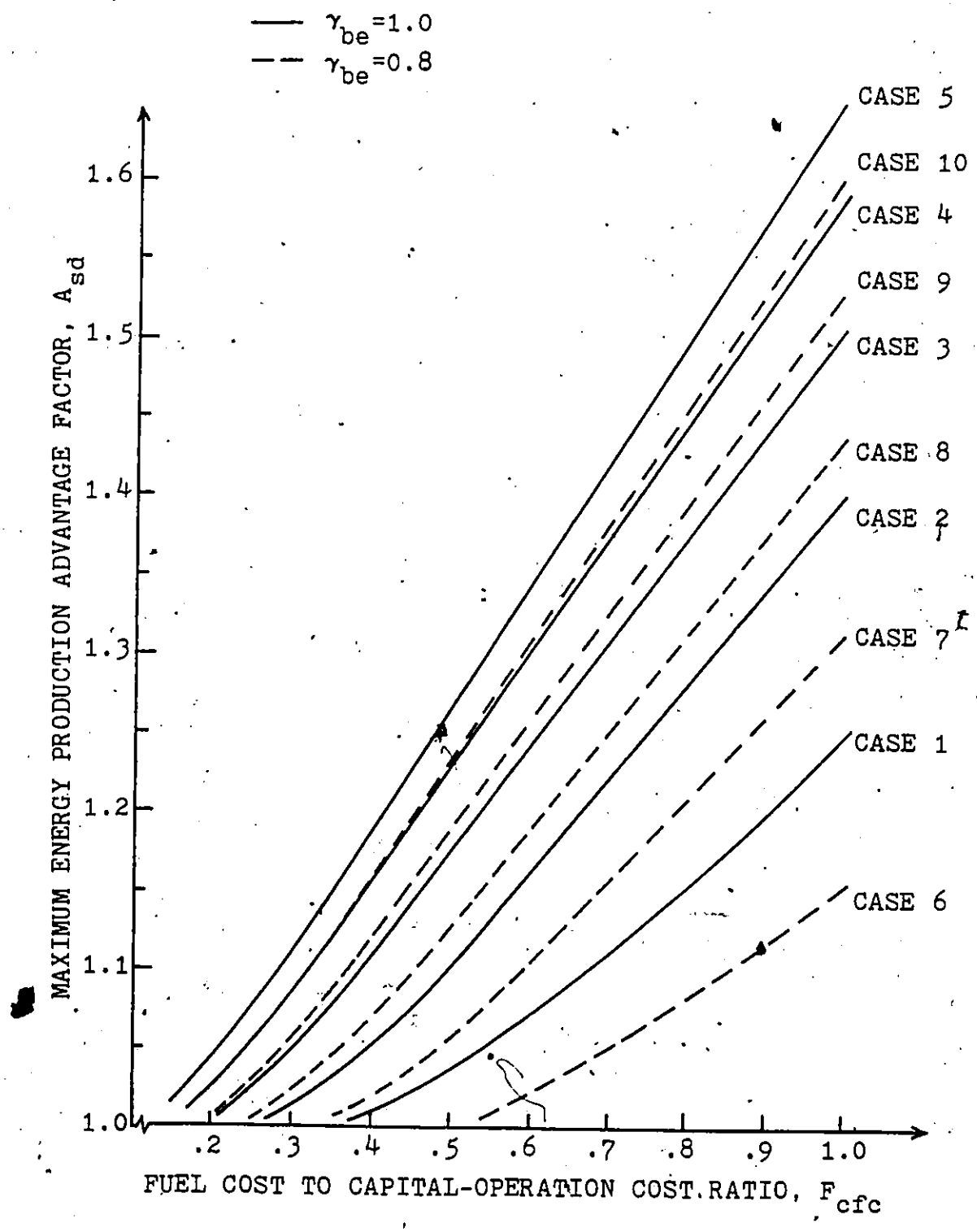

Fig. 5.6.5 Maximum energy production advantage factor for symbiotic systems without fuel reprocessing.

advantage factor, A_{sd}, as a function of fuel fractional cost, while Fig. 5.6.6 shows the corresponding burnup. Here, the practically linear increase of the advantage factor with respect to the fuel cost fraction, F_{cfc} is noteworthy.

Figure 5.6.7 compares the maximum advantage factor of the system without reprocessing to the system with periodic reprocessing. We note here that the maximum energy advantage factor occurs during the initial stage without reprocessing. The reprocessing cost penalty overrides any gains made by the improvements of the physical characteristics associated with reprocessing. The system with reprocessing will yield advantage factors close to those for a system without reprocessing if a relative active fuel reprocessing cost fraction, w_{rsd}, of two instead of three, is achievable. Fig. 5.6.7 also shows the maximum energy advantage factor for a system without any reprocessing cost penalty, that is w_{rsd} is equal to zero. Here, considerable improvement over the system with a cost penalty and the system without reprocessing is apparent. Figure 5.6.8 compares the maximum energy advantage factor for systems with periodic reprocessing, with a relative mill-grade fuel cost fraction, F_{cmf}, of 0.62 to cases with F_{cmf} equal to 0.76, corresponding to a doubling in mill-grade fuel costs. Although an improvement in the

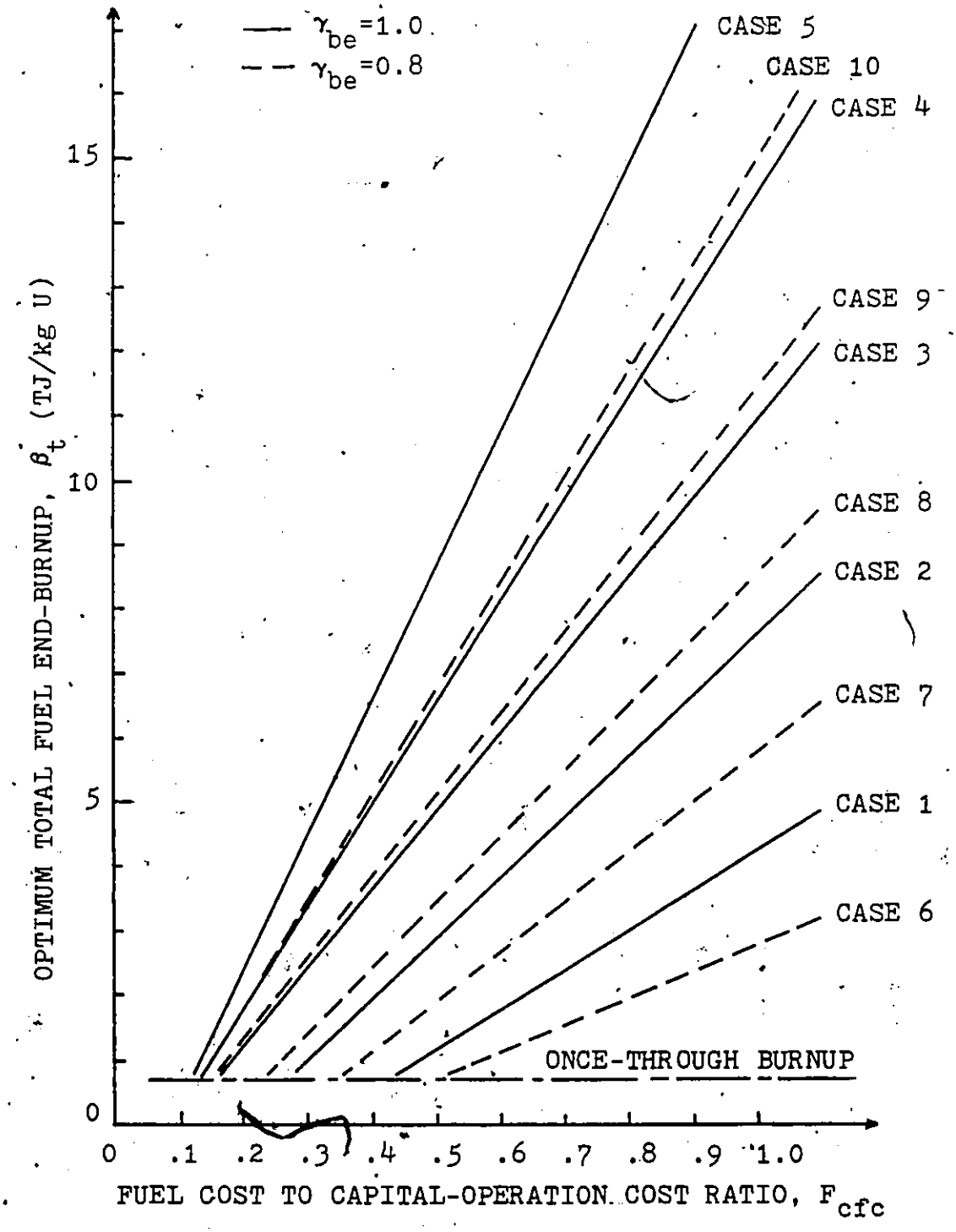

Fig. 5.6.6 Optimum total fuel burnup for symbiotic systems without fuel reprocessing.

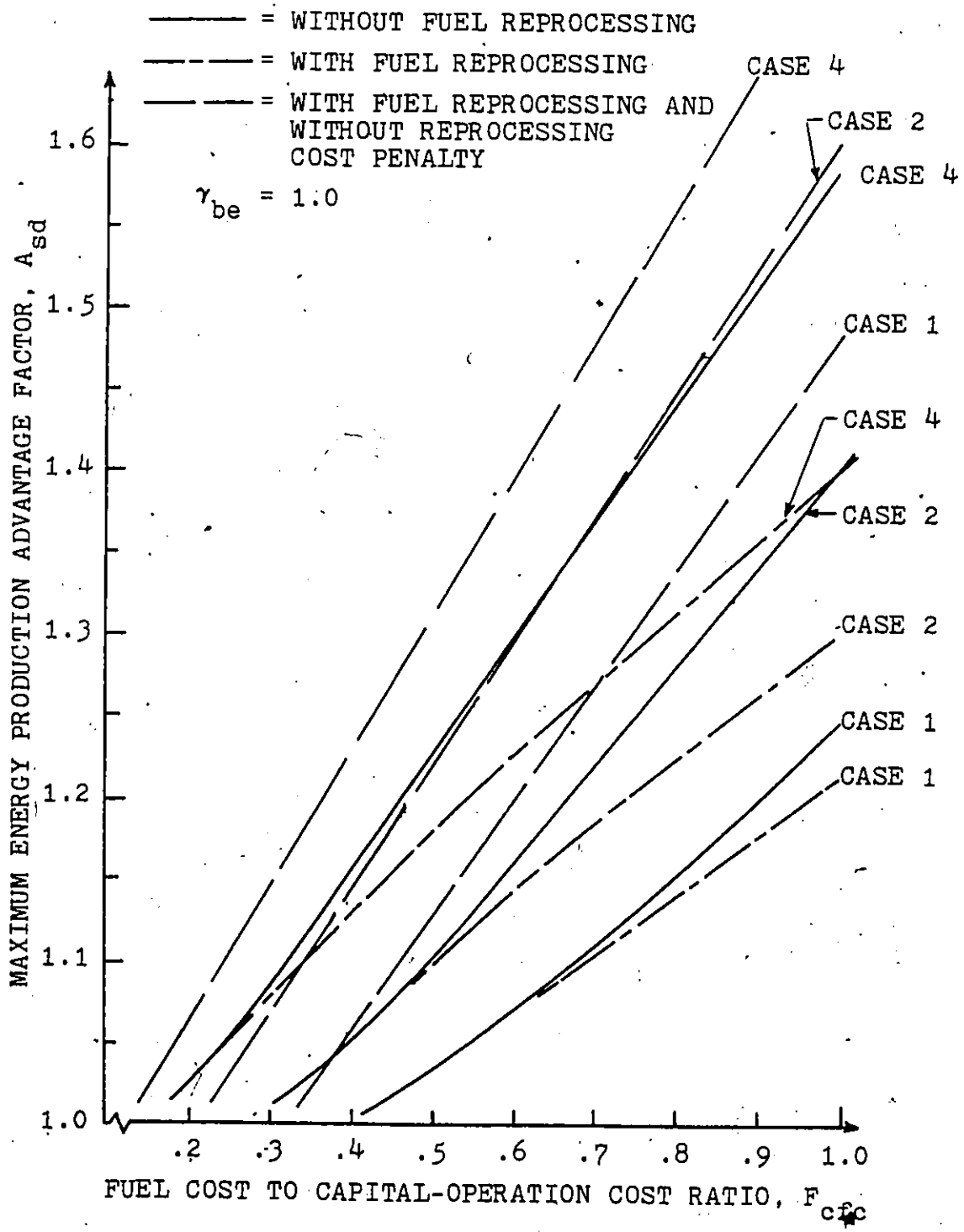

Fig. 5.6.7 Maximum energy production advantage factor for symbiotic systems with and without periodic fuel reprocessing.

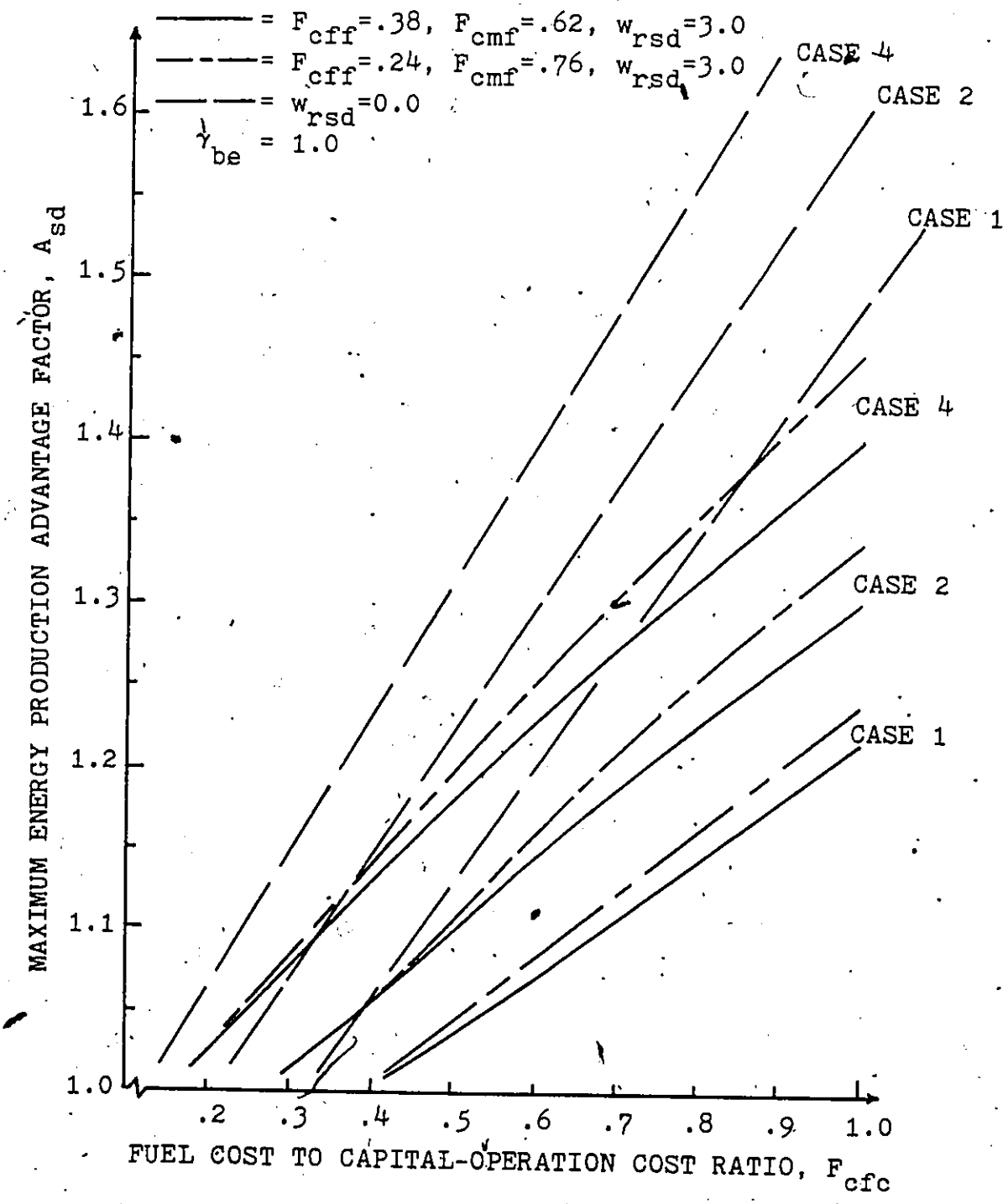

Fig. 5.6.8 Maximum energy production advantage factor for symbiotic systems with periodic fuel reprocessing.

energy advantage factor, A_{sd}, is apparent, results still fall short of those without reprocessing.

So far, only fuel cost effects on the energy advantage factor have been discussed although the breeder cost is also of importance. The breeder lifetime capital-operational cost is, however, relatively insensitive to economic effects, since it appears only relative to the depleter capital-operational cost, as can be seen in Eq. 5.5.1 and Eq. 5.6.8. In exploring the effect of breeder capital-operational cost on the energy advantage factor, A_{sd}, the concept of allowed breeder cost fraction emerges. This is the fraction, f_{abc}, of the presently estimate cost of the breeder subsystem which will yield a system energy production advantage factor, A_{sd}, of unity. This condition can be expressed as

$$F_{es} = \left(1 + \frac{f_{abc}}{Q_{td}}\right)(2.8 + Q_{tb}) + \frac{F_{cfc}}{f_s}\left(0.38\left(1 + 3.0\,\frac{M_r}{M_{oh}}\right) + 0.62\right)\Big)/(1 + F_{cfc}), \quad (5.6.9)$$

which upon rearranging yields

$$f_{abc} = \left(F_{es}(1 + F_{cfc}) - 1 - \frac{F_{cfc}}{f_s}\left(0.38\left(1 + 3.0\,\frac{M_r}{M_{oh}}\right) + 0.62\right)\right)\Big/\left((2.8 + Q_{tb})/Q_{td}\right). \quad (5.6.10)$$

The allowed breeder cost fraction, f_{abc}, is summarized in Fig. 5.6.9 and Fig. 5.6.10 for the systems with reprocessing

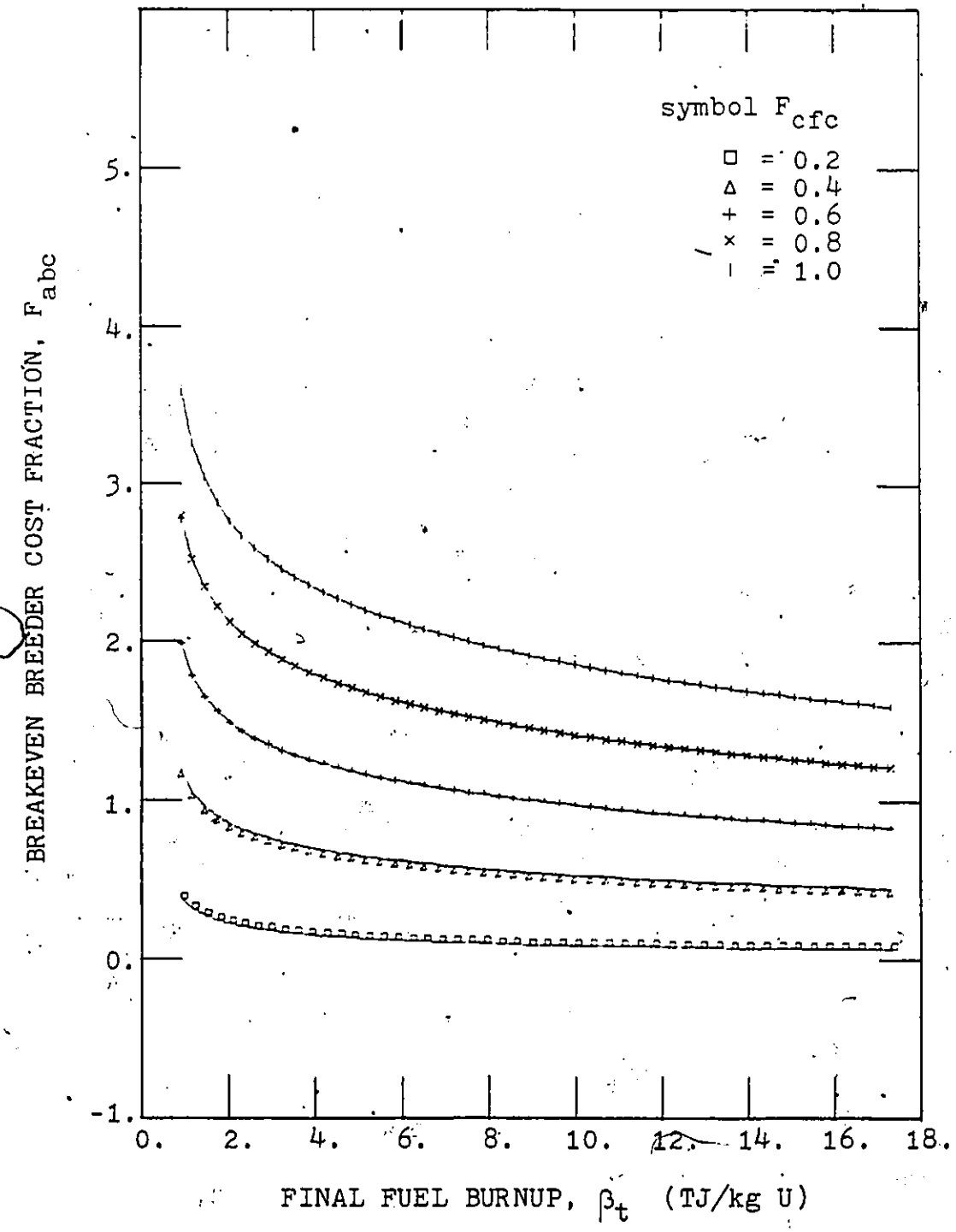

Fig. 5:6.9a Symbiotic system breakeven breeder cost fraction without fuel reprocessing; case 1 of Table 4.6.1.

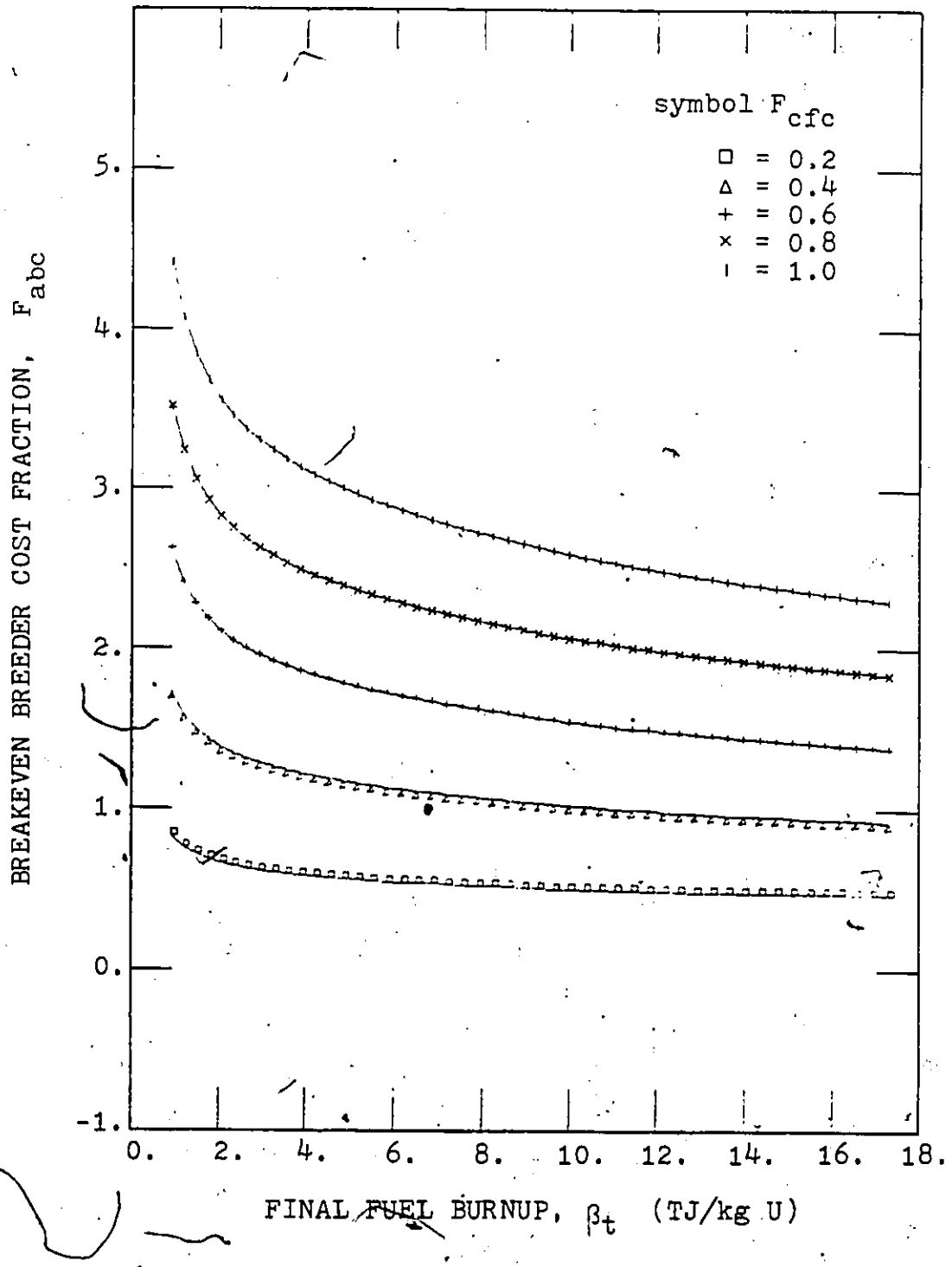

Fig. 5.6.9b Symbiotic system breakeven breeder cost fraction without fuel reprocessing; case 2 of Table 4.6.1.

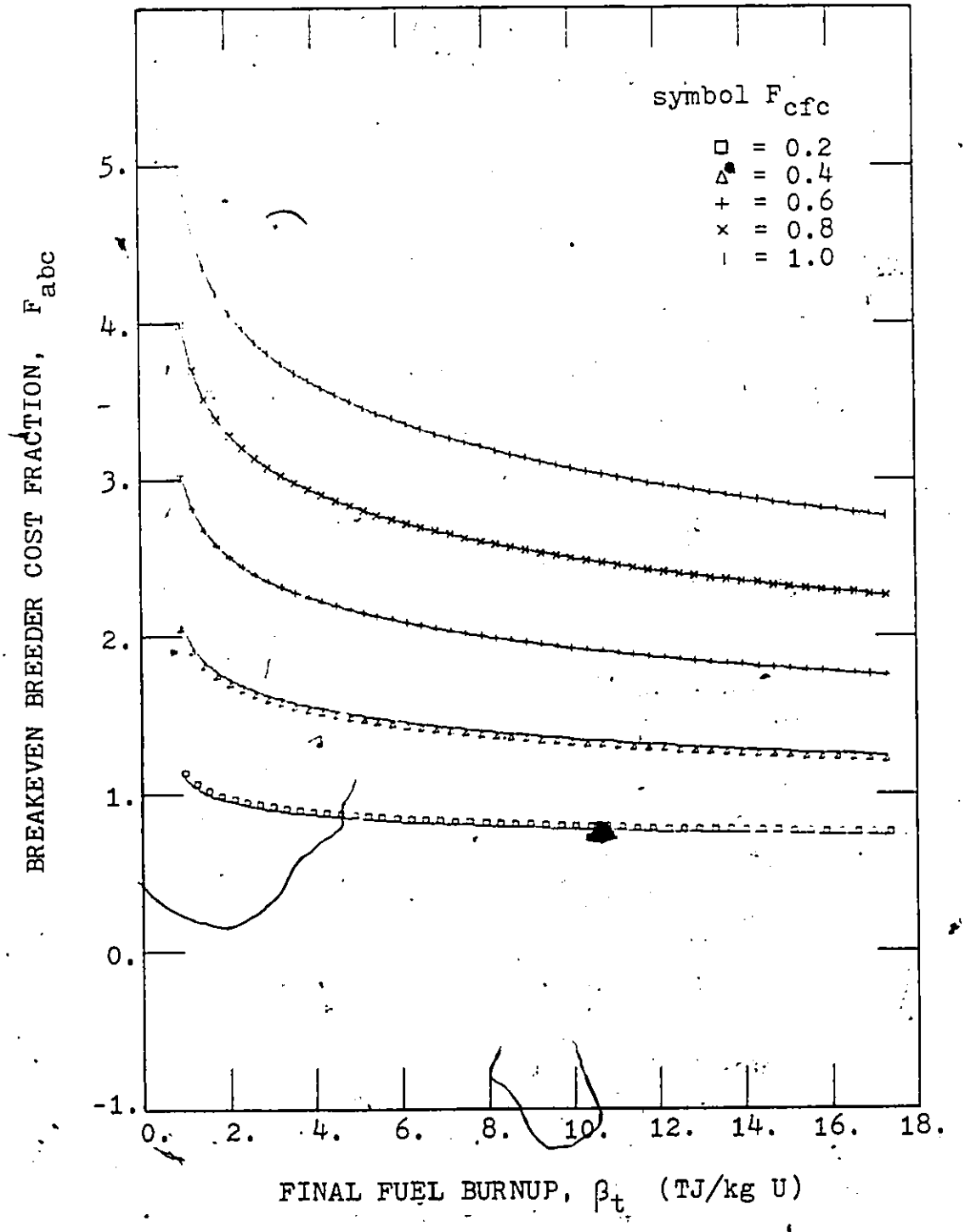

Fig. 5.6.9c Symbiotic system breakeven breeder cost fraction without fuel reprocessing; case 3 of Table 4.6.1.

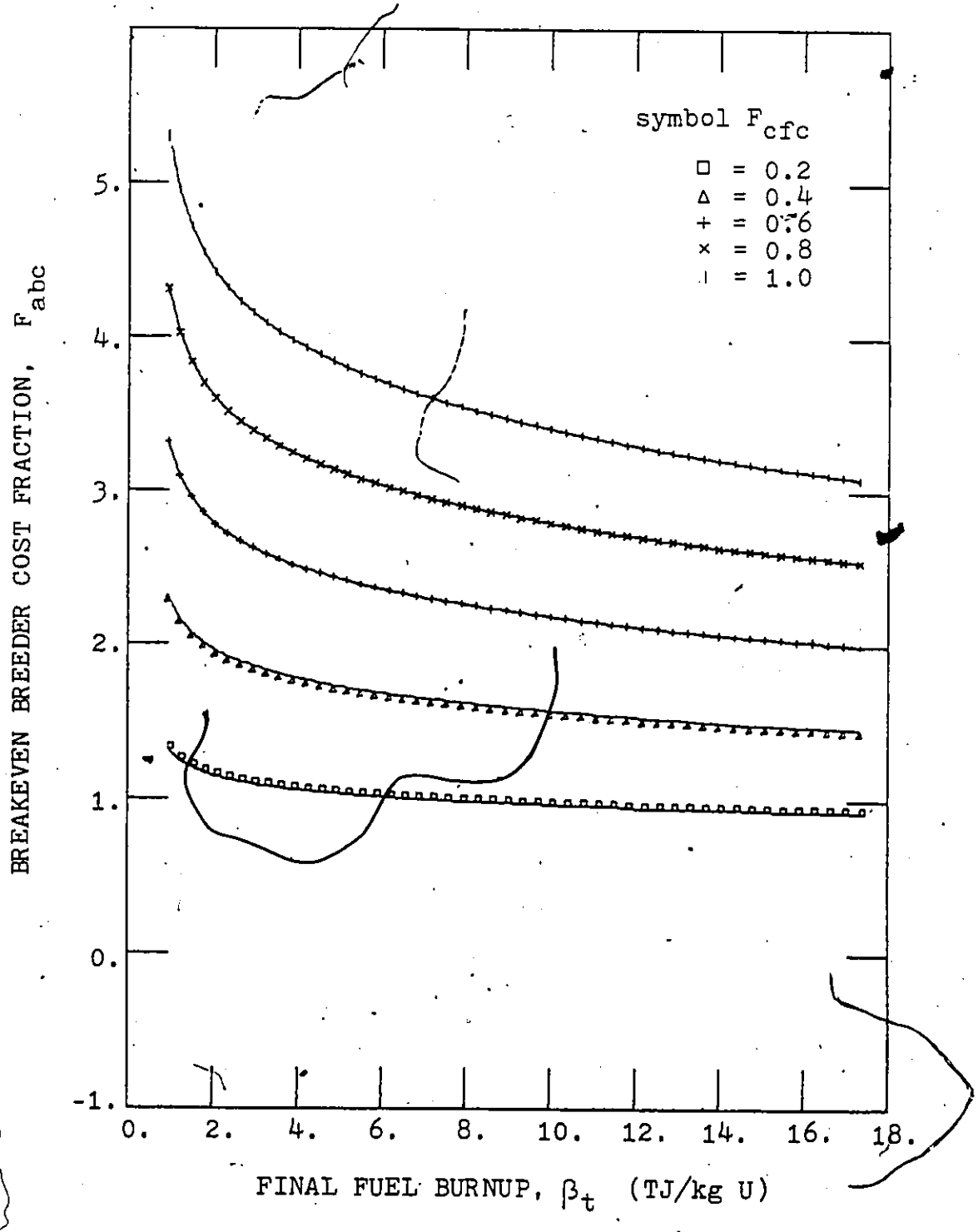

Fig. 5.6.9d Symbiotic system breakeven breeder cost fraction without fuel reprocessing; case 4 of Table 4.6.1.

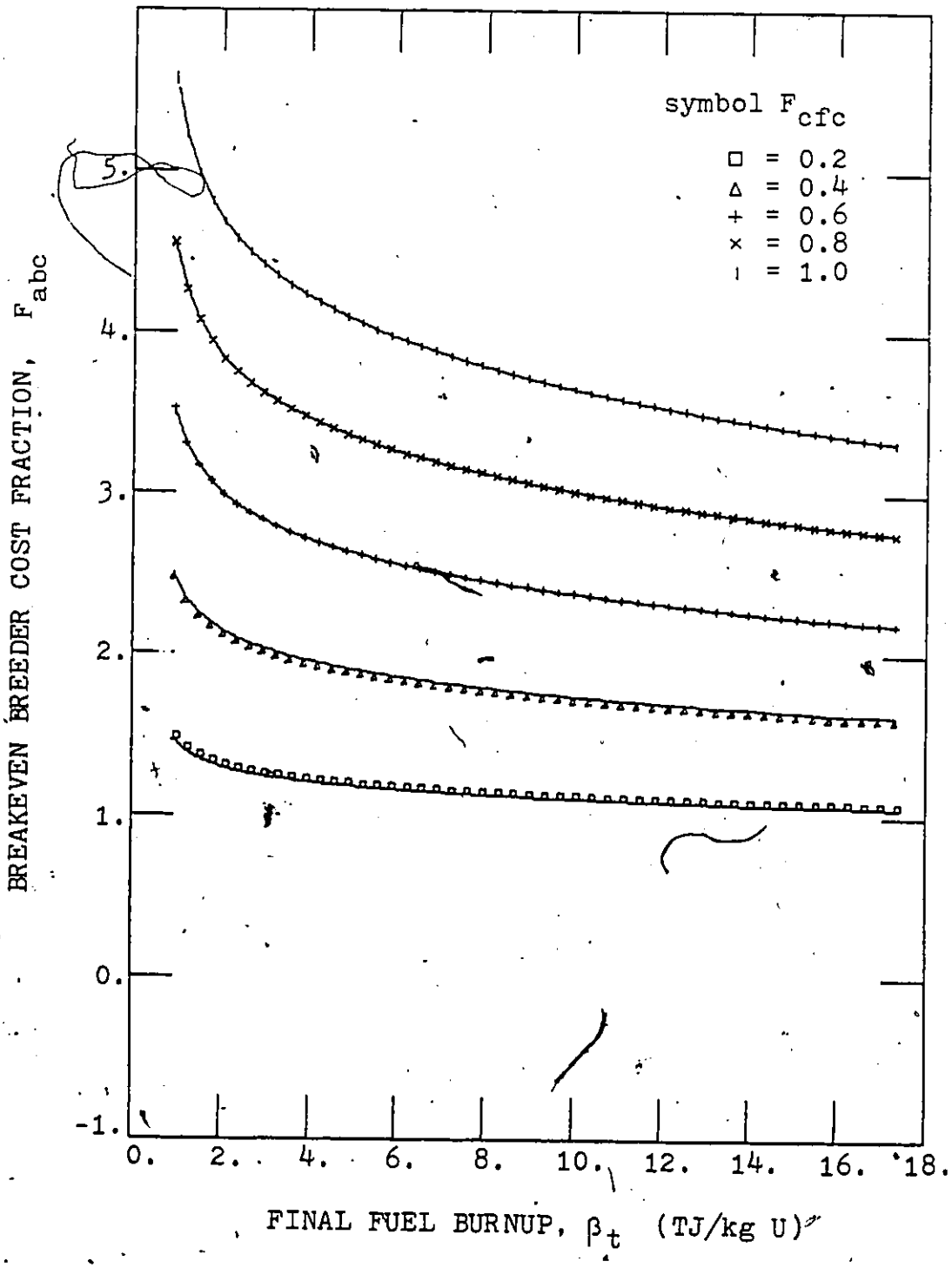

Fig. 5.6.9e Symbiotic system breakeven breeder cost fraction without fuel reprocessing; case 5 of Table 4.6.1.

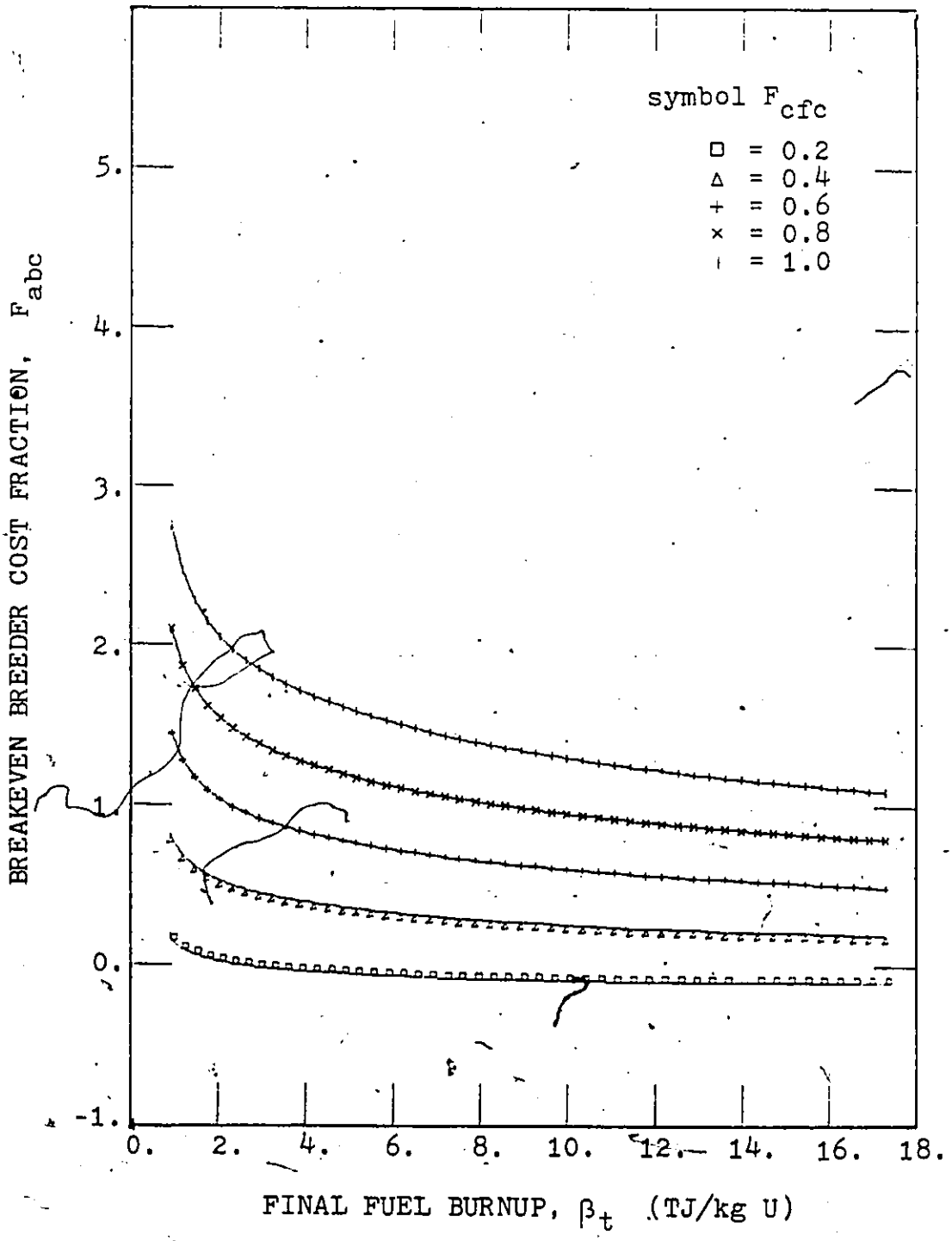

Fig. 5.6.9f Symbiotic system breakeven breeder cost fraction without fuel reprocessing; case 6 of Table 4.6.1.

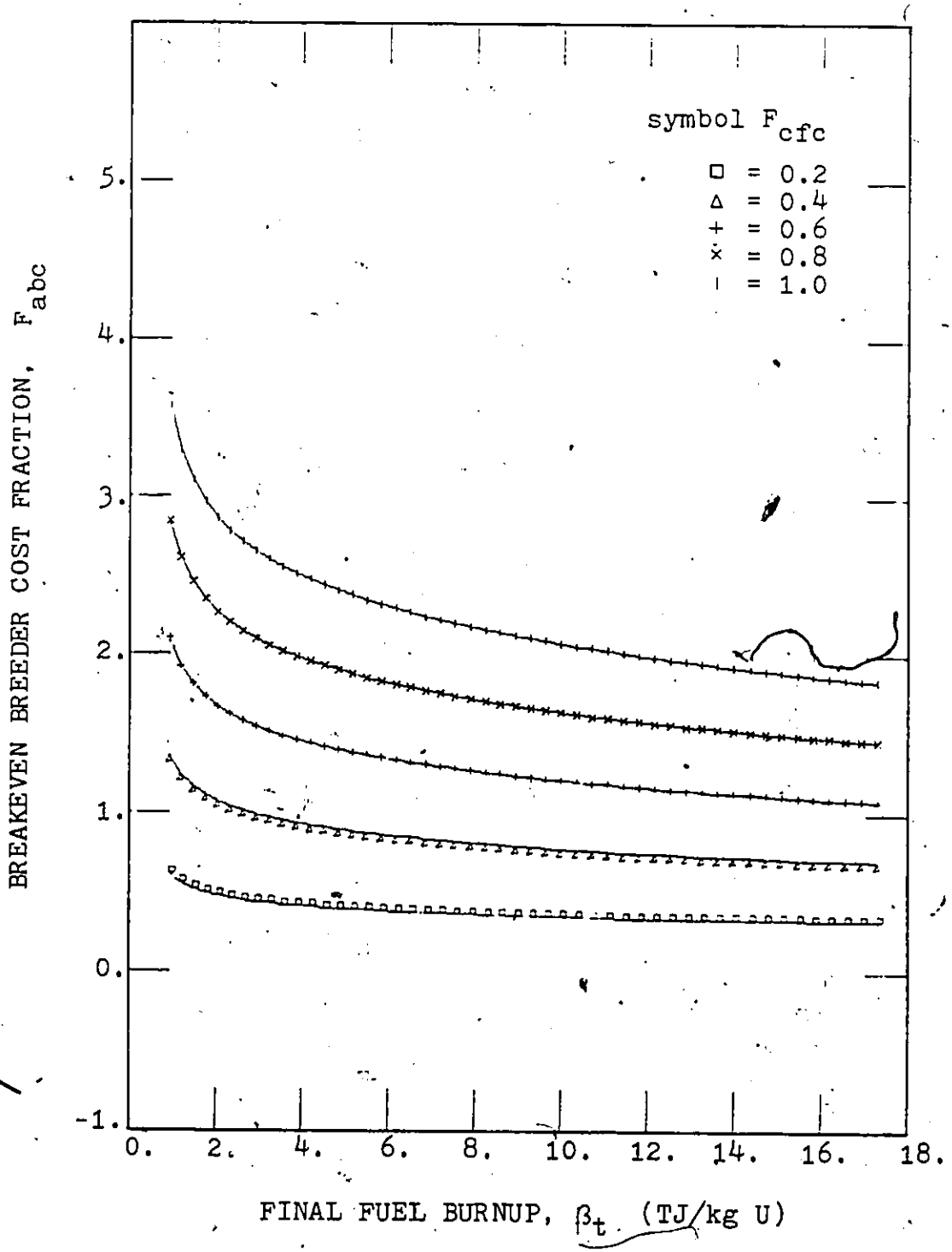

Fig. 5.6.9g Symbiotic system breakeven breeder cost fraction without fuel reprocessing; case 7 of Table 4.6.1.

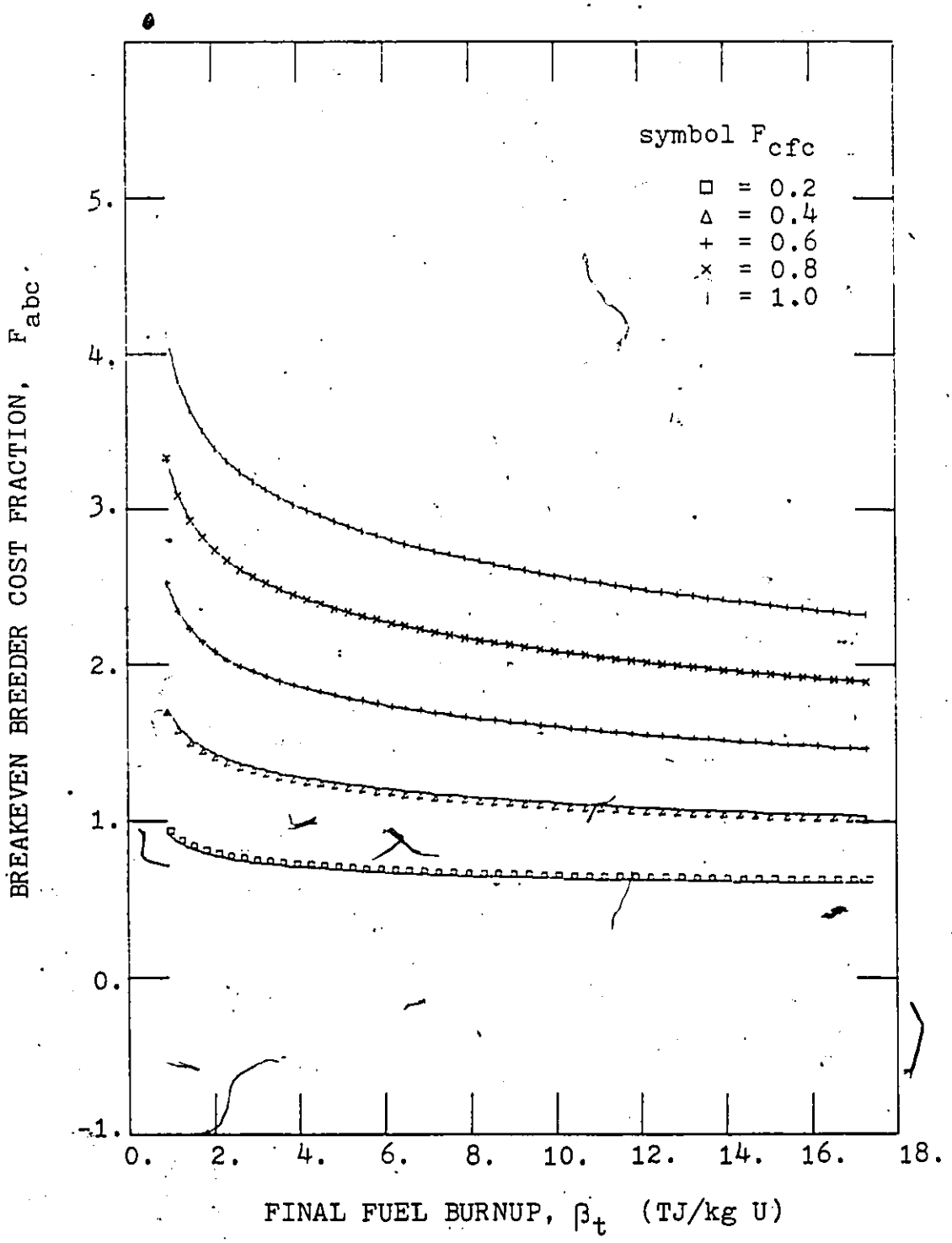

Fig. 5.6.9h Symbiotic system breakeven breeder cost fraction without fuel reprocessing; case 8 of Table 4.6.1.

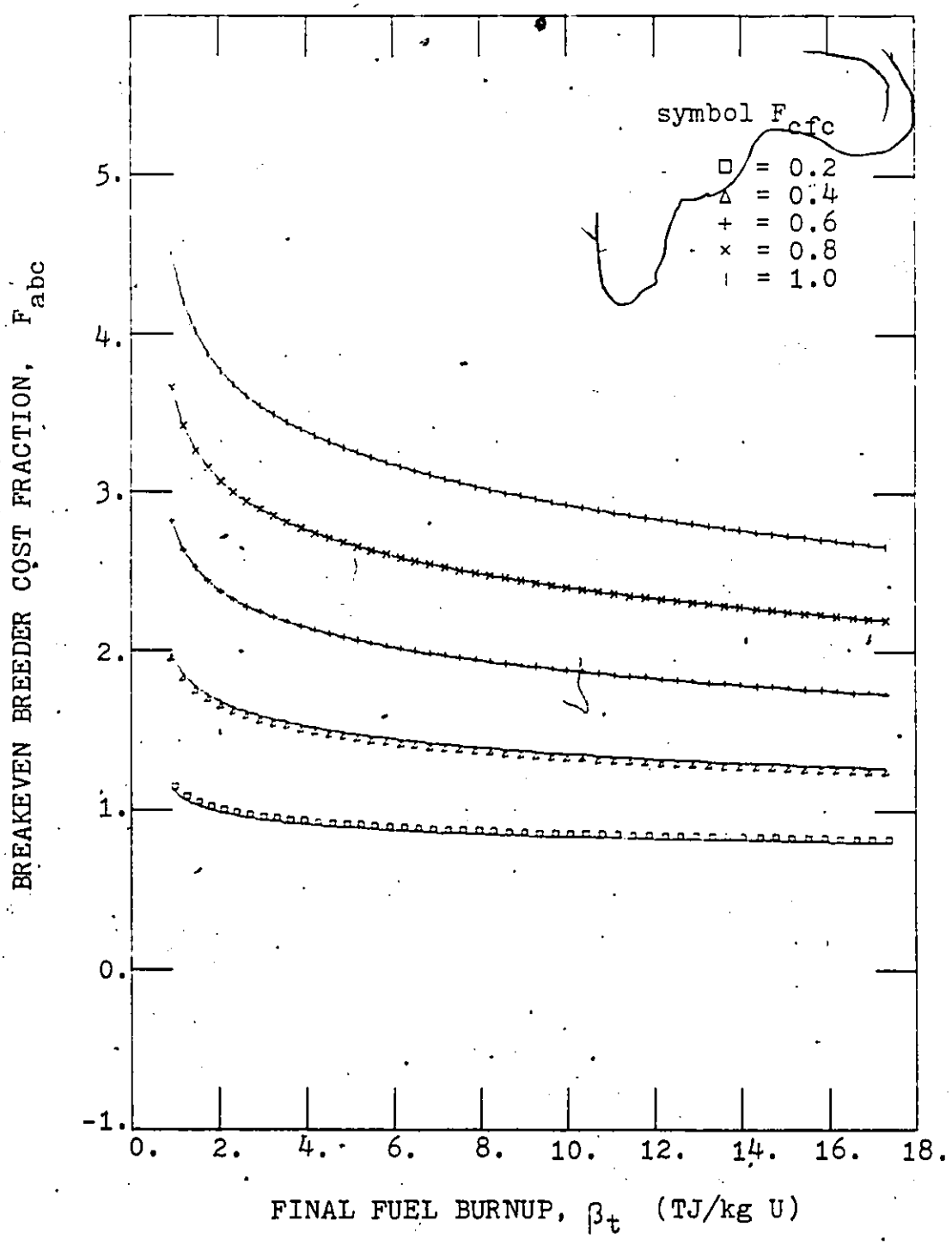

Fig. 5.6.9i Symbiotic system breakeven breeder cost fraction without fuel reprocessing; case 9 of Table 4.6.1.

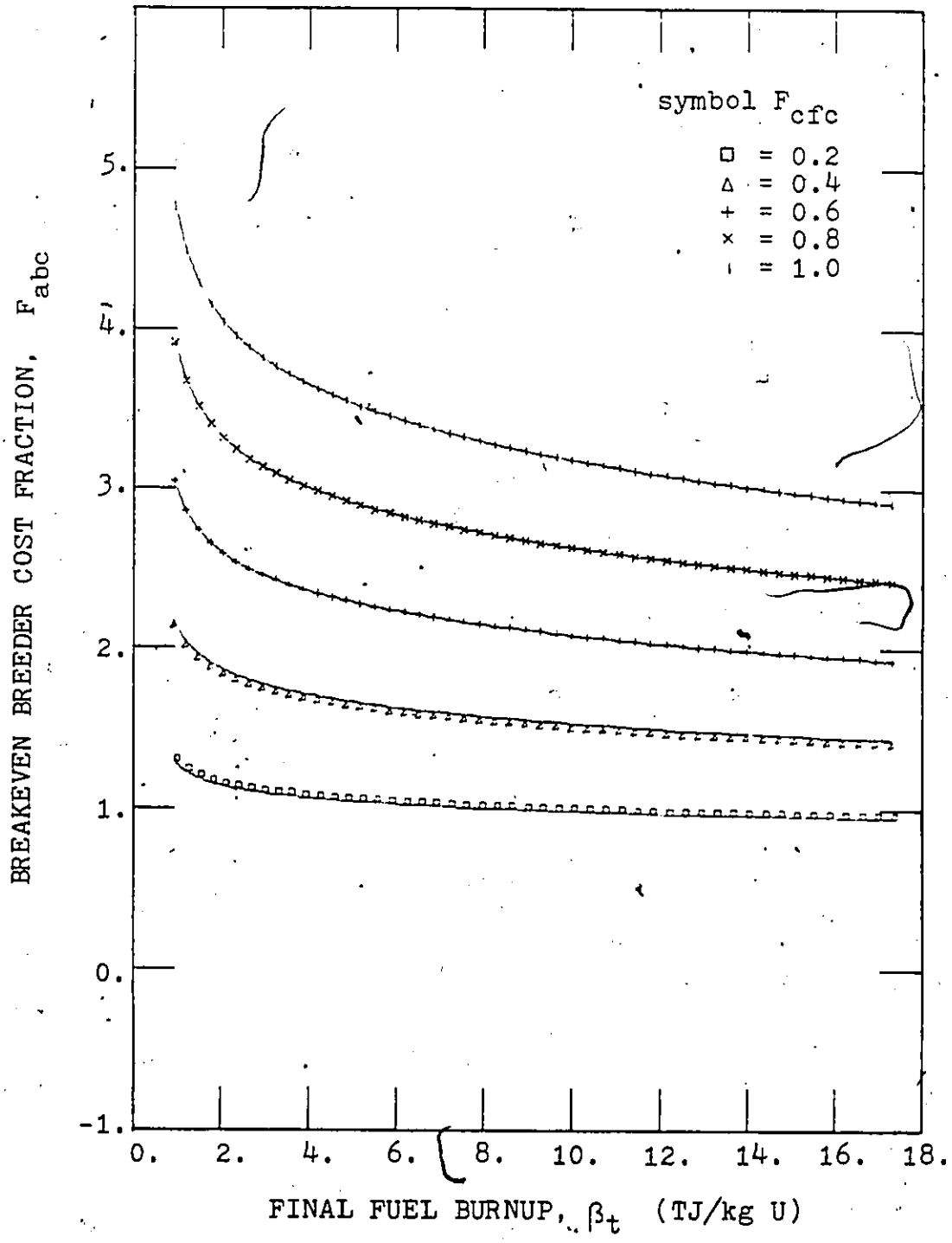

Fig. 5.6.9j Symbiotic system breakeven breeder cost fraction without fuel reprocessing; case 10 of Table 4.6.1.

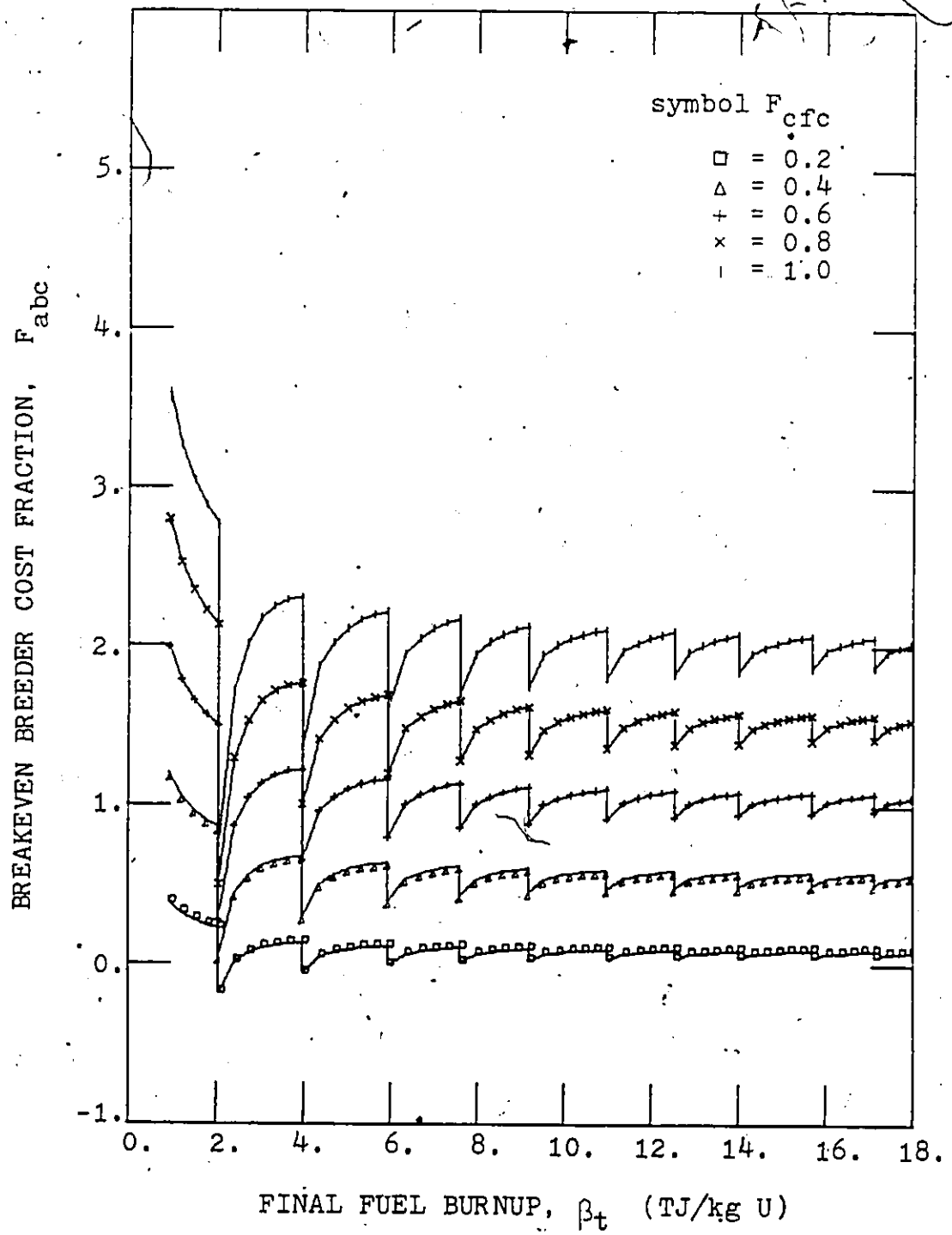

Fig. 5.6.10a Symbiotic system breakeven breeder cost fraction with periodic reprocessing; case 1 of Table 4.6.1.

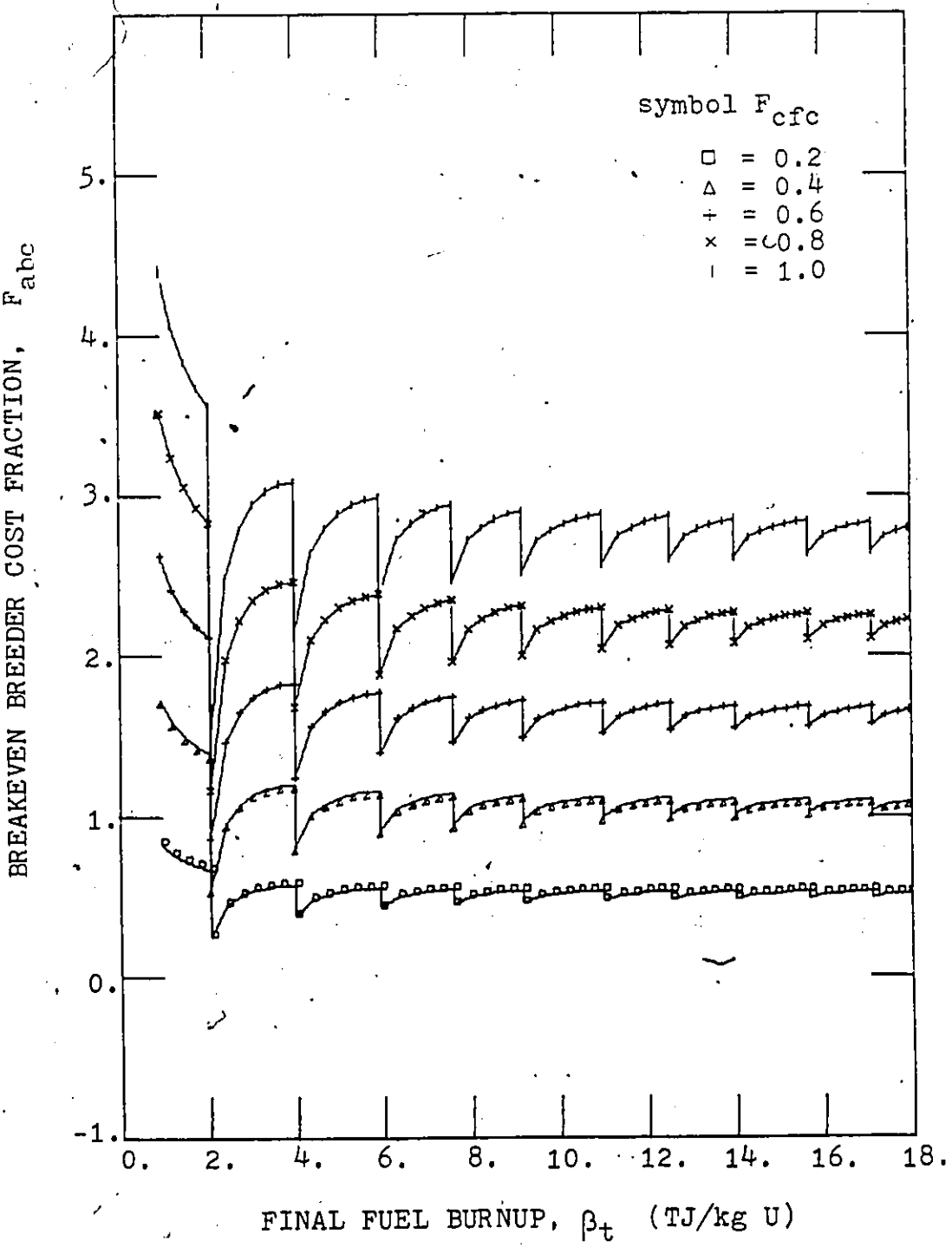

Fig. 5.6.10b Symbiotic system breakeven breeder cost fraction with periodic reprocessing; case 2 of Table 4.6.1.

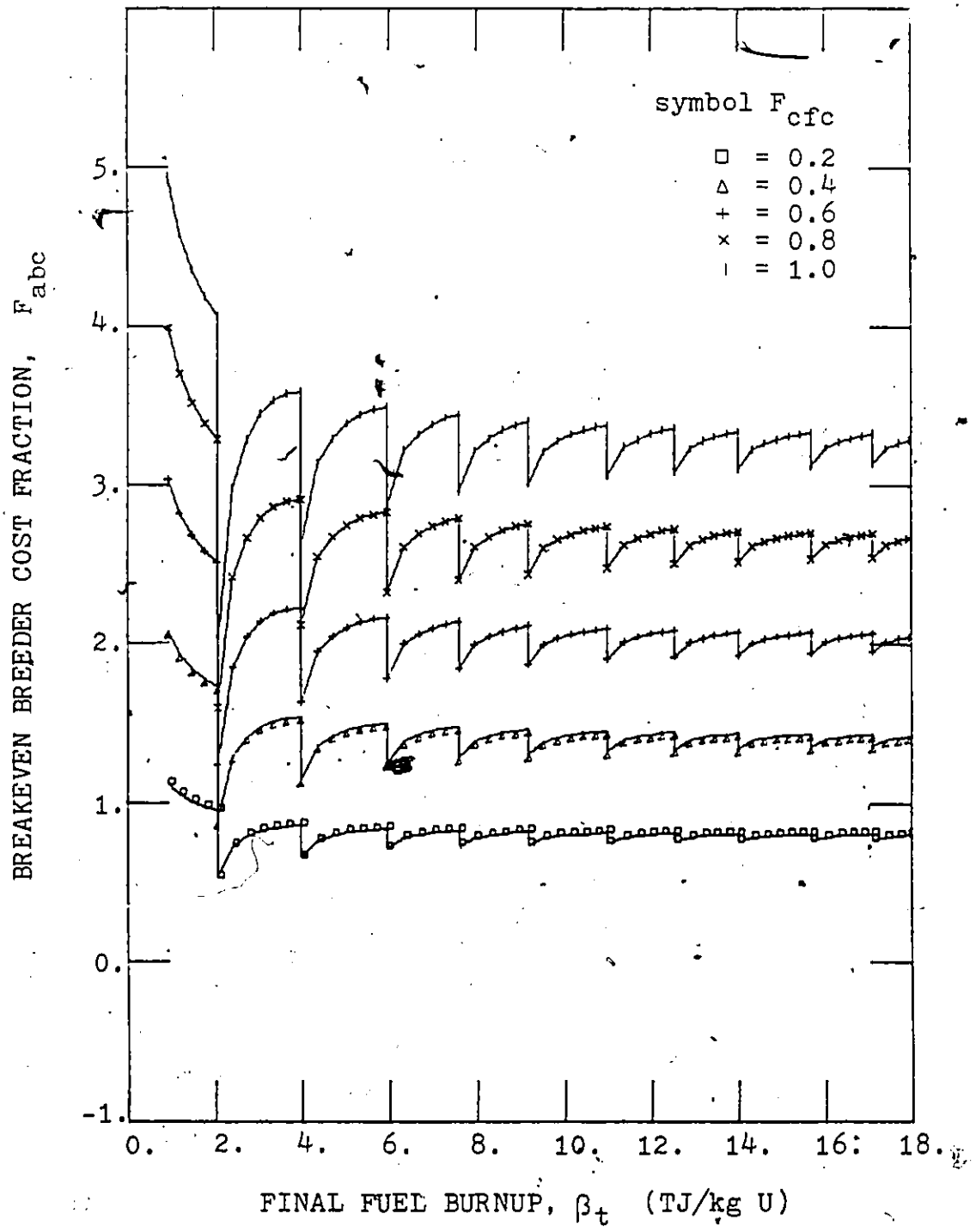

Fig. 5.6.10c Symbiotic system breakeven breeder cost fraction with periodic reprocessing; case 3 of Table 4.6.1.

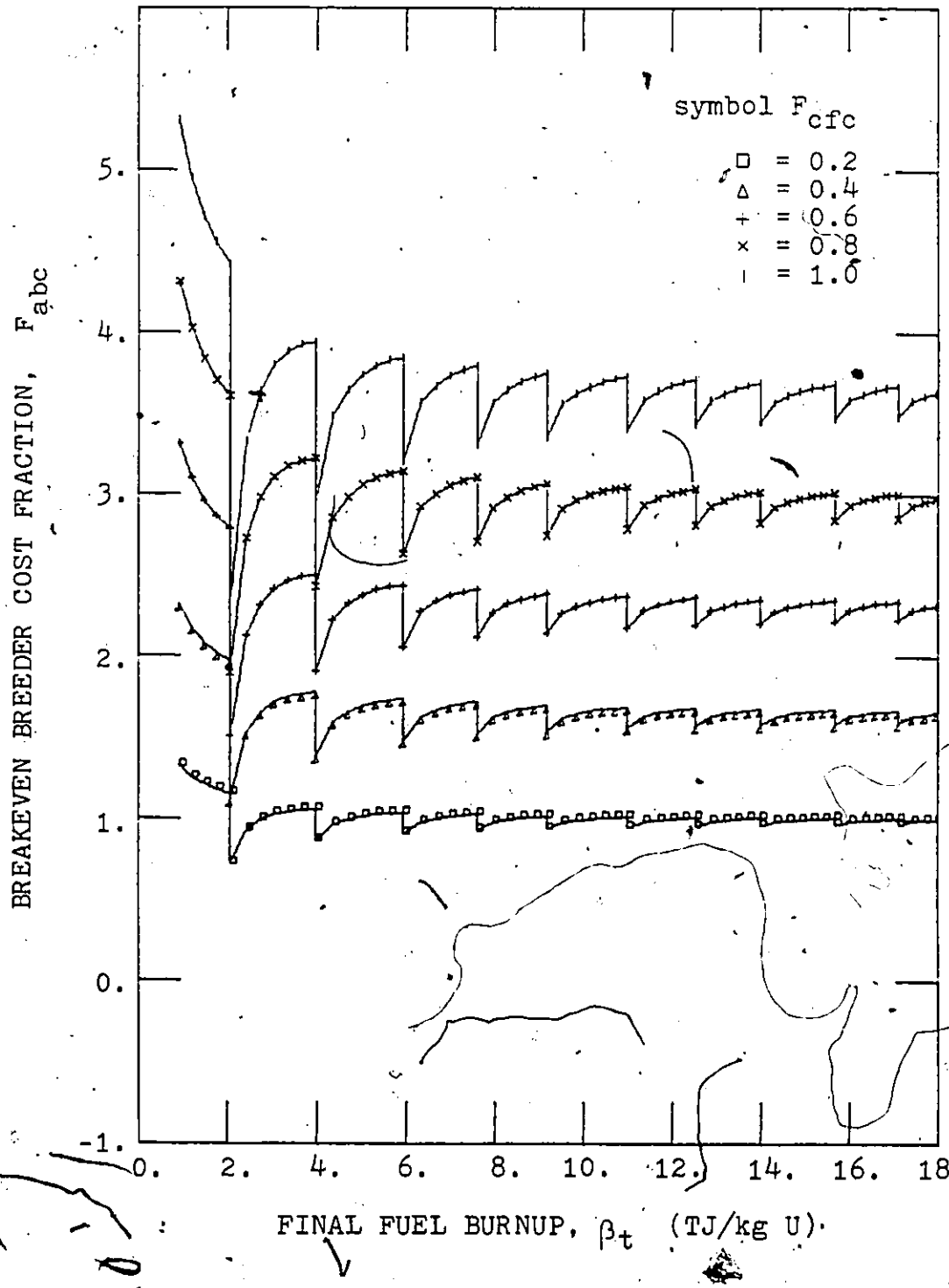

Fig. 5.6.10d Symbiotic system breakeven breeder cost fraction with periodic reprocessing; case 4 of Table 4.6.1.

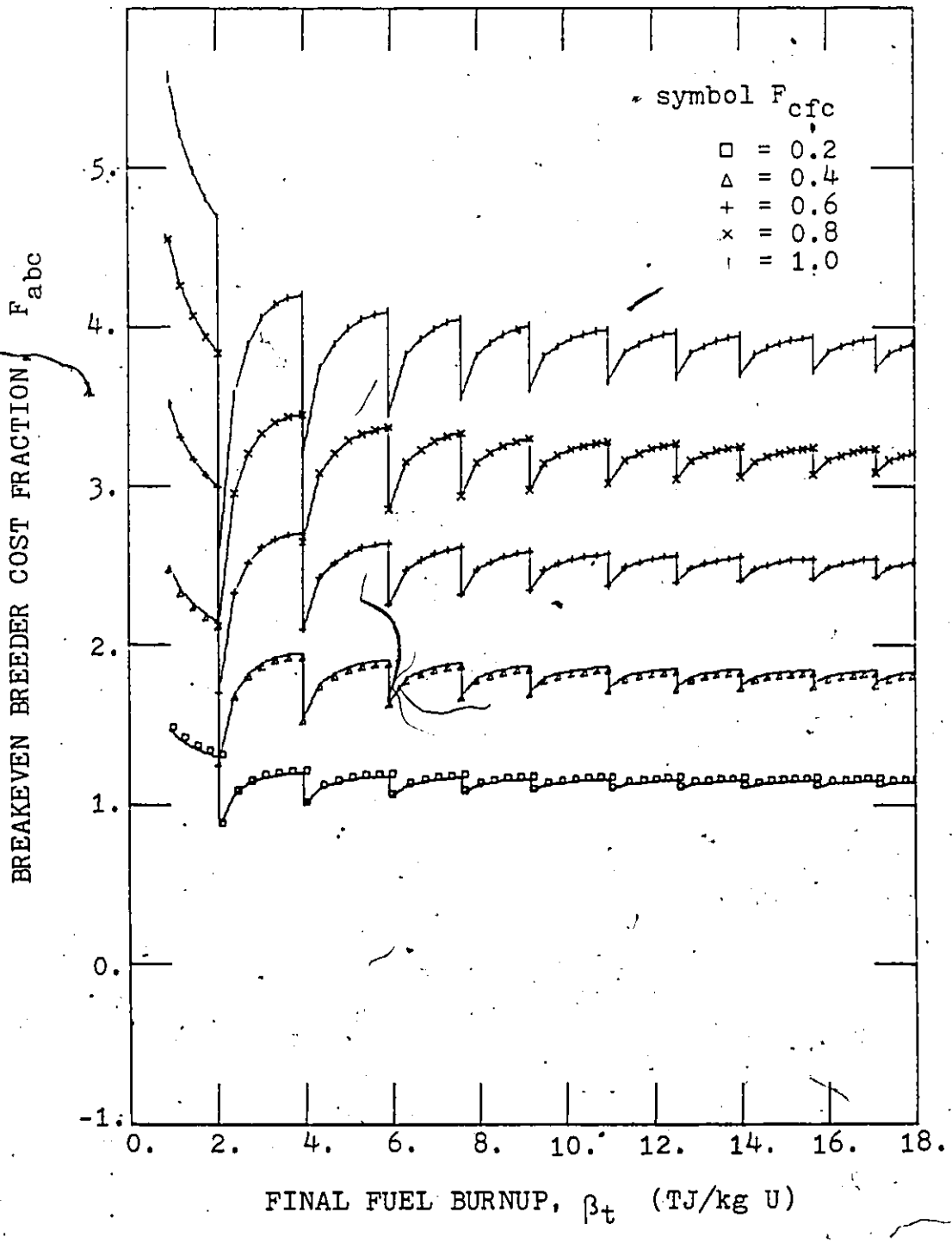

Fig. 5.6.10e Symbiotic system breakeven breeder cost fraction with periodic reprocessing; case 5 of Table 4.6.1.

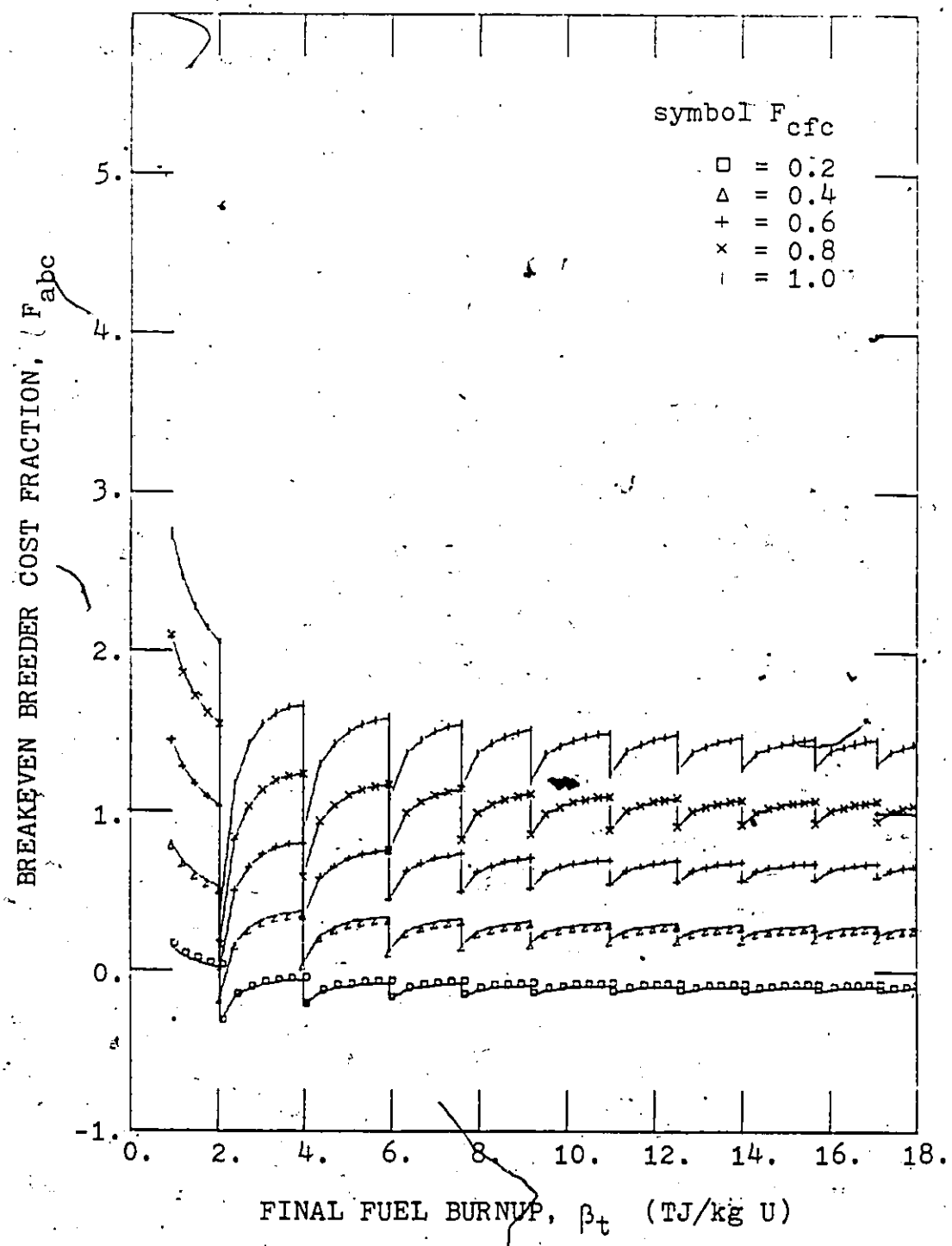

Fig. 5.6.10f Symbiotic system breakeven breeder cost fraction with periodic reprocessing; case 6 of Table 4.6.1.

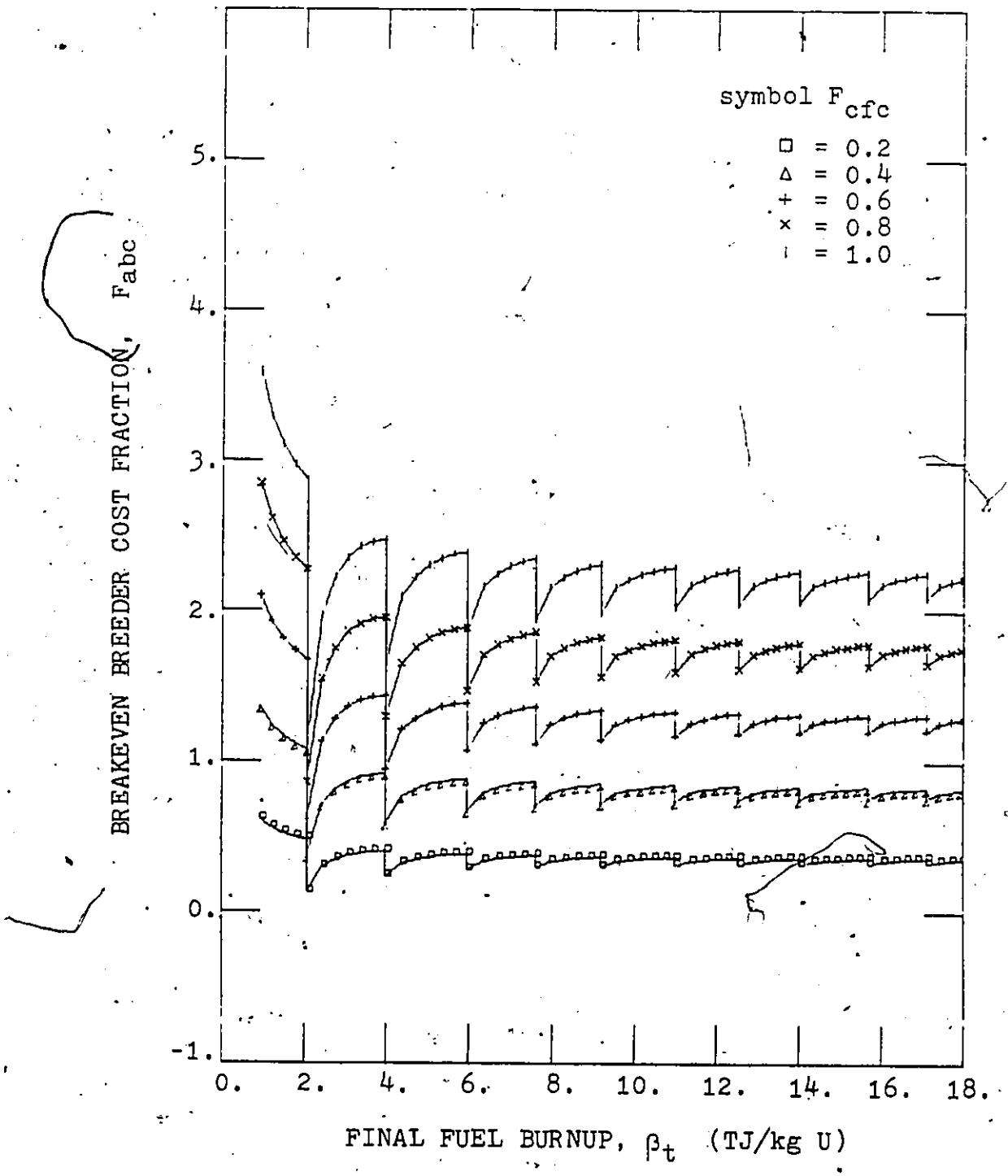

Fig. 5.6.10g Symbiotic system breakeven breeder cost fraction with periodic reprocessing; case 7 of Table 4.6.1.

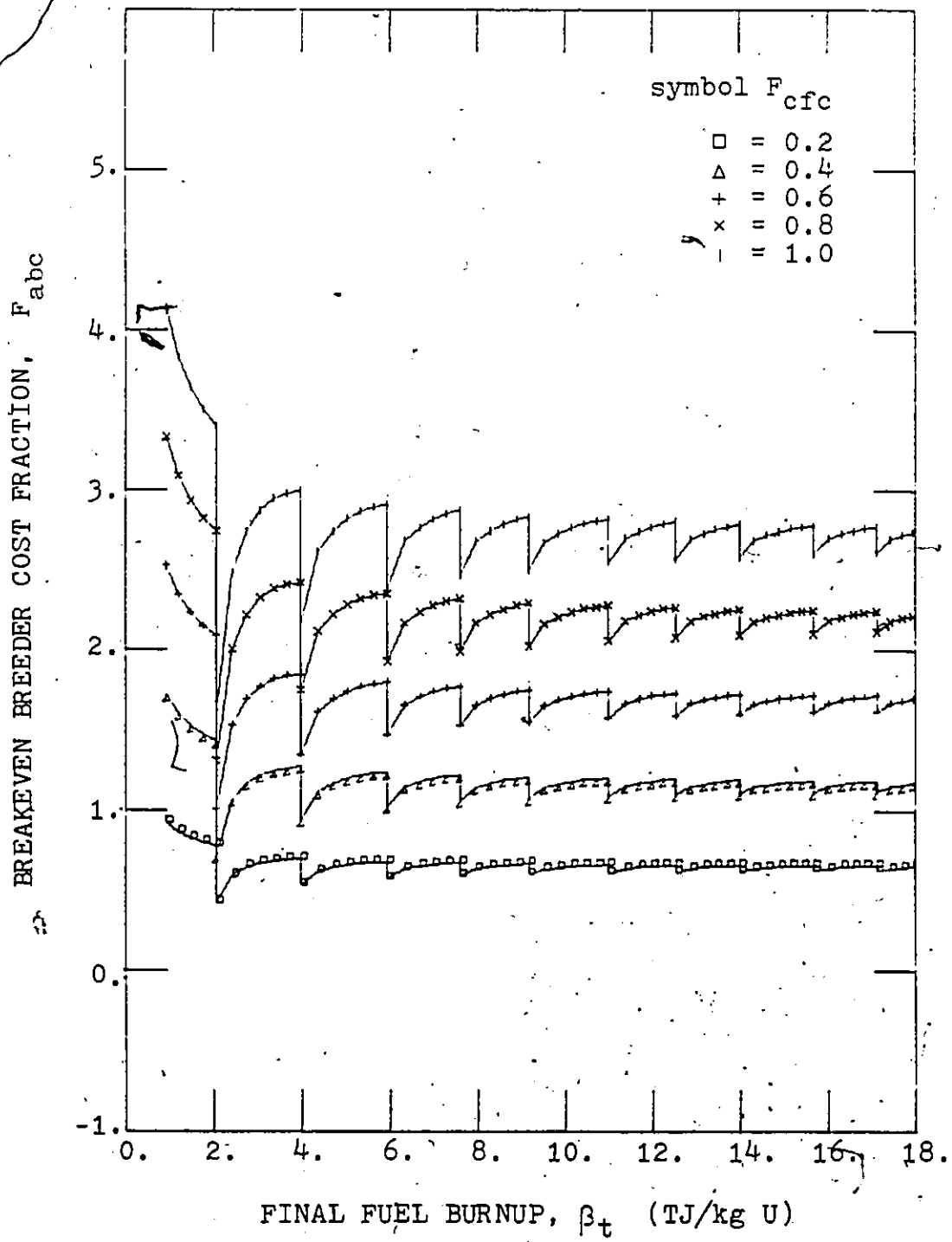

Fig. 5.6.10h Symbiotic system breakeven breeder cost fraction with periodic reprocessing; case 8 of Table 4.6.1.

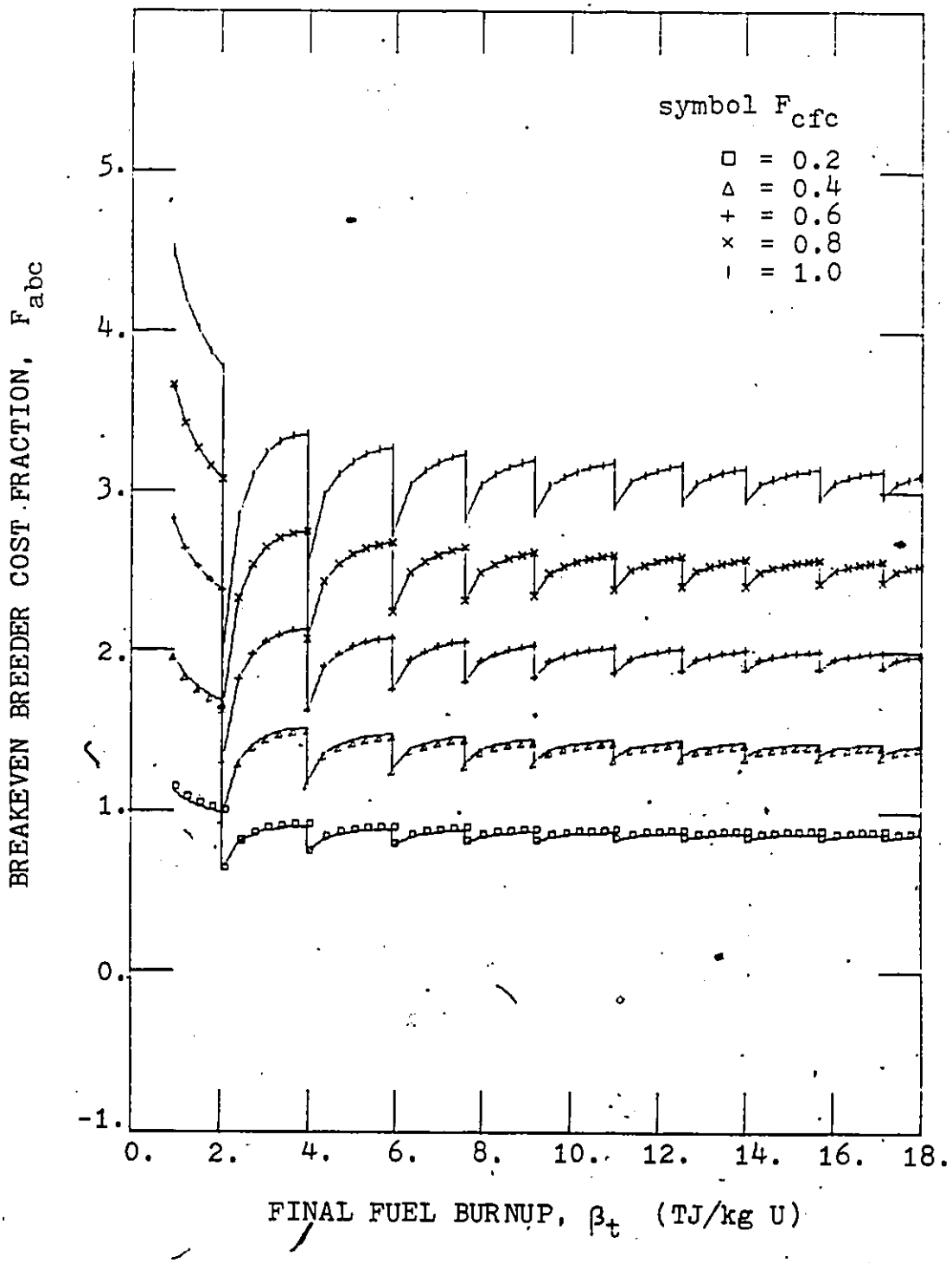

Fig. 5.6.10i Symbiotic system breakeven breeder cost fraction with periodic reprocessing; case 9 of Table 4.6.1.

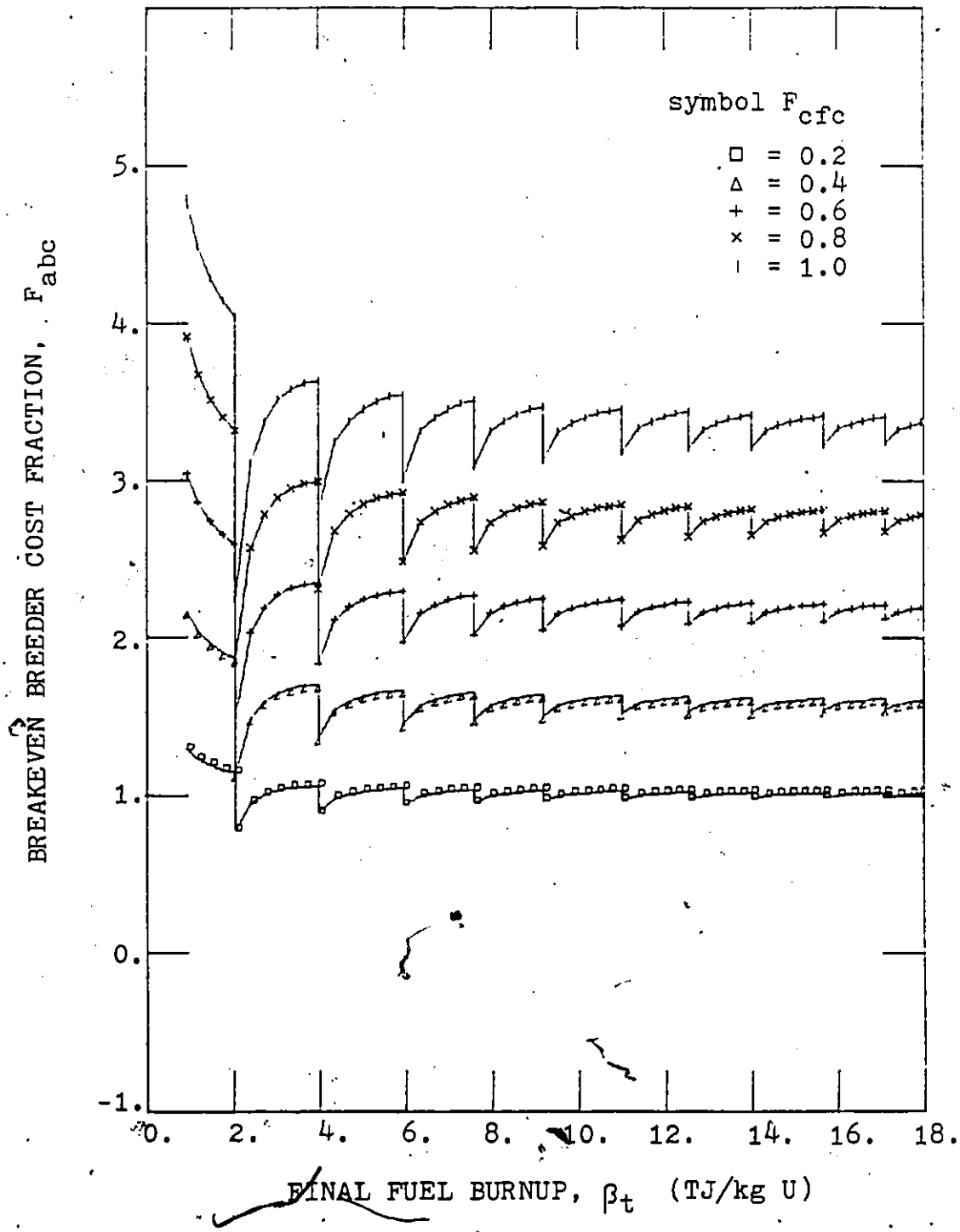

Fig. 5.6.10j Symbiotic system breakeven breeder cost fraction with periodic reprocessing; case 10 of Table 4.6.1.

and without periodic reprocessing. Again, results are shown for all cases defined in Table 4.6.1 and the set of relative fuel cost fractions, F_{cfc}, given in Table 5.6.1.

As expected, breakeven breeder costs are in the range of present cost estimates for F_{cfc} greater than 0.6. Below this value, the breeder cost will have to be substantially reduced before energy production breakeven is achieved. In isolated cases, as shown in Fig. 5.6.9f and Fig. 5.6.10f, the breakeven breeder cost fraction, f_{abc}, becomes negative and therefore cannot even theoretically be achieved. For these cases, the electrical power cost requirements of the breeder subsystem exceed the fuel cost savings of the symbiotic system. For energy production breakeven, the electrical power requirements of the breeder would, therefore, have to be reduced as well.

From energy advantage factor results and related results, it can be concluded that a symbiotic system based on uranium-plutonium fuel rejuvenation without reprocessing is presently only feasible under favourable operating conditions. For an increased fuel cost fraction the symbiotic system becomes attractive even for less favourable operating conditions.

CHAPTER 6

CONCLUSION

With the emergence of spallation neutron sources, nuclear systems based on fissile fuel rejuvenation without reprocessing appear most attractive alternatives in securing future nuclear fuel requirements. The associated nuclear systems involve fission-independent neutron sources produced in heavy element targets of linear accelerator proton beams. These neutron sources may consequently be used to breed nuclear fuels directly in converter reactor spent fuel elements. The rejuvenated fuel elements can then be reintroduced into the depleter reactor for further burnup. The breeder associated depleter subsystem conceived and analyzed here was capable of burning natural uranium suitable for heavy water moderated reactor systems.

A nuclear reactor system can be based on the uranium-plutonium or the thorium-uranium fuel cycle. The thorium cycle shows greater net breeding potential than the uranium cycle since its depleter subsystem conversion ratio is significantly larger. In the analysis undertaken here, the thorium cycle high fissile fuel inventory requirements combined with the feature that natural thorium contains no fissile fuel produces, for moderate fuel burnup levels, net

fissile fuel consumption characteristics inferior to those of natural uranium based fuels. Here it should be noted that in a system without fuel reprocessing, no value is credited to fissile isotopes contained in final burnup fuel elements. Cost savings due to lower thorium fuel costs only have a small effect on the overall system cost characteristics since fuel requirements for systems with fuel recycling are considerably below those without fuel recycling.

In the symbiotic system analysis undertaken here, several major system parameters emerged. One of the most critical system factors is the magnitude of the effective independent breeder neutron source. However, this neutron source characteristic is also one of the most difficult parameters to be obtained experimentally or theoretically. Consequently cases spanning a neutron source range from 24 neutrons to 66 neutrons per 1 GeV accelerator proton have been employed here.

The fuel requirements of the depleter subsystem were described by the fuel stretching factor. For maximum fuel cost saving, a fuel stretching factor as high as possible should be aimed for. Comparing the fuel stretching factor with the fuel utilization factor shows that for a system without reprocessing approximately 10% of the fuel burnup takes place in the breeder subsystem. This fraction is

decreased to 5% for the system with periodic chemical reprocessing.

The system breeder-depleter power utilization factor is generally above 20 for moderate fuel burnups, but may exceed 100 for low fuel burnups. It plays an important role in defining the size of the breeder subsystem. A system breeder-depleter power utilization factor as high as possible is generally aimed for since it yields the lowest breeder subsystem cost while at the same time favorably affecting the overall system power balance.

Similar to the breeder-depleter power utilization factor, a breeder internal power utilization factor emerged with values ranging from 2 to 8. Its effect on the system properties is small since an increase favorably affects the system power balance while at the same time increasing the breeder cost.

A net system conversion efficiency was determined from the power utilization factors, the associated system conversion efficiencies, as well as the accelerator electrical drive power. It falls generally between 0.20 and 0.30 for systems without reprocessing while for systems with periodic reprocessing it ranges from 0.24 to 0.30.

It had been shown that the breeder subsystem electrical power load of the symbiotic system can be obtained from the systems net power advantage ratio. For an

electrical power self-sufficient breeder subsystem this ratio is equal to one while a value less than one describes a breeder consuming electrical power. For moderate burnup levels the net power advantage ratio was generally found to be greater than 0.90, but reached values above 1.20 for systems with high breeder fission multiplication. Depending on the degree of fission multiplication in the breeder subsystem, this factor increased or decreased with fuel burnup.

The wide response characteristics of the major system parameters with increasing system fuel burnup renders single system parameter optimizations inappropriate. An overall system optimization, therefore, included system parameter correlations. One particularly useful correlation factor is the energy production advantage factor which not only shows the effect of parameter interaction but also gives the degree of improvement of the symbiotic system over the once-through conventional reactor system. The prominent feature of the energy production advantage factor is its peak at generally low fuel burnups. An optimum fuel stretching factor, as shown in Fig. 6.1, was typically found to fall between 4 and 9 for present relative fuel cost estimates, but exceeded 20 for high fuel cost fractions. The corresponding energy production advantage factor is shown in Fig. 6.2. Here a factor marginally greater than one was

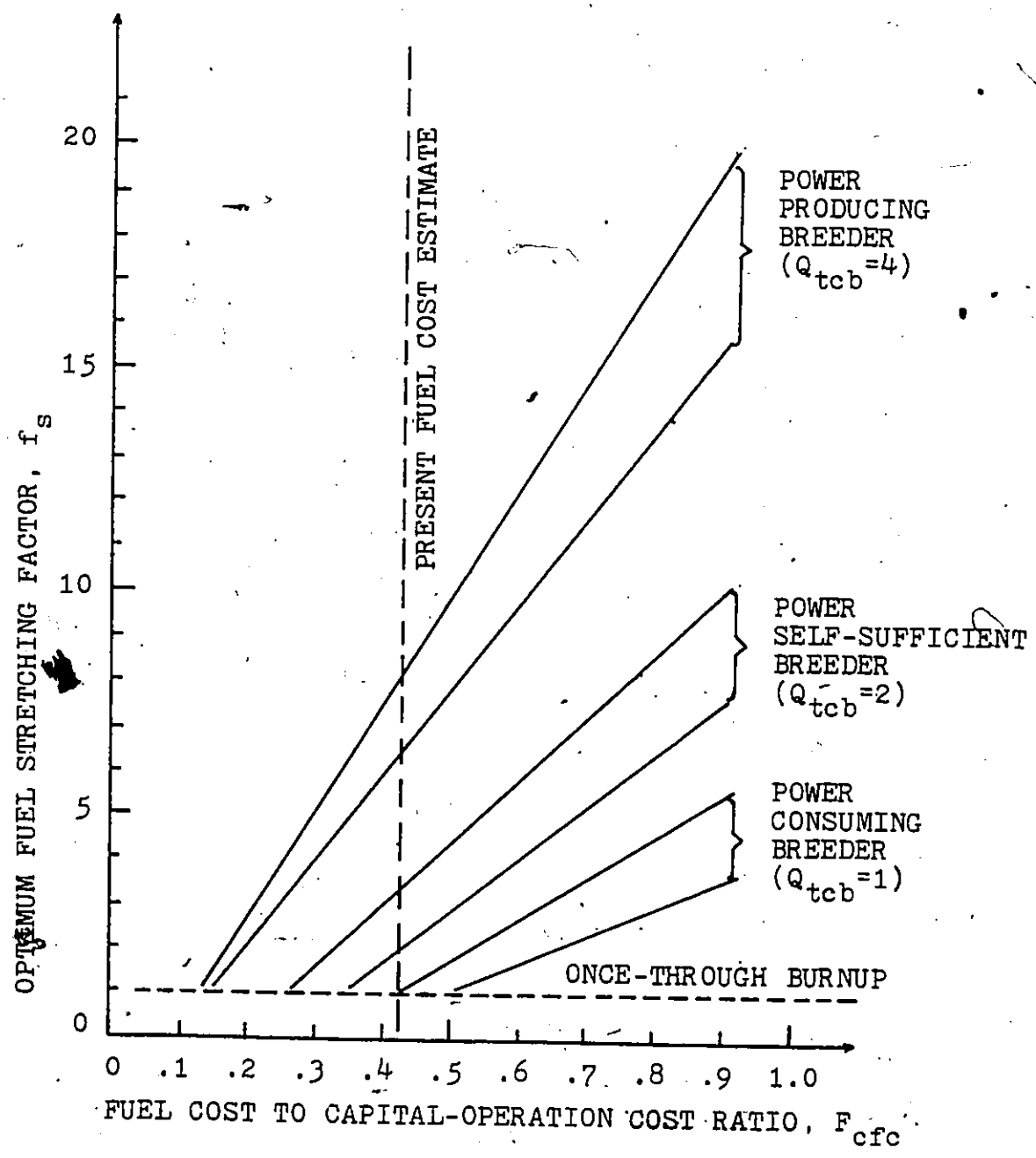

Fig. 6.1 Optimum fuel stretching factor for symbiotic systems without fuel reprocessing.

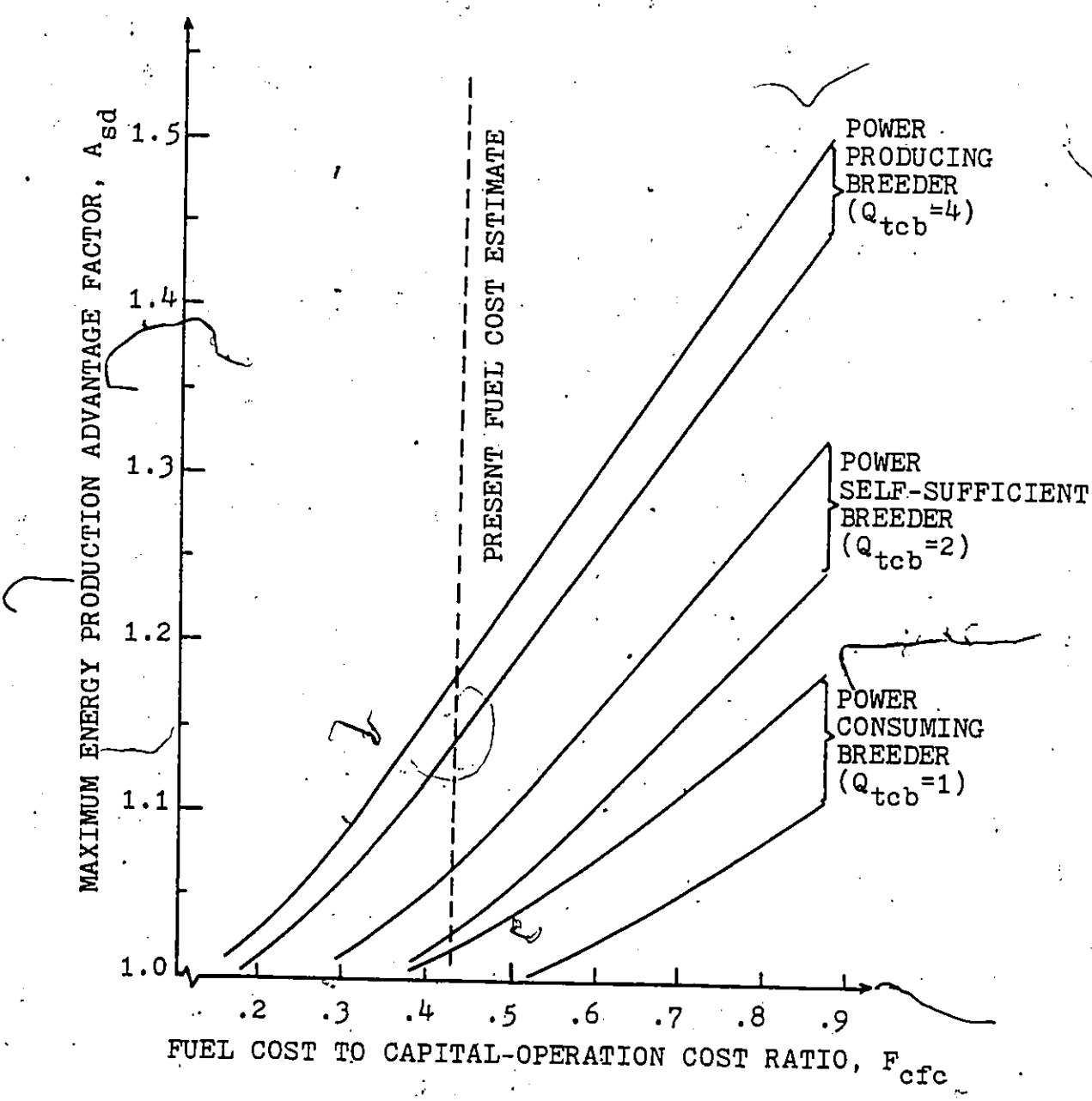

Fig. 6.2 Maximum energy production advantage factor for symbiotic systems without fuel reprocessing.

only achieved for electrical power breakeven breeder subsystems. For fuel cost fractions of at least 0.60, however, the power advantage factor was greater than unity even for the non-fission accelerator breeder targets.

The results for the system with periodic chemical reprocessing shows considerable improvements in the fissile fuel breeding characteristics over the system without any reprocessing. Presently estimated active fuel reprocessing costs, however, completely override this advantage.

The examination of spallation-fission system concepts resulted in a comprehensive analysis of symbiotic systems based on nuclear fuel rejuvenation without reprocessing. The parameter space used in this analysis was chosen to include a wide range of operational options for relevant economic environments. This provides a clear course of action for the evolution of future nuclear energy systems.

REFERENCES

1. W.B. Lewis, "The Significance of the Yield of Neutrons from Heavy Elements Excited to High Energies", AECL-968, Atomic Energy of Canada Limited, Chalk River, Canada (1952).

2. N. Bohr, "Neutron Capture and Nuclear Constitution", Nature, 137, 344 (1936).

3. R. Serber, "Nuclear Reactions at High Energies", Phys. Rev., 72, 1114 (1947).

4. L. Yaffe, Nuclear Chemistry, Academic Press, New York (1968).

5. E.K. Hyde, The Nuclear Properties of the Heavy Elements, Vol. III, "Fission Phenomena", Dover Publications, Inc., New York (1971).

6. B.S.P. Shen and M. Merker, Spallation Nuclear Reactions and their Applications, D. Reidel Publishing Company, Dordrecht-Holland (1976).

7. W.E. Crandall and G.P. Millburn, "Neutron Production at High Energies", J. Appl. Phys., 29(4), 698 (1958).

8. R.G. Vasil'kov, V.I. Gol'danskii, B.A. Pimenov, Yu. N. Pokotilovskii, and L.V. Chistyakov, "Neutron Multiplication in Uranium Bombarded with 300-660 MeV Protons", Atomnaya Energiya, 44(4), 329 (1978).

9. G.A. Bartholomew and P.R. Tunnicliffe, "The AECL Study for an Intense Neutron Generator", AECL-2600, Atomic Energy of Canada Limited, Chalk River, Canada (1966).

10. J.S. Fraser, J.S. Hewitt, J. Walker, "Neutron Spectra and Angular Distribution Produced by 1 GeV Protons on a Thick Lead Target", Phys. in Canada 22(2), 62 (1966).

11. R.R. Fullwood, J.D. Cramer, R.A. Haarman, R.P. Forrest, Jr., R.G. Schrandt, "Neutron Production by Medium-Energy Protons on Heavy Metal Targets", LA-4789, Los Alamos Scientific Laboratory, USA (1972).

12. R.G. Fluharty, P.A. Seeger, D.R. Harris, J.J. Koelling, O.L. Deutch, "Transport of Neutrons Induced by 800 meV Protons", Proc. Symp. Nucl. Data Sci. Technol. 1, 607, Paris (1973).

13. G.J. Russel, P.A. Seeger, R.G. Fluharty, "Parametric Studies of Target/Moderator Configurations for the Weapons Neutron Research (WNR) Facility", LA-6020, Los Alamos Scientific Laboratory, USA (1977).

14. G. Manning, "Spallation Neutron Sources for Neutron Beam Research", Contemp. Phys., 19(6), 505 (1978).

15. J.C.D. Milton and J.S. Fraser, "A Monte-Carlo Calculation of Neutron Production in Heavy Element Targets by Protons in the Range 0.3-1 BeV", AECL-2259, Atomic Energy of Canada Limited, Chalk River, Canada (1965).

16. V.S. Barashenkov and V.D. Toneev, "Neutron Fluxes Generated by High Energy Protons in Thick Blocks of Uranium", Atomnaya Energiya, 35(3), 163 (1973).

17. W.A. Coleman and T.W. Armstrong, "The Nucleon-Meson Transport Code NMTC", ORNL-4606, Oak Ridge National Laboratory, USA (1970).

18. K.C. Chandler and T.W. Armstrong, "Operating Instructions for the High-Energy Nucleon-meson Transport Code HETC", ORNL-4744, Oak Ridge National Laboratory, USA (1972).

19. V.S. Barashenkov, H.W. Bertini, K. Chen, G. Friedlander, G.D. Harp, A.S. Iljinov, J.M. Miller and V.D. Toneev, "Medium Energy Intranuclear Cascade Calculations: A Comparative Study", Nucl. Phys., A187, 531 (1972).

20. D.C. Irving, R.M. Freestone, Jr., and F.B.K. Kam, "05R, a General-Purpose Monte Carlo Neutron Transport Code", ORNL-3622, Oak Ridge National Laboratory, USA (1965).

21. E.A. Straker, P.N. Stevens, D.C. Irving and V.R. Cain, "The MORSE Code - A Multigroup Neutron and Gamma-Ray Monte Carlo Transport Code", ORNL-4585, Oak Ridge National Laboratory, USA (1970).

22. W.W. Engle, Jr., "A Users Manual for ANISN, A One-Dimensional Discrete Ordinates Transport Code with Anisotropic Scattering", Union Carbide Corporation Tech. Report K-1639 (1967).

23. M. Bercovitch, H. Carmichael, G.C. Hanna, and E.P. Hincks, "Yield of Neutrons per Interaction in U, Pb, W, and Sn by Protons of Six Energies Between 250 and 900 MeV Selected from Cosmic Radiation", Phys. Rev., 119(1), 412 (1960).

24. J.S. Fraser, R.E. Green, J.W. Hilborn, J.C.D. Milton, W.A. Gibson, E.E. Gross and A. Zucher, "Neutron Production in Thick Targets Bombarded by High Energy Protons", Phys. in Canada, 21(2), 17 (1965).

25. D. West and E. Wood, "Neutron Yield from Protons and Deuterons of Momenta between 0.85 and 1.7 GeV/c Totally Absorbed in Lead", Can. J. Phys., 49, 2061 (1971).

26. L.R. Veeser, R.R. Fullwood, A.A. Robba and E.R. Shunk, "Neutrons Produced by 740 MeV Protons on Uranium", Nucl. Instr. and Meth. 117, 509 (1974).

27. V.S. Barashenkov, V.D. Toneev, and S.E. Chigrinov, "On the Calculation of the Electronuclear Neutron Generation Technique", Atomnaya Energiya, 37(6), 475 (1974).

28. Y. Nakahara and H. Takahashi, "Analysis of Neutron Yield Produced by High-Energy Protons", Trans. Am. Nucl. Soc. 30, 739 (1978).

29. H. Takahashi, "Fission Reaction in the High-Energy Proton Nucleus Collision", Trans. Am. Nucl. Soc. 34, 771 (1980).

30. W.J. Hartmann and A.A. Harms, "Neutron-Return Effects of Accelerator-Driven Breeding Blankets", Trans. Am. Nucl. Soc. 33, 799 (1979).

31. V.S. Barashenkov, V.D. Toneev, and S.E. Chigrinov, "Interaction of High-Energy Deuteron Beams in Matter", Societ Atomic Energy, 37, 1256 (1974).

32. M. Steinberg, J.R. Powell, H. Takahashi, P. Grande, and H.J.C. Kouts, "Electronuclear Fissile Fuel Production", Atomkernenergie, 32, 39 (1978).

33. D.J. Rose and M.C. Melville, Jr., Plasmas and Controlled Fusion, The M.I.T. Press, Cambridge, Massachusetts (1973).

34. H. Jung, "Two Suggestions Regarding Controlled Fusion: Approximation Equations for Fusion-Fission Reactors and Fusion-Reaction-Tube Reactors", Nuclear Fusion, 9, 169 (1969).

35. L.M. Lidsky, "Fission-Fusion Symbiosis: General Considerations and Specific Example", Proceedings Nuclear Fusion Reactor Conference, 17-19 September 1969, Culham Laboratory, United Kingdom.

36. A.A. Harms, "Synergetic Nuclear Energy Systems Concepts", page 211-245 in Advances in Nuclear Science and Technology, Vol. 12, edited by J. Lewis and M. Becker, Plenum Publishing Corp., New York, USA (1980).

37. S.O. Schriber, "Electronuclear Fuel Production Using High Energy Accelerators", Atomkernenergie, 32, 49 (1978).

38. J.S. Fraser, "High Power Accelerators for Spallation Breeders of Fissile Material", Bull. Am. Phys. Soc., 22, 158 (1977).

39. C.W. Gordon, "Synergetics of Nuclear Breeding Systems", Ph.D. Dissertation, McMaster University, Canada (1979).

40. A.A. Harms and C.W. Gordon, "A Parametric Analysis of the Spallation Breeder", Nucl. Sci. Eng., 63, 336 (1977).

41. M. Steinberg, J. Powell, K. Batchelor, H. Takahashi, J. Blewett, T.V. Sheedan, H. Ludewig, V. Dang, P. Grand, O. Lazareth, and H.J. Kouts, "Linear Accelerator Breeder (LAB): A Preliminary Analysis and Proposal", BNL-50592, Brookhaven National Laboratory, USA (1976).

42. H.J.C. Kouts and M. Steinberg, Editors, "Proceedings of an Information Meeting on Accelerator-Breeding", Brookhaven National Laboratory, CONF-770107 (1977).

43. F.R. Mynatt, R.G. Alsmiller, J. Barish, T.A. Gabriel, D.E. Bartine, T.J. Burns, J.A. Martin, M.J. Saltmarsh and E.S. Bettis, "Preliminary Report on the Promise of Accelerator Breeding and Converter Reactor Symbiosis (ABACS) as an Alternative Energy System", ORNL/TM-5750, Oak Ridge National Laboratory, USA (1977).

44. W.L. Talbert, J., G.J. Russell, R.E. Malenfant, "An Experimental Program to Validate Analysis of Accelerator Breeder Concepts", LA-UR-77-2552, Los Alamos Scientific Laboratory, Los Alamos, USA (1977).

45. G.A. Bartholomew, J.S. Fraser and P.M. Garvey, "Accelerator Breeder Concept", AECL-6363, Atomic Energy of Canada Limited, Chalk River, Canada (1978).

46. R.A. Lewis, P.S. Lam, E.U. Khan, P.B. McCa[illegible]y, D. Stahl, E.F. Parker, "A Preliminary Study of the Accelerator Breeder Concept", Trans. Am. Nucl. Soc., 28, 754 (1978).

47. P.M. Garvey, J.S. Fraser, J.C.D. Milton, F.M. Kiely, B.D. Pate, I.M. Thorson, "Accelerator Breeder Target Neutronics: AECL's Underlying Research Program", Trans. Am. Nucl. Soc., 28, 754 (1978).

48. J.S. Fraser, C.R. Hoffmann, S.O. Schriber, P.M. Garvey, and B.M. Townes, "A Review of Prospects for an Accelerator Breeder", AECL-7260, Atomic Energy of Canada Limited, Chalk River, Canada (1981).

49. J.S. Fraser, C.R.J. Hoffmann and P.R. Tunnicliffe, "The Role of Electrically Produced Neutrons in Nuclear Power Generation", AECL-4658, Atomic Energy of Canada Limited, Chalk River, Canada (1973).

50. P.R. Tunnicliffe, B.G. Chidley and J.S. Fraser, "High Current Proton Linear Accelerators and Nuclear Power", AECL-5622, Atomic Energy of Canada Limited, Chalk River, Canada (1976).

51. V.G. Vasil'kov, V.I. Gol'danskii, V.P. Dzhelepov and V.P. Dmitrievskii, "The Electronuclear Method of Generating Neutrons and Producing Fissionable Materials", Soviet Atomic Energy, 29, 858 (1970).

52. V.A. Davidenko, "On Electronuclear Breeding", Soviet Atomic Energy, 29, 866 (1970).

53. C.M. Van Atta, J.D. Lee and W. Heckrotte, "The Electronuclear Conversion of Fertile to Fissile Material", UC[illegible]2144, Lawrence Livermore Laboratory, USA (1976).

54. R.G. Alsmiller, Jr., J. Barish, D.E. Bartine, T.J. Burns, T.A. Gabriel, "Medium-Energy Nucleon-Meson Transport Calculations and Electronuclear Fuel Production", Trans. Am. Nucl. Soc. 28, 756 (1978).

55. R.E. Malenfant, "Electro-Nuclear Fuel Producer", Trans. Am. Nucl. Soc. 28, 758 (1978).

56. M. Steinberg, J.R. Powell, H. Takahaski, P. Grand, and H.J.C. Kouts, "Electronuclear Fissile Fuel Producers", BNL-24356, Brookhaven National Laboratory, USA (1978).

57. H. Takahashi, H. Ludewig, "Analysis of an Accelerator-Driven Reactor Fuel Cycle", Trans. Am. Nucl. Soc. 27, 432 (1977).

58. E. Greenspan, "Preliminary Report on the Promise of Accelerator-Driven Natural-Uranium-Fueled Light-Water-Moderated Breeding Power Reactors", ORNL/TM-6138, Oak Ridge National Laboratory, USA (1978).

59. M. Steinberg, H. Takahashi, "Linear Accelerator Driven and Regenerative Reactor Systems", Trans. Am. Nucl. Soc., 28, 757 (1978).

60. H. Takahashi, "Uranium and Thorium Fuel Cycle in Linear Accelerator Driven and Regenerative Reactors", Trans. Am. Nucl. Soc. 28, 759 (1978).

61. A.A. Harms and W.J. Hartmann, "Spent Nuclear Fuel Re-Enrichment without Reprocessing", Annals of Nuclear Energy, 5, 213 (1978).

62. P. Grand and H.J.C. Kouts, "Conceptual Design and Economic Analysis of a Light Water Reactor Fuel Regenerator", BNL-50838-UC-80, Brookhaven National Laboratory, USA (1978).

63. H. Takahashi, M. Steinberg, P. Grand, J. Powell, H. Kouts, "Analysis of the Nonprocessing Two-Cycle Scenario for LWR Fuel Regenerated by Linear Accelerator Reactor", Trans. Am. Nucl. Soc. 30, 345 (1978).

64. H. Takahashi, M. Steinberg, P. Grand, J. Powell, H. Kouts, "Analysis of the AIROX Process for LWR Fuel Element Regenerated by Linear Accelerator Reactor", Trans. Am. Nucl. Soc. 32, 399 (1979).

65. J. Dorning, F. Gunnison, "On the Feasibility of an Accelerator-Driven Rejuvenator for Light-Water Reactor Fuel", Trans. Am. Nucl. Soc. 32, 799 (1979).

66. W.J. Hartmann and A.A. Harms, "Nuclear Fuel Rejuvenation Based on In Situ Reenrichment and Fission Product Removal", Trans. Am. Nucl. Soc. 33, 408 (1979).

67. A.F. Henry, Nuclear Reactor Analysis, The M.I.T. Press, Cambridge, Massachusetts (1975).

68. J.R. Lamarsh, Introduction to Nuclear Reactor Theory, Addison-Wesley Publishing Co. Inc., Reading, Massachusetts (1972).

69. L.J. Templin, "Fast Reactors", in Reactor Physics Constants, ANL-5800, Argonne National Laboratory, USA (1963).

70. C.A. Westcott, "Effective Cross Section Values for Well Moderated Thermal Reactor Spectra", AECL-1101, Atomic Energy of Canada Limited, Chalk River, Canada (1962).

71. G.J. Phillips and J. Griffiths, "LATREP User's Manual", AECL-3857, Atomic Energy of Canada Limited, Chalk River, Canada (1976).

72. W.H. Walker, "The Effect of New Data on Reactor Poisoning by Non-Saturating Fission Products", AECL-2111, Atomic Energy of Canada Limited, Chalk River, Canada (1964).

73. R.E. Schenter, W.L. Bunch and W.W. Little, "Effect of the Time Dependence of Fission Product Cross Sections in Fast Reactors", Nucl. Sci. Eng., 47, 471 (1972).

74. "Data Base for a CANDU-PHW Operating on the Thorium Cycle", INFCE/WG8/CAN/Doc4, AECL-6596, Atomic Energy of Canada Limited, Chalk River, Canada (1979).

75. J.J. Duderstadt and L.J. Hamilton, Nuclear Reactor Analysis, John Wiley and Sons, Inc., New York, USA (1976).

76. "Data Base for a CANDU-PHW Operating on a Once-Through Natural Uranium Cycle", INFCE/WG8/CAN/Doc2, AECL-6593, Atomic Energy of Canada Limited, Chalk River, Canada (1979).